1986

Gas flow through bubbles in a fluidised bed /

Hai-Kwang Chen
Lehigh University

GAS FLOW THROUGH BUBBLES

IN A FLUIDISED BED

by

Hai-Kwang Chen

A Thesis

Presented to the Graduate Committee

of Lehigh University

in Candidacy for the Degree of

Master of Science

in

Mechanical Engineering

Lehigh University

1986

CERTIFICATE OF APPROVAL

This thesis is accepted and approved in partial fulfillment of the requirements for the degree of Master of Science in Mechanical Engineering.

February 26, 1986

(Date)

Edward K Levy

Professor in Charge

F. Erdogan

Chairman of Department

ACKNOWLEDGMENTS

I would like to express my deepest gratitude and appreciation to Professor E. K. Levy, my advisor, for his guidance and encouragement to make this research work possible. I am grateful to Professor T. J. Delph for his assistance on finite element method. I am also indebted to Mr. Yi-Der Lee and Ching-Hwei Chue for their great help and valuable suggestions.

Special thanks are to my dear parents and my whole family for their endless love.

TABLE OF CONTENTS

LIST OF TABLES

LIST OF FIGURES

ABSTRACT

A theoretical model was developed to determine the behavior of gas flow through an erupting bubble in a fluidised bed. The deformation of the free surface, the motion of particles and gas, the pressure distribution and the flow rate of gas into and out of a bubble were calculated for a bubble rising through the bed and erupting at the free surface. The finite element method combined with a finite difference integration technique was used to solve this problem.

Solutions were obtained for a slow bubble at several different minimum fluidising velocities. The results show that the gas flow rate through the free surface and through the rising bubble increase rapidly when the bubble approaches the free surface, and when the bubble erupts, both the flow pattern of gas and particles and the shape of the free surface change significantly.

1. INTRODUCTION

The fluidization technique and fluidised beds have been applied to a wide variety of industrial fields, such as energy conversion and chemical processing. In practical applications of fluidised beds, elutriation frequently plays a significant role. The elutriation of particles from a gas fluidised bed may be explained based on the rising bubble. Gas bubbles are formed and rise upward through the fluidised bed, and the particles around and behind the bubble can be carried up out of the bed. The elutriation process consists of bubble eruption and transport of particles above the bed surface.

Many extensive studies on elutriation have been made, and many correlations have been proposed. Zenz and Weil [1] listed the major factors governing the freeboard phenomena and suggested a correlation to estimate the elutriation rate constant. George and Grace [2] correlated the volume of particles ejected into the freeboard as a function of the bubble diameter. Levy et al [3] have shown that the bubble through flow coefficient is much larger than is predicted by classical bubble models. On the mechanisms of bubble eruption, Rowe and Partridge [4] have shown that the particles carried in the cloud and the wake of a rising bubble are continually exchanged with the fresh particles in the dense phase. Do et al [5] performed experiments to show the ejected particles originated in the bulge material at the nose of the bursting bubbles and not from the bubble wake, and four

different mechanisms of bubble eruption and particle ejection were observed by Levy et al [6].

The previous studies are mainly empirical. The first useful theoretical approach to bubble motion was made by Davidson in 1961 [7], whose model successfully accounts for the pressure distribution and the movements of both gas and solids around a rising single bubble. Other alternate models were made by Jackson[8], Murray[9], Collins[10] to describe the behavior of gas and particles in an infinite fluidised bed.

In studying the behavior of bubbles near the bed free surface in a bed of finite dimensions, it is necessary to use different boundary conditions that were considered in [7,8,9,10]. It is also necessary to account for the deformation of the free surface as the bubble erupts. Radcliff [11] used hydrodynamics theory with a finite difference technique coupled with the finite element method to solve this problem. The present study extends Radcliff's model to analyze the phenomenon of an erupting bubble. The gas through flow coefficient is computed. The results of this study coupled with experimental studies can obtain a better understanding of gas flow through the bubble in a fluidised bed.

2. THE DAVIDSON MODEL

The first analysis of the flow of fluidising fluid around a spherical bubble which moves in an incipiently fluidised bed was derived by Davidson [12]. The model, which describes the motion of fluid and particles in the neighborhood of a rising bubble, was developed for both two and three dimensional beds. The following assumptions were made:

(a) The three dimensional bubble was assumed to have a circular cross section. Based on experimental observations, the flow near the front of a spherical-cap bubble was assumed to be the same as a potential flow a round a sphere with radius **a**. The radius **a** is also the radius of the spherical-cap.

(b) Davidson assumed that the particle phase behaves as an incompressible fluid, so the whole bed has the same bulk density outside the bubble. The continuity equation for the particles is expressed as

$$\text{div } (v_p) = 0. \tag{1}$$

where v_p is the particle velocity.

For a bubble with velocity u_b, which moves in a bed of particles. the solution of equation (1) can be found. The velocity potential for the particle motion is then

$$\phi = -u_b \left(a + \frac{r_b^3}{2a^2}\right) \cos\theta \tag{2}$$

where **a** and θ are the polar coordinates and r_b is the radius of the bubble in Figure 1. It should be noted that equation (2) refers to a bubble that is kept stationary by a downward flow of particles.

(c) The fluidising gas is assumed to be incompressible. The continuity equation of the fluidising gas is

$$\text{div } (u_g) = 0. \tag{3}$$

where u_g is the interstitial gas velocity

(d) According to D'Arcy's law, the difference between the interstitial gas and particle velocities is a constant k times the pressure gradient (grad p). That is

$$u_g - v_p = - k \text{ grad } p \tag{4}$$

where k is a constant characteristic of the particles and of the fluidising gas.

Combining equations (1),(3) and (4)

$$\text{div grad } p = 0. \tag{5}$$

This shows that the pressure distribution is unaffected by the motion of particles. Applying the following pressure boundary conditions

(i) the pressure gradient $\frac{\partial p}{\partial z}$ has a constant value at large distances above and below the rising bubble and

(ii) at **a** $= r_b$, the pressure throughout the bubble is constant, the solution for the pressure distribution is

$$p = -J \left(\mathbf{a} - \frac{r_b^3}{\mathbf{a}^2}\right) \cos \theta \tag{6}$$

where J is the pressure gradient in the vertical direction far from the bubble which just supports the weight of the particles.

$$J = -\left(\frac{\partial p}{\partial z}\right)_{\infty} \tag{7}$$

The interstitial fluid velocity far from the bubble relative to the particles $u_{g\infty}$, must be k times the pressure gradient

$$u_{g\infty} = k\ J \tag{8}$$

The superficial fluid velocity at minimum fluidization u_{mf} is

$$u_{mf} = u_{g\infty}\ \epsilon_{mf} \tag{9}$$

where ϵ_{mf} is the voidage of the bed at the minimum fluidization velocity.

From equation (4), the fluidising fluid velocity can be found. The corresponding three dimensional axi-symmetric results are

$$u_r = \left[\frac{r_b^3}{a^3}\ (u_b+2u_{g\infty}) - (u_b-u_{g\infty})\ \right] \cos\theta \tag{10}$$

$$u_\theta = \left[\frac{r_b^3}{a^3}\ \left(\frac{u_b}{2}+u_{g\infty}\right) + (u_b-u_{g\infty})\ \right] \sin\theta \tag{11}$$

The Davidson theory also shows that the upward flow rate of gas through a bubble is

$$\dot{q} = 3u_{g\infty}\ \epsilon_{mf}\ \pi r_b^2 = 3u_{mf}\ \pi r_b^2 \tag{12}$$

3. PRESENT ANALYSIS

The objective of this study is to develop an analytical model for predicting the behavior of the motion of the particles and gas and to account for the gas flow rate through the free surface and through the rising bubble as the bubble approaches the free surface.

Several assumptions are proposed for the present analysis

(a)Although this assumption doesn't coincide with experimental observations, since the bubble will grow as it rises, in order to have a steady flow problem, the gas bubble is assumed to remain constant in size and spherical in shape and keep a constant speed with only a vertical direction component through the bed.

(b) The voidage of the bed remains constant at minimum fluidization (ϵ_{mf}) when the bubble rises. The value of ϵ_{mf} depends on the shape and size of the particles. According to Jackson [13], the value of 0.4 is appropriate for approximately spherical particles. Therefore in the present study the value 0.4 is assigned to ϵ_{mf}. The bulk density of the particle phase will be equal to a constant $\rho_s(1-\epsilon_{mf})$. The particle phase will then be assumed to be an incompressible fluid. The continuity equation of the particle phase is

$$\nabla \cdot v_p = 0. \tag{13}$$

Experiments also show that a bed at minimum fluidization can be treated as a liquid of negligible viscosity. So the particle phase's behavior is assumed to be irrotational and inviscid,

$$\nabla \times v_p = 0. \tag{14}$$

From above restrictions (13)and(14), the particle phase flow is incompressible and irrotational. The particle velocity potential exists and satisfies Laplace's equation.

$$\nabla^2\phi = 0. \tag{15}$$

(c) Because the voidage is ϵ_{mf} everywhere, the gas flow is treated as an incompressible fluid. The continuity equation for the interstitial gas velocity is

$$\nabla \cdot u_g = 0. \tag{16}$$

The relation between gas velocity and the particle velocity must satisfy D'Arcy's law.

$$u_g = v_p - k\,\nabla p \tag{17}$$

Taking the divergence of the equation of D'Arcy's law and combining equations (13)and(16), Laplace's equation for the pressure p will be derived

$$\nabla^2 p = 0. \tag{18}$$

According to the above assumptions, the derived governing equations are the same as those from the Davidson's theory. If a fluidised bed with finite dimensions is considered, different boundary conditions should be applied to solve the present model. When a bubble approaches the free surface, the bubble motion will result in the deformation of the free surface and a variation of the value of the particle velocity potential function at the surface.

It is necessary to derive additional equations to obtain the above dynamic boundary conditions. According to the theory of kinetic

conditions at the surface [14](shown in Figure 2.), the equation of the free surface is

$$z_f - \eta - z_o = 0. \tag{19}$$

where z_o is the level of the undisturbed bed

z_f is the height of the free surface

η is the deformation of the free surface. $\eta = \eta(r,t)$

Since the free surface moves with the particles

$$D(z_f - \eta - z_o) / Dt = 0. \tag{20}$$

where t is time. so that

$$\frac{\partial \eta}{\partial t} + v_r \frac{\partial \eta}{\partial r} = v_z \tag{21}$$

where v_r and v_z are the particle velocities at the free surface in the r,z directions

Another dynamic boundary condition can be determined from the pressure conditions at the free surface. Using the unsteady Bernoulli equation, the pressure p is

$$p = \rho_s (1 - \epsilon_{mf})(\frac{\partial \phi}{\partial t} - g z_f - \frac{1}{2} v_p \bullet v_p) + C(t) \tag{22}$$

where C(t) is an instantaneous constant.

C(t) may be replaced by an absolute constant C by adding a suitable function of t to ϕ. Applying this equation to the surface, then

$$p_f = \rho_s (1 - \epsilon_{mf})(\frac{\partial \phi}{\partial t} - g (z_o + \eta) - \frac{1}{2} v_p \bullet v_p) + C \tag{23}$$

where p_f is the pressure at free surface

For the initial condition at t= 0., $\eta = 0.$ $\frac{\partial \phi}{\partial t} = 0.$ and $v_p = 0.$

the equation will become

$$p_f = \rho_s (1 - \epsilon_{mf})(g z_o) + C \tag{24}$$

Subtracting (24) from (23), the dynamic boundary condition can be expressed

$$\frac{\partial \phi}{\partial t} = g\,\eta + \frac{1}{2}\,v_p \cdot v_p \tag{25}$$

Using the finite difference technique, (21)and(25) may be written as

$$\eta^{N+1} - \eta^{N} = \Delta t \left(\frac{\partial \phi}{\partial z} - \frac{\partial \phi}{\partial r}\,\frac{\partial \eta}{\partial r} \right)^{N} \tag{26}$$

$$\phi^{N+1} - \phi^{N} = \Delta t \left(g\,\eta + \frac{1}{2} \left(\frac{\partial \phi}{\partial r}\,\frac{\partial \phi}{\partial r} + \frac{\partial \phi}{\partial z}\,\frac{\partial \phi}{\partial z} \right)^{N} \right. \tag{27}$$

where N and N+1 are consecutive levels of time separated by the interval Δt.

The deformation of the free surface (η) and the potential at the surface (ϕ) can be obtained by the above explicit method.

From D'Arcy's law, the constant k times $\frac{\partial p}{\partial z}$ for the bubble far away from the upper and lower surfaces will equal the interstitial gas velocity $u_{g\infty}$.

$$u_{g\infty} = - k \left(\frac{\partial p}{\partial z} \right)_{\infty} \tag{28}$$

and the superficial gas velocity at minimum fluidization u_{mf} is

$$u_{mf} = \epsilon_{mf}\, u_{g\infty} = - \epsilon_{mf}\, k \left(\frac{\partial p}{\partial z} \right)_{\infty} \tag{29}$$

Because ϵ_{mf} and $\left(\frac{\partial p}{\partial z} \right)_{\infty}$ are constant, the choice of k will affect the value of u_{mf} which dominates the type of flow pattern. As the bubble erupts from the surface, the gas flow pattern is different from that for a bubble deep in the bed. In order to understand the characteristic of the erupting bubble, it is necessary to have information about the gas flow rates through the bubble and the surface.

In spherical coordinates, the differential area dA is

$$dA = r_b^2 \sin\theta \; d\theta \; d\phi \tag{30}$$

If $u_n(\theta)$ is the absolute interstitial gas velocity normal to the sphere surface (shown in Figure 3.), the net volumetric flow rate of gas across the surface of the bubble can be expressed as

$$\dot{q}_{net} = \int \epsilon_{mf} \; u_n(\theta) \; dA$$

$$= \int_0^{2\pi} \int_0^{\pi} \epsilon_{mf} \; u_n(\theta) \; r_b^2 \; \sin\theta \; d\theta \; d\phi$$

$$= 2\pi r_b^2 \; \epsilon_{mf} \int_0^{\pi} u_n(\theta) \; \sin\theta \; d\theta \tag{31}$$

To satisfy the principle of conservation of mass, $\dot{q}_{net}=0$. There exists an angle θ_1 such that

$$\dot{q}_{out} = 2\pi r_b^2 \; \epsilon_{mf} \int_{\theta_1}^{\pi} u_n(\theta) \; \sin\theta \; d\theta$$

This can also be written

$$\dot{q}_{out} = - \; 2\pi r_b^2 \; \epsilon_{mf} \int_0^{\theta_1} u_n(\theta) \; \sin\theta \; d\theta = - \; \dot{q}_{in} \tag{32}$$

since

$$\dot{q}_{out} + \dot{q}_{in} = 0. \tag{33}$$

The magnitude of the total flow rate of gas into or out of the bubble is

$$\dot{q}_{out} = \left| \; 2\pi r_b^2 \; \epsilon_{mf} \int_0^{\theta_1} u_n(\theta) \; \sin\theta \; d\theta \; \right| \tag{34}$$

or $$\dot{q}_{out} = u_{GB} \; \pi r_b^2 \tag{35}$$

where u_{GB} is the average absolute superficial gas velocity flowing through the bubble.

u_{GB} is also defined by [3]

$$u_{GB} = u_b + m_b u_{mf} \tag{36}$$

where m_b is the through flow coefficient of the bubble

u_b is the bubble velocity

Combining the above three equations, m_b can be directly obtained from

$$m_b = \frac{u_{GB}}{u_{mf}} - \frac{u_b}{u_{mf}} \tag{37}$$

$$m_b = \frac{2\epsilon_{mf} \int_0^{\theta_1} u_n(\theta) \sin\theta \, d\theta}{u_{mf}} - \frac{u_b}{u_{mf}} \tag{38}$$

The total gas flow rate across the effective circular eruption area at the free surface of the bed is

$$\dot{q}_{FS} = \epsilon_{mf} \int_0^{r_1} u_z \, 2\pi r \, dr \tag{39}$$

or $$\dot{q}_{FS} = u_{GF} \pi r_1^2 \tag{40}$$

where r_1 is the effective radius of the circular eruption area through which gas flows vertically across the surface of the bed in Figure 4.

u_z is the vertical component of interstitial gas velocity at the bed free surface.

u_{GF} is the average absolute superficial gas velocity flowing through the area πr_1^2 at the free surface of the bed.

and

$$u_{GF} = u_b + m_f\, u_{mf} \tag{41}$$

So $$m_f = \frac{u_{GF}}{u_{mf}} - \frac{u_b}{u_{mf}} \tag{42}$$

IF u_{GF} is replaced by $\frac{\dot{q}_{FS}}{\pi r_1^2}$ then

$$m_f = \frac{\epsilon_{mf} \int_0^{r_1} u_z\, 2\pi r\, dr}{\pi r_1^2\, u_{mf}} - \frac{u_b}{u_{mf}} \tag{43}$$

where m_f is the through flow coefficient at the free surface

The effective radius r_1 can be related to the bubble radius r_b through

$$\alpha_f = \frac{r_1}{r_b} \tag{44}$$

where α_f is the bubble flow area shape factor

The preceding analysis provides a set of equations which model the behavior of the particle and gas phase in a fluidised bed. The following governing equations will be used to solve the present model.

$$\nabla^2 \phi = 0. \tag{15}$$

$$\nabla^2 p = 0. \tag{18}$$

$$u_g = v_p - k\, \nabla p \tag{17}$$

$$\eta^{N+1} - \eta^{N} = \Delta t \left(\frac{\partial \phi}{\partial z} - \frac{\partial \phi}{\partial r} \frac{\partial \eta}{\partial r} \right)^{N} \tag{26}$$

$$\phi^{N+1} - \phi^{N} = \Delta t \left(g \eta + \frac{1}{2} \left(\frac{\partial \phi}{\partial r} \frac{\partial \phi}{\partial r} + \frac{\partial \phi}{\partial z} \frac{\partial \phi}{\partial z} \right)^{N} \right. \tag{27}$$

$$m_b = \frac{2\epsilon_{mf} \int_0^{\theta_1} u_n(\theta) \sin\theta \, d\theta}{u_{mf}} - \frac{u_b}{u_{mf}} \tag{38}$$

$$m_f = \frac{\epsilon_{mf} \int_0^{r_1} u_z \, 2\pi r \, dr}{\pi r_1^2 \, u_{mf}} - \frac{u_b}{u_{mf}} \tag{43}$$

It is convenient to nondimensionlize the equations, using the following reference quantities.

d_b bubble diameter

u_b bubble velocity

$\rho_s(1- \epsilon_{mf}) \, d_b \, g / g_c$ undisturbed pressure

The dimensionless ratios are

time $\Delta T = \dfrac{\Delta t \, u_b}{d_b}$

velocity potential $\Phi = \dfrac{\phi}{d_b \, u_b}$

pressure $P = \dfrac{p}{\rho_s(1-\epsilon_{mf}) \, d_b \, g/g_c}$

velocity $U_g = \dfrac{u_g}{u_b}$ $\quad V_p = \dfrac{v_p}{u_b}$

$U_z = \dfrac{u_z}{u_b}$ $\quad U_n(\theta) = \dfrac{u_n(\theta)}{u_b}$

length $H = \dfrac{\eta}{d_b}$ $\quad R = \dfrac{r}{d_b}$ $\quad Z = \dfrac{z}{d_b}$

The dimensionless governing equations become

$$\nabla^2 \Phi = 0. \tag{45}$$

$$\nabla^2 P = 0. \tag{46}$$

$$U_g = V_p - K \nabla P \tag{47}$$

$$H^{N+1} - H^N = \Delta T \left(\frac{\partial \Phi}{\partial Z} - \frac{\partial \Phi}{\partial R} \frac{\partial H}{\partial R} \right)^N \tag{48}$$

$$\Phi^{N+1} - \Phi^N = \Delta T \left(\frac{H}{Frd} + \frac{1}{2} \left(\frac{\partial \Phi}{\partial R} \frac{\partial \Phi}{\partial R} + \frac{\partial \Phi}{\partial Z} \frac{\partial \Phi}{\partial Z} \right)^N \right. \tag{49}$$

$$m_b = \frac{2 \int_0^{\theta_1} U_n(\theta) \sin \theta \, d\theta}{K} - \frac{1}{K \epsilon_{mf}} \tag{50}$$

$$m_f = \frac{\int_0^{R_1} U_z \, 2\pi R \, dR}{\pi R_1^2 K} - \frac{1}{K \epsilon_{mf}} \tag{51}$$

Two parameters K and Frd appear in the above equations. The ratio K can be considered a dimensionless interstitial gas velocity far from the bubble (see appendix A). The quantity Frd is the Froude number, which is defined by the relation

$$Frd = \frac{u_b^2}{d_b \, g} \tag{52}$$

The bubble velocity can be written

$$u_b = u_{g\infty} - u_{mf} + 0.711 \sqrt{g \, d_b}$$

which gives

$$Frd = \frac{(u_{g\infty} - u_{mf} + 0.711 \sqrt{g\, d_b})^2}{d_b\, g}$$

For conditions near minimum fluidization or for bubbles near the top of a very deep bed, this reduces to

$$Frd = (0.711)^2 = 0.50552$$

4. NUMERICAL SOLUTION TECHNIQUE

Several approximate numerical analysis methods are available for solving the above equations. The most commonly used method is the finite difference scheme, but since the position of the bubble and the shape of the free surface change with time, the finite difference technique becomes difficult to use. The finite element method can represent the flow structure by an assemblage of finite elements. It can specify the element mesh density around the bubble and near the free surface as finely as necessary. And because of the flexibility it provides, it is particularly well suited for this problem.

A specific finite element software package developed by Structural Dynamics Research Corporation (SDRC) and General Electric CAE (Computer-Aided Engineering) International Inc. was used in this study. The CAE software system provides a complete computer aided design (CAD) capability with the SUPERTAB programs and a general purpose finite element analysis program (SUPERB). SUPERTAB interactive graphics uses geometric modeling and mesh generation to allow rapid creation of models for finite element analysis. SUPERB uses the finite element method of numerical analysis to solve partial differential equations.

Another two computer programs developed by Radcliff will be used. One is VPARTS, which combines the data from SUPERTAB and SUPERB to create the VPART1.DAT and STEP1.DAT files. The VPART1.DAT file contains the information on potential, node coordinate and velocity

for all nodes. The STEP1.DAT file involves the value of potential and position at the free surface for the present time step and the next time step. The other is UGAS, which uses D'Arcy's law to compute the gas velocity and to create the UGAS1.DAT file, The UGAS1.DAT file contains the direction and magnitude of gas velocity for all nodes. The source code of the above programs can be found at the Energy Research Center, Lehigh University. in Bethlehem Pennsylvania.

The solution procedure always follows an orderly step-by-step process. To summarize in general terms how the CAE software system and programs works, we will list these steps.

1. Model creation and mesh generation

The new data for the free surface comes from the previous step N. These data contain the values of the potential function and position coordinates for the new time step N+1, which are used to create the geometrical model for this time step. For the initial time step where the bubble is deep in the bed, the shape of the free surface is flat and the velocity potential on the free surface is $\Phi=0$.

SUPEBTAB will directly write out two files, the UNIVERSAL file and the INPUT file. These contain the information on node coordinate and element connection.

It should be noted that an axisymmetric parabolic-quadrilateral isoparametric element was used as mesh generation process (see appendix B).

2. Calculate the motion of the particles and potential field

After the CAE software system generates appropriate nodes and elements, the boundary conditions are added to complete the finite element model.

The governing equation and the boundary conditions (shown in Figure 5.) are

$$\nabla\Phi^2 = 0.$$

(a) free surface $\Phi = \Phi^N$

(b) surface of sphere $\frac{\partial\Phi}{\partial N} = -\cos\theta$

(c) bottom edge $\frac{\partial\Phi}{\partial Z} = 0.$

(d) right edge and else where $\frac{\partial\Phi}{\partial R} = 0.$

SUPERB solves directly for the potential Φ throughout the solution domain at time level N and it derives the solutions of particle velocities in the R and Z directions.

3. Calculate the new time step N+1

The explicit finite difference technique is used to modify the free surface boundary conditions, The difference in shape and potential between the present time step N and next time step N+1 is calculated by VPARTS.

The governing equations are

$$H^{N+1} = H^N + \Delta T \left(\frac{\partial\Phi}{\partial Z} - \frac{\partial\Phi}{\partial R} \frac{\partial H}{\partial R} \right)^N$$

$$\Phi^{N+1} = \Phi^N + \Delta T \left(\frac{H}{Frd} + \frac{1}{2} \left(\frac{\partial\Phi}{\partial R} \frac{\partial\Phi}{\partial R} + \frac{\partial\Phi}{\partial Z} \frac{\partial\Phi}{\partial Z} \right)^N \right.$$

where Φ^N, H^N, $\frac{\partial\Phi^N}{\partial R}$, $\frac{\partial\Phi^N}{\partial Z}$, come from step 2. The resulting values of H^{N+1}, Φ^{N+1} are used by step 1 for the next time step N+1

4. Calculate the pressure distribution

The pressure field has the same domain and same type of governing equation (Laplace's equation) as the potential field. Therefore the same INPUT file from step 1 can be used with adjustment of the boundary conditions.

The governing equation and the boundary conditions (shown in Figure 6.) are

$$\nabla P^2 = 0.$$

(a) free surface $\quad P = 0.$

(b) surface of sphere $\quad P = P_s$

(c) centerline $\quad \frac{\partial P}{\partial R} = 0.$

(d) else where $\quad P = Z_o + H - Z$

where P_s is the dimensionless constant pressure at the bubble surface.

Z_o is the dimensionless height of the undisturbed free surface. The derivation of the pressure boundary condition (d) is described in appendix A

SUPERB solves directly for the pressure P and computes the pressure gradients in the R and Z directions.

5. Calculate the gas velocity

UGAS uses particle velocities from step 2 and pressure gradients from step 3 to insert into the D'Arcy law to computer the interstitial gas velocity field.

The governing equation is

$$U_g = V_p - K \nabla P$$

The dimensionless group K is selected for different interstitial gas velocities far from the bubble.

It should be noted that any results for gas velocities should be to make certain they satisfy the mass conservation principle. This means the gas flow into the bubble must equal gas flow out the bubble. In addition, the gas flow rate through the bottom of bed should be the same as the gas flow rate across the free surface.

6. Calculate the through flow coefficient

The gas flow rate is computed by the program CUBINT. The CUBINT is a method of numerical integration for unequal spaces using cubic interpolation [15] and it can easily be applied to the surface around the bubble and free surface.

The through flow coefficient of the bubble can be obtained from

$$m_b = \frac{2 \int_0^{\theta_1} U_n(\theta) \sin\theta \, d\theta}{K} - \frac{1}{K \epsilon_{mf}}$$

the through flow coefficient of the free surface is

$$m_f = \frac{\int_0^{R_1} U_z \, 2\pi R \, dR}{\pi R_1^2 K} - \frac{1}{K \epsilon_{mf}}$$

5. RESULTS AND DISCUSSION

In this study, a cylindrical bed $\pi(\frac{20d_b}{2})^2 \times 20d_b$ is selected. This selection is based on Radcliff's analysis [11], in which he tried different domain sizes and compared the solutions for bubbles deep in the bed to Davidson's results [12]. Figure 7 illustrates this axisymmetric domain of the bed with the bubble being located at the center of the bed.

For a bubble deep in the bed, the Davidson solution is in reasonable agreement with experimental observations for some bubble characteristics such as cloud behavior. To verify the validity of the numerical method in this study, comparisons of the results with the Davidson solution are demonstrated. The particle and gas velocities (K= 0.5, 1.1, 10) are calculated by both the present and Davidson models at the initial time step. The relative error formula is defined by

$$\text{Error} = \frac{\text{(present solution - Davidson solution)}}{\text{(Davidson solution)}} \text{ X 100 \%}$$

and notations are as follows

0	:	10 %	$\geq$	Error	>	0 %
1	:	20 %	$\geq$	Error	>	10 %
2	:	30 %	$\geq$	Error	>	20 %
3	:	40 %	$\geq$	Error	>	30 %
4	:	50 %	$\geq$	Error	>	40 %
5	:	60 %	$\geq$	Error	>	50 %
6	:	70 %	$\geq$	Error	>	60 %
7	:	80 %	$\geq$	Error	>	70 %
8	:	90 %	$\geq$	Error	>	80 %
9	:			Error	>	90 %

The comparisons of the particle velocities are shown in Figures 8-13, which indicate the accuracy of this model especially in the area near the bubble. Furthermore, in order to have a more detailed comparison of these two solutions, the relative error in the range of 0 - 10% for absolute particle velocity in the area near the bubble was broken down into ten individual percentage distributions. The notations shown in Figure 14 are listed below

A	:	1 %	$\geq$	Error	>	0 %
B	:	2 %	$\geq$	Error	>	1 %
C	:	3 %	$\geq$	Error	>	2 %
D	:	4 %	$\geq$	Error	>	3 %
E	:	5 %	$\geq$	Error	>	4 %
F	:	6 %	$\geq$	Error	>	5 %
G	:	7 %	$\geq$	Error	>	6 %
H	:	8 %	$\geq$	Error	>	7 %
I	:	9 %	$\geq$	Error	>	8 %
O	:	10 %	$\geq$	Error	>	9 %

The gas velocities are also presented in Figures 15-35 in the same way. These pictures exhibit several characteristics. Because of the finite dimensions of bed in this study, the differences between the particle velocities from this work and Davidson's show the largest values near the domain boundaries. Nevertheless the results in the area near the bubble are in good agreement with Davidson's solution. For the gas velocity, the vertical component of gas velocity is generally much larger than the radial component and thus it dominates the gas flow field. The radial component of gas velocity can be neglected in comparison with the magnitude of gas velocity. The results for the vertical component and the magnitude of gas velocity

generally are in close agreement with those of the Davidson model, particularly near the bubble.

For purposes of understanding the phenomena of elutriation and bubble eruption, the region between the bubble and the free surface is of particular concern. From the sequential graphics of Figure 36, the location of bubble surface on plots of deformation of free surface for different bubble positions is presented. Figures 37-42 show the finite element grid patterns for bubble center heights z_c at 10, 16.25 and 19.85 d_b. As the bubble approaches the free surface, the area in the bulge becomes particularly important and a much finer element mesh is needed in this region such that the error due to numerical interpolation can be reduced to a minimum. The element grid pattern used for $\frac{c}{d_b} = 19.85$ is illustrated in Figure 43.

A numerical instability in the integration with time was observed and this was found to depend on Δt and the size of the elements in the bulge. Figures 44-50 characterize this unstable behavior. Figure 44 shows the deformation of the free surface where a coarse mesh in the bulge and a large time step ($\Delta t = 0.05 \frac{u_b}{d_b}$) were used. Figure 45 displays the deformation of the free surface for a fine mesh in the bulge. These two graphs demonstrate the influence of the size of element in the bulge. The instability manifested itself in irregularities in the deformation of the free surface as the bulge

became thin. This is seen at $\frac{z_c}{d_b} = 19.7$ in Figures 46 and 47. The time increment also plays an important role in the numerical instability. In comparison with Figure 44, the deformation of the free surface for a small time step ($\Delta t = 0.02 \frac{u_b}{d_b}$) is calculated and plotted in Figure 48. As the bulge becomes thin, differences in the solution for the shape of the free surface due to Δt appear. This is shown in Figures 49 and 50. There are many papers dealing with this kind of numerical inaccuracy. Usually the finer mesh does not mean more accurate results. For this problem, it was hoped to get a convergent solution despite the existence of the oscillation due to the instability. The use of a smaller time step size proved to be helpful in securing stable solutions.

Based on the above results, mesh sizes and time steps were selected for the final calculations shown here. The calculations were completed within 30 time steps in this study. There are two kinds of parameters which can be used to indicate time scale. The first parameter is the vertical position of the bubble center, which was the basic variable used to create the mesh geometry and calculate the deformation of free surface. The bulge thickness at the bubble centerline characterizes the region between the bubble and the free surface and is also a significant parameter.

Table 1 shows the position of the bubble center and the bulge thickness at the bubble centerline for all the computational time steps. Figure 51 plots the bulge thickness at the bubble centerline

with respect to the position of the bubble center. It shows a linear relationship until the position of the bubble center is higher than 19.5 d_b.

The motion of the particle and gas are presented by vector fields. Figures 52-57 show the behavior of the particle flow for three different bubble positions z_c = 10, 16.25, 19.85 d_b. These pictures demonstrate that the particle velocities are quite small except in the immediate region of the bubble. The gas velocity vector field is presented in Figures 58-73. These illustrate that the vertical component of gas velocity dominates the gas flow field except in the vicinity of the bubble. For values of $K \gg 1$, the graphs of the vector fields for absolute gas velocity and gas velocity relative to the bubble are nearly identical. For $K \simeq 1$ and $K < 1$, the gas velocities relative to the bubble velocity show different characteristics from the absolute gas velocity, and this depends on the choice of the specific value of K. For slow bubbles ($K > 1$), the gas enters the bottom of the bubble and leaves at the top. This is illustrated in Figures 74-79. For a fast bubble ($K < 1$), Figures 80-83 show that there is one region where the gas is in circulation around the bubble. The rest of the gas of the bed does not mix with the circulating gas and bypasses the cloud region.

The characteristics of the particle motion were examined at the free surface. Figure 84 shows an increase in the vertical component of particle velocity when the bubble is near the free surface. This can be used to explain why, as the bubble rises, the fluidised bed has a

deformation at the free surface. Figure 85 shows the full free surface with respect to the position of the bubble center. A plot of the region near the bubble centerline is given in Figure 86 and Figure 87 shows the deformation of the free surface at the bubble centerline as a function of bulge thickness. The numerical values are also listed in Table 1.

Multiple solutions for gas flow are possible, each occurring with a specific value of bubble pressure. However for a given bubble position and value of K only one gas flow field result satisfies conservation of mass for the bubble. In this study, six values of the interstitial gas velocity far from the bubble (K = 1.1, 2, 5, 10, 100, 1000) were selected. For a given value of K, the gas velocity fields at each time step depend on the particle velocities and pressure gradients at that same time step. For each solution for the gas velocity field, calculations of conservation of mass were made to evaluate the gas flow rate into and out of the moving bubble. At each time step, the gas flow rate was calculated. If it did not show a balance in gas flow through the bubble, the pressure in the bubble was adjusted until the residual gas flow through the bubble W_r equaled zero. Fortunately, a nearly linear relationship exists between the residual gas flow through the bubble and the pressure in the bubble. Table 2 lists the residual gas flow rate through the bubble with respect to different bubble pressures at bubble heights 10, 14, 17, 19 and 19.85 d_b. The data for the case K=100 are plotted in Figure 88 to

demonstrate the linear relationship above, A similar phenomenon for different K values can also be shown by the same procedure. It is convenient to use this relationship to find the appropriate pressure in the bubble at which mass is conserved.

All of the final pressure gradients and gas velocity fields shown in this study were derived corresponding to these pressures. Those pressures at which the conservation of mass is satisfied throughout the bubble are tabulated in Table 3 and the gas flow rates through the bubble corresponding to these pressure are calculated and listed in Table 4. The relation between the through flow coefficient for the bubble and the bulge thickness was also calculated by equation (50) for various values of the voidage at minimum fluidization (ϵ_{mf}): 0.4, 0.45 and 0.5. The results are tabulated in Tables 5-7 and shown in Figures 89-91.

The horizontal and vertical gas velocity components and the magnitude of the gas velocities around the bubble are plotted corresponding to the angle variation in Figures 92-109. These results display the variation of the gas velocities and the gas velocity increase in the bulge area of the bubble as the bubble approaches the free surface.

In order to investigate the gas behavior at the free surface of the bed more thoroughly, the absolute vertical gas velocities on the free surface are plotted in Figures 110-115. These give a picture of the gas motion at the free surface. Figures 116-121 show an increase

in gas velocity at the free surface in the vicinity of the bubble centerline when the bubble is near the free surface.

When the bubble erupts from the free surface of a gas fluidised bed, the effective diameter for gas flow across the free surface of the bed and the gas flow rate through the moving bubble and free surface are of interest. The magnitudes of the bubble through flow coefficient and the effective area of flow were calculated. From the definition of the effective diameter (Figure 4) and figures of vertical gas velocity at free surface (Figures 116-121), the effective diameter $2r_1$ can be determined at the location of the intersection of the vertical gas velocity profile and the interstitial minimum fluidization gas velocity profile which is the closest to the bubble centerline. A meaningful value for effective diameter for gas flow does not occur until the position of the bubble center reaches a certain height. Table 8 shows the effective diameter with respect to the bulge thickness for different K's. These results are also plotted in Figure 122. These show an decrease in the effective diameter with a decrease of the bulge thickness. The gas flow rates at the free surface across the circular eruption area within this effective diameter were computed and are tabulated in Table 9. Using the above information and the equation (51), the through flow coefficient at the free surface can be calculated. The results are contained in Tables 10-12, and graphically illustrated in Figures 123-125 for various values of ϵ_{mf}.

Summary

The results of computations of the gas flow through a bubble in a fluidised bed are presented here. Several characteristics can be concluded as follows.

1. Significant variations in gas flow behavior occur near the bulge region. Nevertheless these phenomena do not show up until the bubble rises to a certain distance in the bed.

2. For the purpose of improving the numerical accuracy and avoiding computational instability, sufficiently small time steps should be used.

3. The gas velocity field is affected primarily by the Froude number and the value of K. However the particle velocity field is only a function of the Froude number.

4. This model was used to predict the behavior of the slow bubble. For a bubble deep in the bed, the difference between the results from this model and Davidson's are small for values of K >10.

5.For slow bubbles, the bubble through-flow coefficient is larger than that predicted by the Davidson model when the bubble reaches the free surface. The value of through flow coefficient is a function of the value of voidage at minimum fluidization.

The results presented here are backed up on the magnetic tape, which may be requested at the Research Center. Lehigh University, Bethlehem, Penn.

Table 1. The deformation of free surface and the bulge thickness at the bubble centerline related to the position of the bubble center

the position of bubble center z_c	bulge thickness Δ	the deformation of free surface η
10.0000	9.5000	.0000
11.0000	8.5004	.0000
12.0000	7.5006	.0006
13.0000	6.5009	.0009
14.0000	5.5013	.0013
14.7500	4.7512	.0012
15.5000	4.0009	.0009
16.2500	3.2499	.0000
17.0000	2.5003	.0003
17.5000	2.0026	.0026
18.0000	1.5083	.0083
18.2500	1.2643	.0143
18.5000	1.0228	.0228
18.7500	.7847	.0347
19.0000	.5522	.0552
19.1000	.4648	.0648
19.2000	.3804	.0804
19.3000	.3014	.1014
19.4000	.2282	.1282
19.5000	.1612	.1612
19.5500	.1336	.1836
19.6000	.1111	.2111
19.6500	.0849	.2349
19.7000	.0695	.2695
19.7300	.0541	.2841
19.7600	.0468	.3068
19.7900	.0356	.3068
19.8200	.0326	.3526
19.8500	.0171	.3671
19.8600	.0243	.3843

Table 2. The residual gas flow through the bubble with respect to the bubble pressure

the bubble center height at 10.00

K	P_b=9.9 W_r	P_b=10.0 W_r	P_b=10.1 W_r	the appropriate bubble pressure
1.1	-.468	.220	.909	9.9680
2.0	-1.042	.210	1.461	9.9832
5.0	-2.954	.175	3.304	9.9944
10.0	-6.141	.117	6.375	9.9981
100.0	-63.507	-.928	61.648	10.0015
1000.0	-637.211	-11.397	614.450	10.0018

the bubble center height at 14.00

K	P_b=5.9 W_r	P_b=5.95 W_r	P_b=6.0 W_r	the appropriate bubble pressure
1.1	-.166	.182	.531	5.9238
2.0	-.677	-.044	.591	5.9535
5.0	-2.380	-.798	.785	5.9752
10.0	-5.219	-2.055	1.111	5.9825
100.0	-56.327	-24.674	6.974	5.9890
1000.0	-567.357	-250.888	65.625	5.9896

the bubble center height at 17.00

K	P_b=2.9 W_r	P_b=2.95 W_r	P_b=3.0 W_r	the appropriate bubble pressure
1.1	-.263	.091	.446	2.9371
2.0	-.709	-.065	.580	2.9550
5.0	-2.196	-.585	1.027	2.9681
10.0	-4.674	-1.451	1.772	2.9725
100.0	-49.274	-17.048	15.177	2.9765
1000.0	-495.305	-173.008	149.198	2.9769

the bubble center height at 19.00

K	P_b=0.9 W_r	P_b=0.95 W_r	P_b=1.0 W_r	the appropriate bubble pressure
1.1	-.482	-.044	.395	.9550
2.0	-.886	-.087	.711	.9555
5.0	-2.229	-.233	1.764	.9558
10.0	-4.468	-.475	3.517	.9560
100.0	-44.760	-5.956	35.089	.9561
1000.0	-447.678	-48.425	350.807	.9561

the bubble center height at 19.85

K	P_b=0.09 W_r	P_b=0.1 W_r	P_b=0.11 W_r	the appropriate bubble pressure
1.1	-.243	.109	.462	.0969
2.0	-.390	.251	.892	.0961
5.0	-.877	.725	2.328	.0955
10.0	-1.690	1.516	4.721	.0953
100.0	-16.317	15.737	47.792	.0951
1000.0	-162.594	158.235	478.497	.0951

Table 3. The pressure at which the conservation of mass is satisfied throughout the bubble as a function of bulge thickness and K

bulge thickness	P_b (K=1.1)	P_b (K=2)	P_b (K=5)	P_b (K=10)	P_b (K=100)	P_b (K=1000)
9.5000	9.9680	9.9832	9.9944	9.9981	10.0015	10.0018
8.5004	8.9517	8.9682	8.9802	8.9843	8.9878	8.9882
7.5006	7.9494	7.9658	7.9779	7.9819	7.9855	7.9859
6.5009	6.9919	6.9902	6.9889	6.9885	6.9881	6.9881
5.5013	5.9238	5.9535	5.9752	5.9825	5.9890	5.9896
4.7512	5.1710	5.1960	5.2144	5.2205	5.2260	5.2265
4.0009	4.4721	4.4795	4.4849	4.4867	4.4884	4.4885
3.2499	3.7070	3.7176	3.7256	3.7283	3.7306	3.7309
2.5003	2.9371	2.9550	2.9681	2.9725	2.9765	2.9769
2.0026	2.4534	2.4594	2.4638	2.4653	2.4666	2.4668
1.5083	1.9695	1.9710	1.9721	1.9725	1.9728	1.9728
1.2643	1.6962	1.7060	1.7092	1.7121	1.7124	1.6829
1.0228	1.4356	1.4467	1.4504	1.4538	1.4541	1.4205
0.7847	1.1765	1.1918	1.2031	1.2068	1.2102	1.2105
0.5522	0.9550	0.9555	0.9558	0.9560	0.9561	0.9561
0.3804	0.7488	0.7493	0.7496	0.7497	0.7498	0.7499
0.2282	0.5500	0.5483	0.5470	0.5466	0.5462	0.5462
0.1336	0.3872	0.3871	0.3871	0.3870	0.3870	0.3870
0.0695	0.2247	0.2260	0.2270	0.2273	0.2276	0.2277
0.0356	0.1424	0.1433	0.1440	0.1442	0.1445	0.1445
0.0171	0.0969	0.0961	0.0955	0.0953	0.0951	0.0951
0.0243	0.0900	0.0892	0.0886	0.0884	0.0883	0.0883

Table 4. The absolute flow rate of gas through a bubble $\dot{q}$ as a function of bulge thickness and K

bulge thickness	$\dot{q}/\epsilon_{mf}$ (K=1.1)	$\dot{q}/\epsilon_{mf}$ (K=2)	$\dot{q}/\epsilon_{mf}$ (K=5)	$\dot{q}/\epsilon_{mf}$ (K=10)	$\dot{q}/\epsilon_{mf}$ (K=100)	$\dot{q}/\epsilon_{mf}$ (K=1000)
9.5000	3.161	5.118	11.673	22.598	219.25	2185.6
8.5004	3.090	5.070	11.676	22.689	220.85	2204.7
7.5006	3.089	5.069	11.676	22.686	220.87	2204.7
6.5009	2.973	4.955	11.585	22.635	221.51	2210.3
5.5013	3.175	5.147	11.721	22.572	219.88	2191.7
4.7512	3.109	5.071	11.613	22.514	218.74	2180.9
4.0009	3.009	4.950	11.438	22.254	216.94	2163.6
3.2499	3.145	5.086	11.572	22.412	217.49	2168.5
2.5003	3.096	4.989	11.300	21.859	211.95	2112.9
2.0026	3.141	5.113	11.688	22.679	220.49	2198.8
1.5083	3.096	5.060	11.627	22.590	219.93	2193.2
1.2643	3.151	5.104	11.615	22.484	218.33	2176.8
1.0228	3.210	5.205	11.870	23.011	223.57	2229.1
0.7847	3.204	5.199	11.708	22.948	222.91	2222.7
0.5552	3.367	5.384	12.109	23.334	225.47	2246.7
0.3804	3.380	5.408	12.169	23.446	226.57	2257.9
0.2282	3.408	5.478	12.377	23.899	231.30	2305.3
0.1336	3.456	5.608	12.780	24.743	240.08	2393.4
0.0695	3.498	5.679	12.950	25.068	243.21	2424.5
0.0356	3.500	5.727	12.148	25.518	248.19	2475.0
0.0171	3.408	5.566	12.769	24.773	240.85	2401.6
0.0243	3.396	5.545	12.716	24.666	239.78	2390.9

Table 5. The through flow coefficient of the bubble as a function of bulge thickness and K for (ϵ_{mf} = 0.4)

bulge thickness	m_b (K=1.1)	m_b (K=2)	m_b (K=5)	m_b (K=10)	m_b (K=100)	m_b (K=1000)
9.5000	1.39	2.01	2.47	2.63	2.77	2.78
8.5004	1.30	1.98	2.47	2.64	2.79	2.80
7.5006	1.30	1.98	2.47	2.64	2.79	2.80
6.5009	1.17	1.90	2.45	2.63	2.80	2.81
5.5013	1.40	2.03	2.48	2.62	2.77	2.79
4.7512	1.33	1.98	2.46	2.62	2.76	2.77
4.0009	1.21	1.90	2.41	2.58	2.74	2.75
3.2499	1.37	1.99	2.45	2.60	2.74	2.76
2.5003	1.31	1.93	2.38	2.53	2.67	2.69
2.0026	1.36	2.00	2.48	2.64	2.78	2.80
1.5083	1.31	1.97	2.46	2.63	2.78	2.79
1.2643	1.37	2.00	2.46	2.61	2.75	2.77
1.0228	1.44	2.06	2.52	2.68	2.82	2.84
0.7847	1.44	2.06	2.48	2.67	2.81	2.83
0.5522	1.62	2.18	2.58	2.72	2.85	2.86
0.3804	1.64	2.19	2.60	2.74	2.86	2.87
0.2282	1.67	2.24	2.65	2.79	2.92	2.93
0.1336	1.73	2.32	2.75	2.90	3.03	3.04
0.0695	1.78	2.37	2.80	2.94	3.07	3.08
0.0356	1.78	2.40	2.85	3.00	3.14	3.15
0.0171	1.67	2.29	2.75	2.90	3.04	3.06
0.0243	1.66	2.28	2.74	2.89	3.03	3.04

Table 6. The through flow coefficient of the bubble as a function of bulge thickness and K for (ϵ_{mf} = 0.45)

bulge thickness	m_b (K=1.1)	m_b (K=2)	m_b (K=5)	m_b (K=10)	m_b (K=100)	m_b (K=1000)
9.5000	1.64	2.15	2.53	2.65	2.77	2.78
8.5004	1.56	2.12	2.53	2.67	2.79	2.80
7.5006	1.56	2.12	2.53	2.67	2.79	2.80
6.5009	1.42	2.04	2.51	2.66	2.80	2.81
5.5013	1.65	2.17	2.54	2.65	2.78	2.79
4.7512	1.58	2.12	2.51	2.64	2.76	2.77
4.0009	1.46	2.04	2.47	2.61	2.74	2.75
3.2499	1.62	2.13	2.50	2.63	2.75	2.76
2.5003	1.56	2.06	2.43	2.56	2.68	2.69
2.0026	1.62	2.14	2.53	2.67	2.79	2.80
1.5083	1.56	2.11	2.52	2.65	2.78	2.79
1.2643	1.63	2.14	2.51	2.64	2.76	2.77
1.0228	1.69	2.20	2.58	2.71	2.82	2.84
0.7847	1.69	2.20	2.54	2.70	2.82	2.83
0.5522	1.88	2.32	2.64	2.75	2.85	2.86
0.3804	1.89	2.33	2.65	2.76	2.86	2.87
0.2282	1.92	2.38	2.71	2.82	2.92	2.93
0.1336	1.98	2.46	2.81	2.93	3.03	3.05
0.0695	2.03	2.50	2.85	2.97	3.07	3.08
0.0356	2.03	2.53	2.90	3.03	3.14	3.15
0.0171	1.92	2.43	2.81	2.93	3.04	3.06
0.0243	1.91	2.42	2.79	2.92	3.03	3.04

Table 7. The through flow coefficient of the bubble as a function of bulge thickness and K for (ϵ_{mf} = 0.5)

bulge thickness	m_b (K=1.1)	m_b (K=2)	m_b (K=5)	m_b (K=10)	m_b (K=100)	m_b (K=1000)
9.5000	1.84	2.26	2.57	2.68	2.77	2.78
8.5004	1.76	2.23	2.57	2.69	2.79	2.80
7.5006	1.76	2.23	2.57	2.69	2.79	2.80
6.5009	1.62	2.15	2.55	2.68	2.80	2.81
5.5013	1.86	2.28	2.58	2.67	2.78	2.79
4.7512	1.78	2.23	2.56	2.67	2.77	2.77
4.0009	1.66	2.15	2.51	2.63	2.74	2.75
3.2499	1.82	2.24	2.55	2.65	2.75	2.76
2.5003	1.77	2.18	2.48	2.58	2.68	2.69
2.0026	1.82	2.25	2.58	2.69	2.79	2.80
1.5083	1.76	2.22	2.56	2.68	2.78	2.79
1.2643	1.83	2.25	2.56	2.66	2.76	2.77
1.0228	1.90	2.31	2.62	2.73	2.83	2.84
0.7847	1.89	2.31	2.58	2.72	2.82	2.83
0.5522	2.08	2.43	2.68	2.77	2.85	2.86
0.3804	2.09	2.44	2.70	2.79	2.86	2.87
0.2282	2.13	2.49	2.75	2.84	2.93	2.93
0.1336	2.18	2.57	2.85	2.95	3.04	3.05
0.0695	2.23	2.62	2.90	2.99	3.08	3.09
0.0356	2.23	2.65	2.95	3.05	3.14	3.15
0.0171	2.13	2.54	2.85	2.95	3.05	3.06
0.0243	2.11	2.53	2.84	2.94	3.03	3.04

Table 8. The effective radius of the circular eruption area through which gas flows vertically across the surface of the bed as a function of bulge thickness and K

bulge thickness	r_1 (K=1.1)	r_1 (K=2)	r_1 (K=5)	r_1 (K=10)	r_1 (K=100)	r_1 (K=1000)
2.5003	2.6210	3.1285	3.8915	4.0418	4.2671	4.2671
2.0026	2.3583	2.4992	2.7028	3.6469	3.6469	3.6469
1.5083	2.3074	2.4690	2.6752	2.7577	2.7886	2.7886
1.2643	1.7959	2.0015	2.2624	2.4008	2.5183	2.5418
1.0228	1.4442	1.5566	1.6577	1.7083	1.7757	1.7757
.7847	1.3178	1.3973	1.4946	1.5363	1.5850	1.5926
.5522	1.2237	1.2639	1.3142	1.3243	1.3459	1.3459
.3804	1.0777	1.1085	1.1393	1.1547	1.1624	1.1624
.2282	.8713	.8964	.9298	.9381	.9465	.9465
.1336	.7009	.7284	.7527	.7638	.7749	.7749
.0695	.5492	.5536	.5580	.5624	.5624	.5624
.0356	.4811	.4853	.4874	.4895	.4916	.4916
.0171	.4517	.4545	.4564	.4574	.4574	.4574
.0243	.4442	.4461	.4480	.4489	.4499	.4499

Table 9. The gas flow rate across the effective circular erupting area at the free surface $\dot{q}_{FS}$ as a function of bulge thickness and K

bulge thickness	$\dot{q}_{FS}/\epsilon_{mf}$ (K=1.1)	$\dot{q}_{FS}/\epsilon_{mf}$ (K=2)	$\dot{q}_{FS}/\epsilon_{mf}$ (K=5)	$\dot{q}_{FS}/\epsilon_{mf}$ (K=10)	$\dot{q}_{FS}/\epsilon_{mf}$ (K=100)	$\dot{q}_{FS}/\epsilon_{mf}$ (K=1000)
2.0026	19.4000	39.550	115.47	419.28	4192.7	41926.0
1.5083	18.6830	38.767	113.49	241.00	2463.4	24634.0
1.2643	11.3620	25.557	81.36	183.02	2012.1	20495.0
1.0228	7.4479	15.651	44.22	93.79	1011.7	10117.0
0.7847	6.3224	12.839	36.51	77.00	817.8	8254.9
0.5522	5.7064	10.901	29.10	58.91	606.2	6061.8
0.3804	4.6689	8.789	22.83	46.64	470.7	4706.2
0.2282	3.4893	6.453	16.78	33.85	341.7	3415.5
0.1336	2.6806	4.941	12.59	25.51	258.6	2584.8
0.0695	2.0435	3.584	8.74	17.44	172.7	1725.6
0.0356	1.8126	3.169	7.67	15.23	151.3	1512.0
0.0171	1.7164	2.951	7.06	13.93	137.3	1371.0
0.0243	1.6846	2.889	6.91	13.62	134.5	1343.2

Table 10. The through flow coefficient at the free surface as a function of bulge thickness and K

(for $\epsilon_{mf} = 0.4$)

bulge thickness	m_f (K=1.1)	m_f (K=2)	m_f (K=5)	m_f (K=10)	m_f (K=100)	m_f (K=1000)
2.0026	-1.26	-0.24	0.51	0.75	0.98	1.00
1.5083	-1.26	-0.24	0.51	0.76	0.98	1.01
1.2643	-1.25	-0.23	0.51	0.76	0.98	1.01
1.0228	-1.24	-0.22	0.52	0.77	1.00	1.02
.7847	-1.22	-0.20	0.54	0.79	1.01	1.03
.5522	-1.17	-0.16	0.57	0.82	1.04	1.06
.3804	-1.11	-0.11	0.62	0.86	1.08	1.11
.2282	-0.94	0.03	0.74	0.97	1.19	1.21
.1336	-0.69	0.23	0.92	1.14	1.35	1.37
.0695	-0.31	0.61	1.29	1.51	1.71	1.73
.0356	-0.01	0.89	1.56	1.77	1.97	1.99
.0171	-0.16	1.02	1.66	1.87	2.06	2.08
.0243	-0.20	1.06	1.69	1.90	2.09	2.11

Table 11. The through flow coefficient at the free surface as a function of bulge thickness and K (for ϵ_{mf} = 0.45)

bulge thickness	m_f (K=1.1)	m_f (K=2)	m_f (K=5)	m_f (K=10)	m_f (K=100)	m_f (K=1000)
2.0026	-1.01	-0.10	0.56	0.78	0.98	1.00
1.5083	-1.00	-0.10	0.57	0.79	0.99	1.01
1.2643	-1.00	-0.10	0.57	0.79	0.99	1.01
1.0228	-0.99	-0.08	0.58	0.80	1.00	1.02
.7847	-0.97	-0.06	0.60	0.82	1.01	1.03
.5522	-0.92	-0.03	0.63	0.85	1.04	1.06
.3804	-0.86	0.03	0.68	0.89	1.09	1.11
.2282	-0.69	0.17	0.79	1.00	1.19	1.21
.1336	-0.44	0.37	0.97	1.17	1.35	1.37
.0695	-0.06	0.75	1.34	1.53	1.72	1.73
.0356	0.25	1.03	1.61	1.80	1.97	1.99
.0171	0.41	1.16	1.72	1.90	2.07	2.08
.0243	0.45	1.20	1.75	1.93	2.09	2.11

Table 12. The through flow coefficient at the free surface as a function of bulge thickness and K

(for ϵ_{mf} = 0.5)

bulge thickness	m_f (K=1.1)	m_f (K=2)	m_f (K=5)	m_f (K=10)	m_f (K=100)	m_f (K=1000)
2.0026	-0.81	0.01	0.61	0.80	0.98	1.00
1.5083	-0.80	0.01	0.61	0.81	0.99	1.01
1.2643	-0.80	0.02	0.61	0.81	0.99	1.01
1.0228	-0.78	0.03	0.62	0.82	1.00	1.02
.7847	-0.76	0.05	0.64	0.84	1.02	1.03
.5522	-0.72	0.09	0.67	0.87	1.05	1.06
.3804	-0.65	0.14	0.72	0.91	1.09	1.11
.2282	-0.49	0.28	0.84	1.02	1.19	1.21
.1336	-0.24	0.68	1.02	1.19	1.35	1.37
.0695	0.14	0.86	1.39	1.56	1.72	1.73
.0356	0.45	1.14	1.66	1.82	1.97	1.99
.0171	0.62	1.27	1.76	1.92	2.07	2.08
.0243	0.65	1.31	1.79	1.95	2.10	2.11

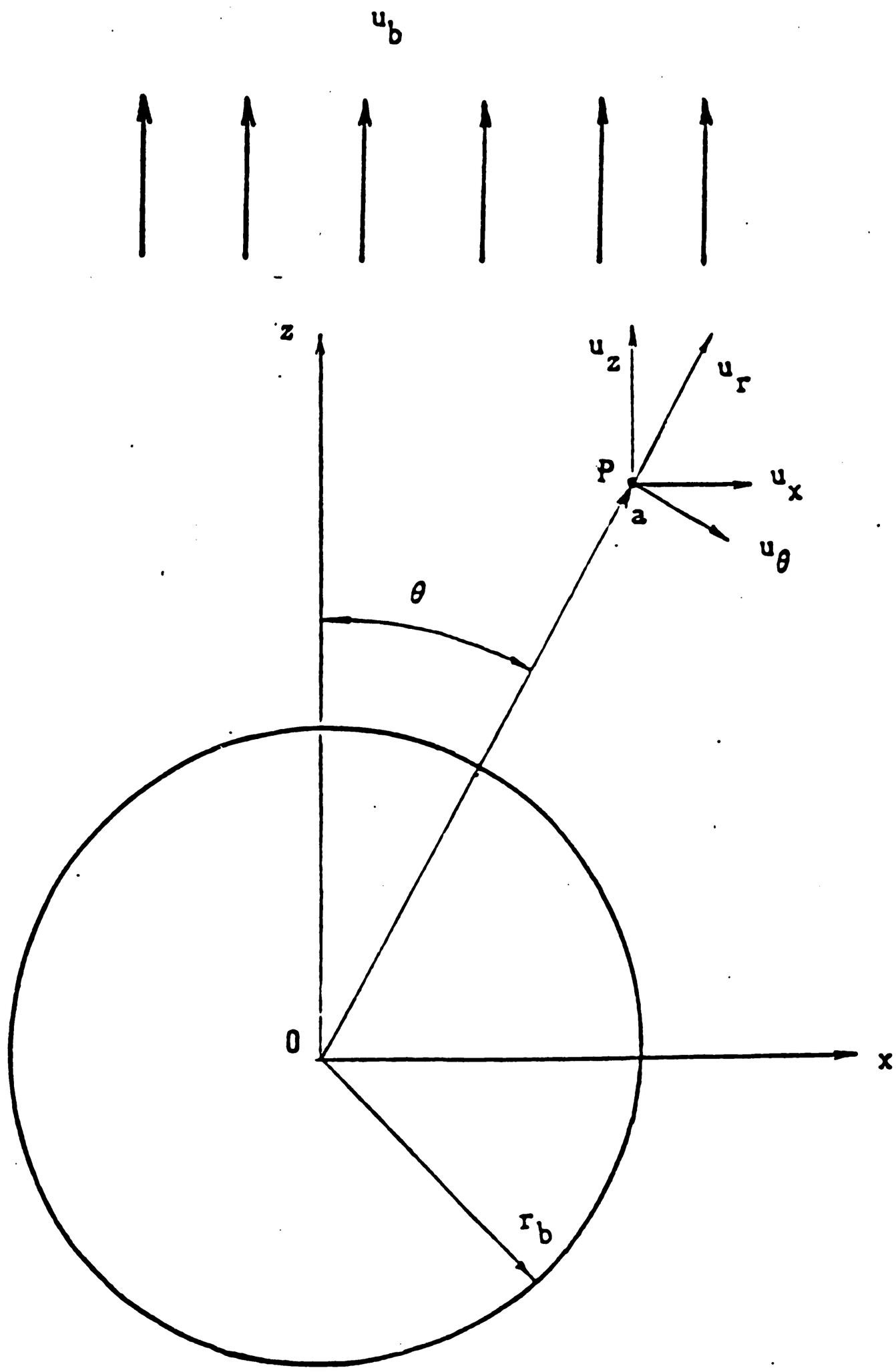

Figure 1. The axes, coordinates and velocities in Davidson model

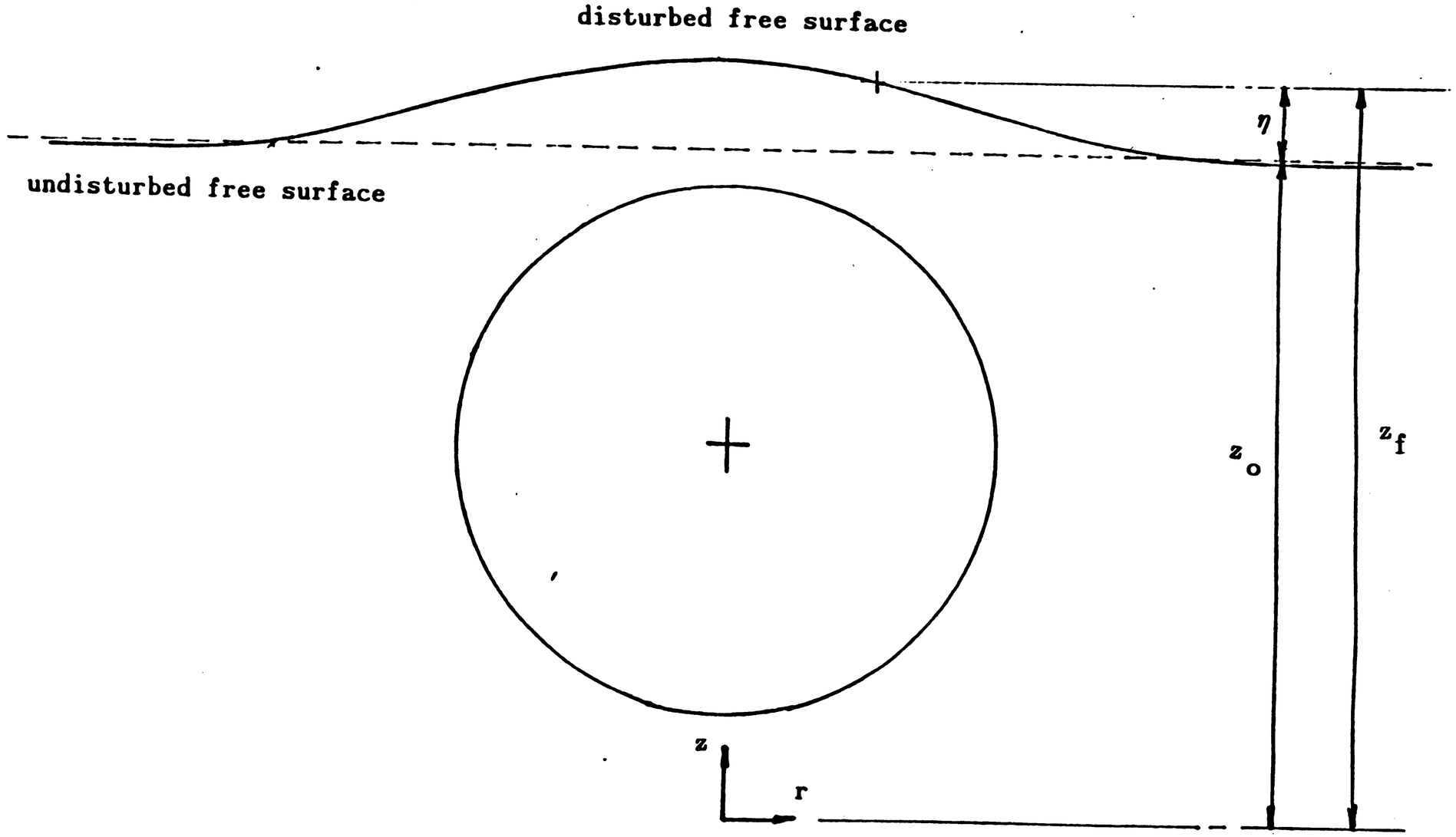

Figure 2. The kinetic condition at the free surface for an erupting bubble

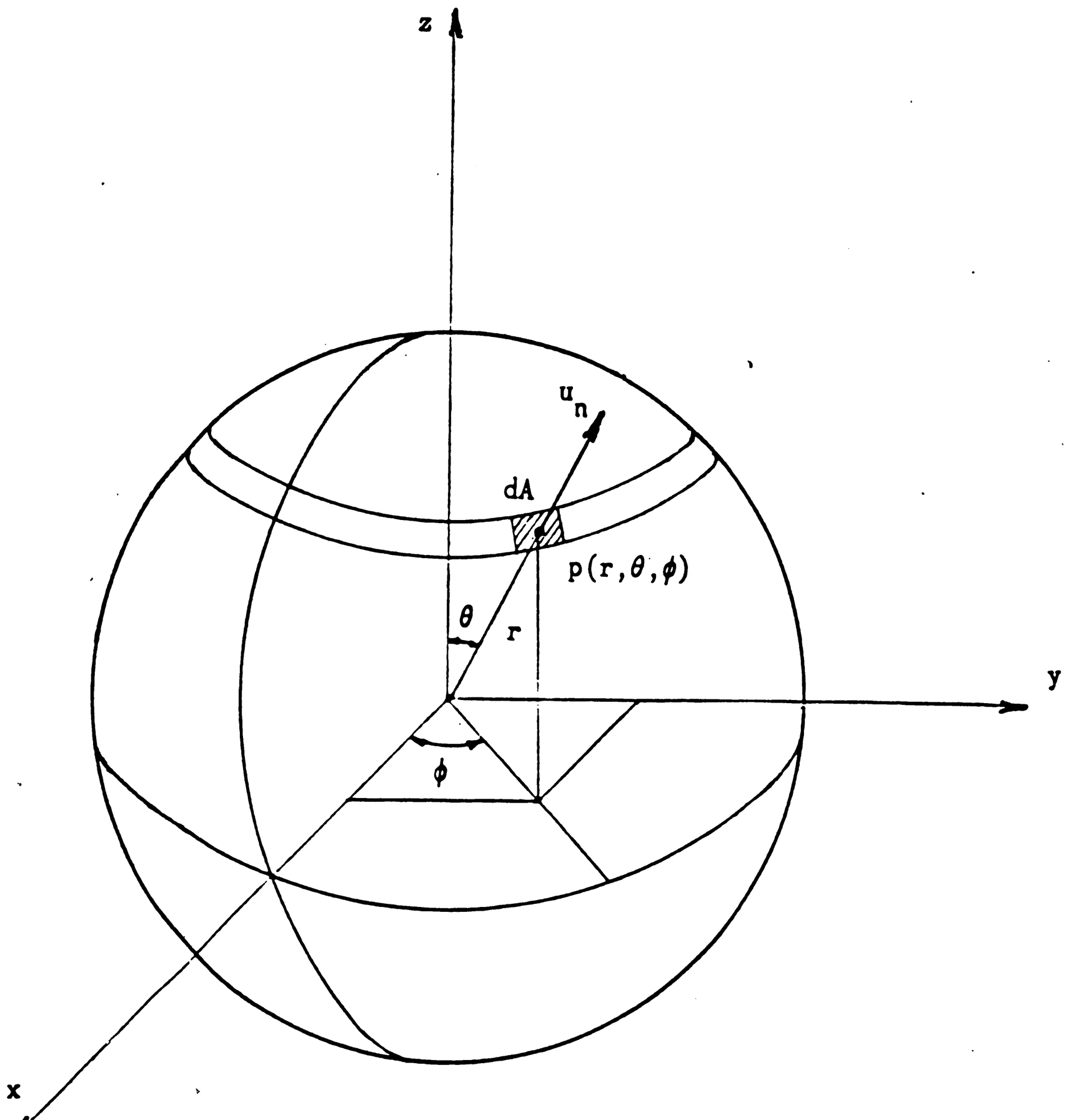

Figure 3. The gas velocity normal to the differential area in the spherical coordinate system

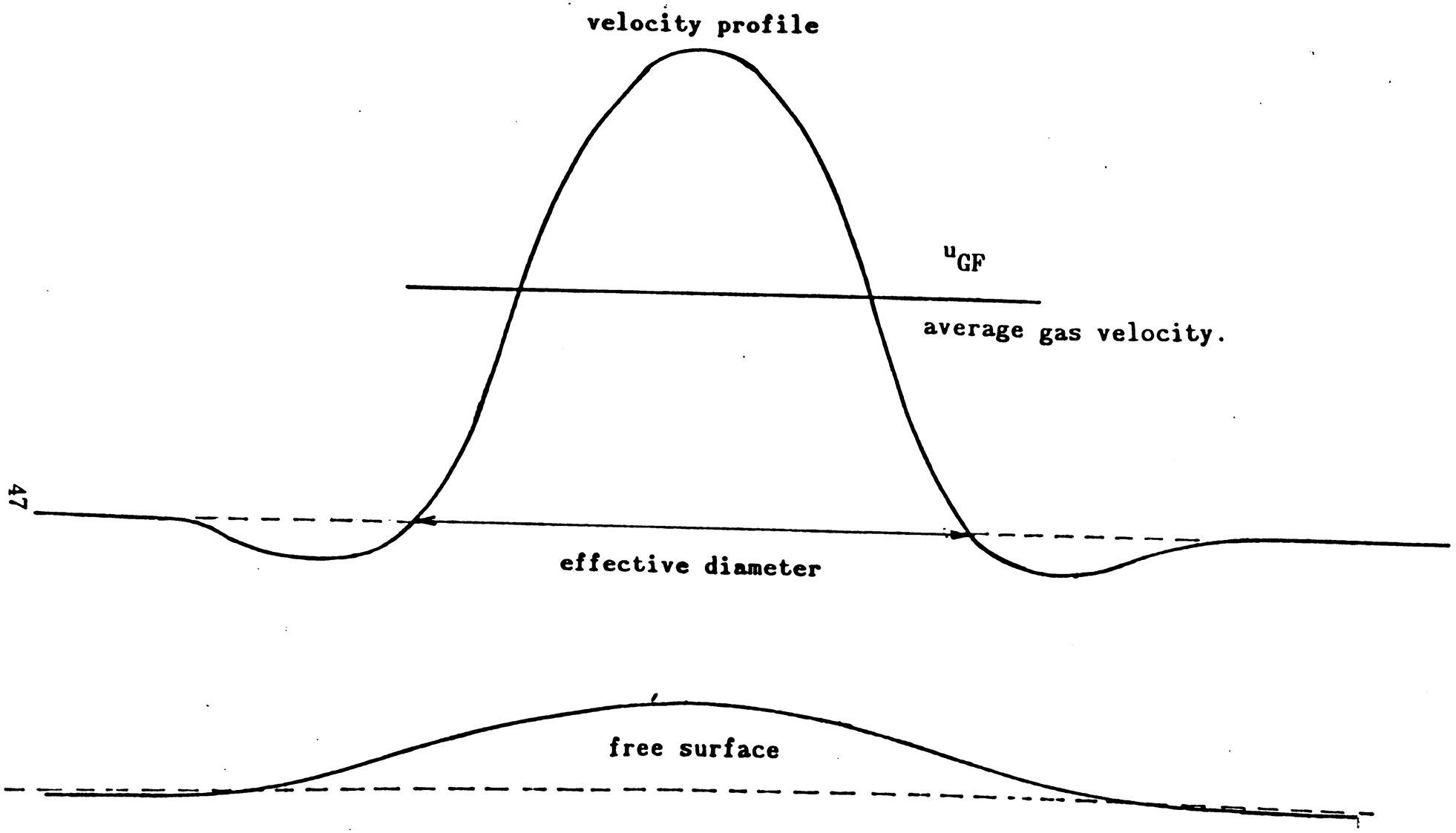

Figure 4. Sketch of velocity profile at the free surface illustrating definition of effective diameter

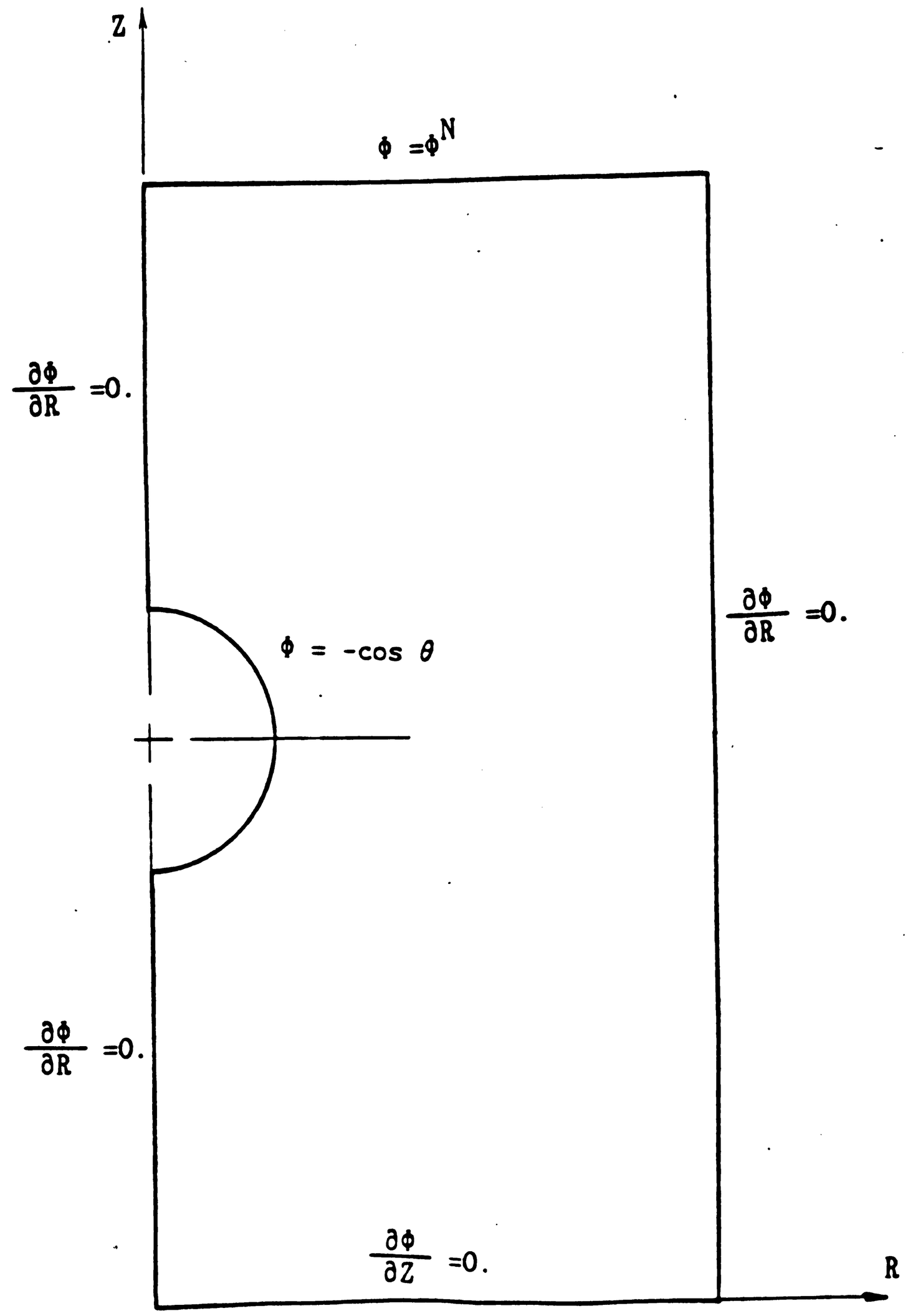

Figure 5. The axes, domain and boundary conditions for the particle velocity potential

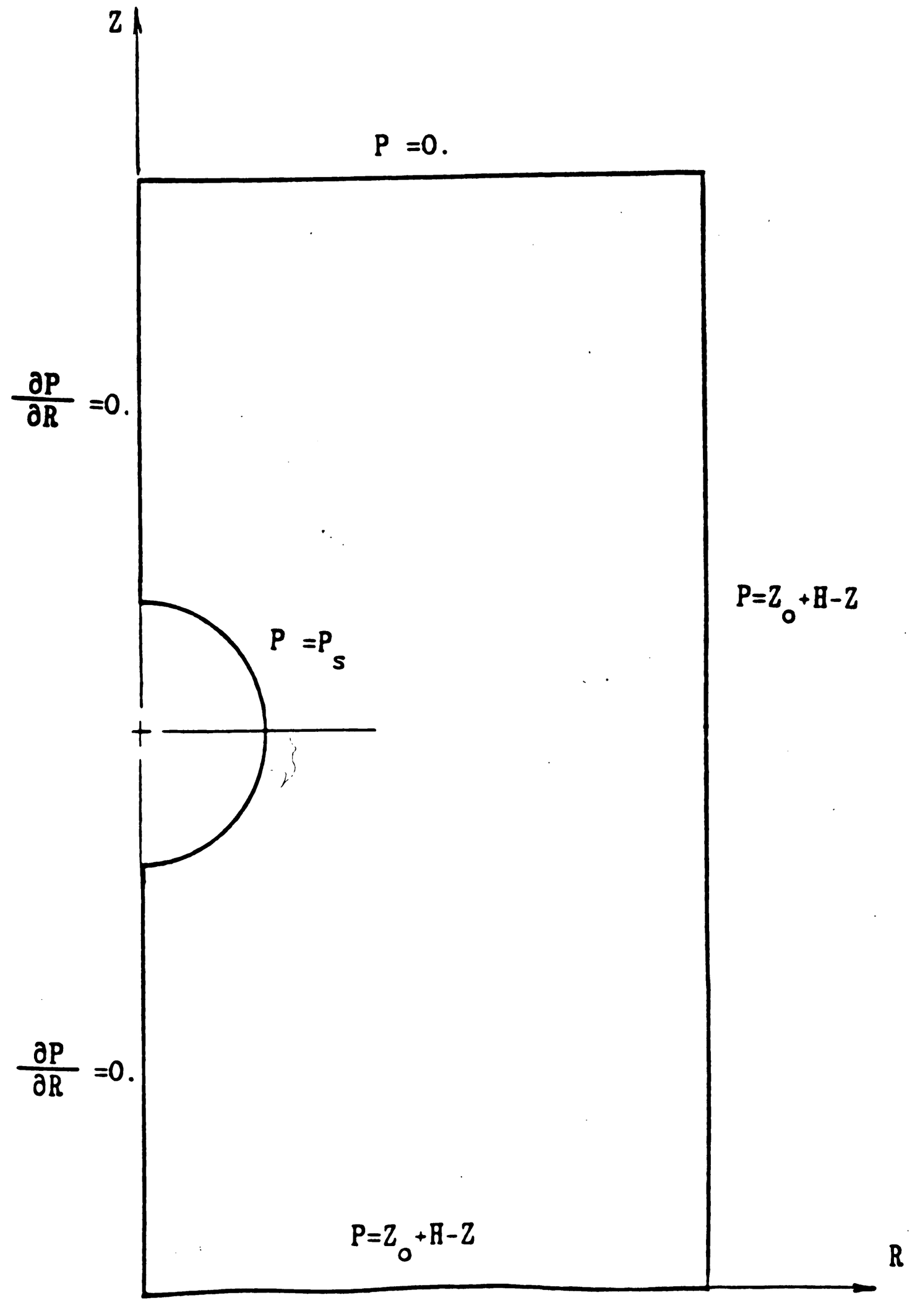

Figure 6. The axes, domain and boundary conditions for the pressure distribution

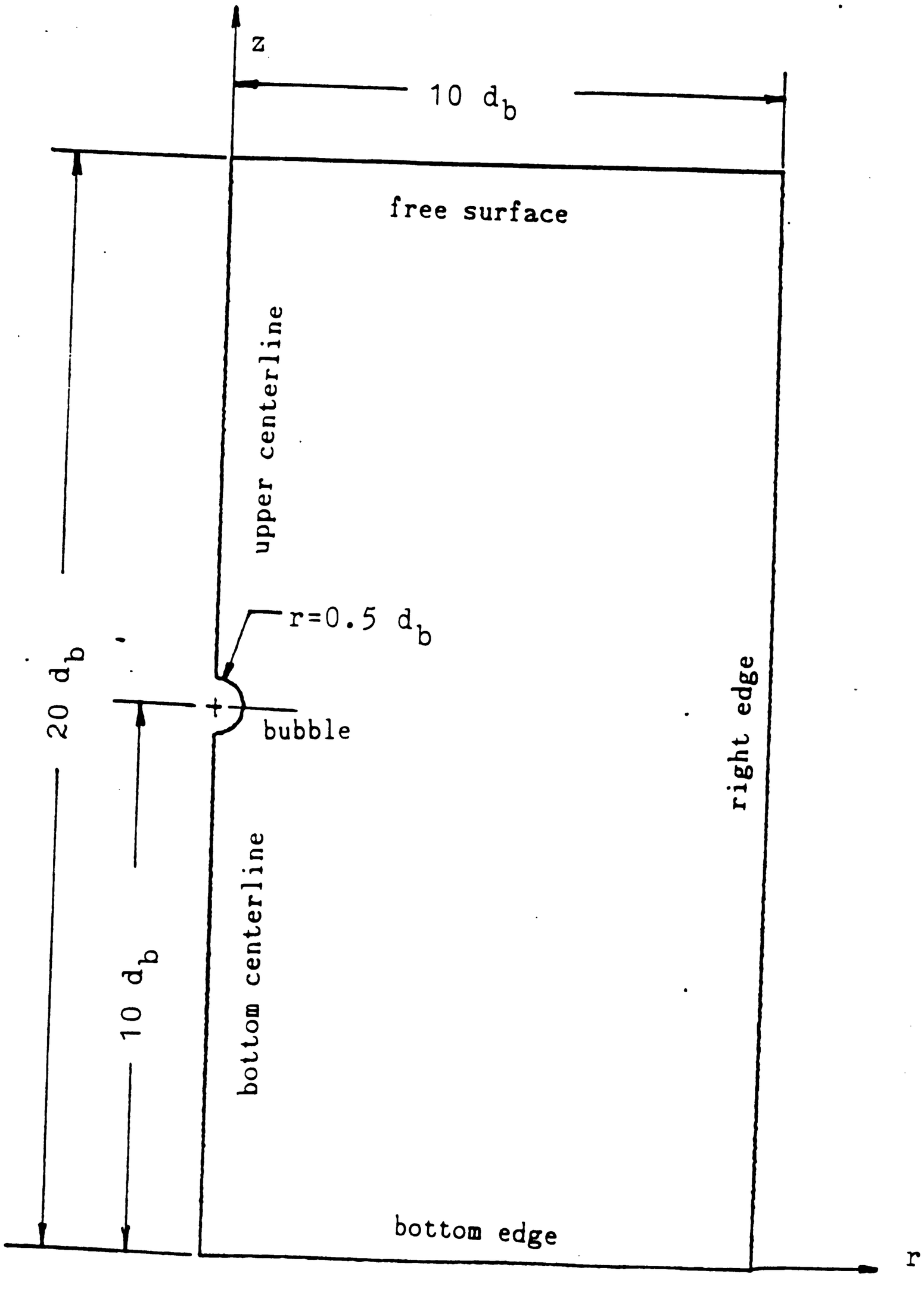

Figure 7. The axes, dimension and boundaries of the axisymmetric portion of the bed

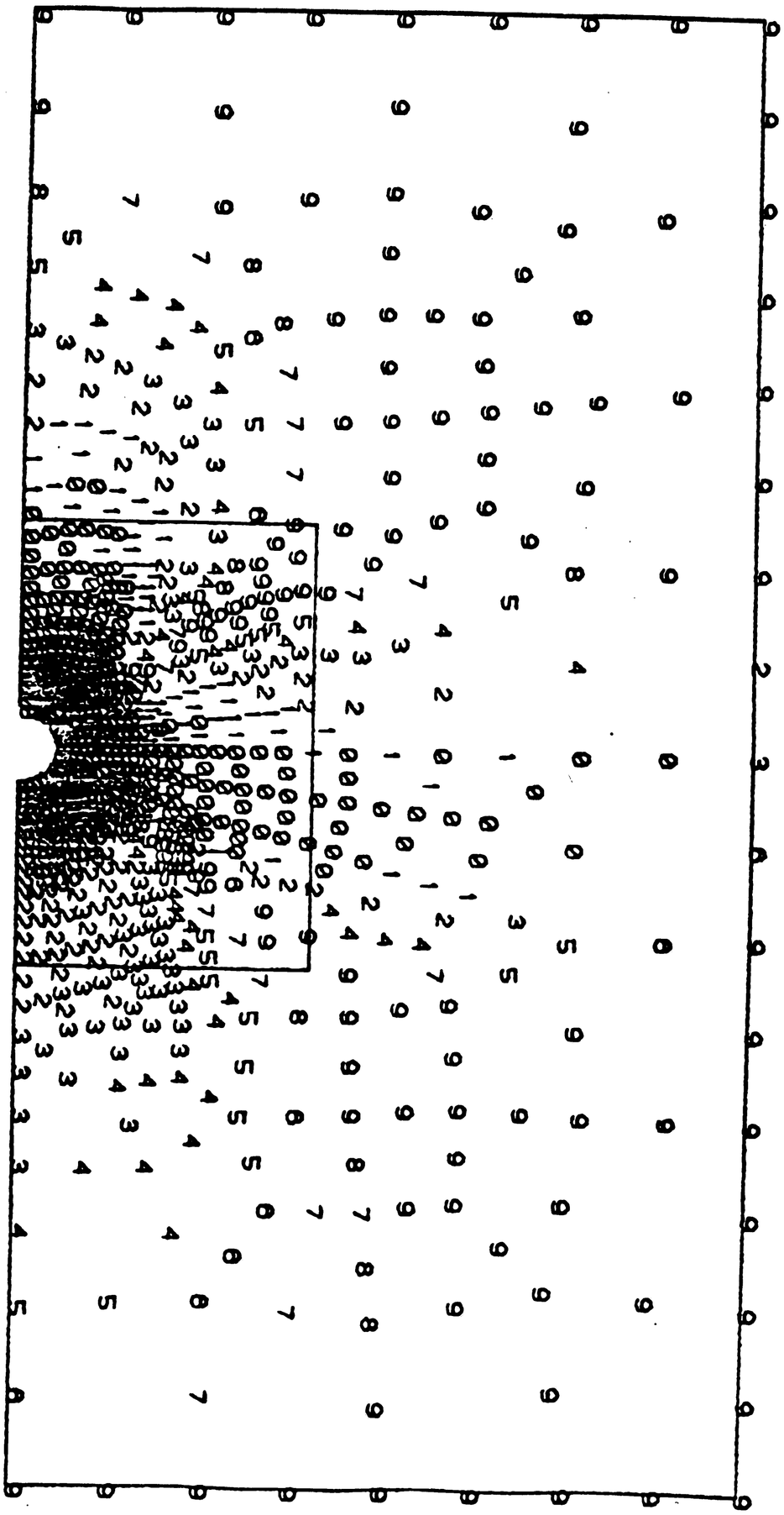

Figure 8. Comparison of the vertical component of particle velocity with Davidson solution for bubble deep in the bed

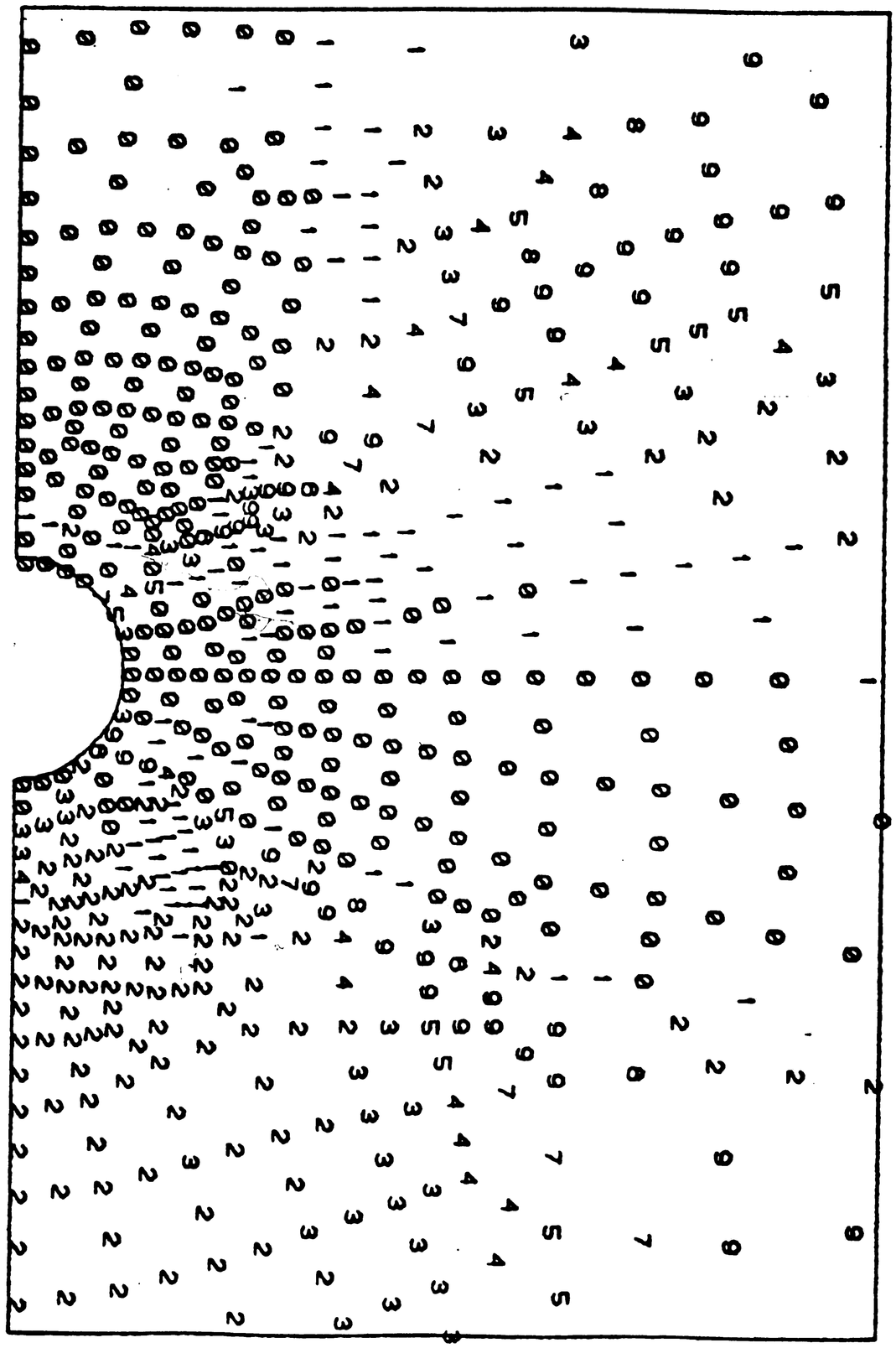

Figure 9. Comparison of the vertical component
of particle velocity with Davidson solution
for bubble deep in the bed
highlighting the area near to the bubble

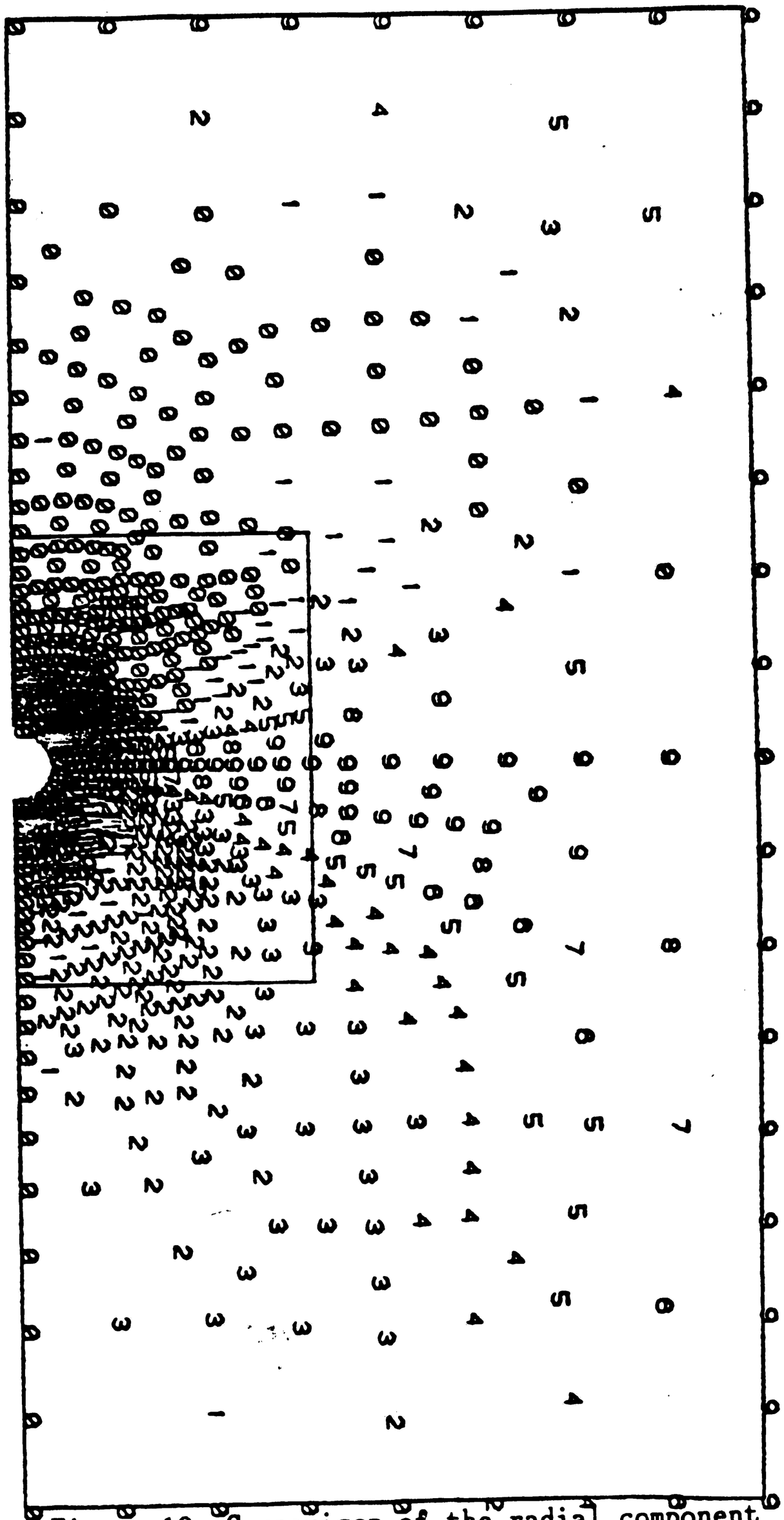

Figure 10. Comparison of the radial component of particle velocity with Davidson solution for bubble deep in the bed

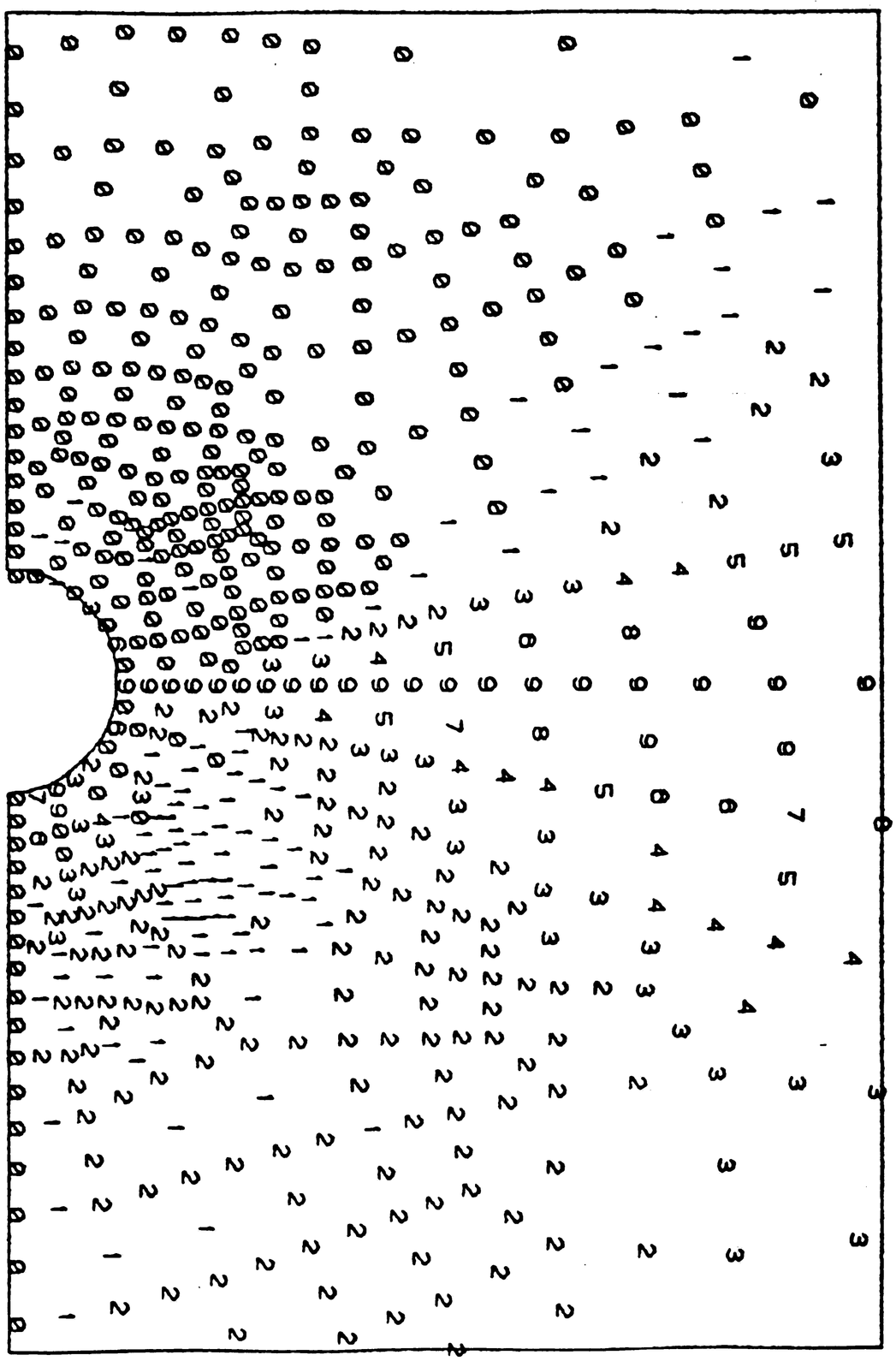

Figure 11. Comparison of the radial component of particle velocity with Davidson solution for bubble deep in the bed highlighting the area near to the bubble

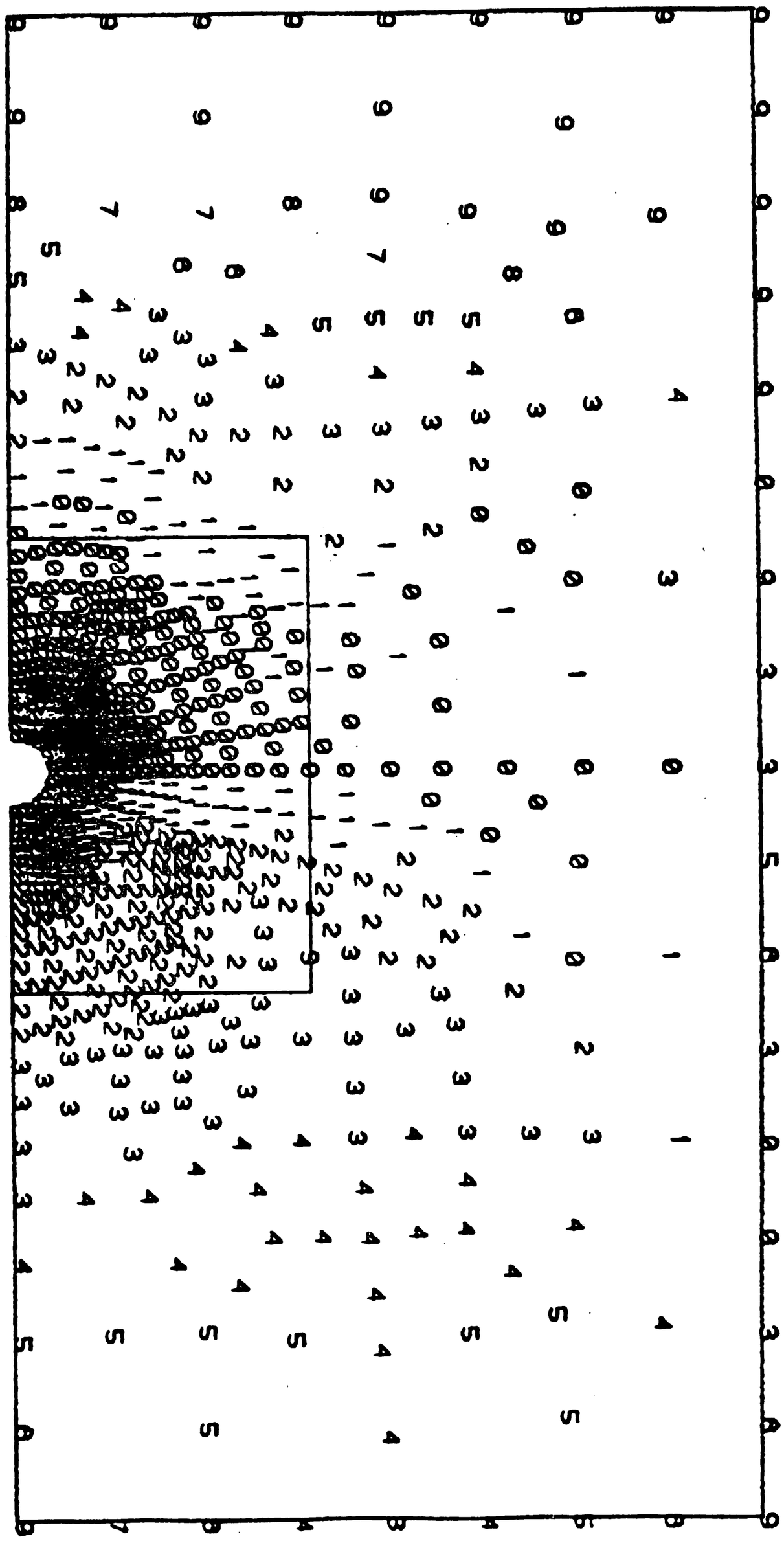

Figure 12. Comparison of the magnitude of particle velocity with Davidson solution for bubble deep in the bed

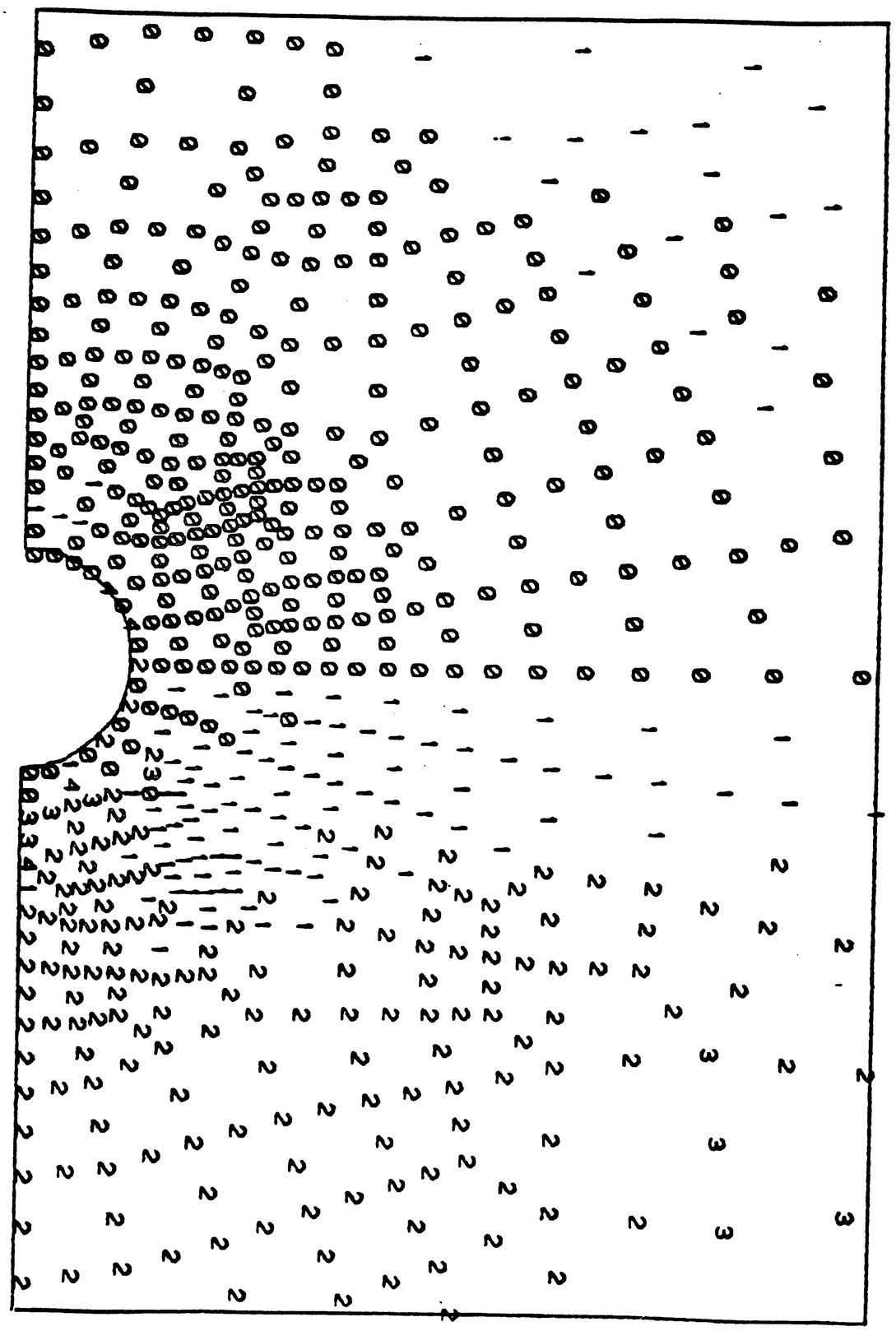

Figure 13. Comparison of the magnitude of particle velocity with Davidson solution for bubble deep in the bed highlighting the area near to the bubble

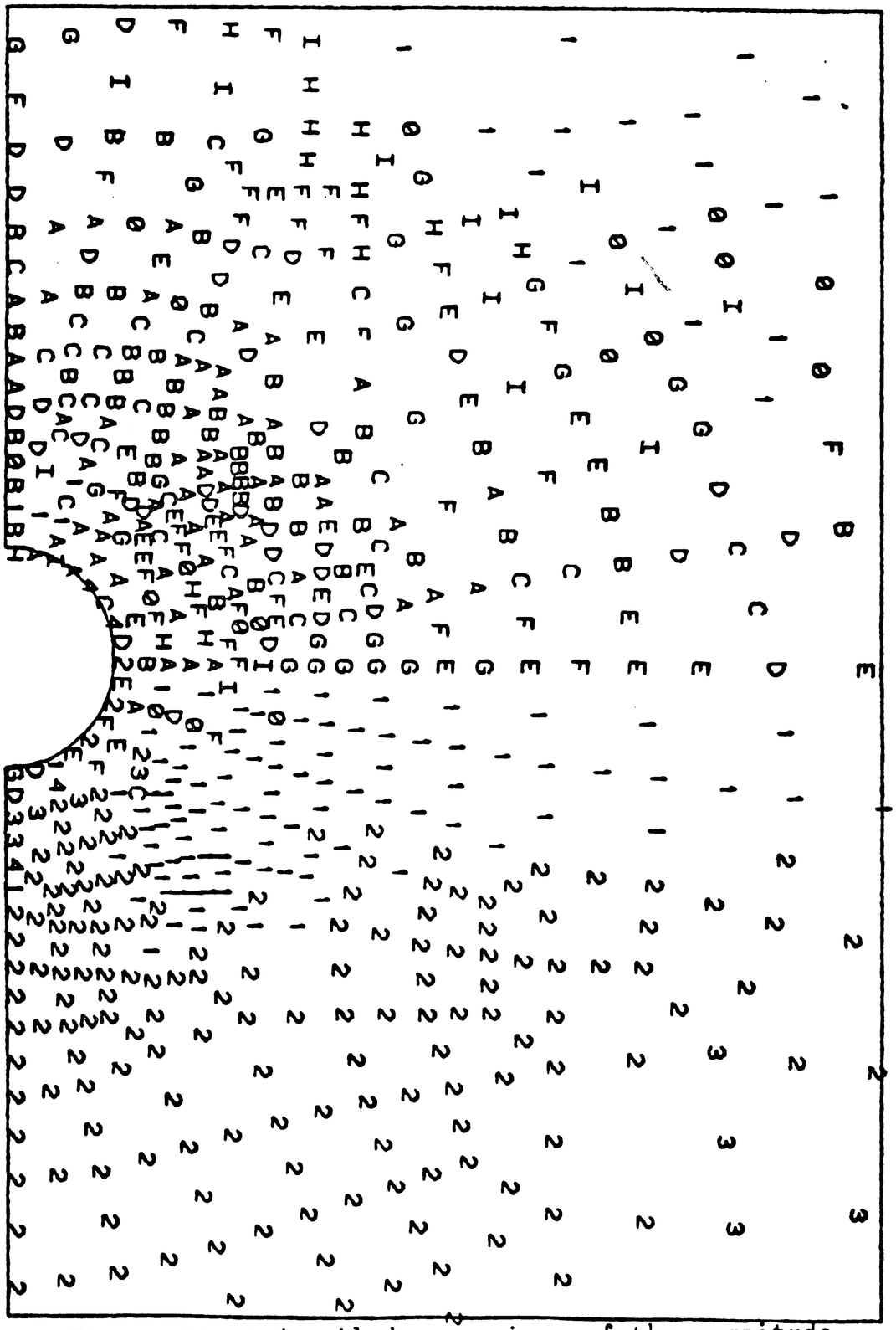

Figure 14. A detailed comparison of the magnitude of particle velocity with Davidson solution for bubble deep in the bed and highlighting the area near to the bubble

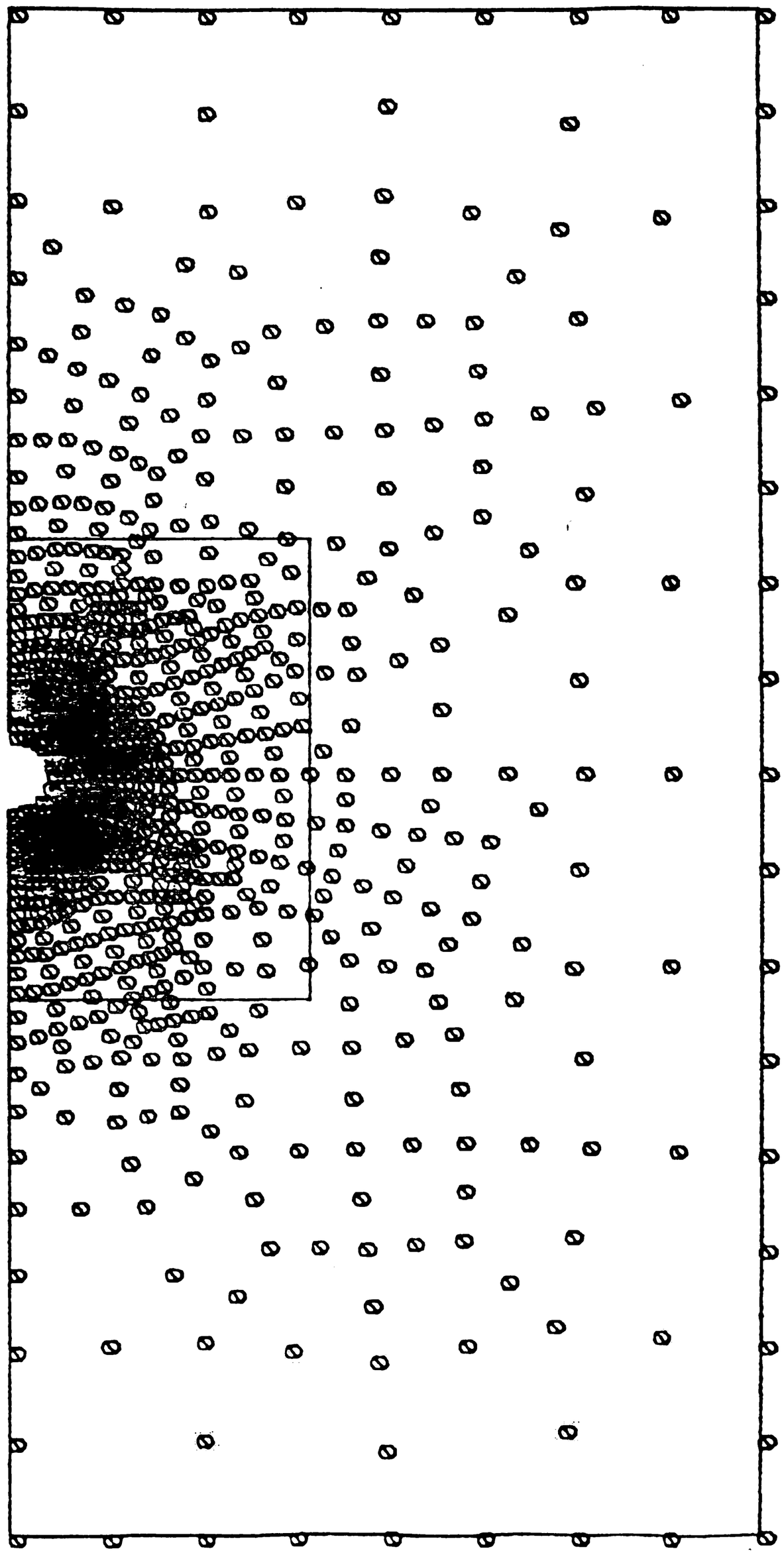

Figure 15. Comparison of the vertical component of gas velocity with Davidson solution for bubble deep in the bed and K = 0.5

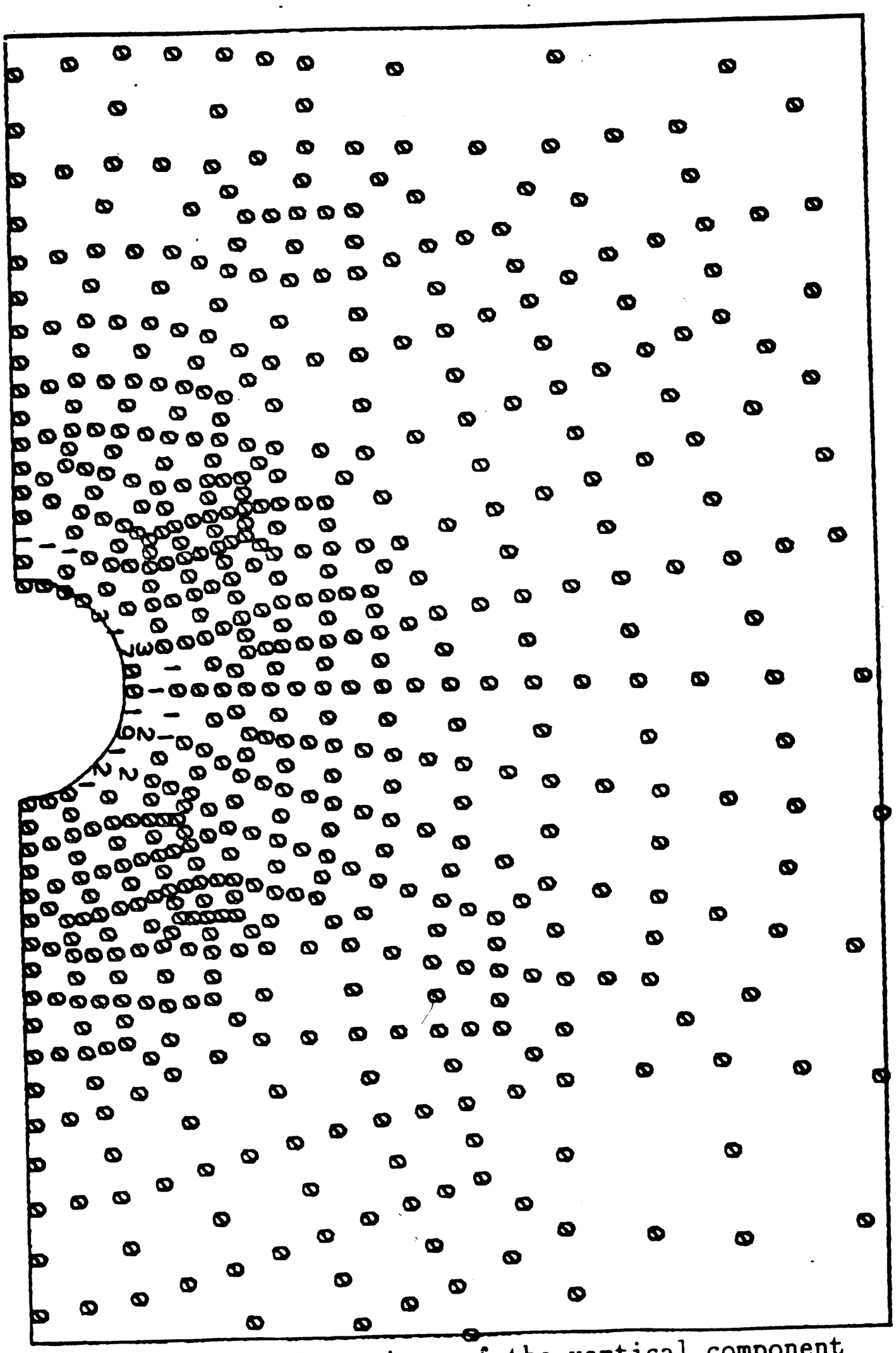

Figure 16. Comparison of the vertical component of gas velocity with Davidson solution for bubble deep in the bed and K = 0.5 highlighting the area near to the bubble

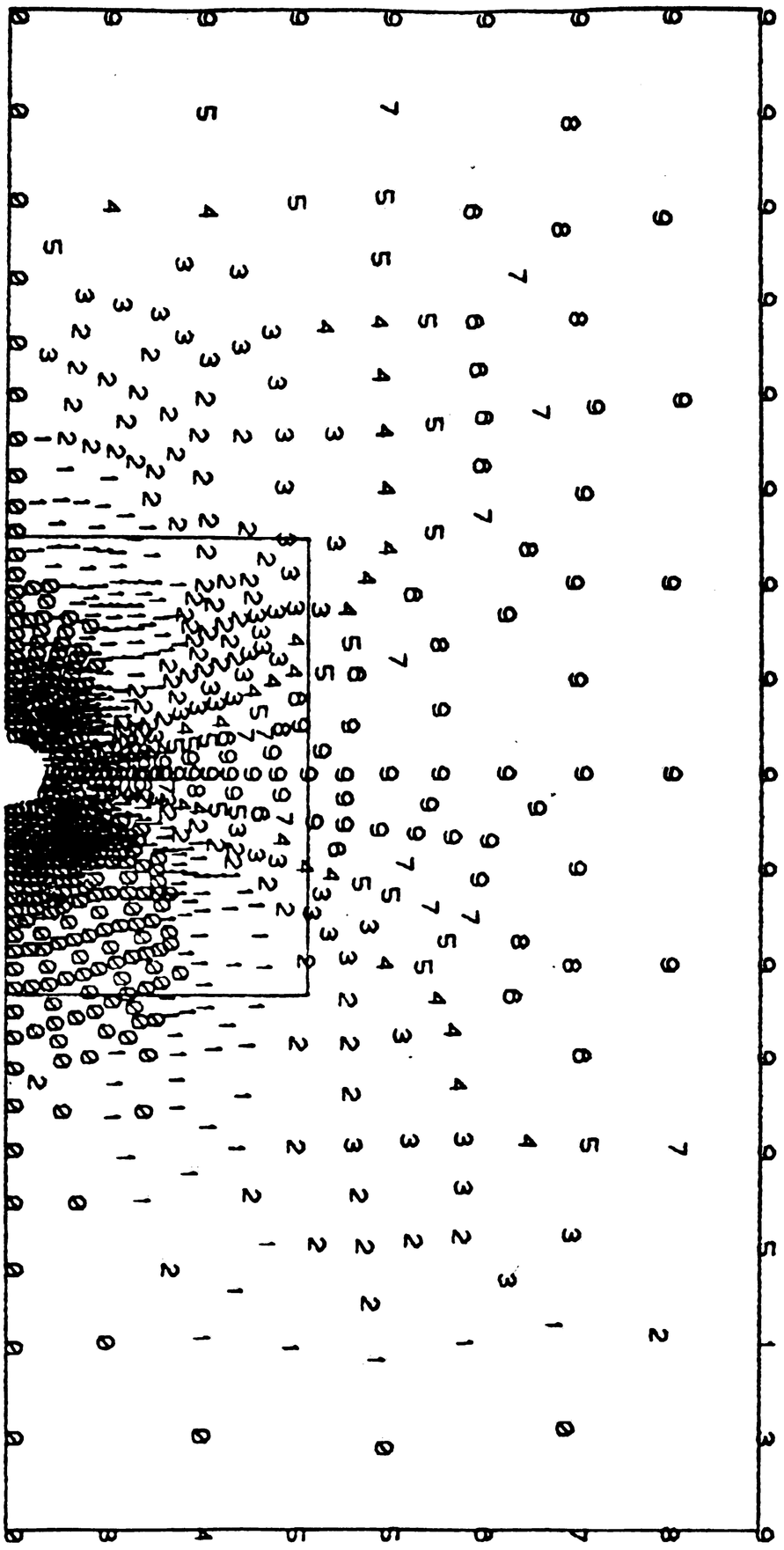

Figure 17. Comparison of the radial component of gas velocity with Davidson solution for bubble deep in the bed and K = 0.5

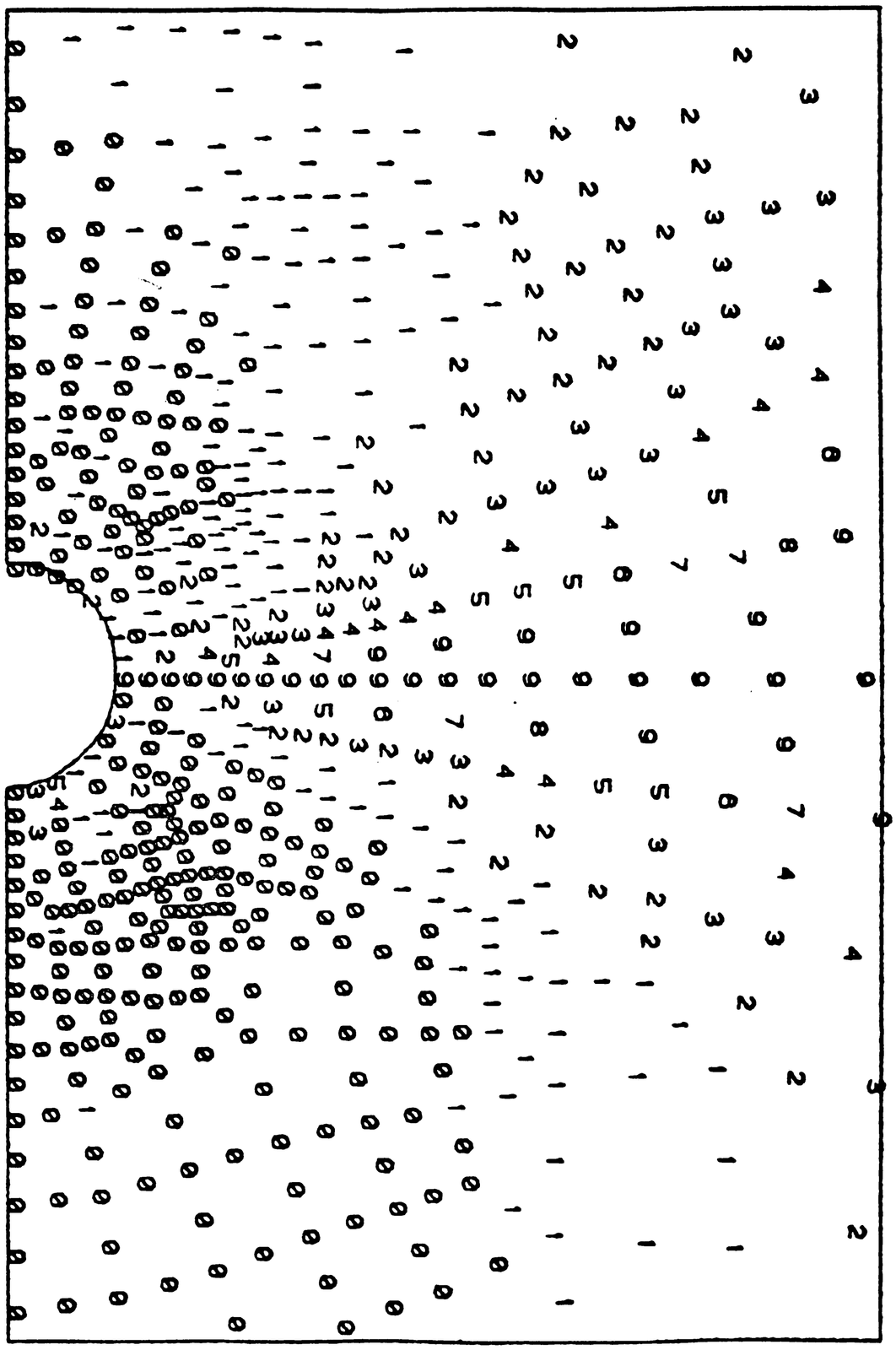

Figure 18. Comparison of the radial component of gas velocity with Davidson solution for bubble deep in the bed and K = 0.5 highlighting the area near to the bubble

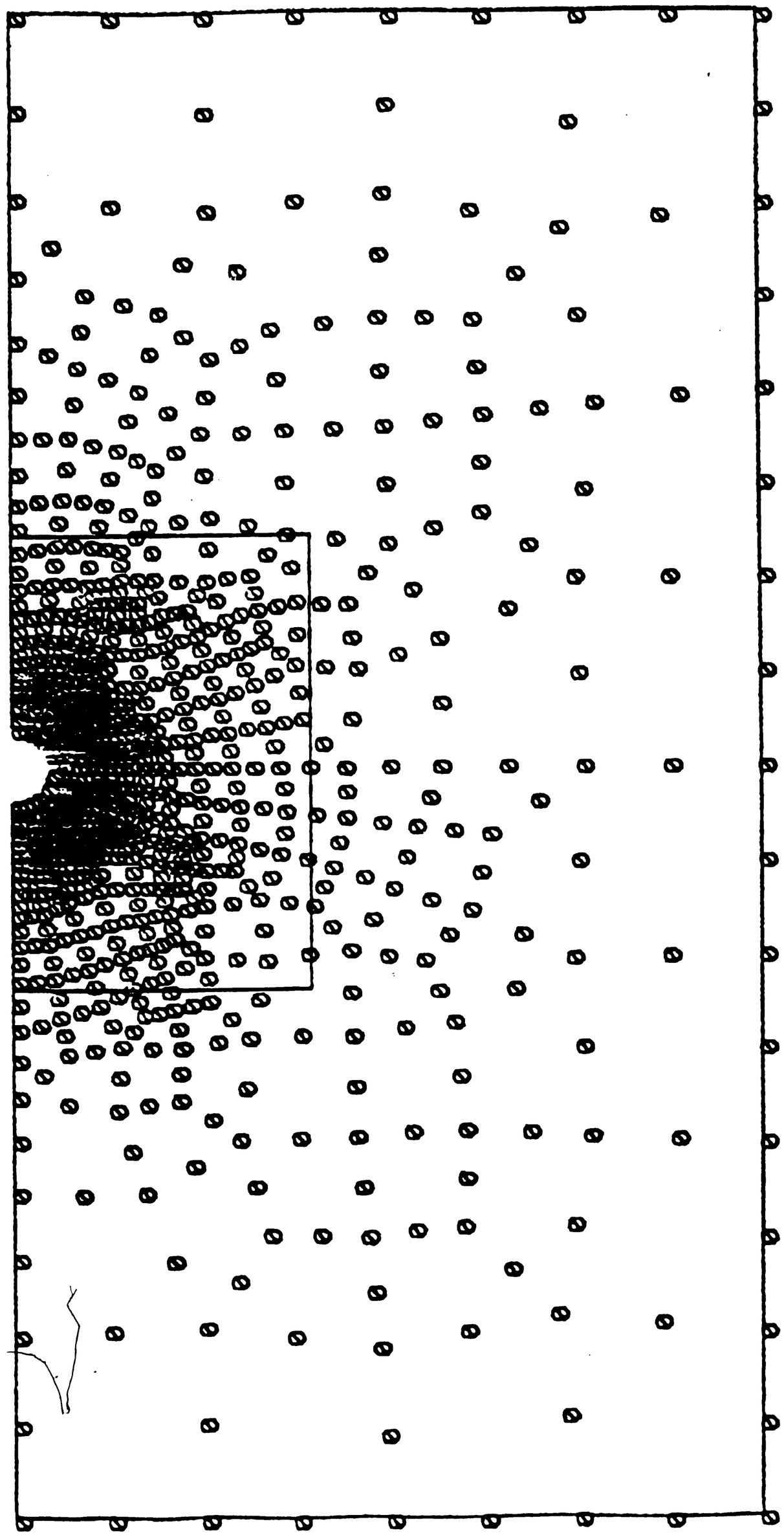

Figure 19. Comparison of the magnitude of gas velocity with Davidson solution for bubble deep in the bed and K=0.5

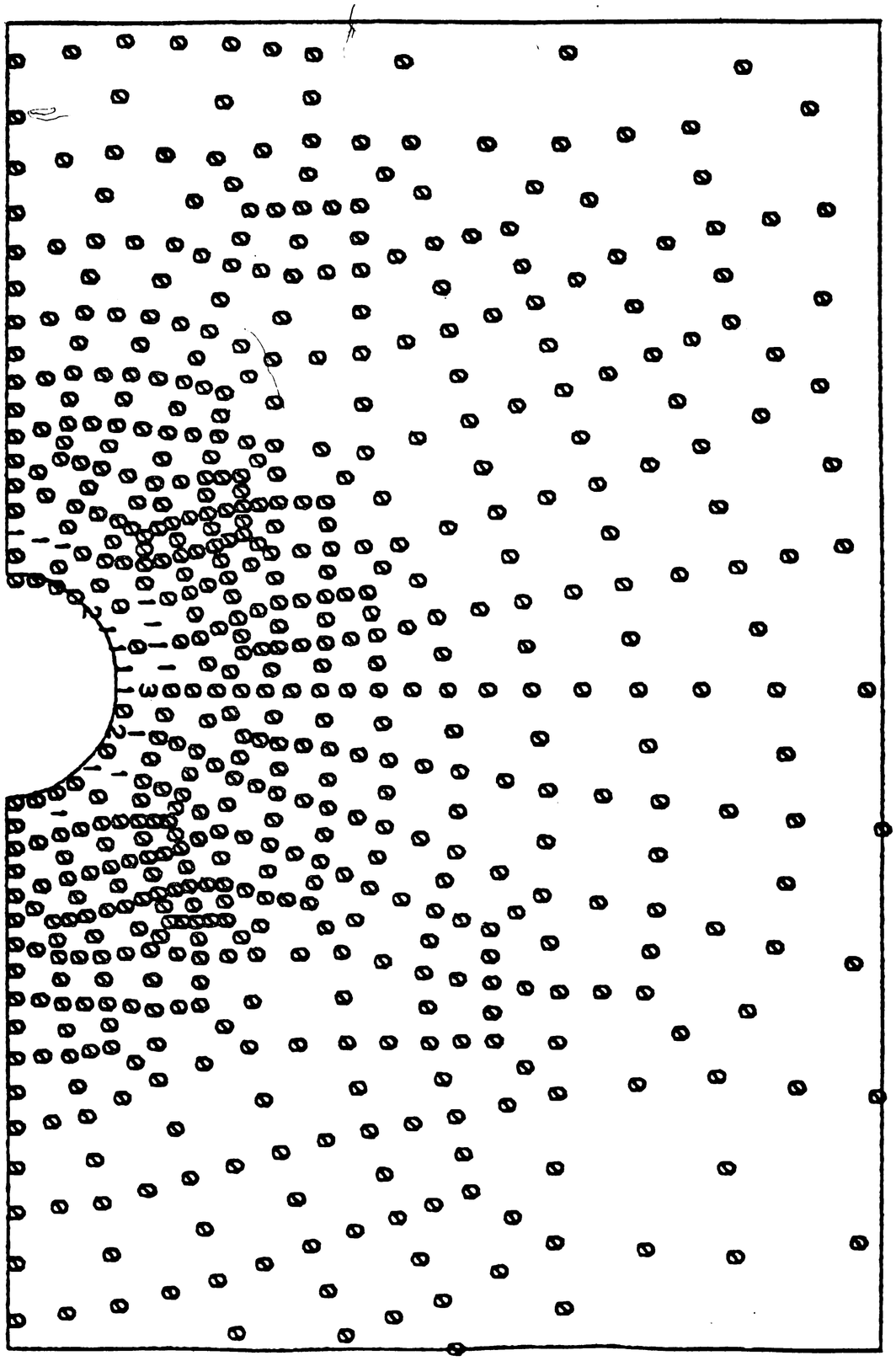

Figure 20. Comparison of the magnitude of gas velocity wiht Davidson solution for bubble deep in the bed and K=0.5 highlighting the area near to the bubble

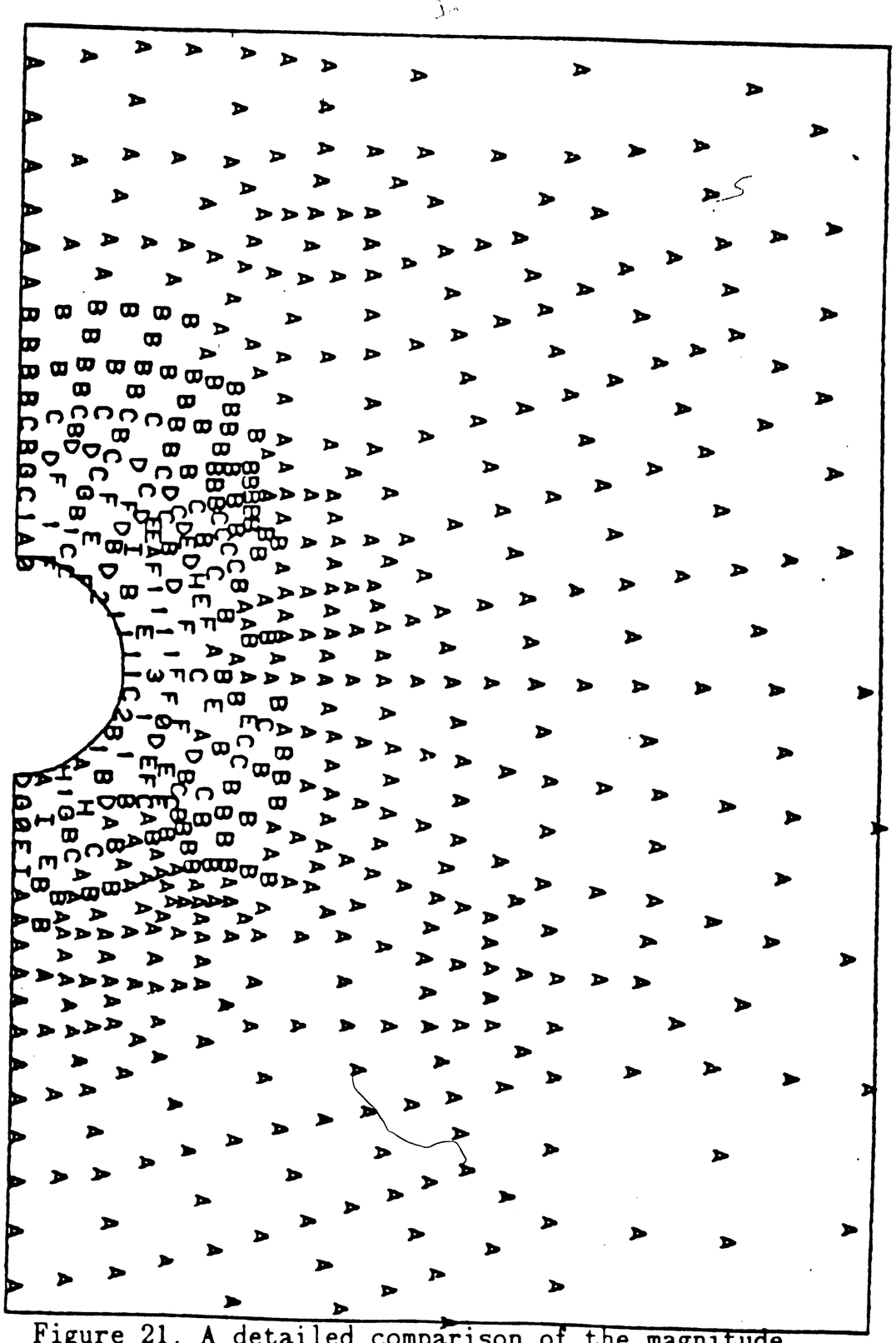

Figure 21. A detailed comparison of the magnitude of gas velocity with Davidson solution for bubble deep in the bed and K= 0.5 highlighting the area near to the bubble

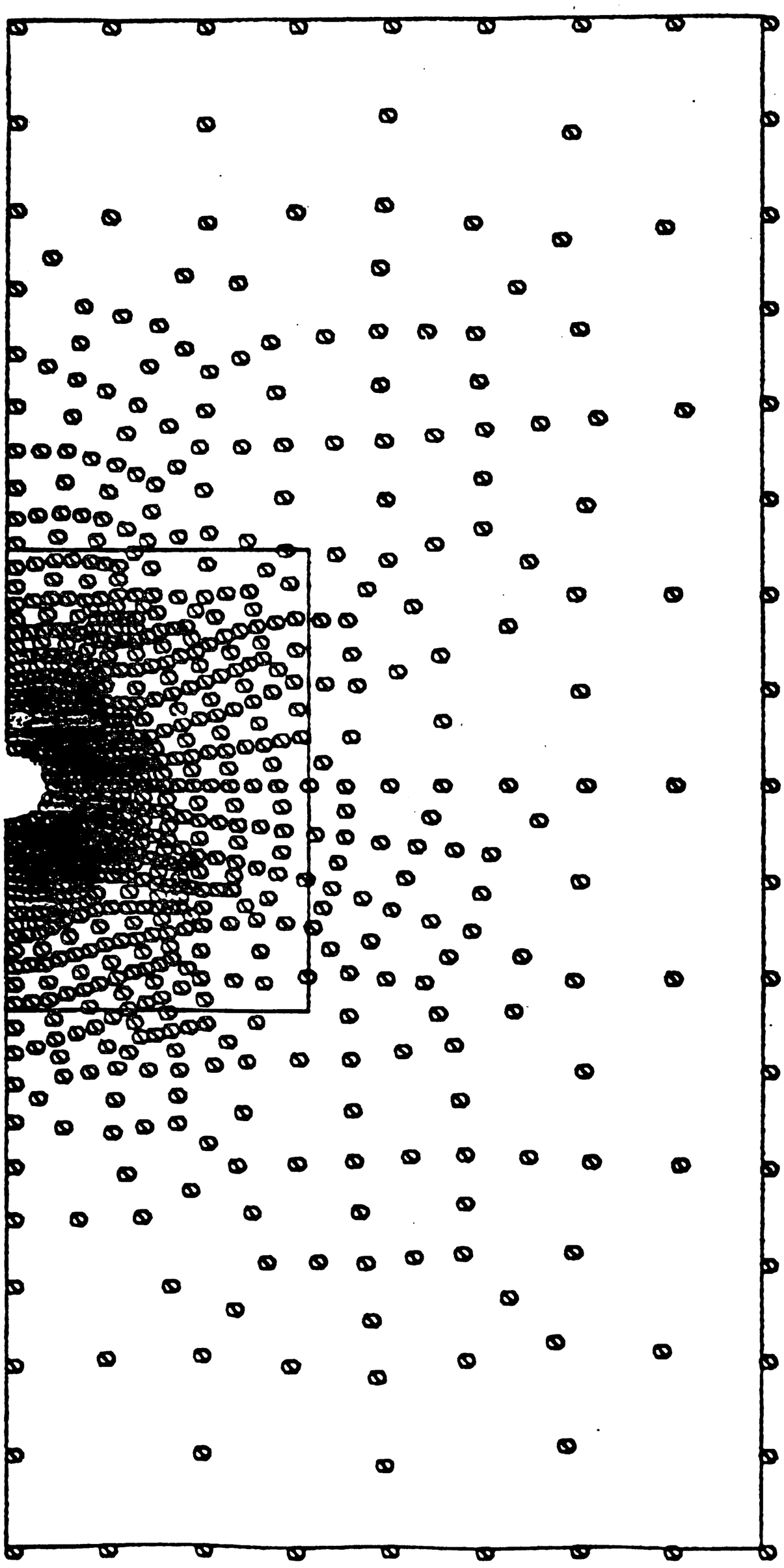

Figure 22. Comparison of the vertical component of gas velocity with Davidson solution for bubble deep in the bed and K = 1.1

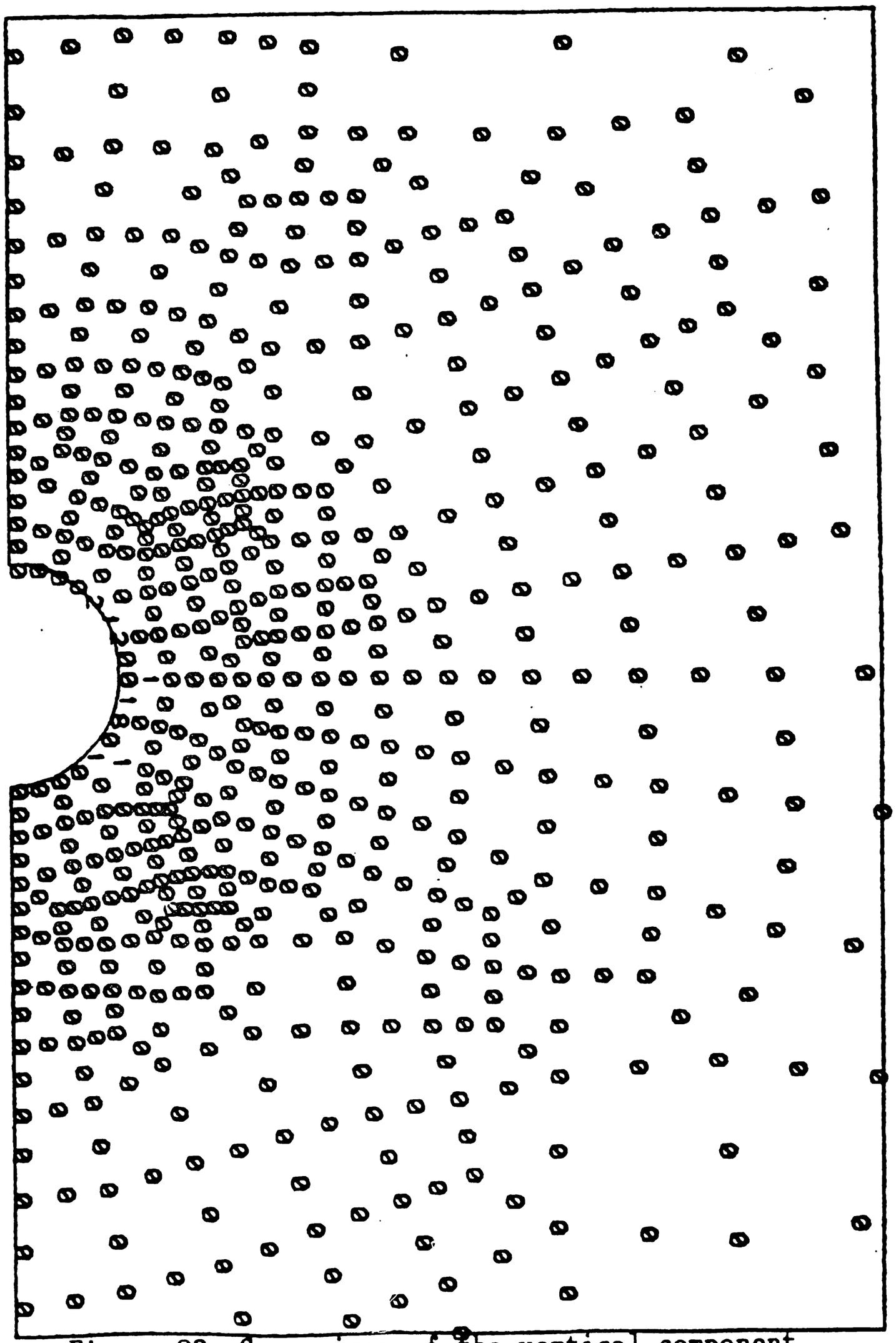

Figure 23. Comparison of the vertical component of gas velocity with Davidson solution for bubble deep in the bed and K = 1.1 highlighting the area near to the bubble

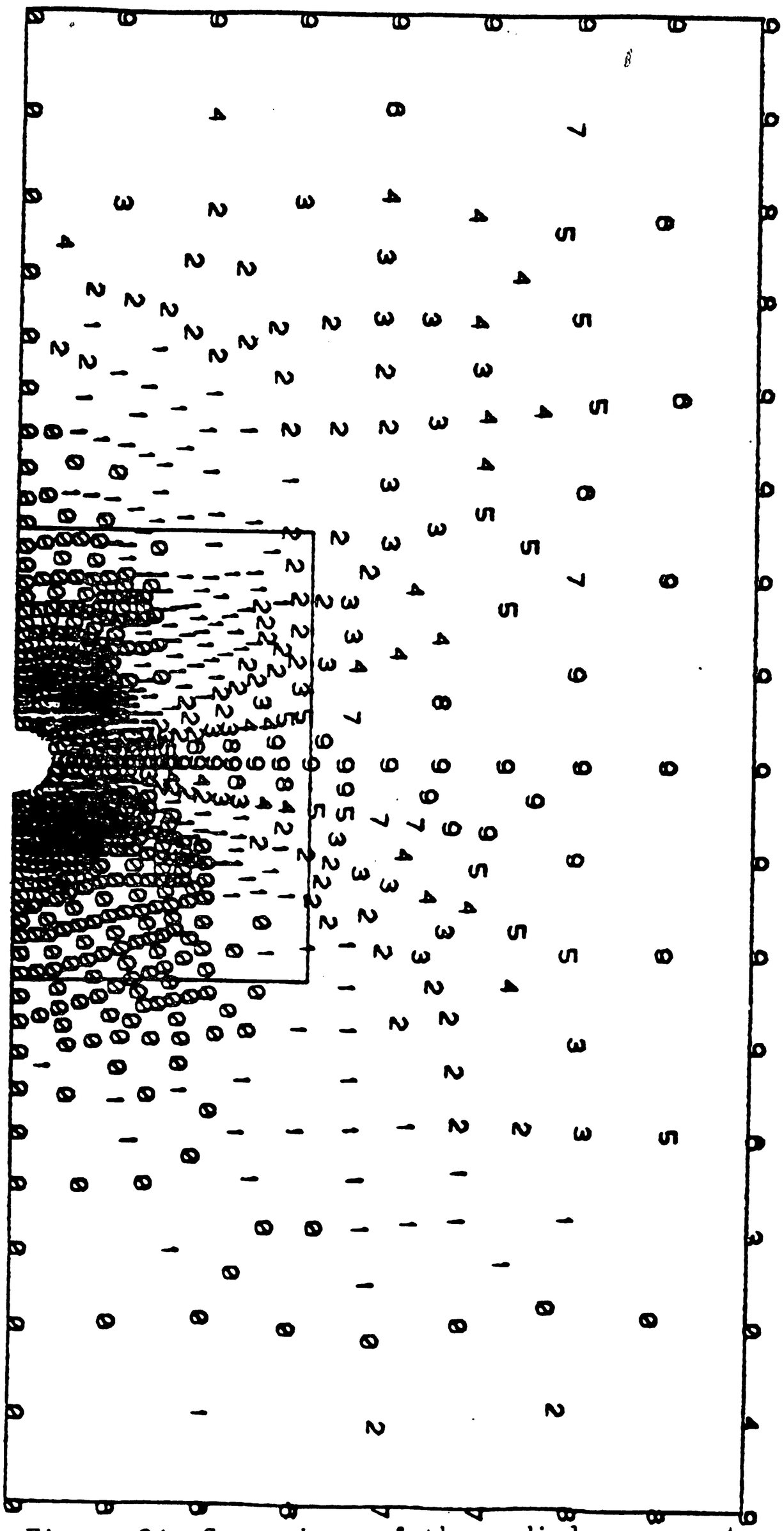

Figure 24. Comparison of the radial component of gas velocity with Davidson solution for bubble deep in the bed and K = 1.1

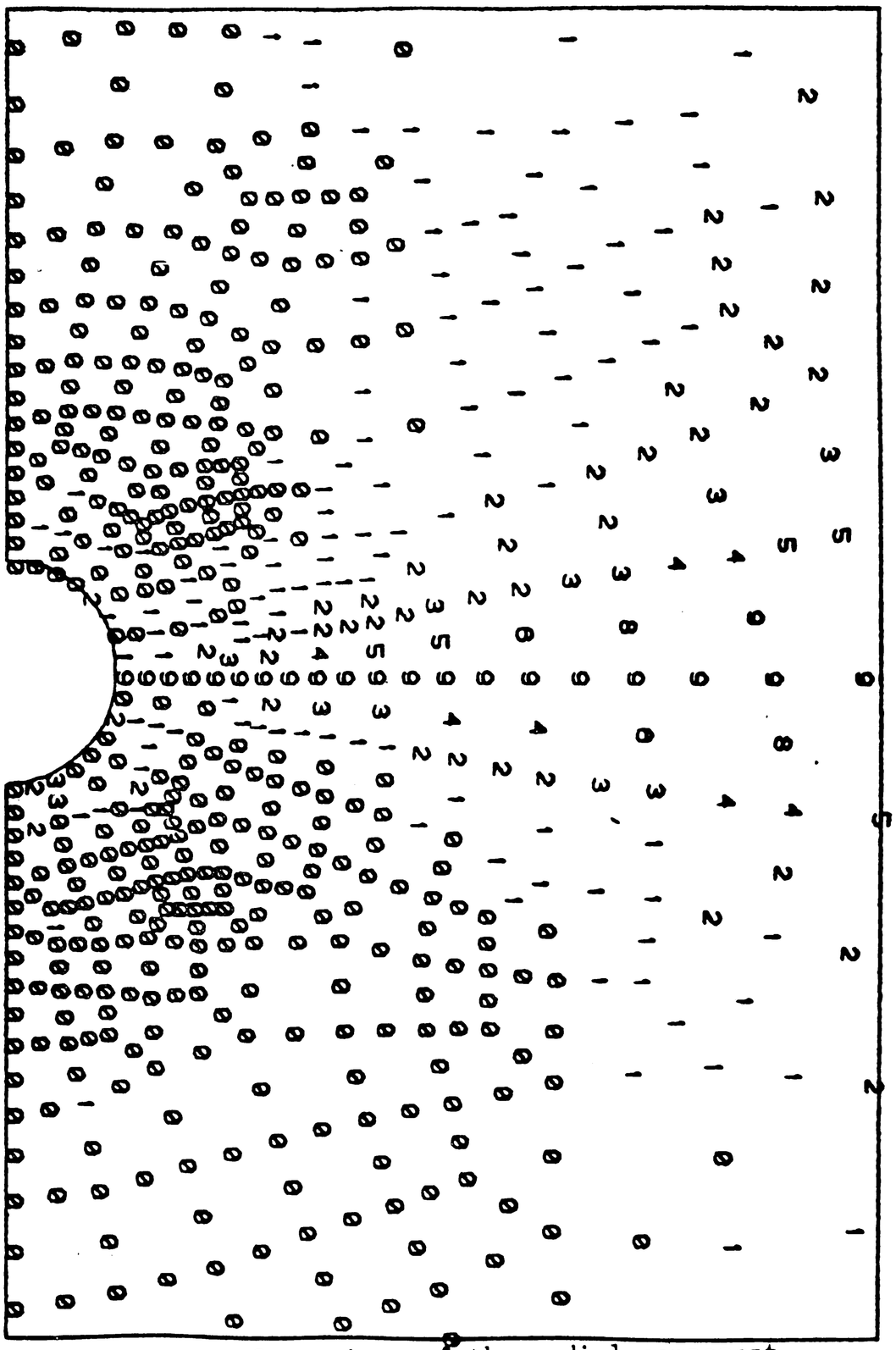

Figure 25. Comparison of the radial component of gas velocity with Davidson solution for bubble deep in the bed and K = 1.1 highlighting the area near to the bubble

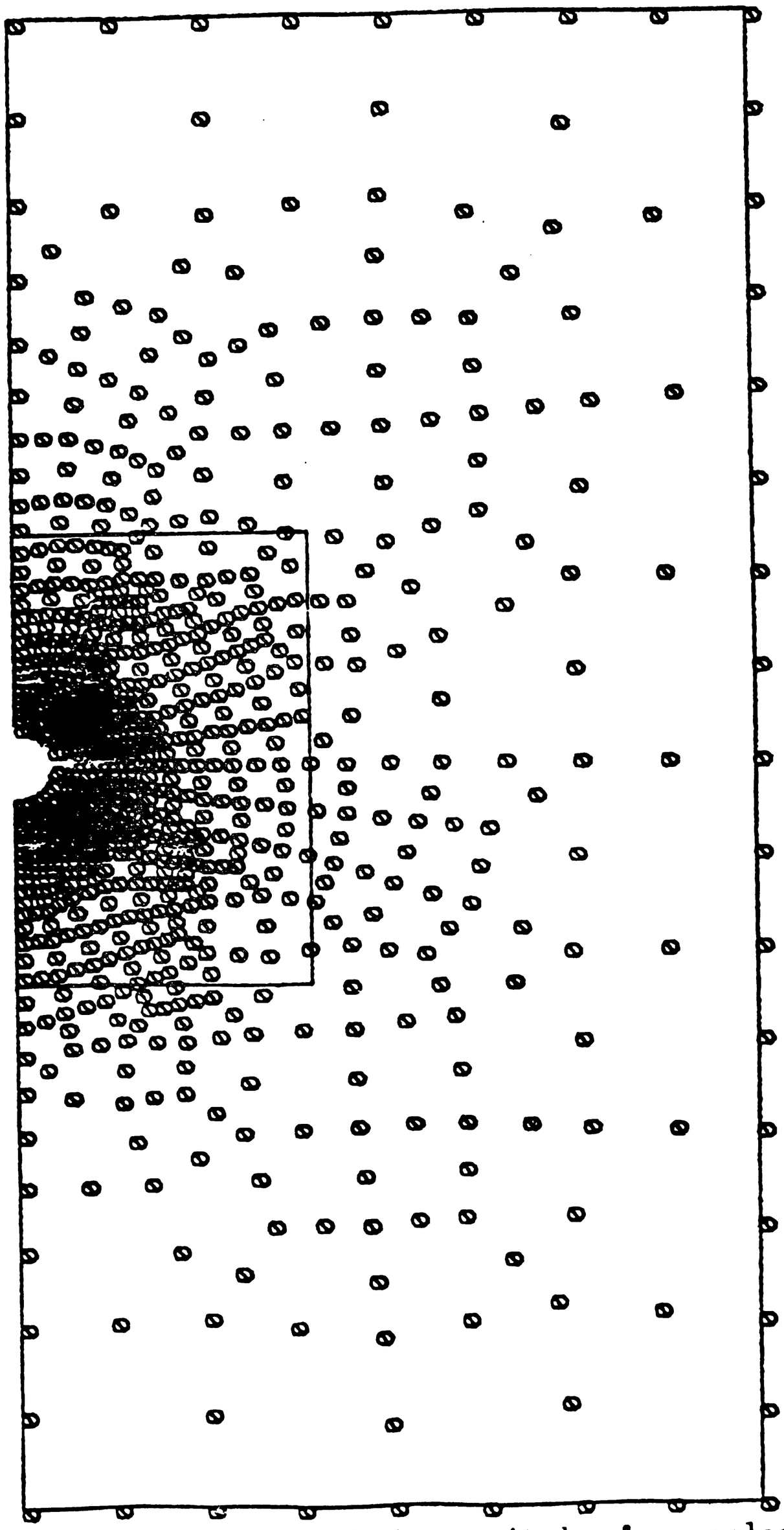

Figure 26. Comparison of the magnitude of gas velocity with Davidson solution for bubble deep in the bed and K=1.1

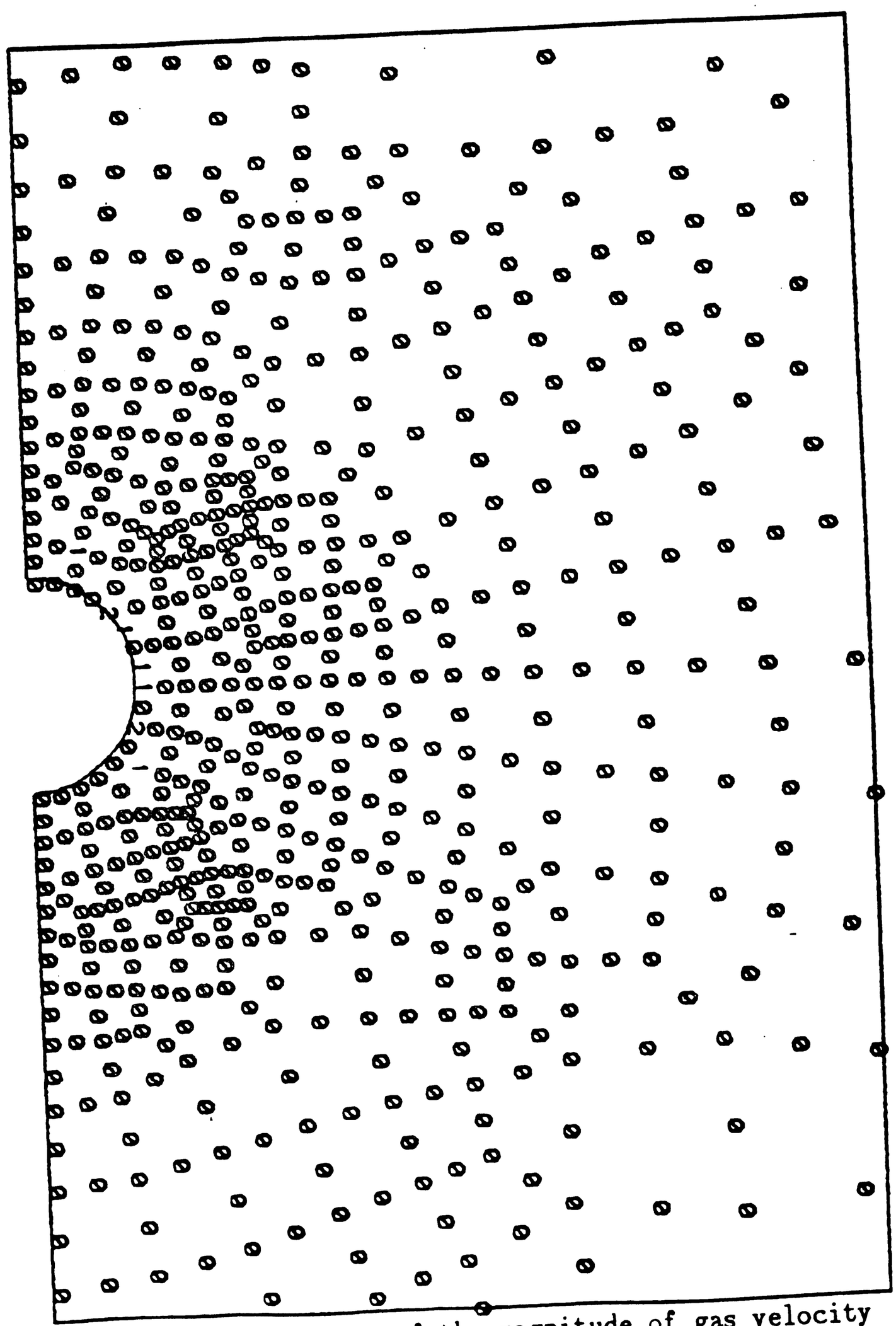

Figure 27. Comparison of the magnitude of gas velocity with Davidson solution for bubble deep in the bed and K=1.1 highlighting the area near to the bubble

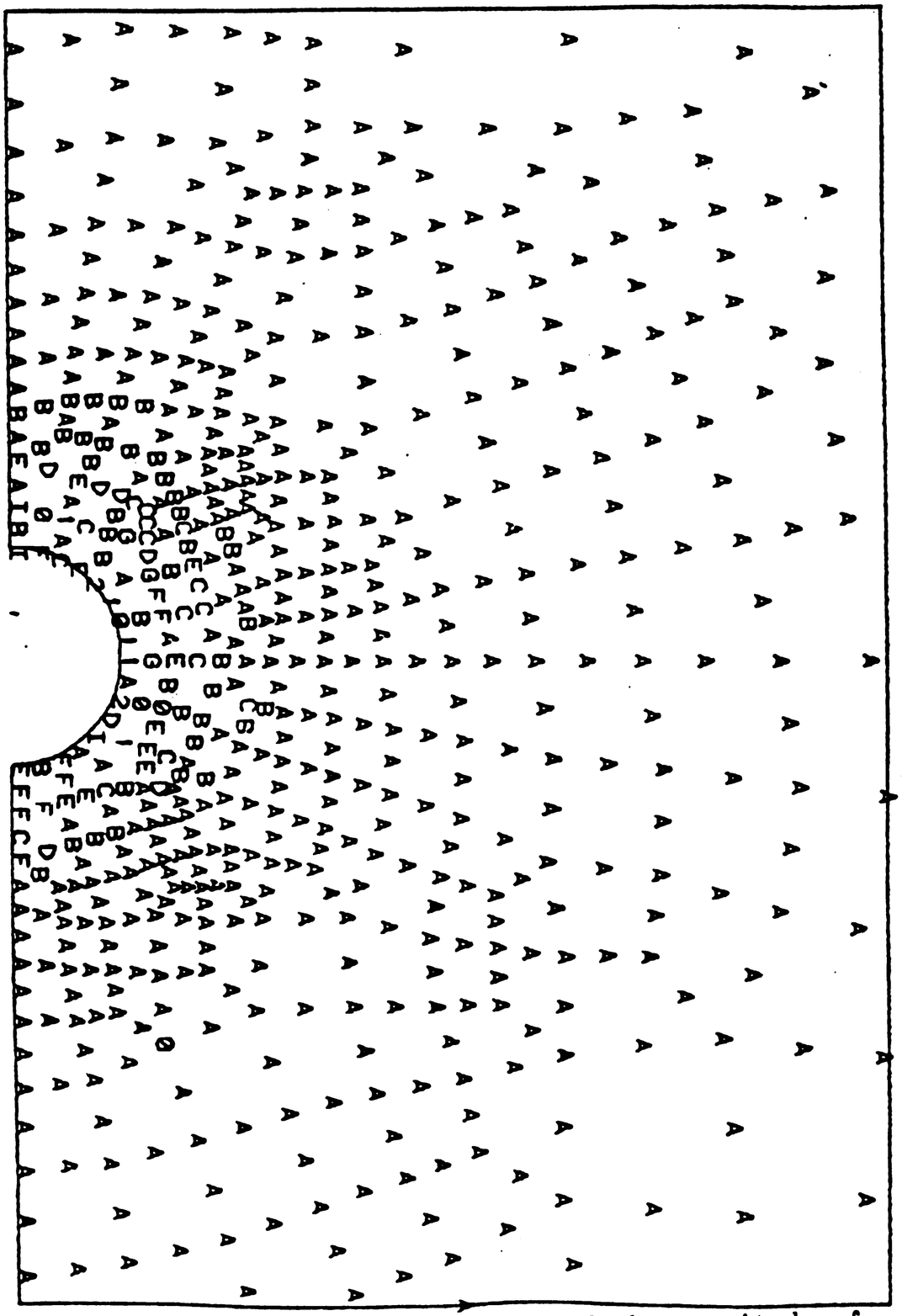

Figure 28. A detailed comparison of the magnitude of gas velocity with Davidson solution for bubble deep in the bed and K= 1.1 highlighting the area near to the bubble

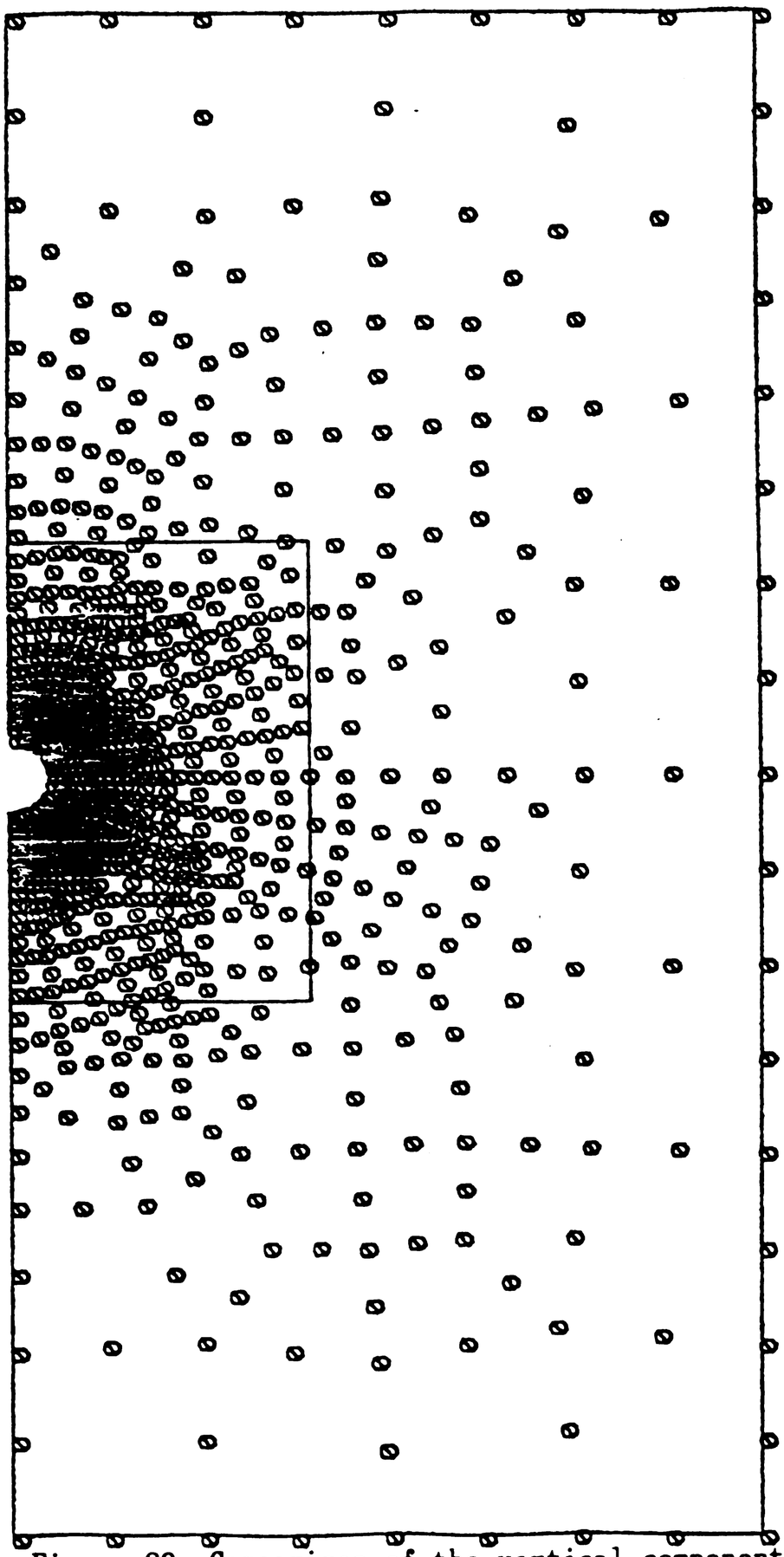

Figure 29. Comparison of the vertical component of gas velocity with Davidson solution for bubble deep in the bed and K = 10

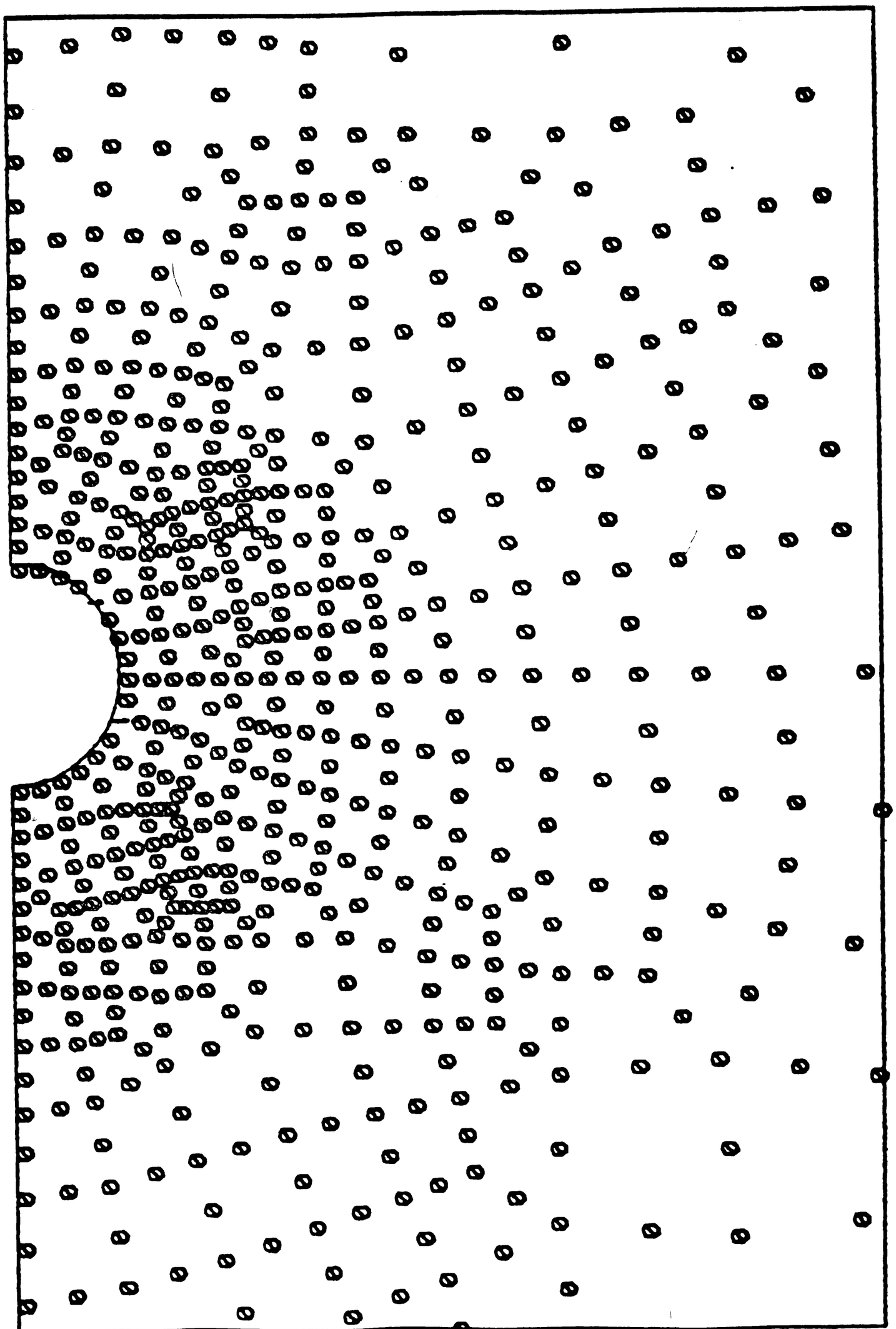

30. Comparison of the vertical component of gas velocity with Davidson solution for bubble deep in the bed and K = 10 highlighting the area near to the bubble

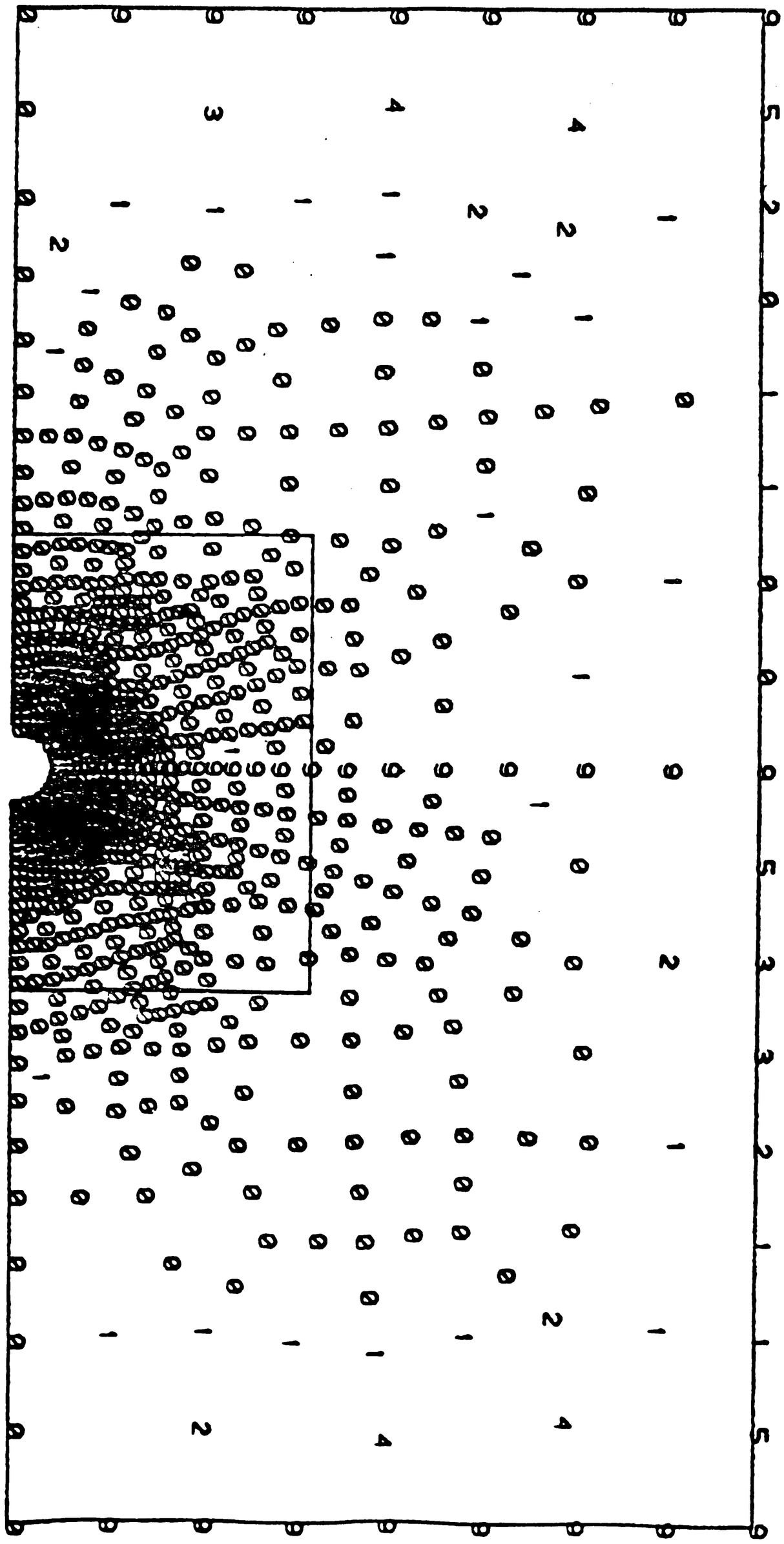

Figure 31. Comparison of the radial component of gas velocity with Davidson solution for bubble deep in the bed and K = 10

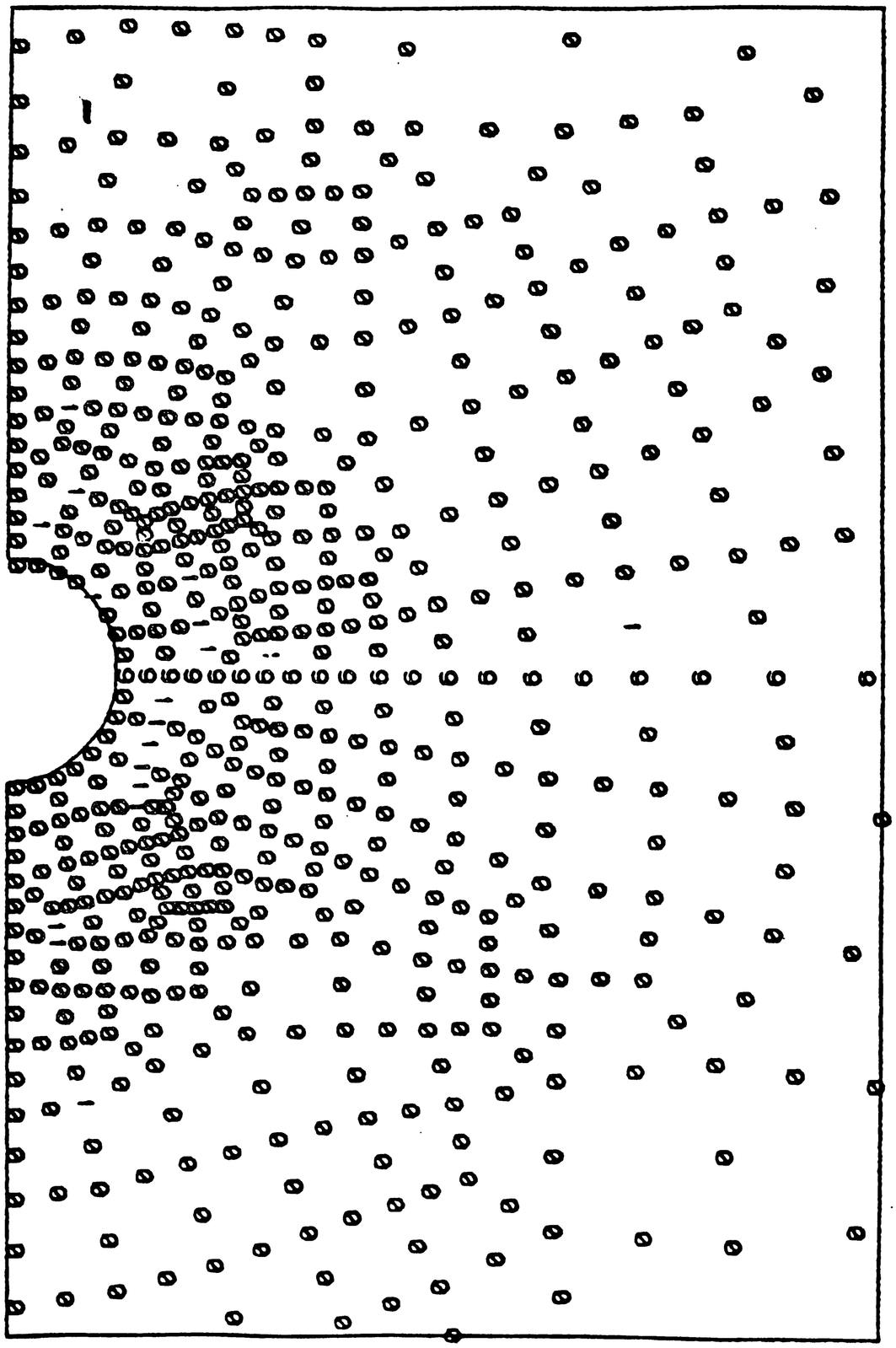

Figure 32. Comparison of the radial component of gas velocity with Davidson solution for bubble deep in the bed and K = 10 highlighting the area near to the bubble

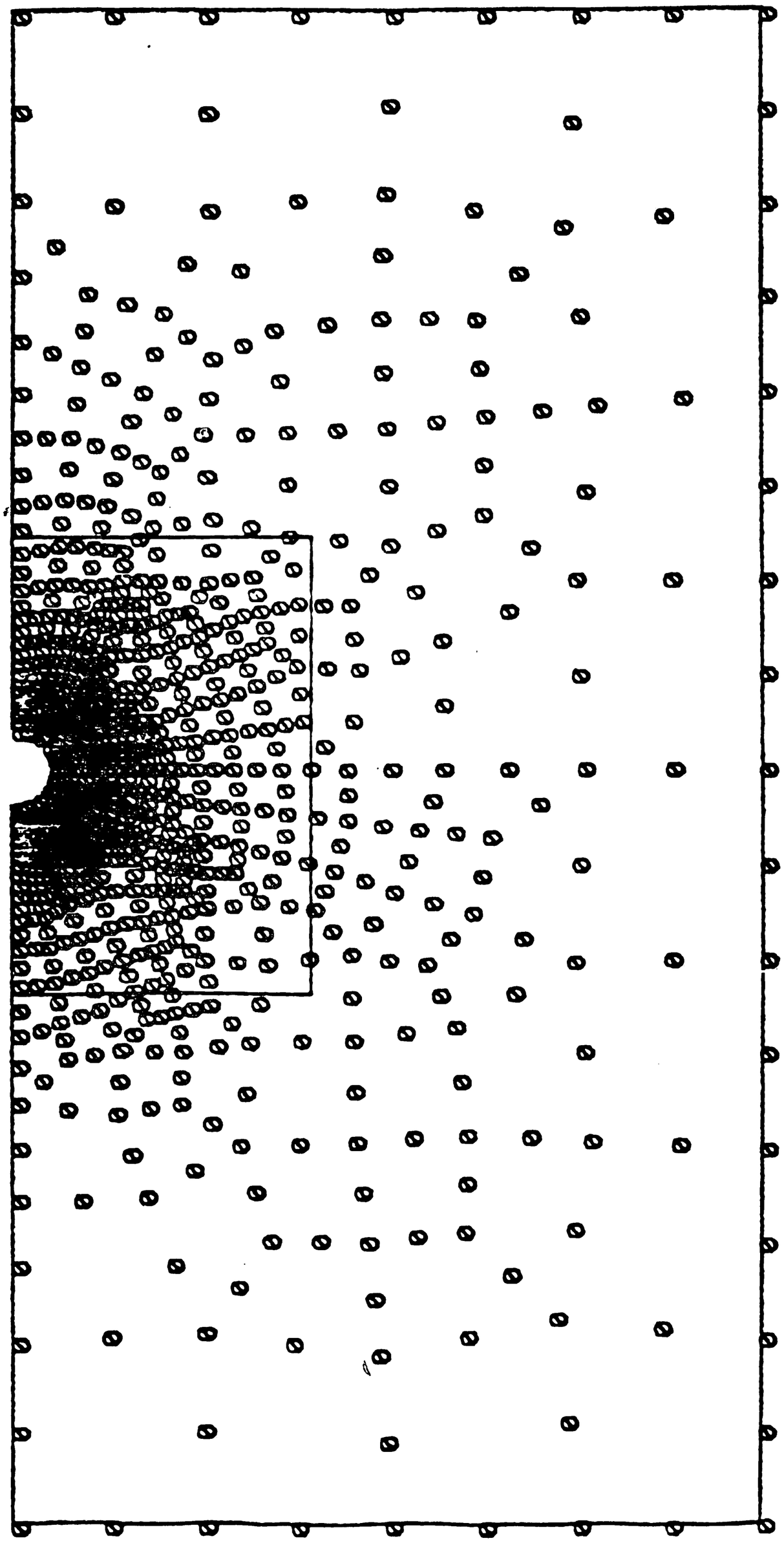

Figure 33. Comparison of the magnitude of gas velocity with Davidson solution for bubble deep in the bed and K=10

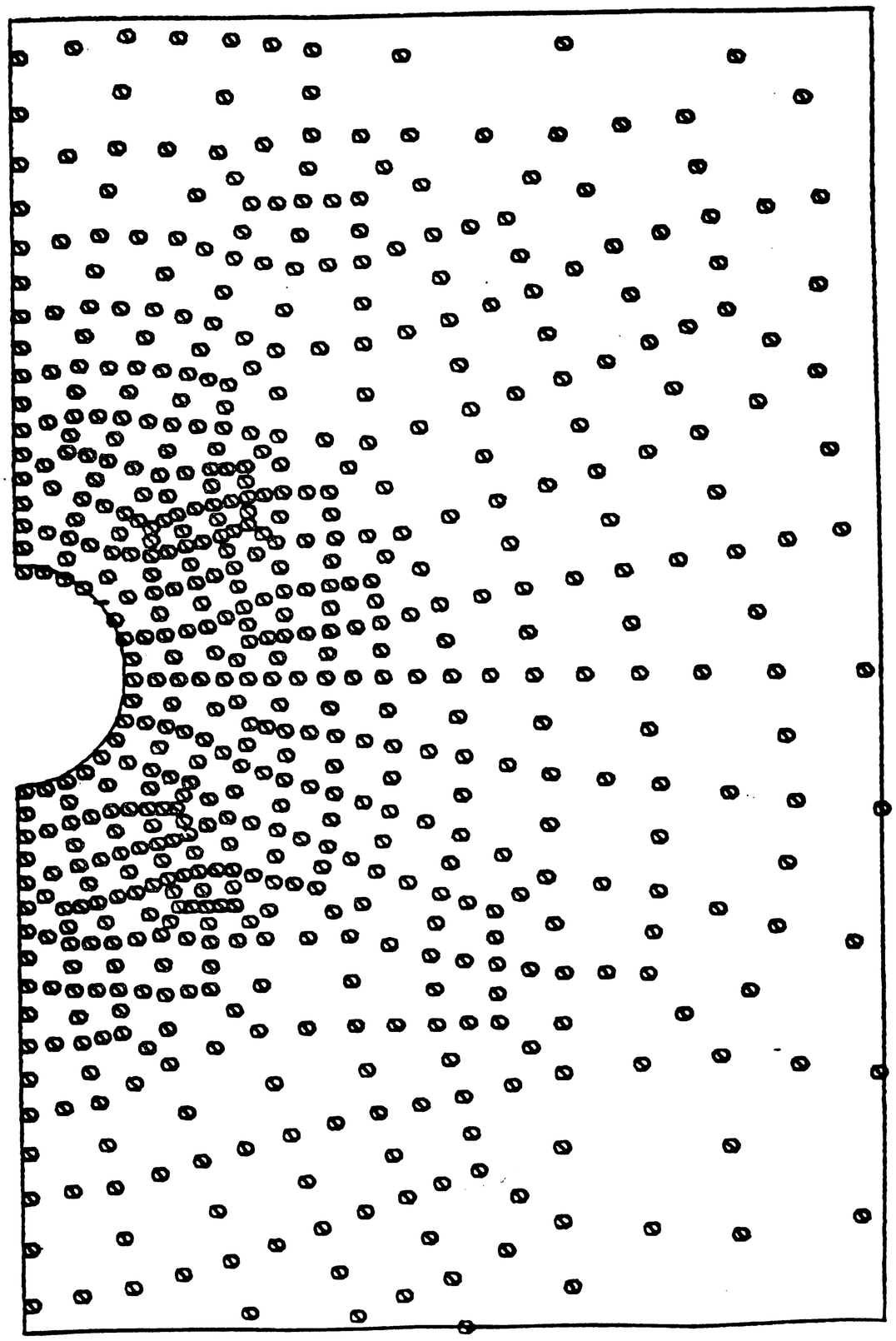

Figure 34. Comparison of the magnitude of gas velocity with Davidson solution for bubble deep in the bed and K=10 highlighting the area near to the bubble

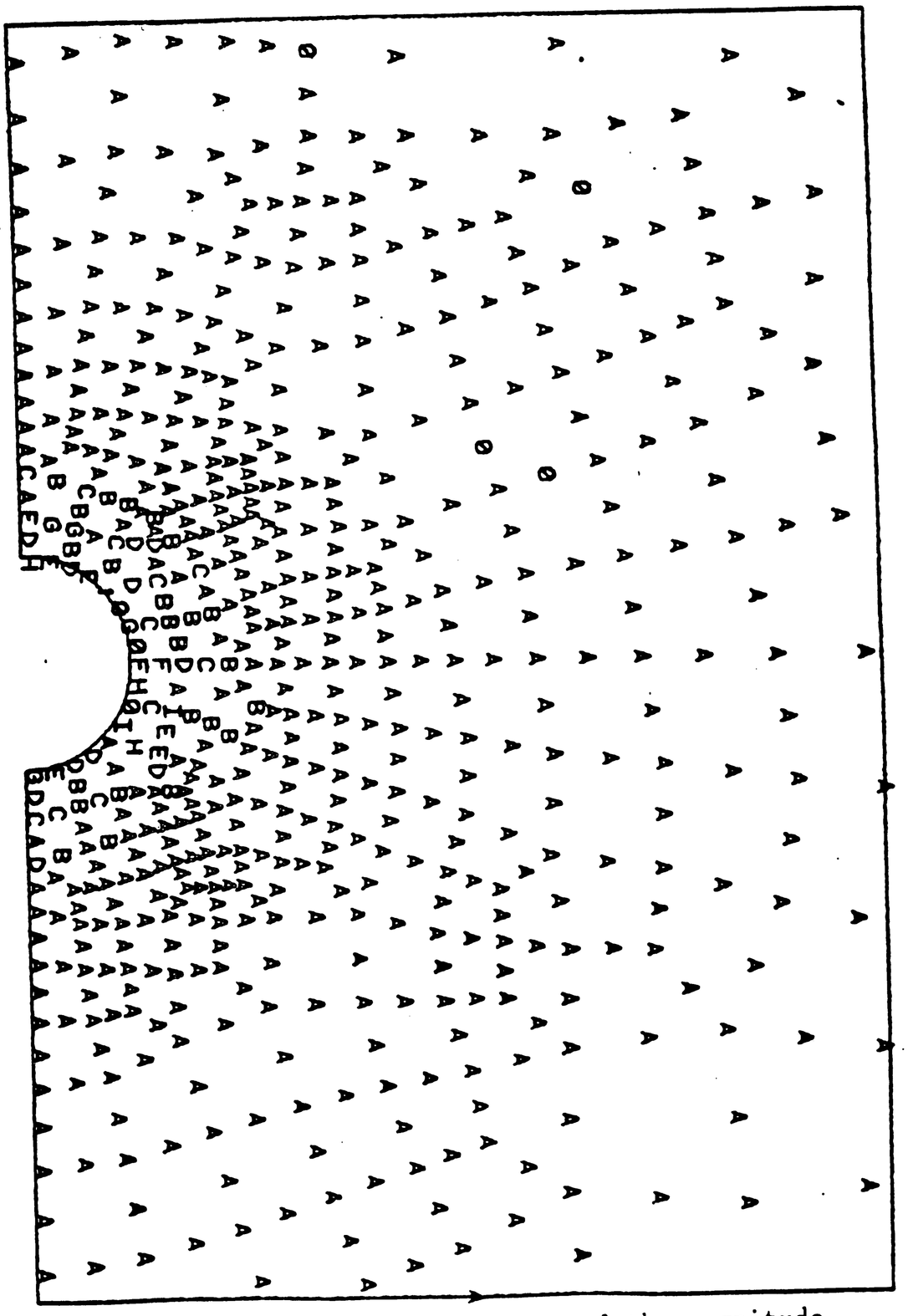

Figure 35. A detailed comparison of the magnitude of gas velocity with Davidson solution for bubble deep in the bed and K= 10 highlighting the area near to the bubble

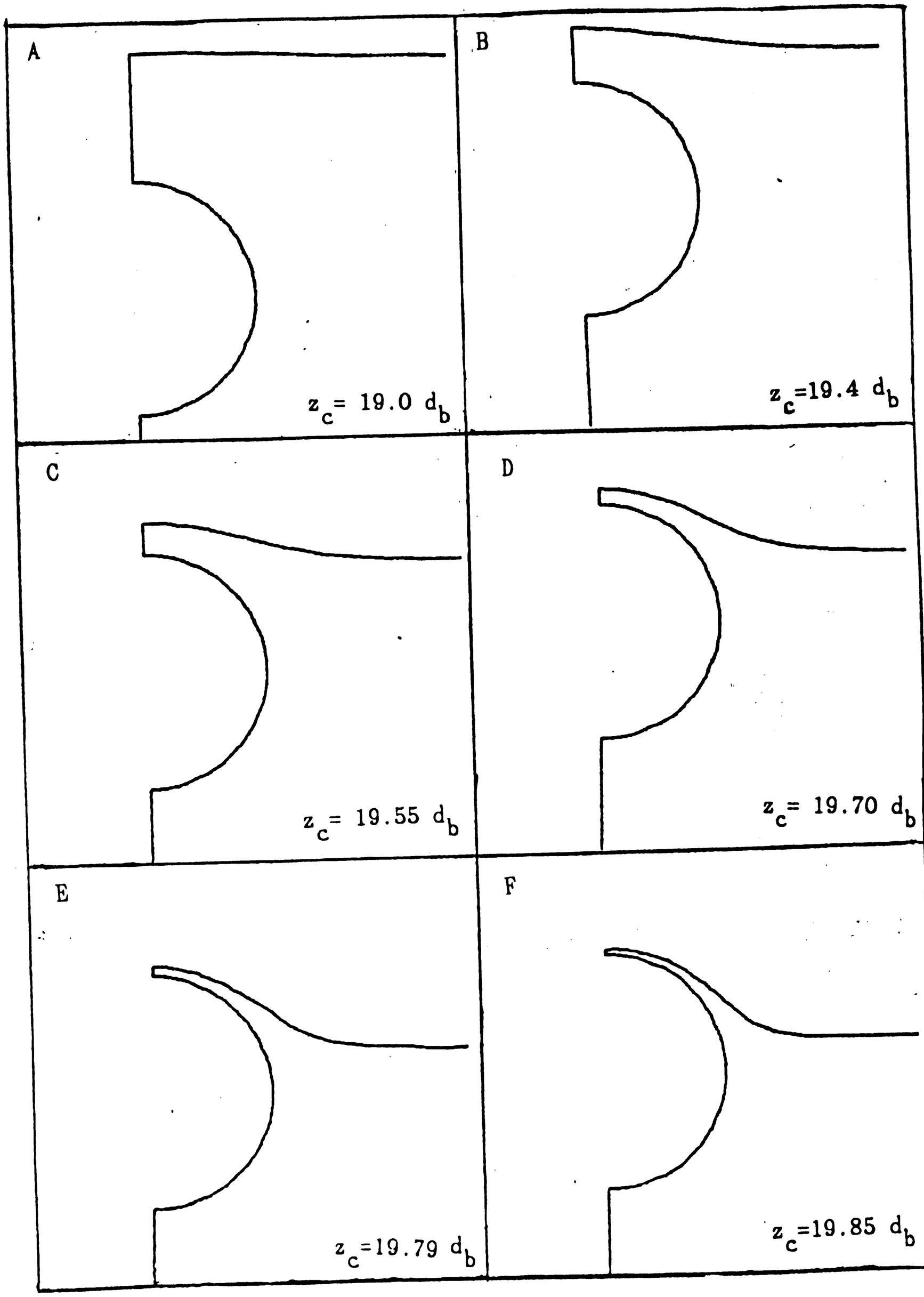

Figure 36. The location of bubble surface on plots of deformation of free surface

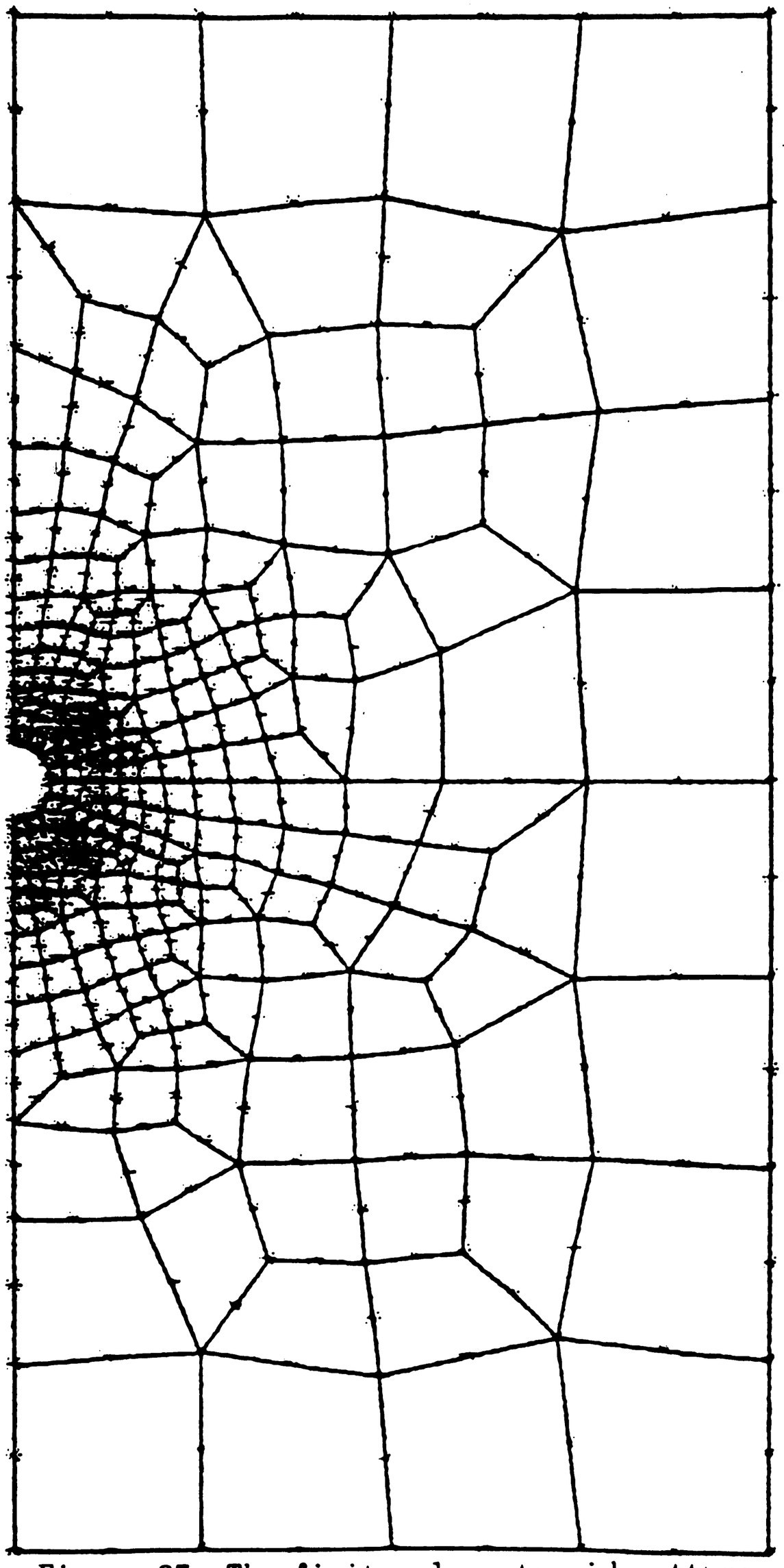

Figure 37. The finite element grid pattern for bubble center height = $10.d_b$

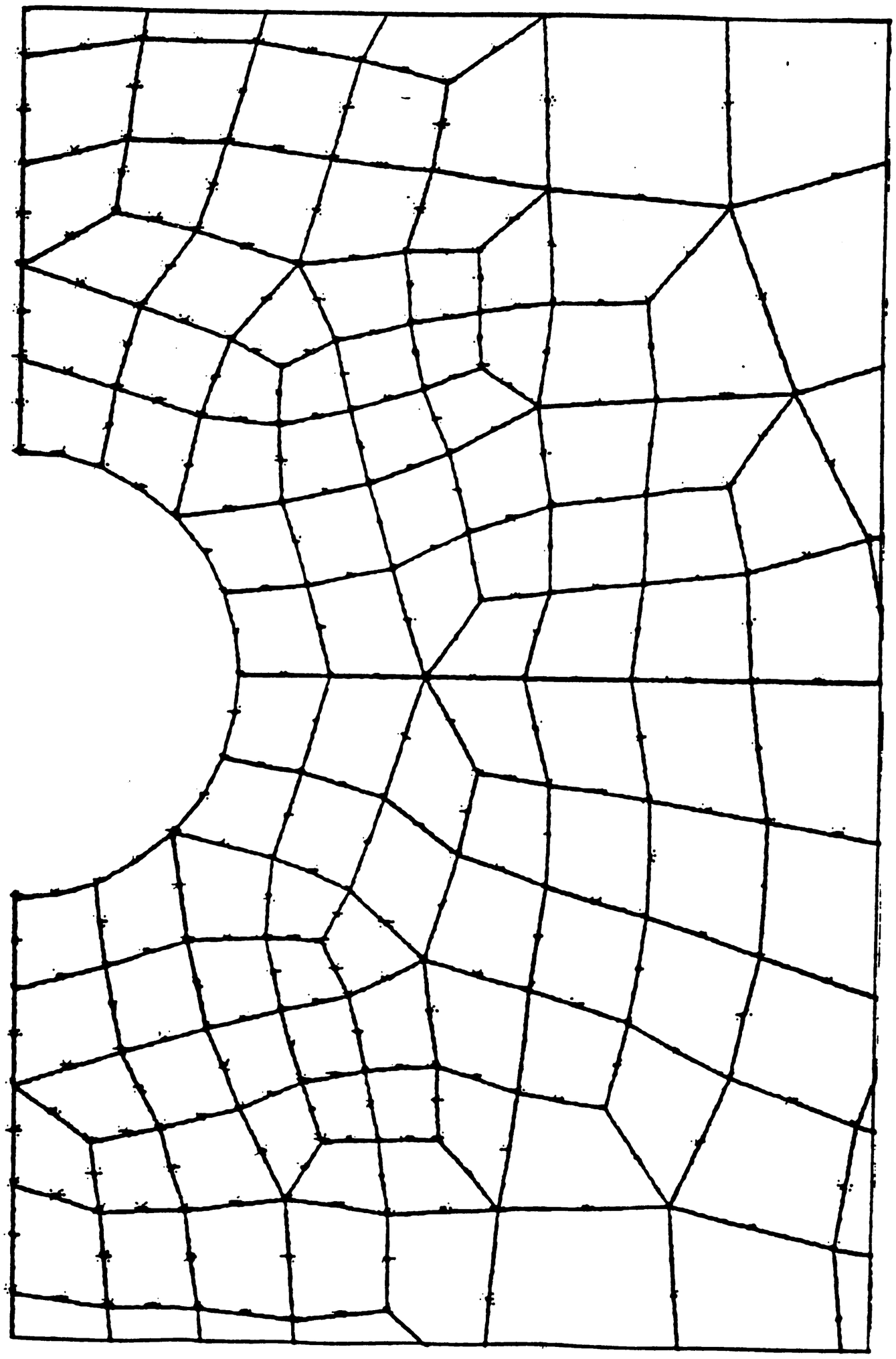

Figure 38. The finite element grid pattern highlighting the area near to the bubble for bubble center height = $10.d_b$

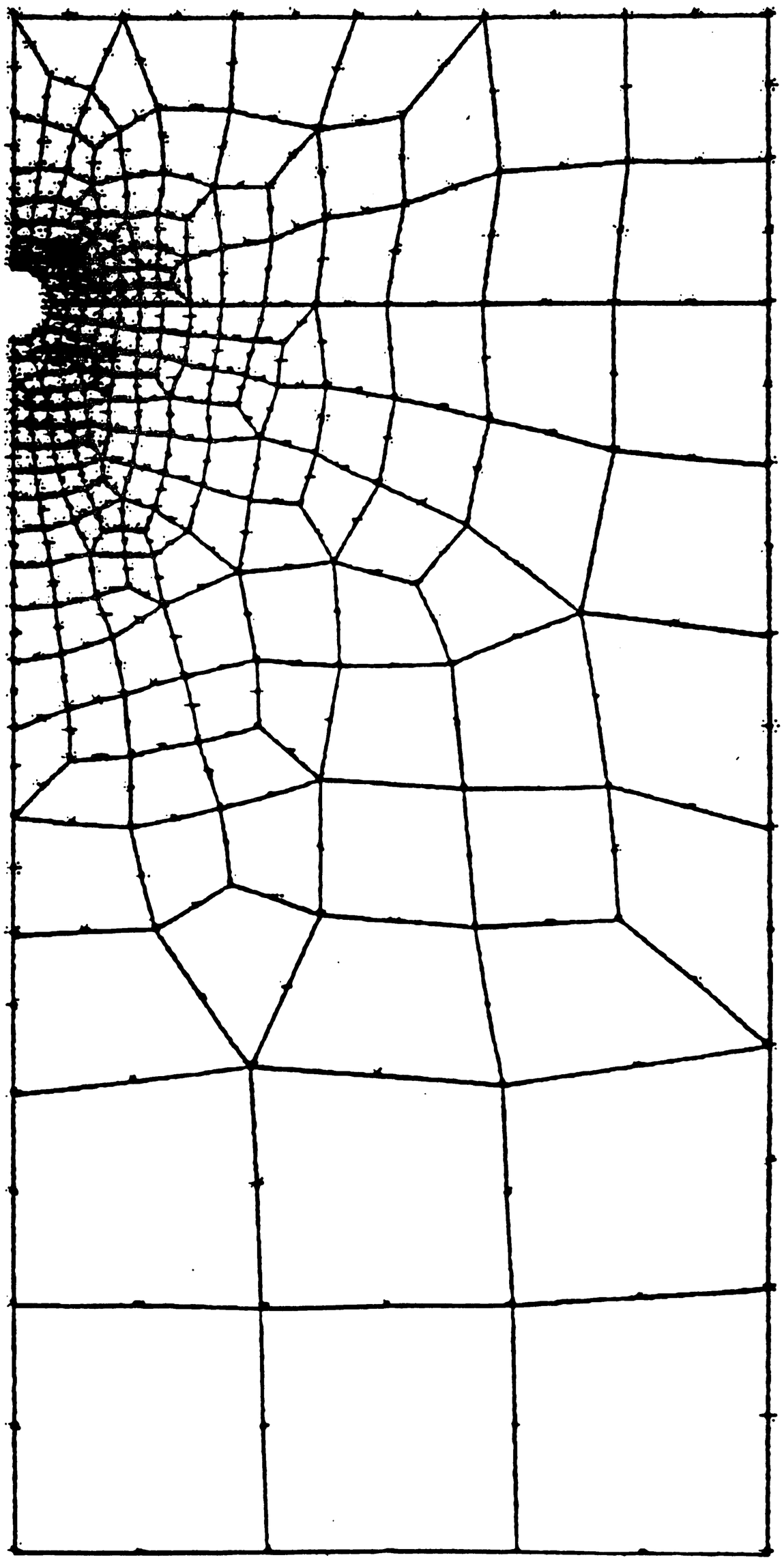

Figure 39. The finite element grid pattern for bubble center height = $16.25d_b$

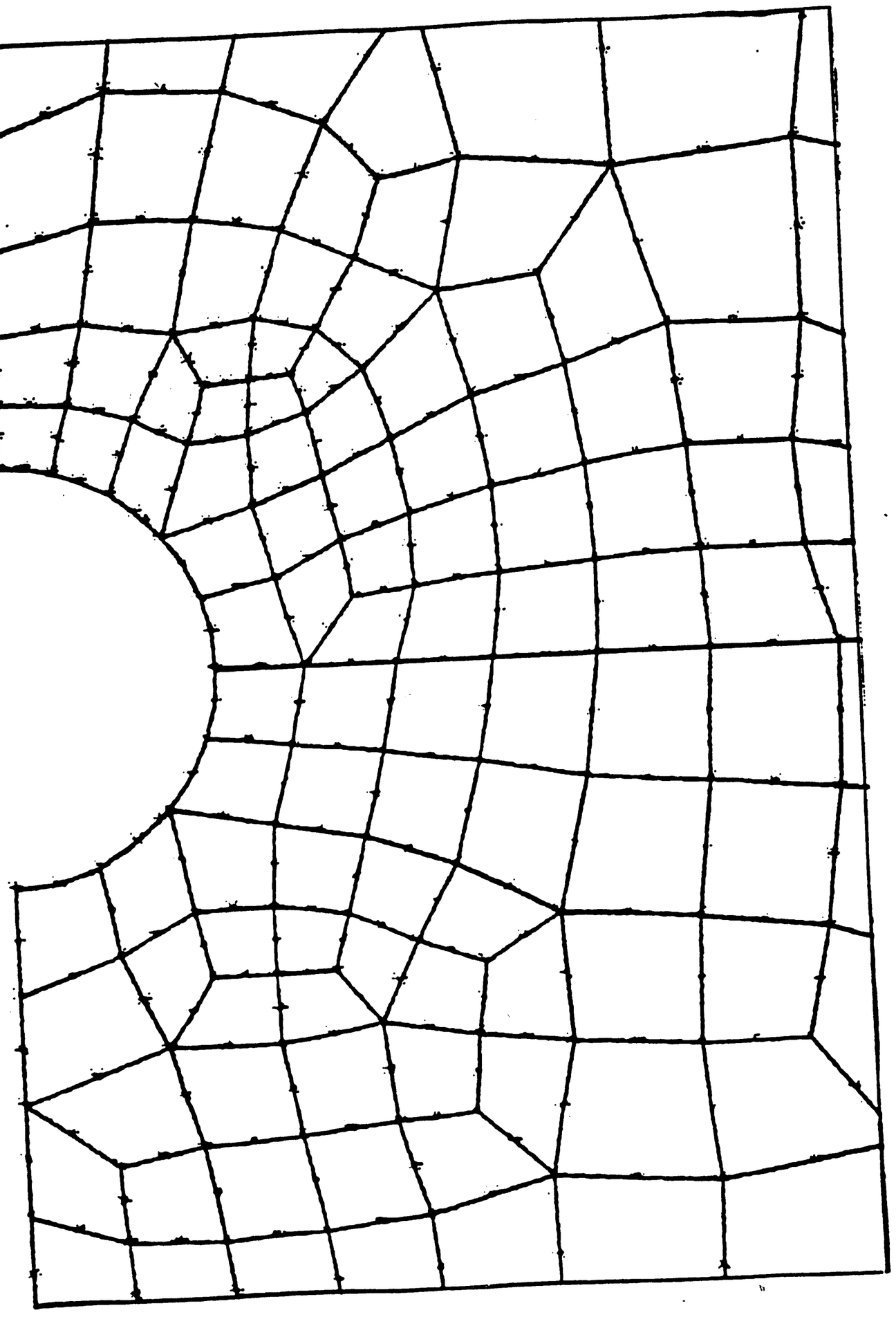

Figure 40. The finite element grid pattern highlighting the area near to the bubble for bubble center height = $16.25d_b$

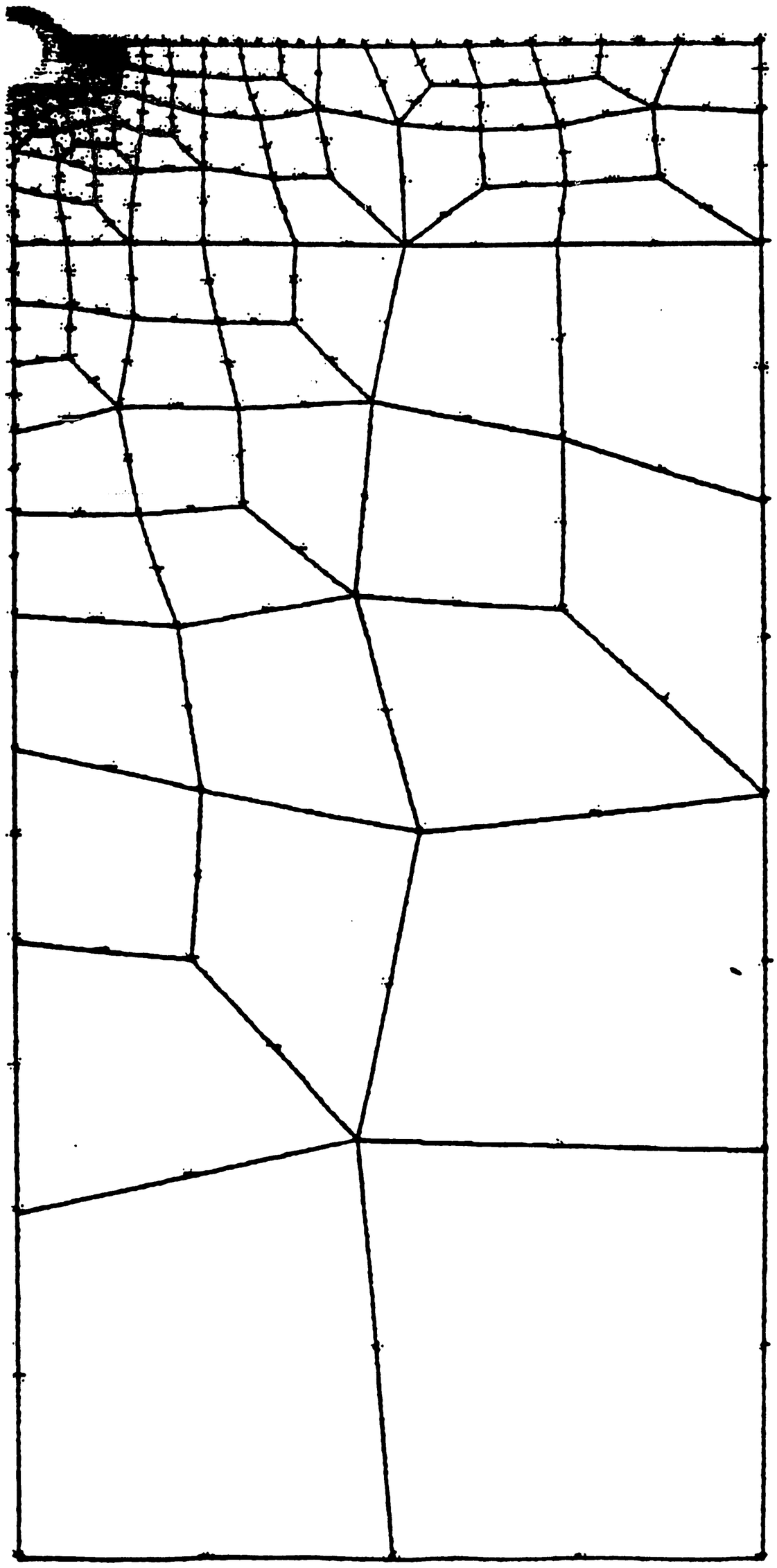

Figure 41. The finite element grid pattern for bubble center height = $19.85d_b$

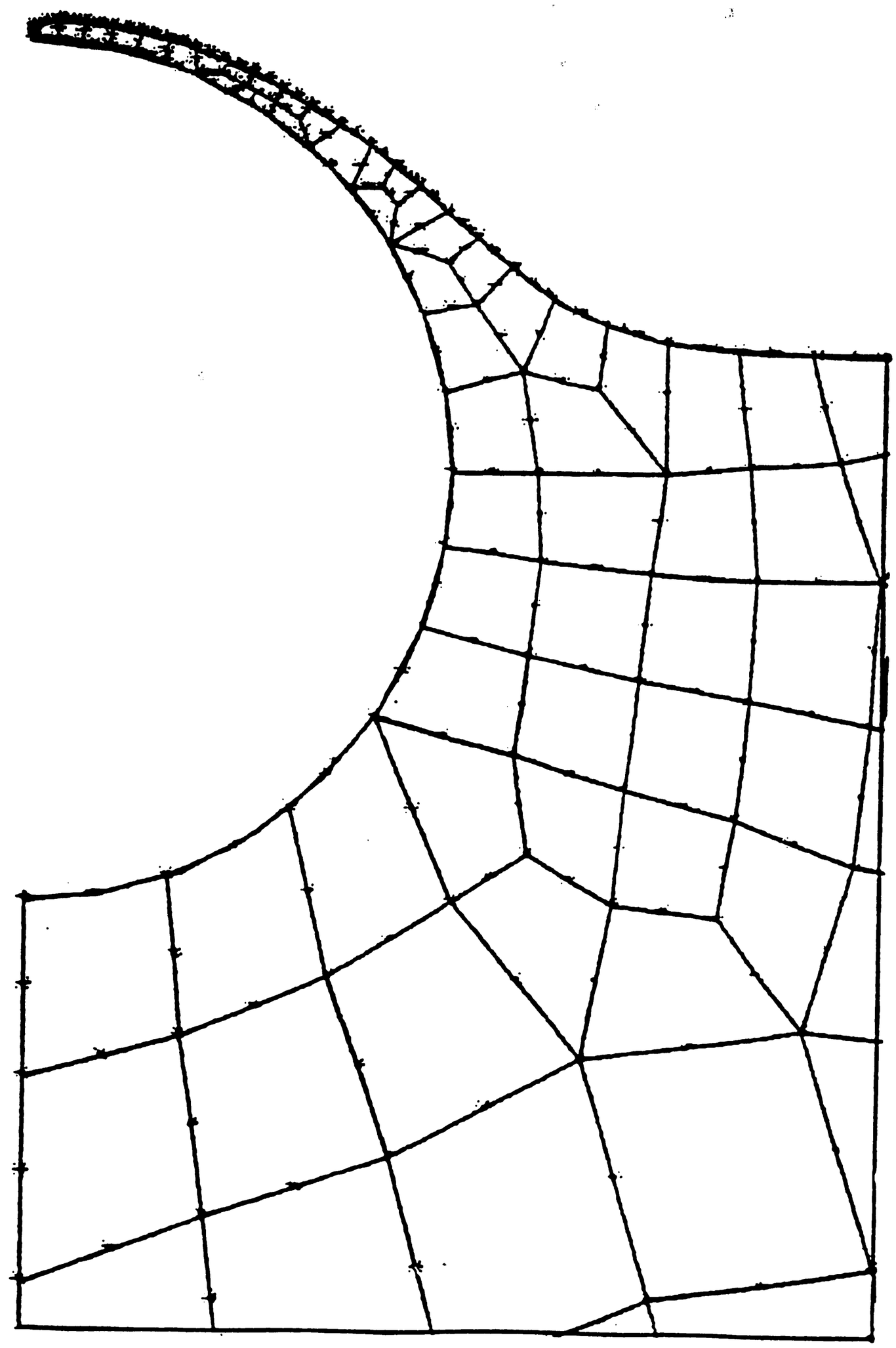

Figure 42. The finite element grid pattern highlighting the area near to the bubble for bubble center height = $19.85d_b$

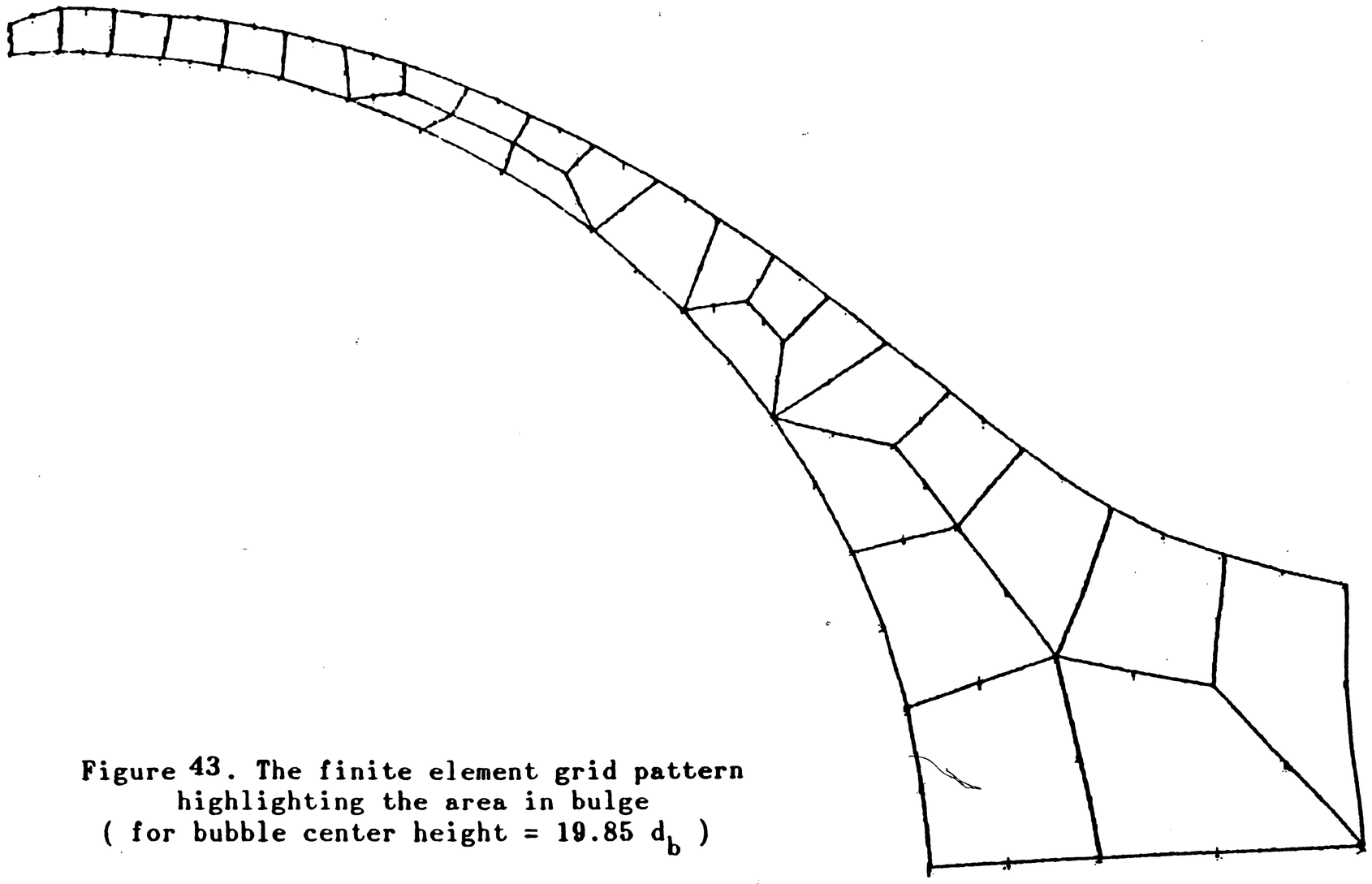

Figure 43. The finite element grid pattern highlighting the area in bulge (for bubble center height = 19.85 d_b)

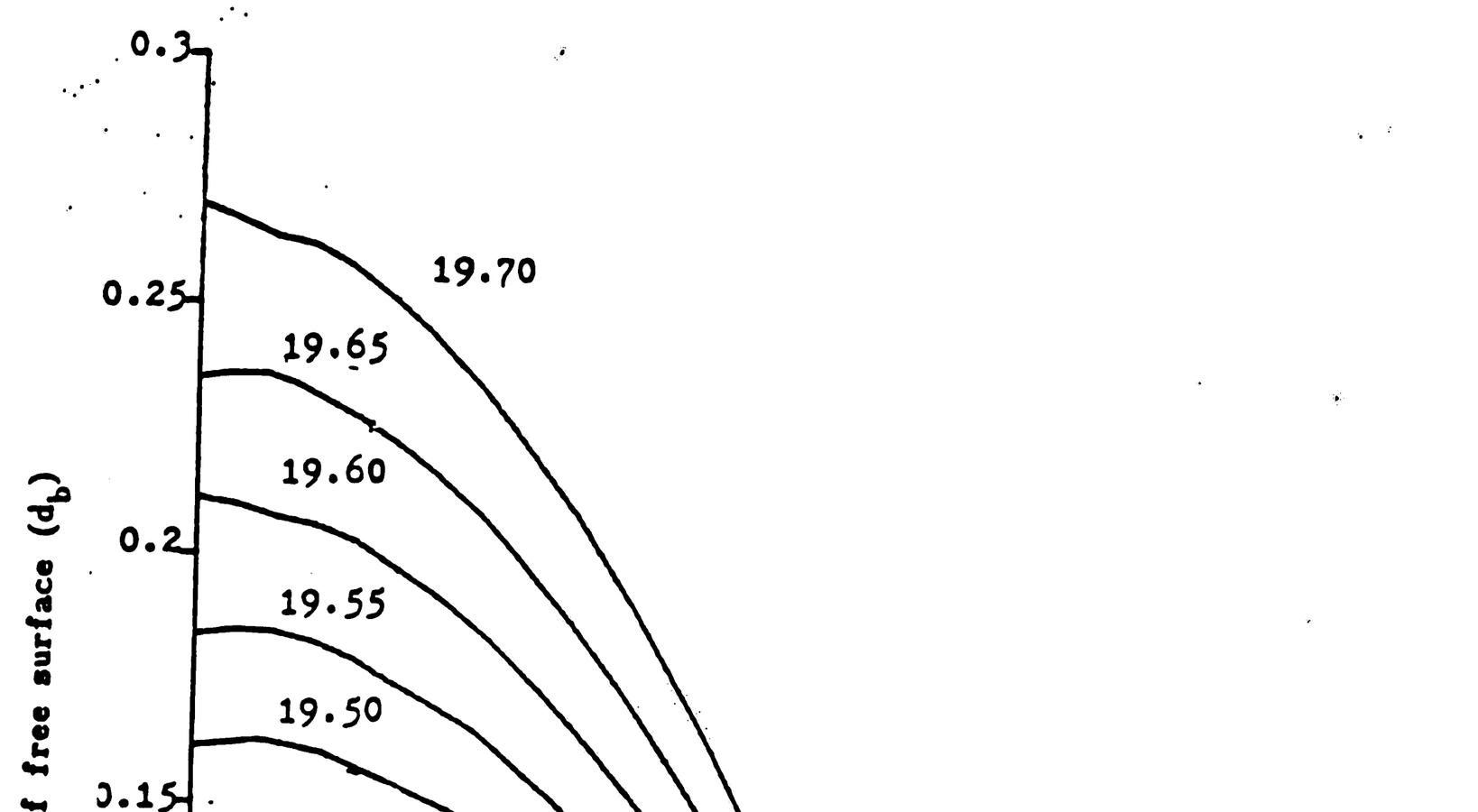

Figure 44. The deformation of the free surface

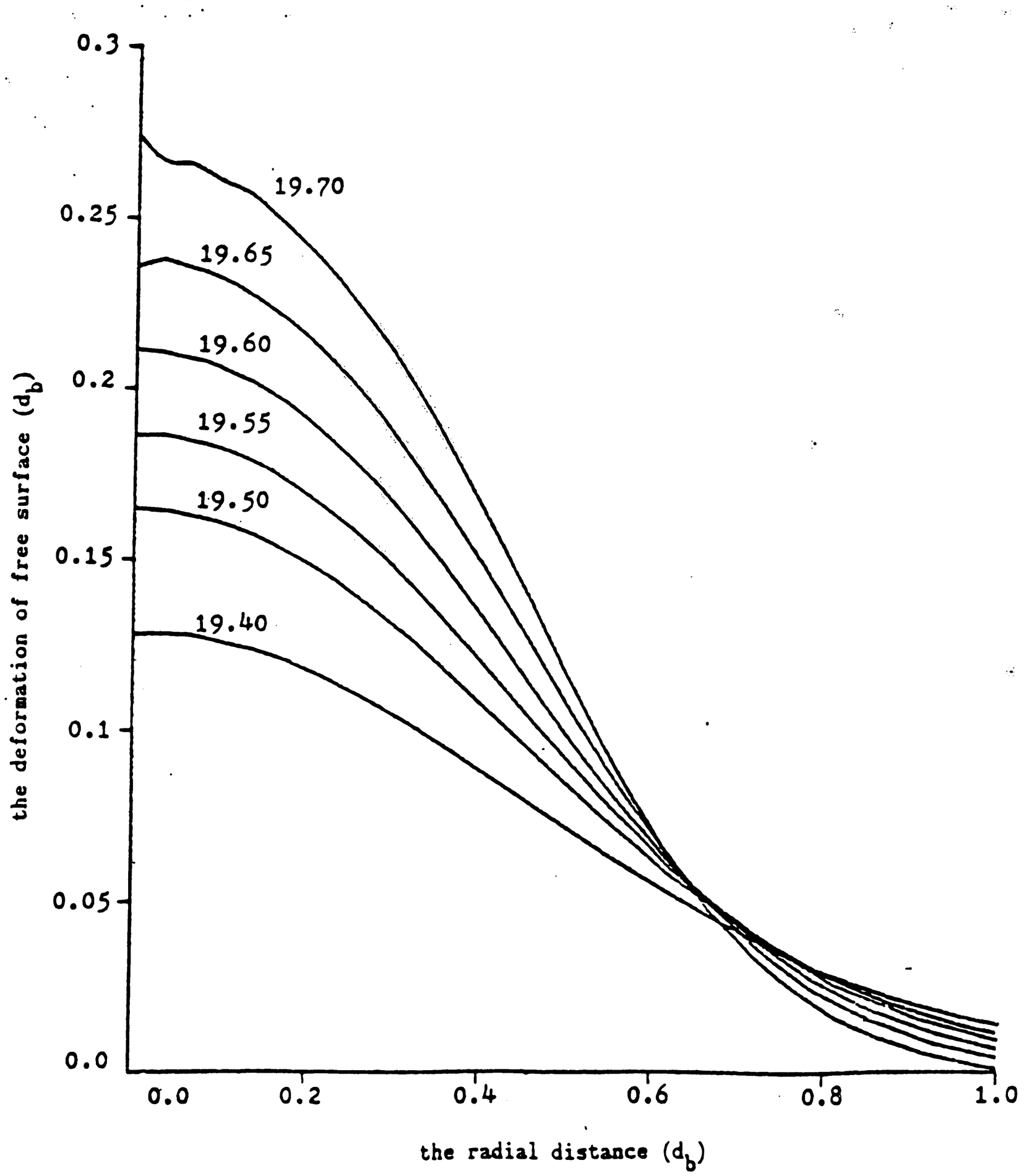

Figure 45. The deformation of the free surface for fine mesh

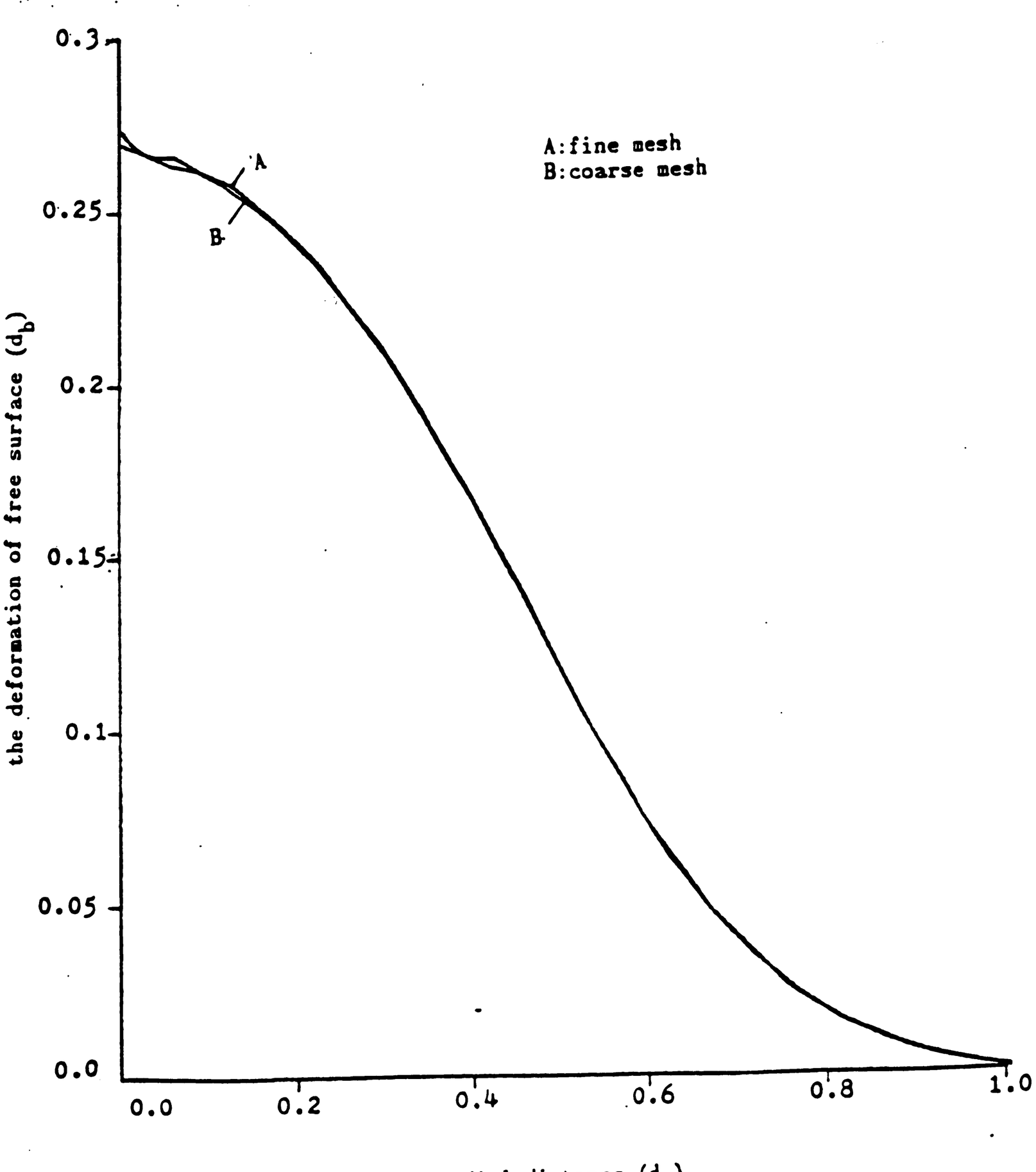

Figure 46. Comparison of the deformation of free surface between the fine and coarse mesh

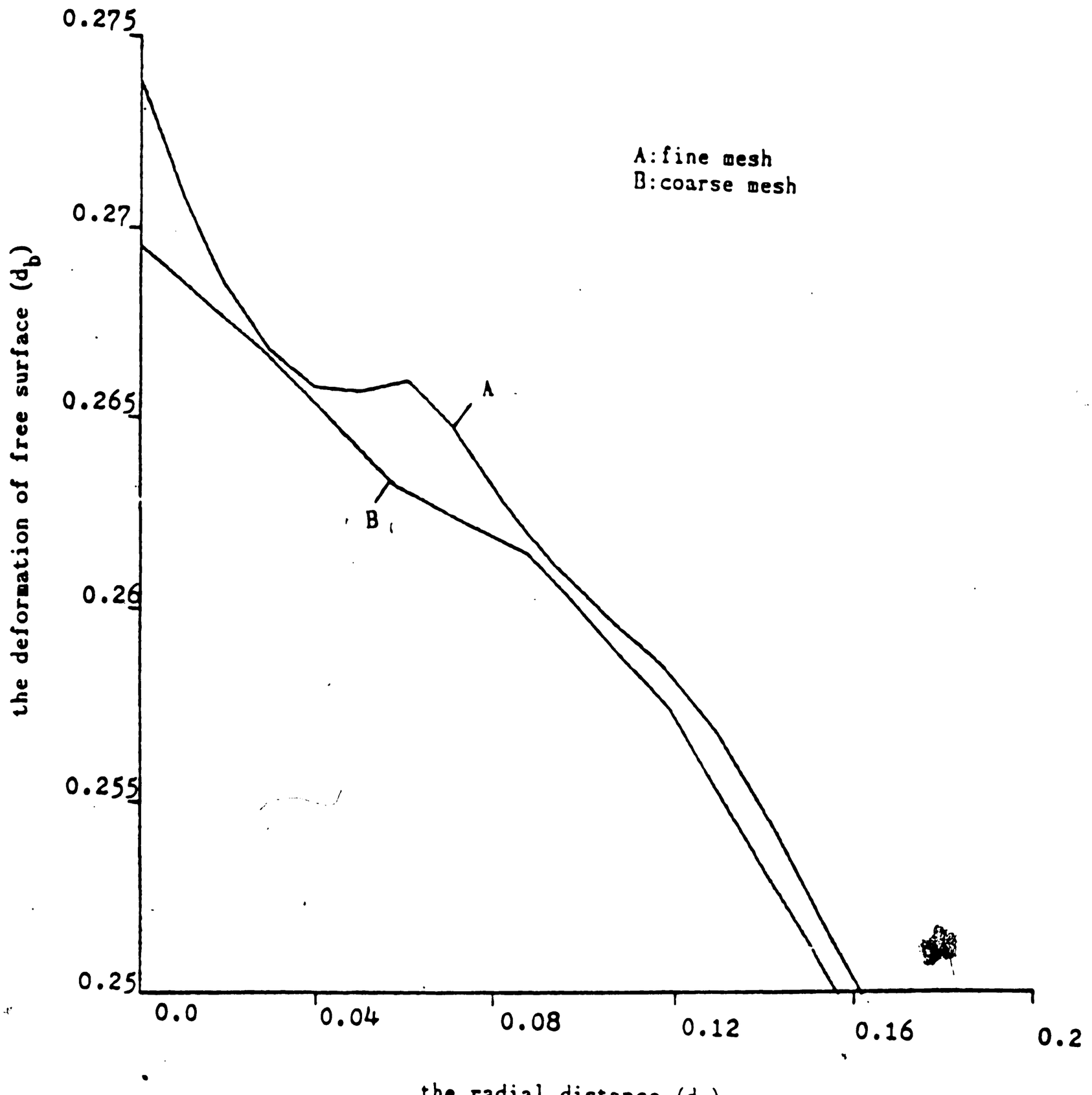

Figure 47. Comparison of the deformation of free surface between the fine and coarse mesh highlighting the area near to the bubble

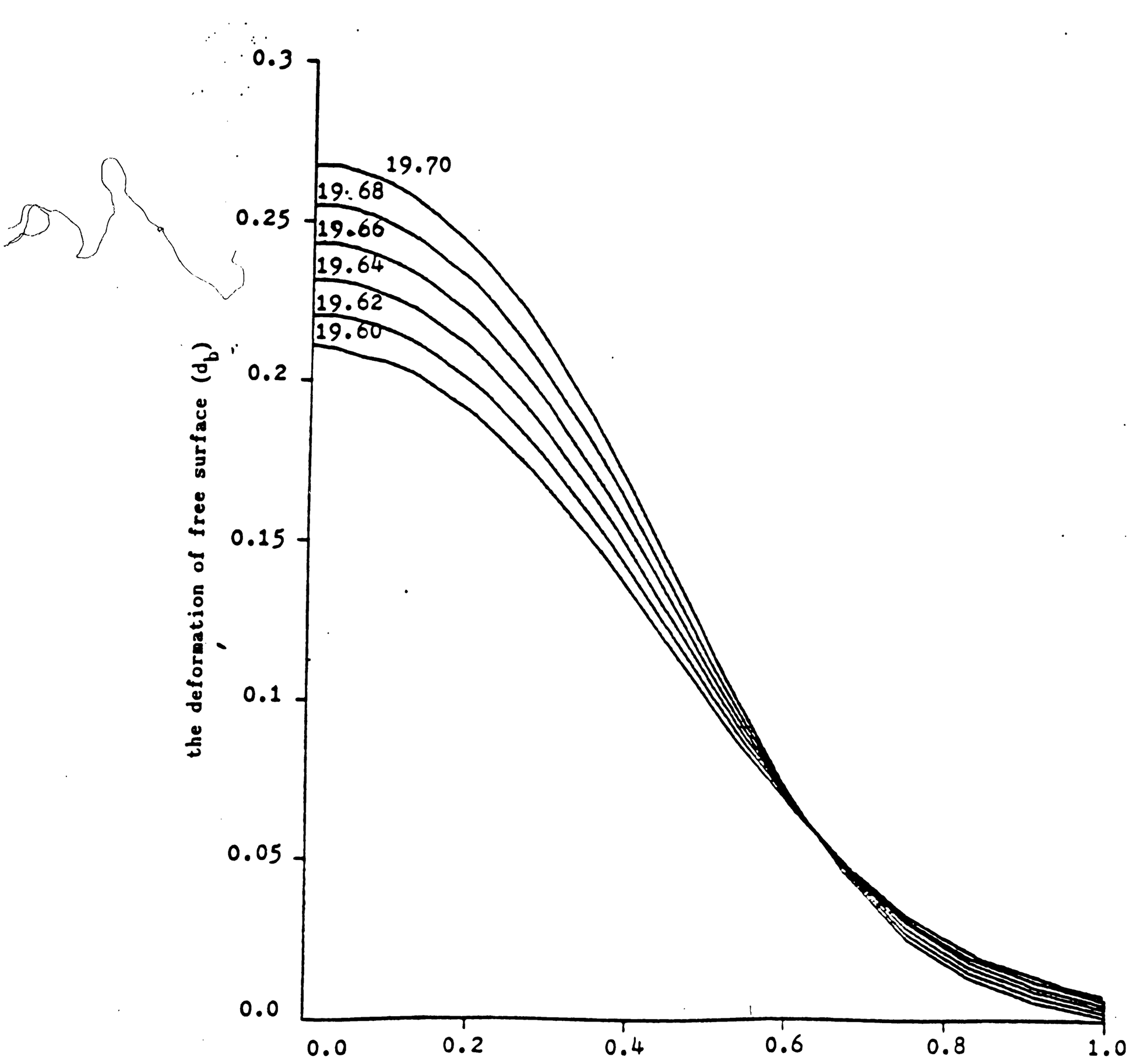

Figure 48. The deformation of the free surface for small time step size

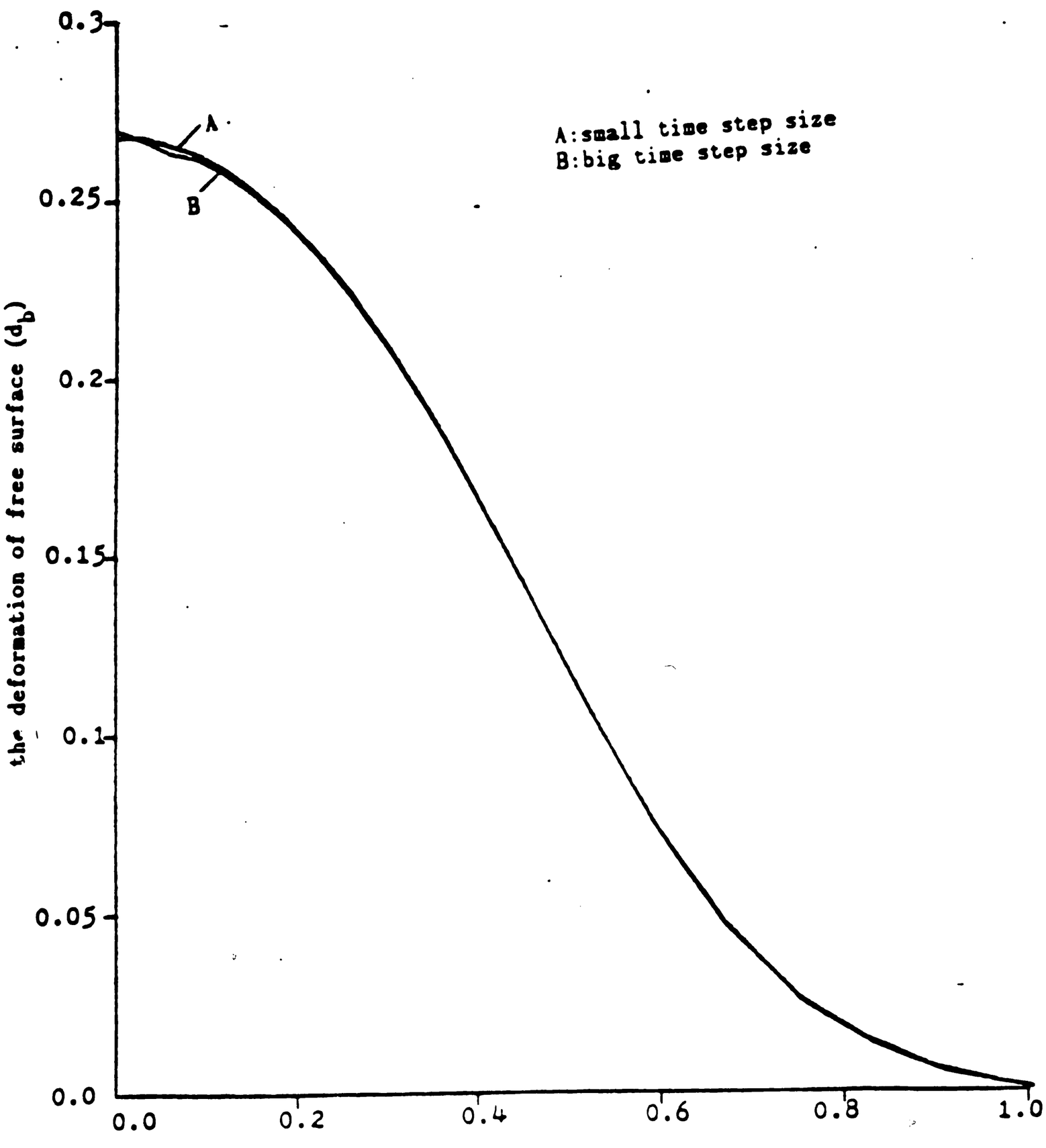

Figure 49. Comparison of the deformation of free surface between the small and large time step size

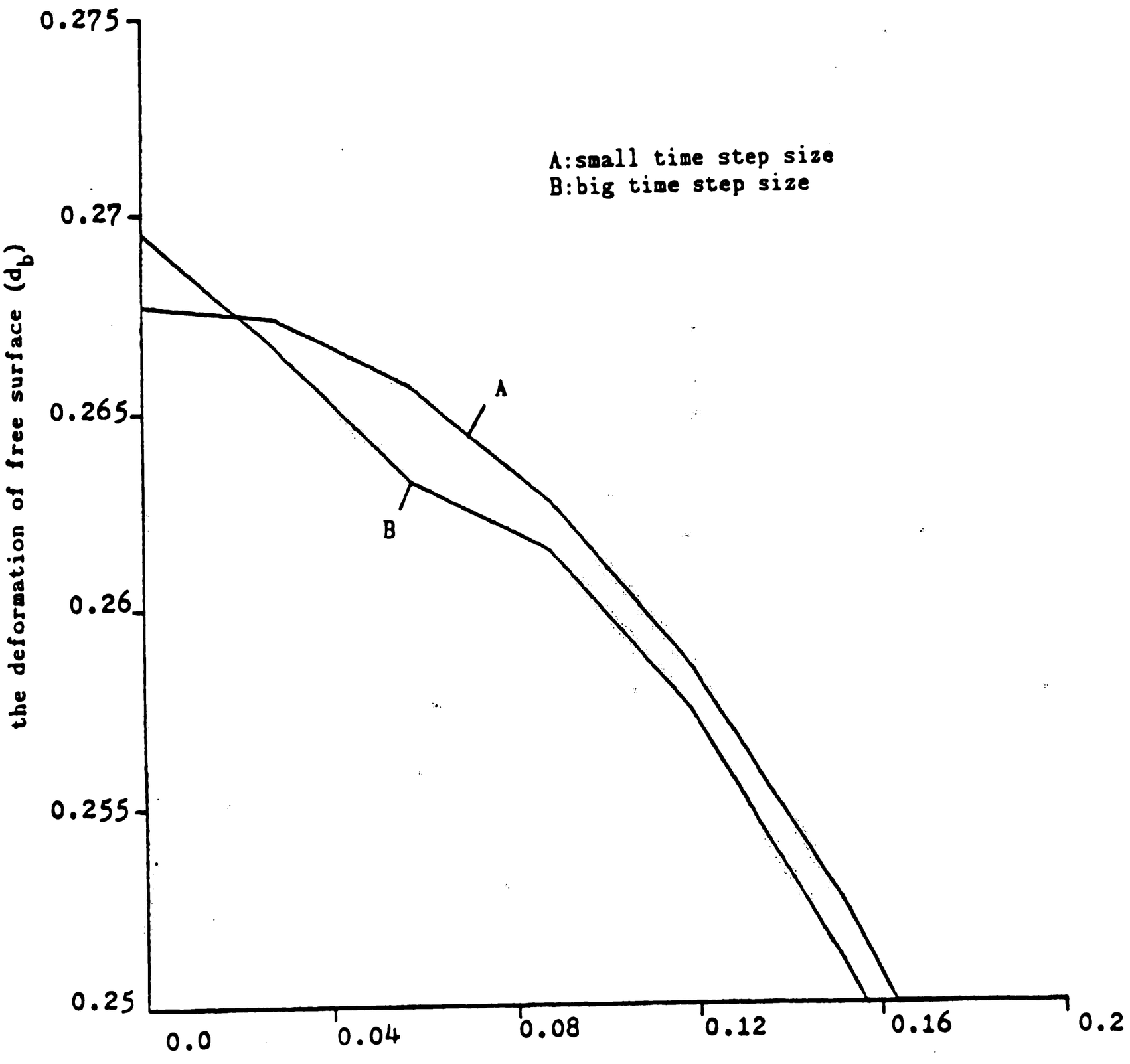

Figure 50. Comparison of the deformation of free surface between the small and large time step size highlighting the area near to the bubble

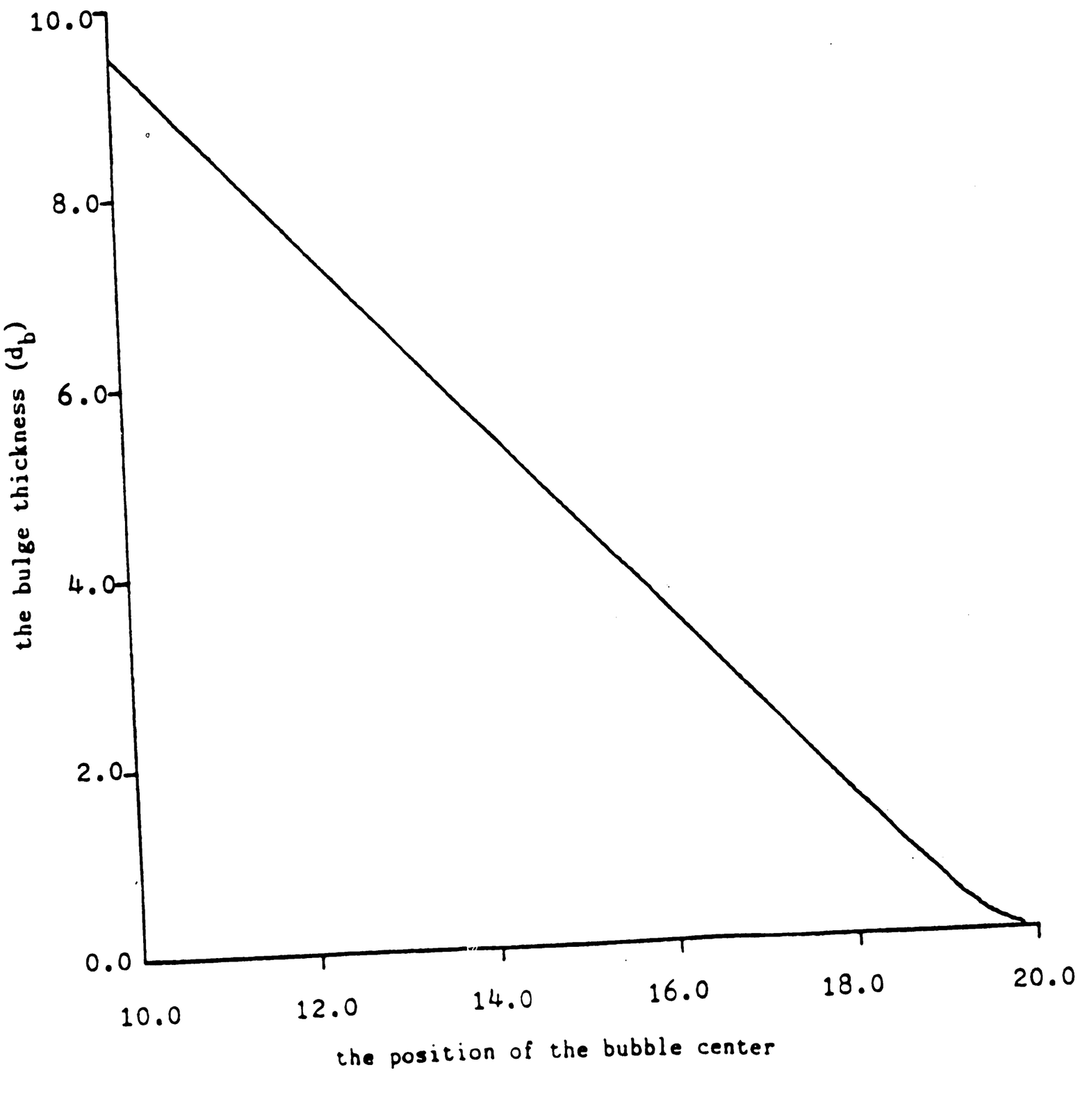

Figure 51. The bulge thickness at bubble centerline related to the bubble center height

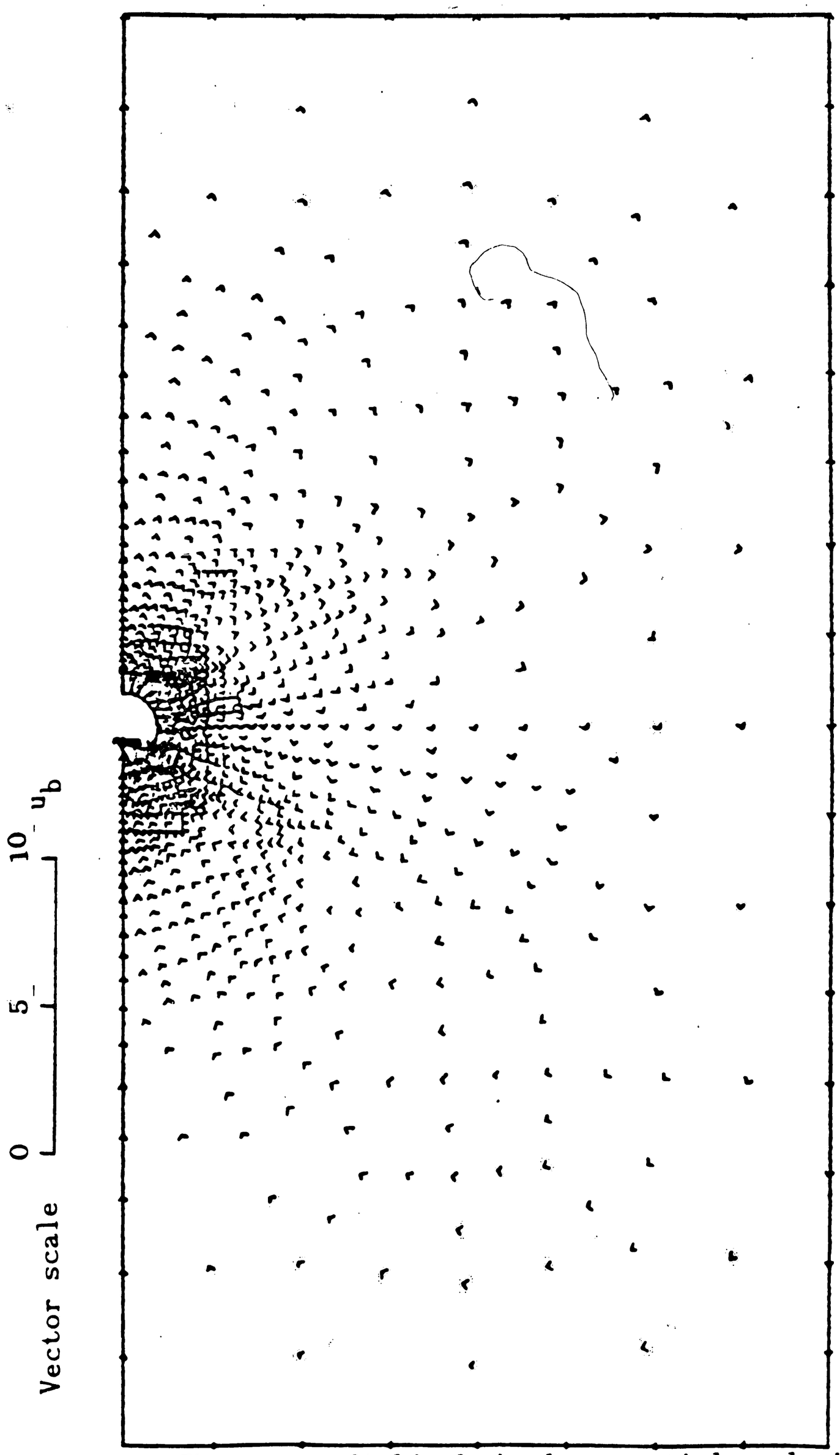

Figure 52. The vector field of absolute particle velocity for bubble center height at 10 d_b

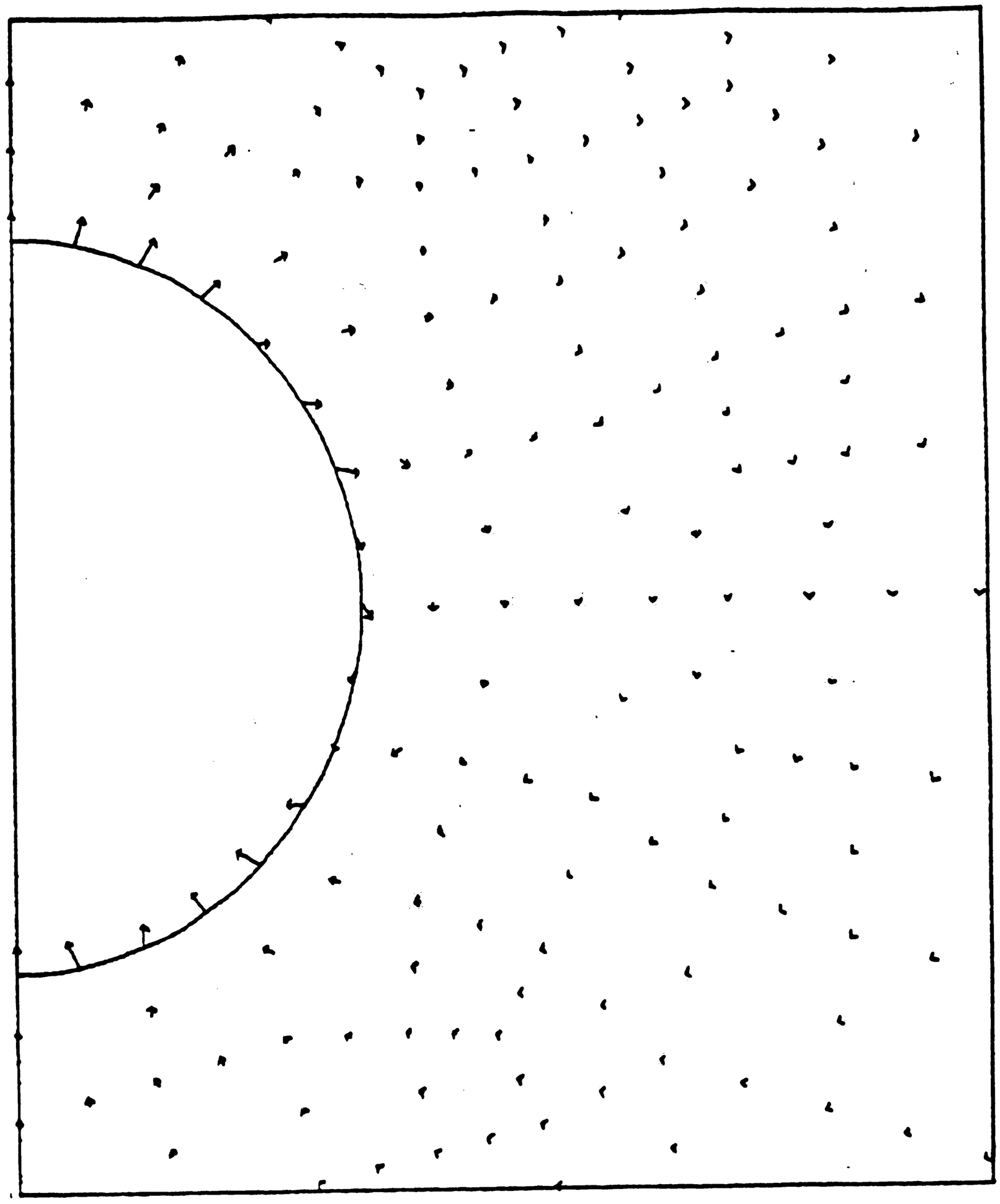

Figure 53. The vector field of absolute particle velocity highlighting the area near to the bubble for bubble center height at 10 d_b

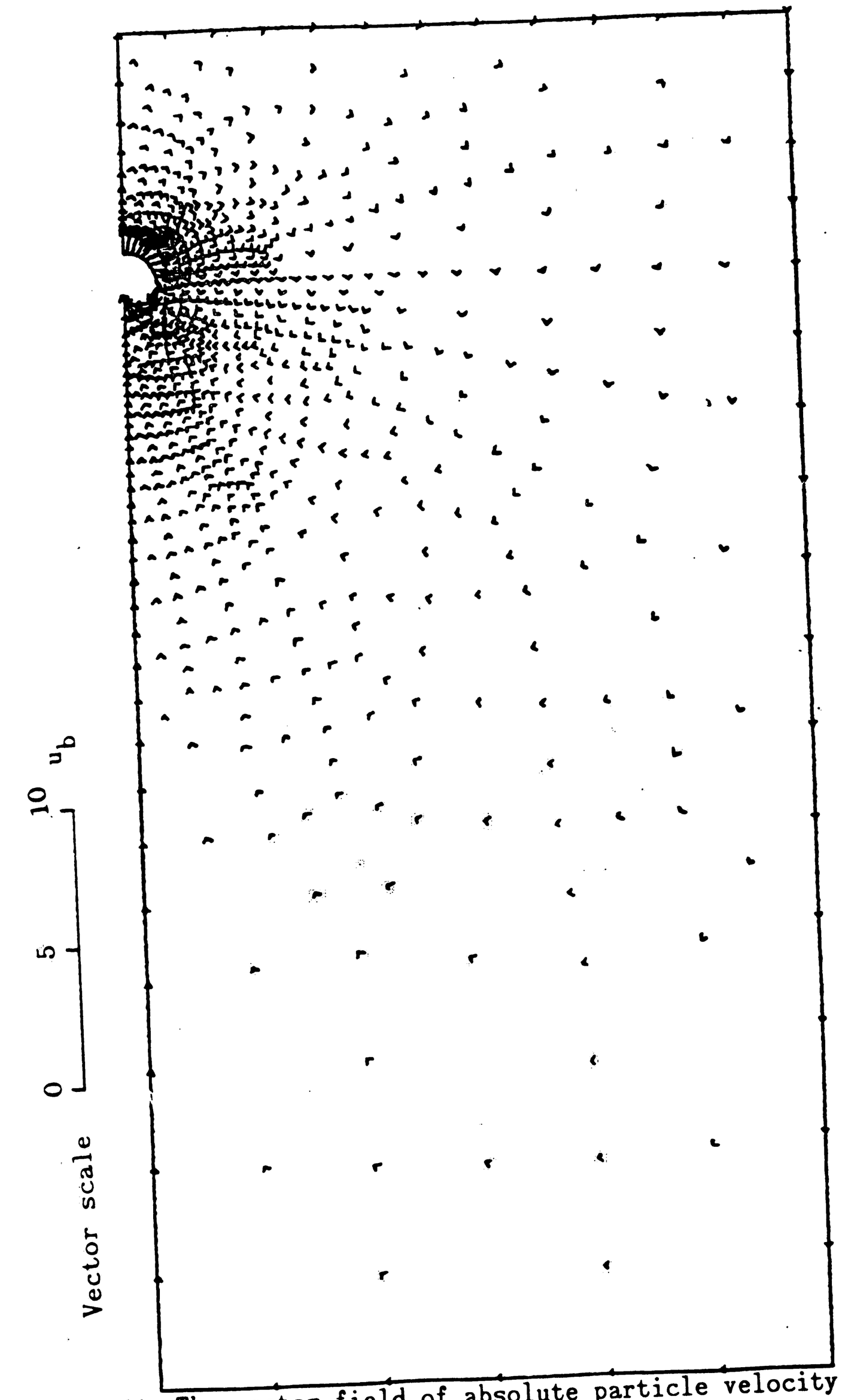

Figure 54. The vector field of absolute particle velocity for bubble center height at 16.25 d_b

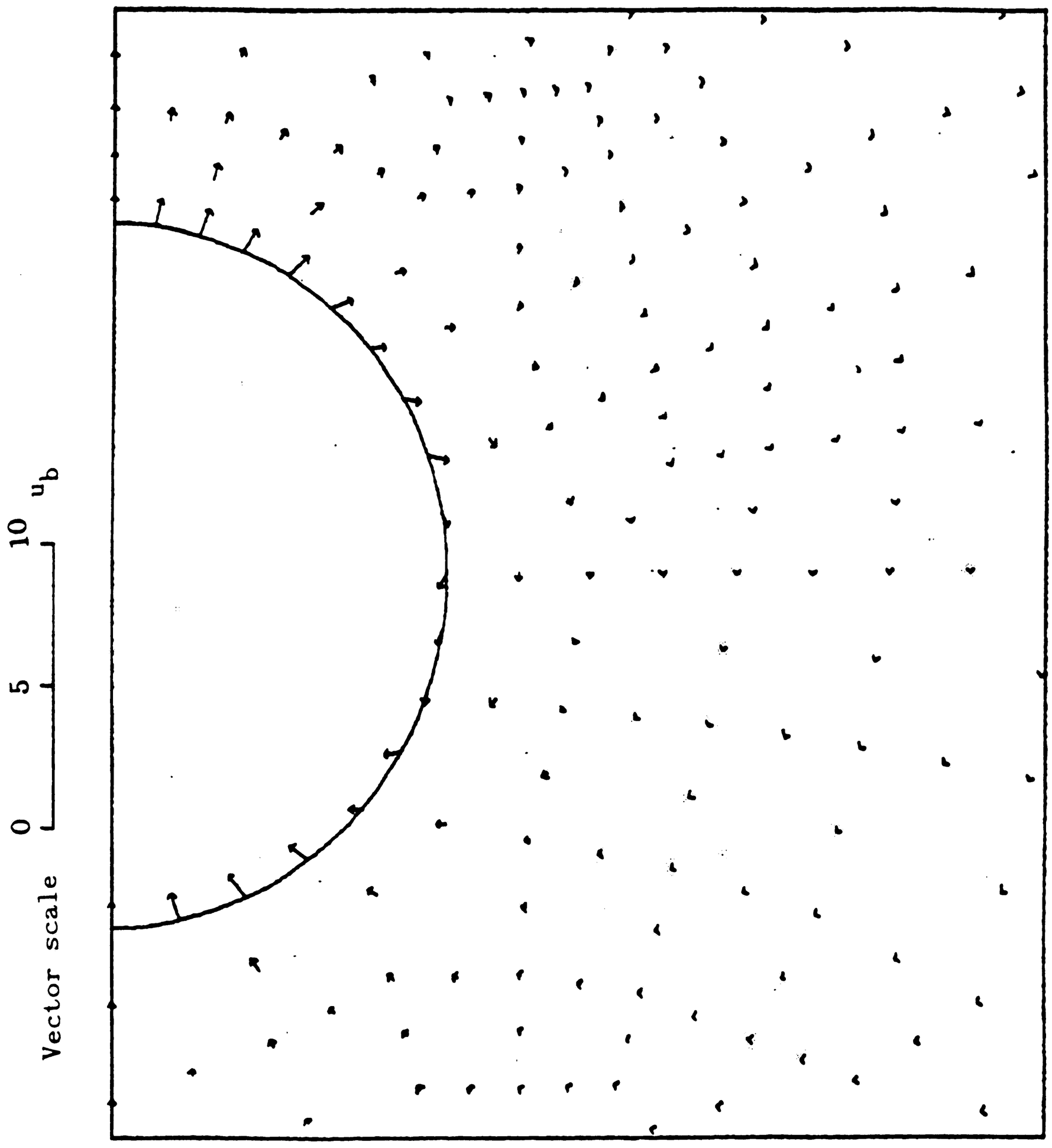

Figure 55. The vector field of absolute particle velocity highlighting the area near to the bubble for bubble center height at 16.25 d_b

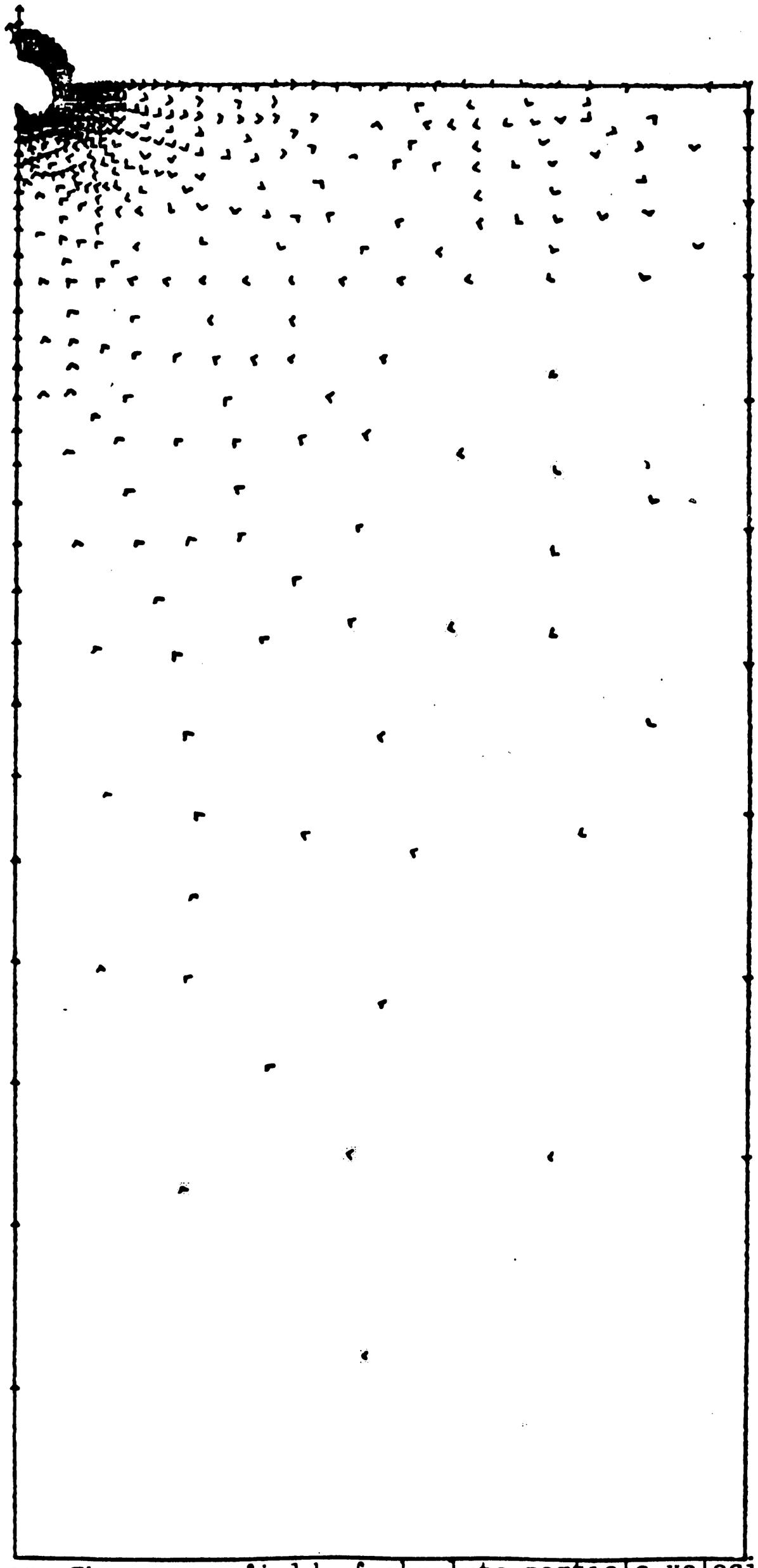

Figure 56. The vector field of absolute particle velocity for bubble center height at 19.85 d_b

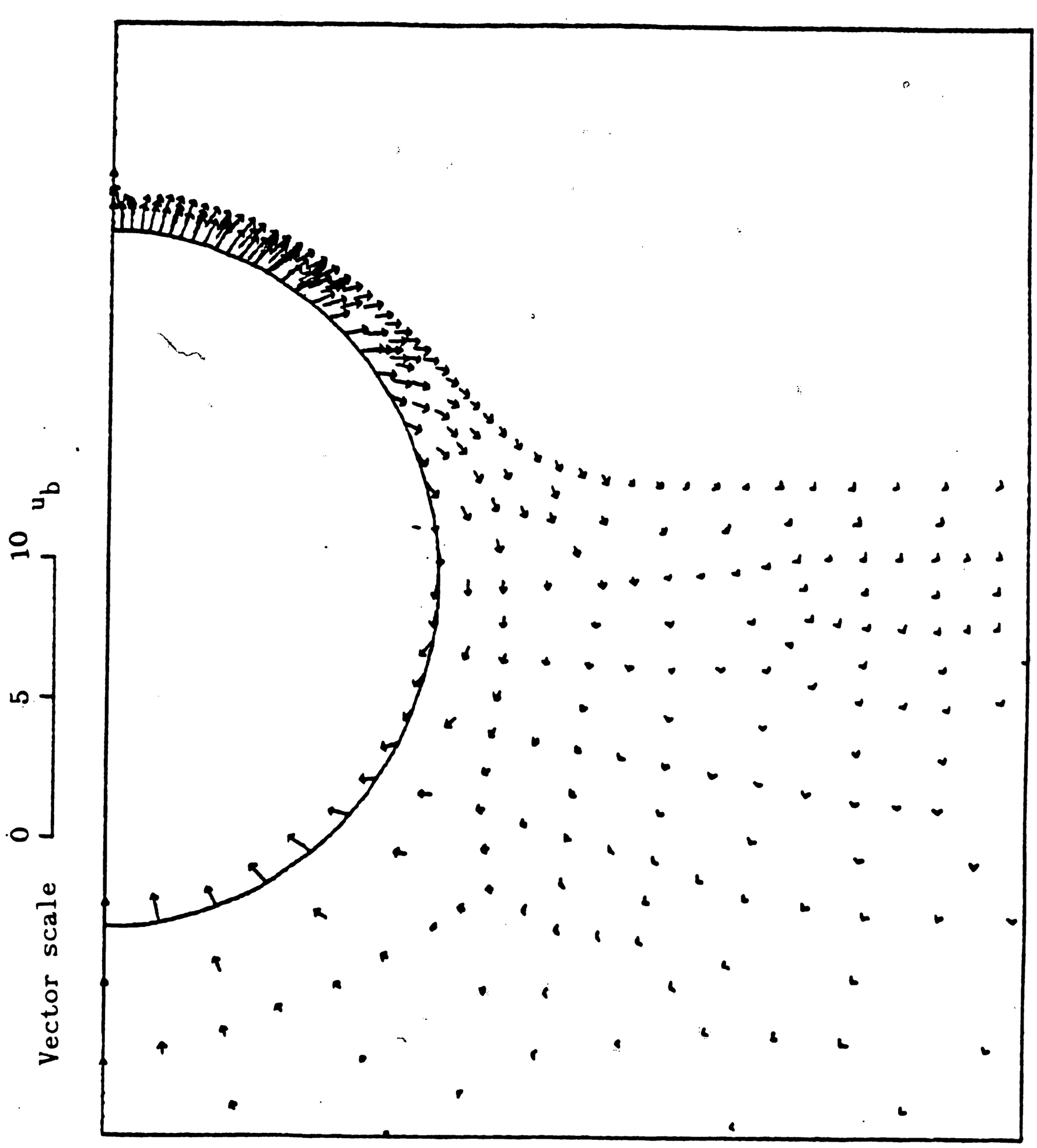

Figure 57. The vector field of absolute particle velocity highlighting the area near to the bubble for bubble center height at 19.85 d_b

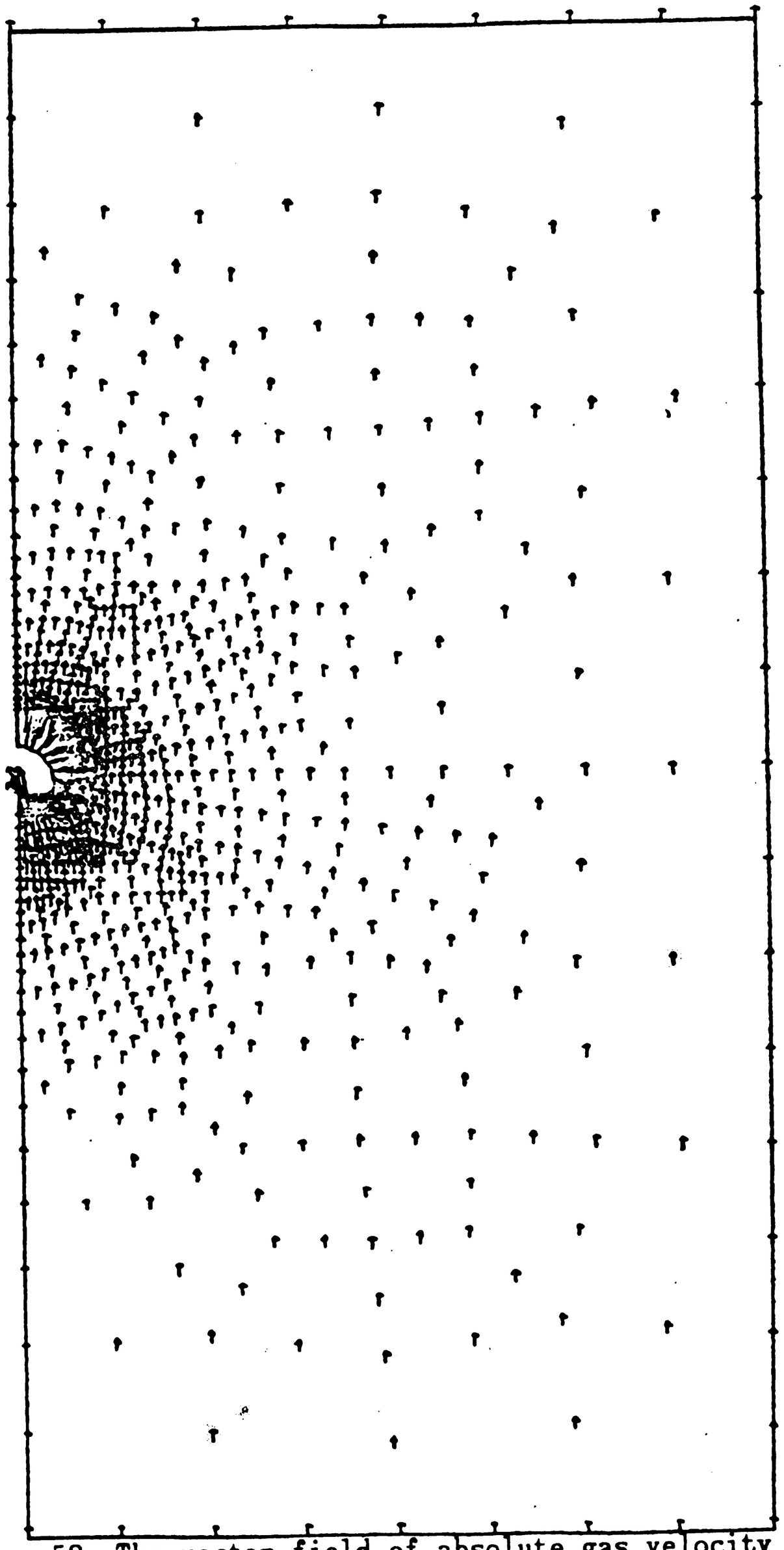

Figure 58. The vector field of absolute gas velocity for bubble center height at 10 d_b and K = 0.5

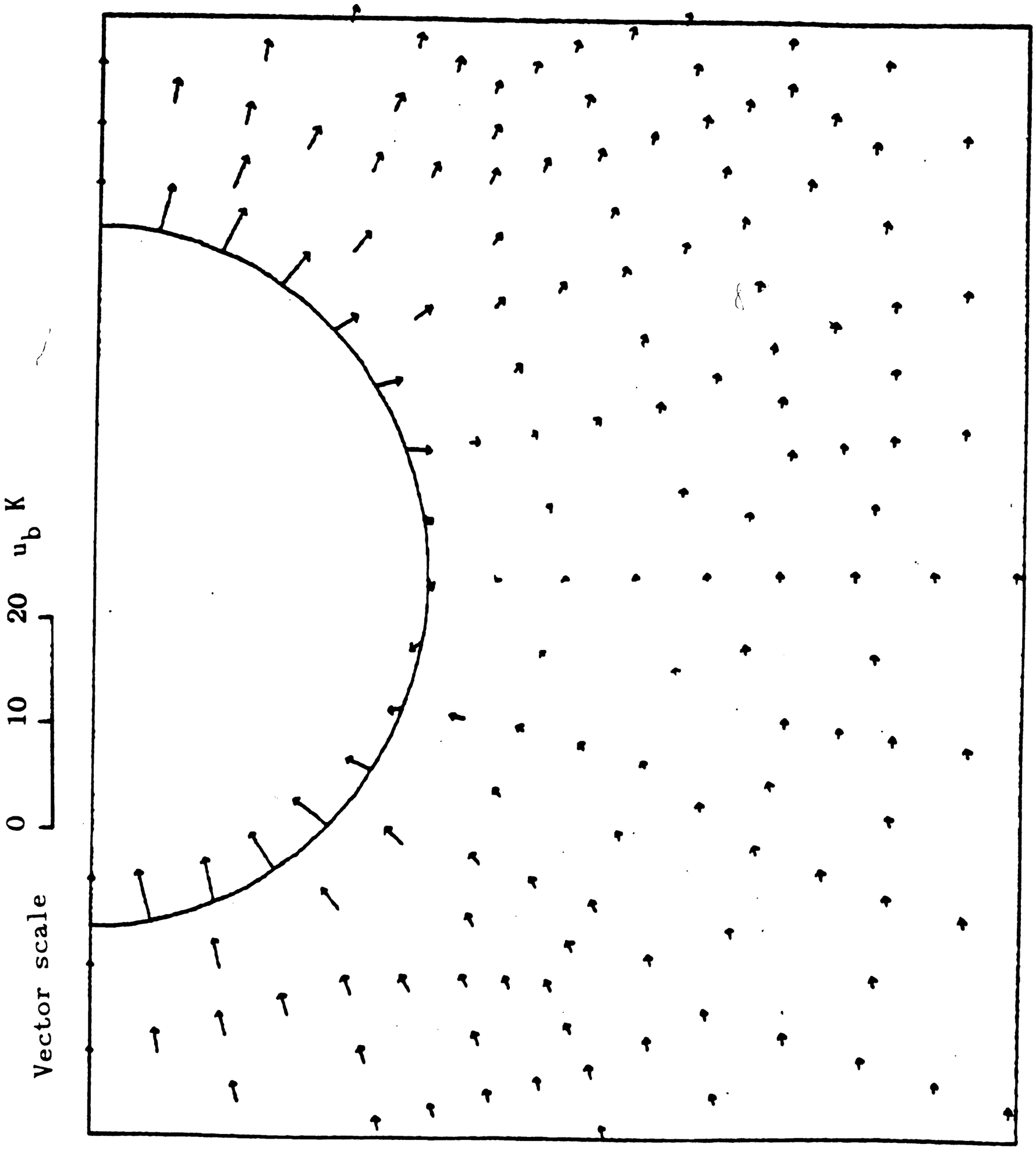

Figure 59. The vector field of absolute gas velocity highlighting the area near to the bubble for bubble center height at 10 d_b and K = 0.5

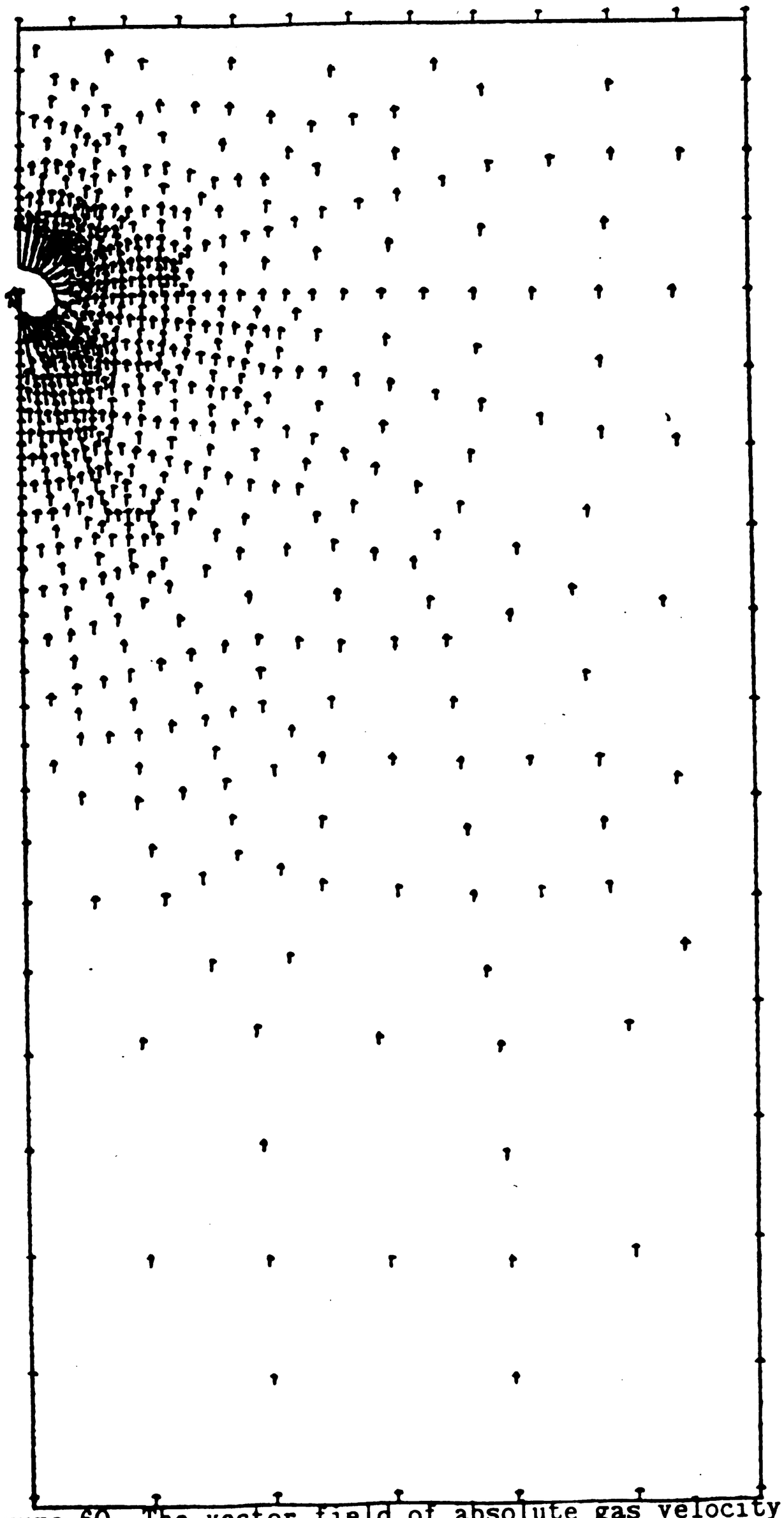

Figure 60. The vector field of absolute gas velocity for bubble center height at 16.25 d_b and K = 0.5

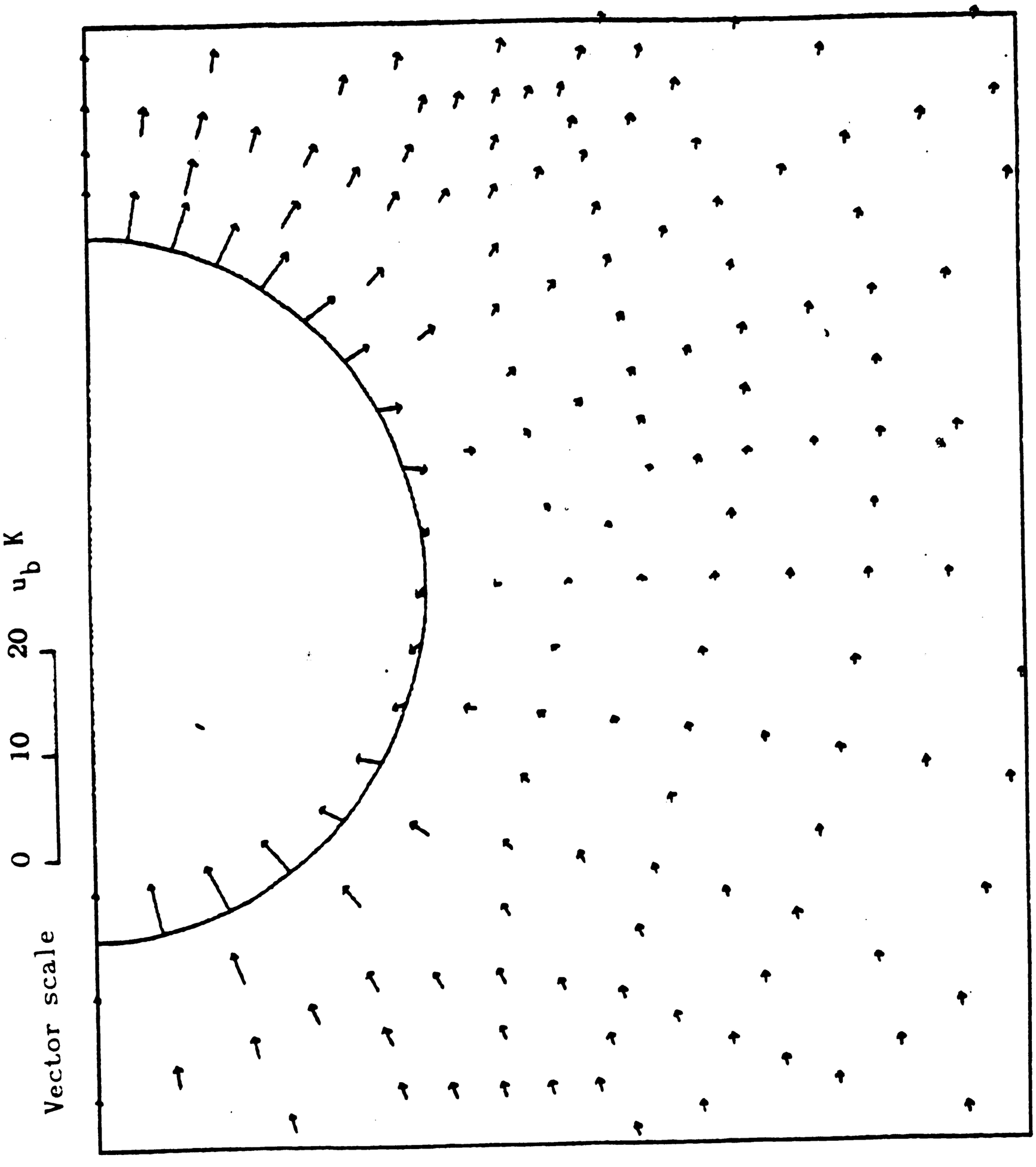

Figure 61. The vector field of absolute gas velocity highlighting the area near to the bubble for bubble center height at 16.25 d_b and K = 0.5

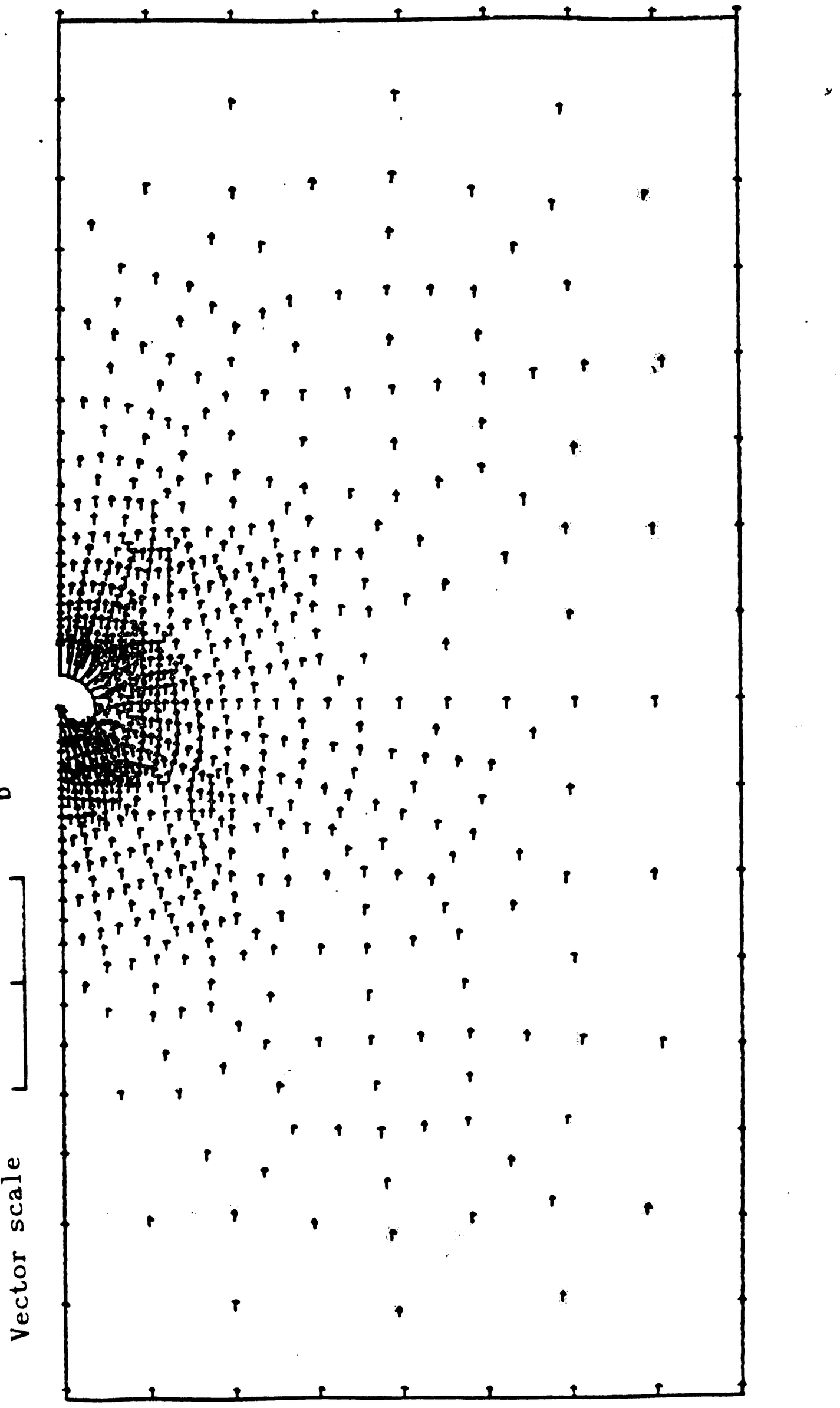

Figure 62. The vector field of absolute gas velocity for bubble center height at 10 d_b and K = 1.1

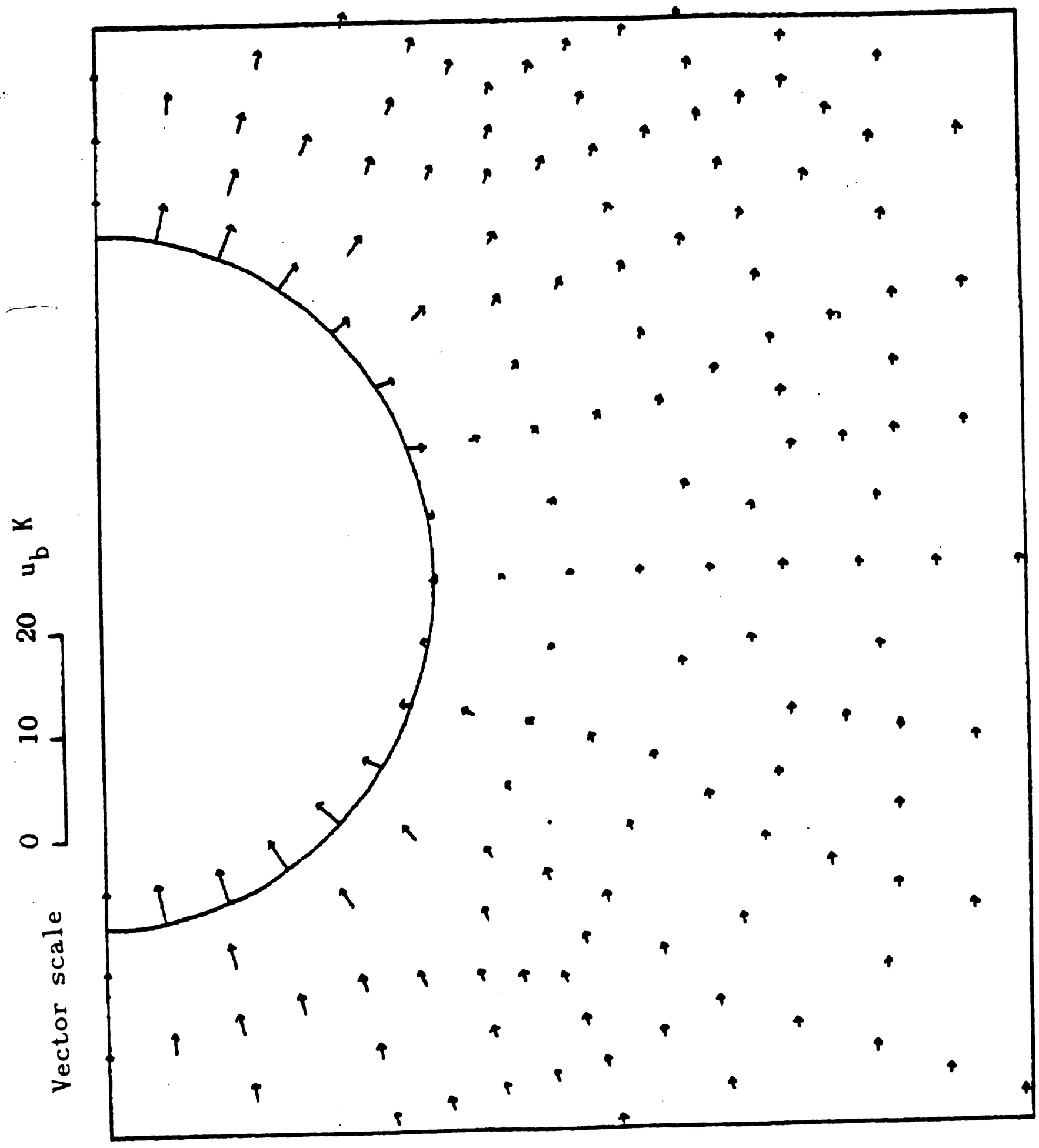

Figure 63. The vector field of absolute gas velocity highlighting the area near to the bubble for bubble center height at 10 d_b and K = 1.1

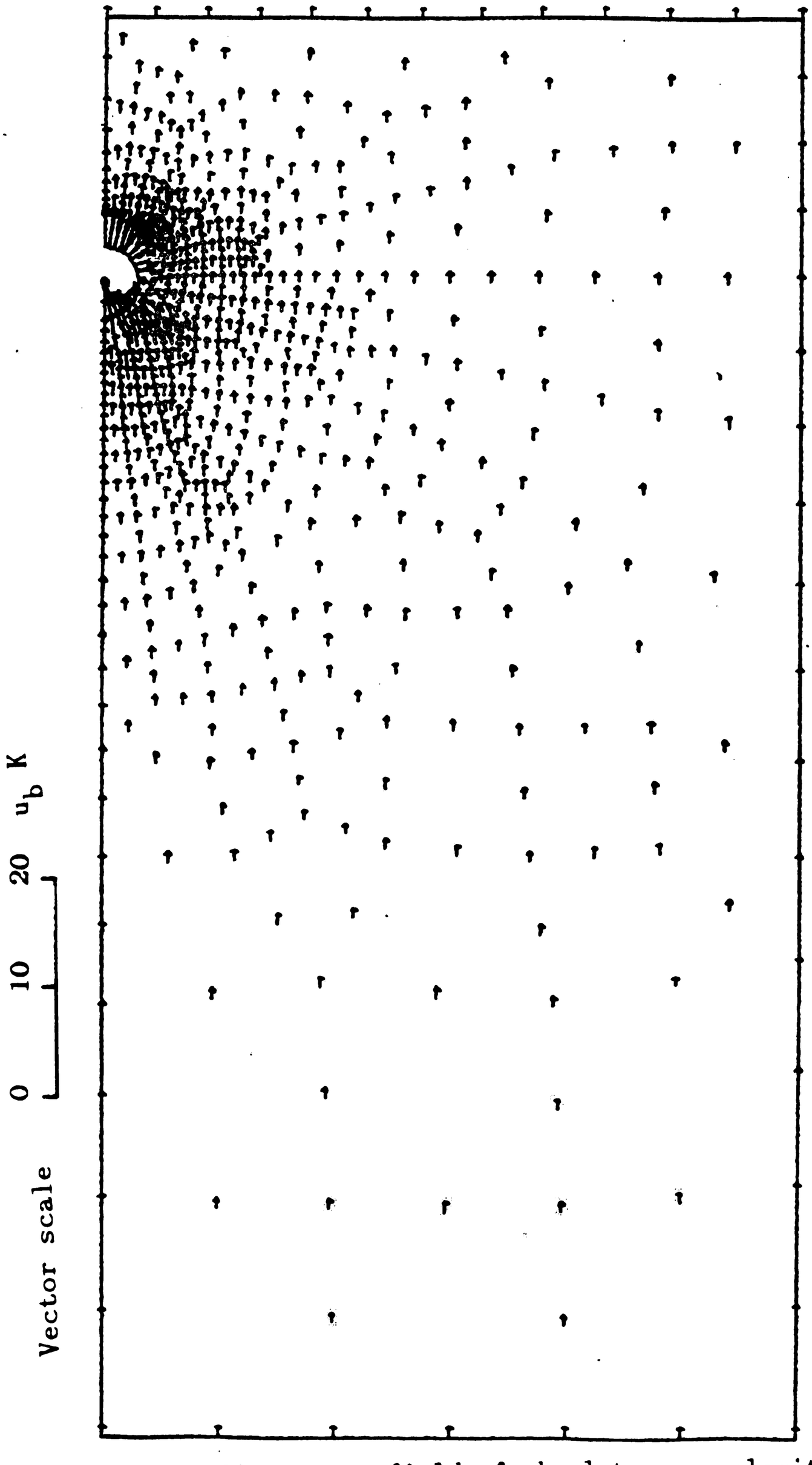

Figure 64. The vector field of absolute gas velocity for bubbel center height at 16.25 d_b and K = 1.1

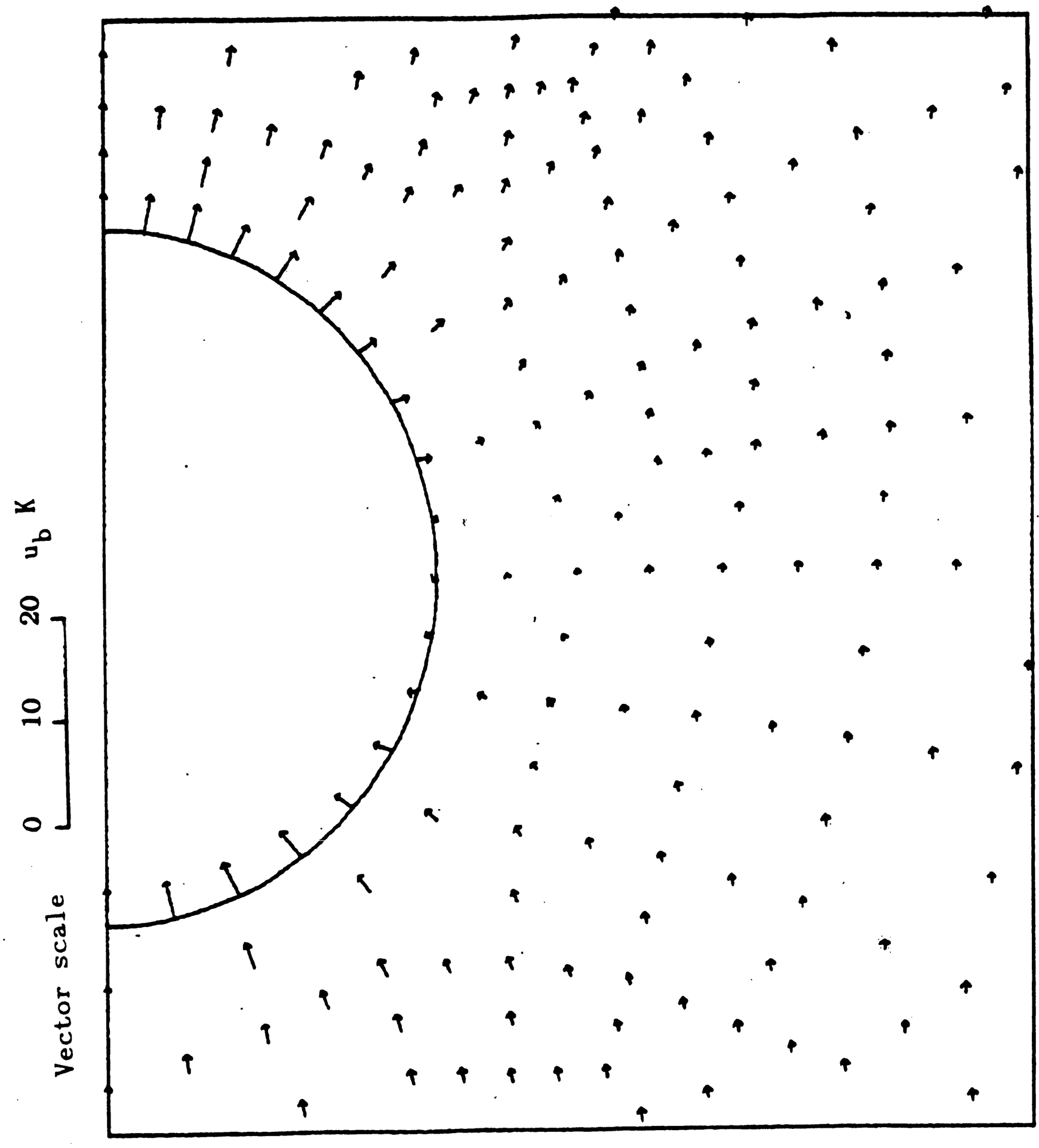

Figure 65. The vector field of absolute gas velocity
highlighting the area near to the bubble
for bubble center height at 16.25 d_b and K = 1.1

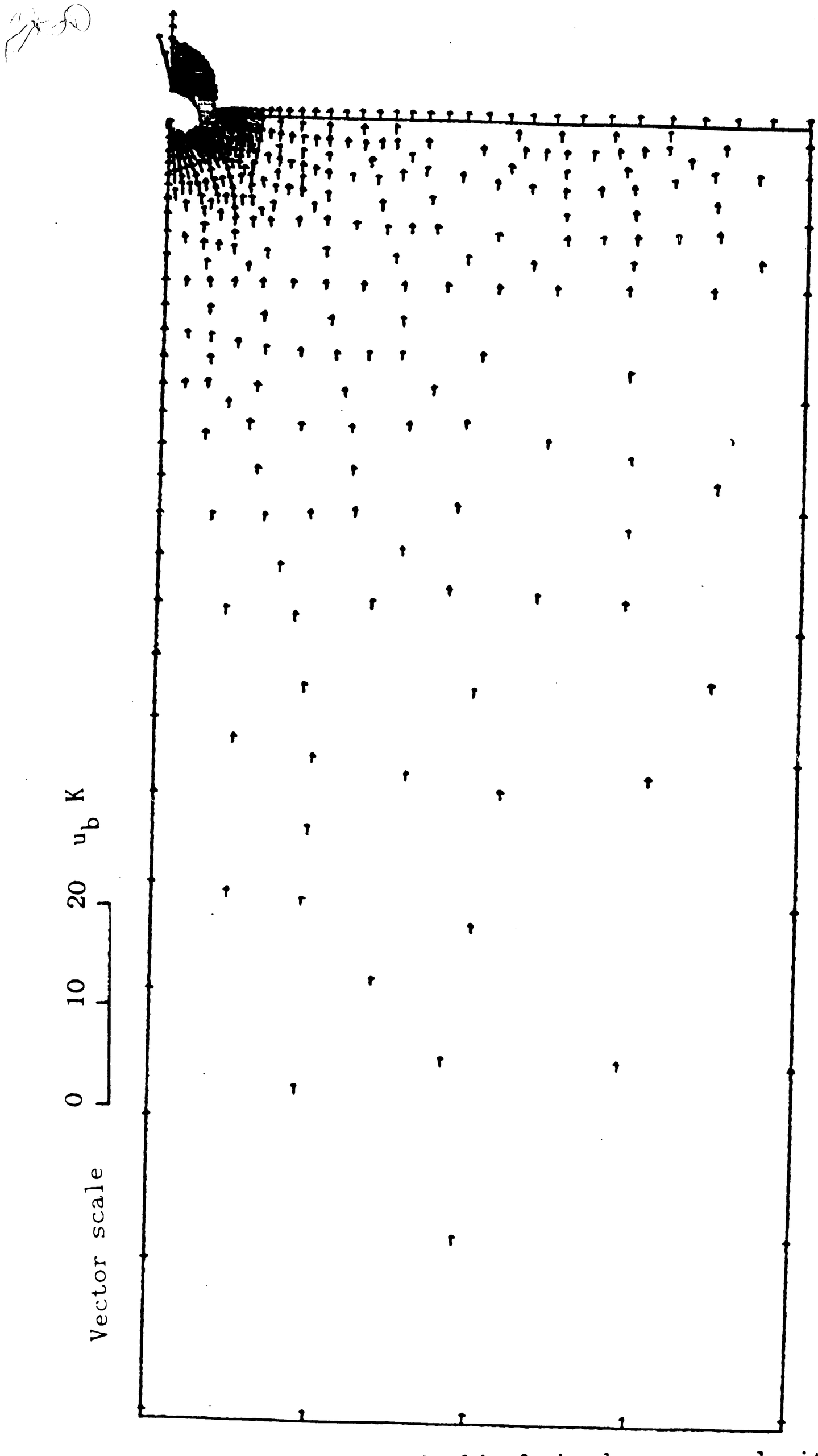

Figure 66. The vector field of absolute gas velocity for bubble center height at 19.85 d_b and K = 1.1

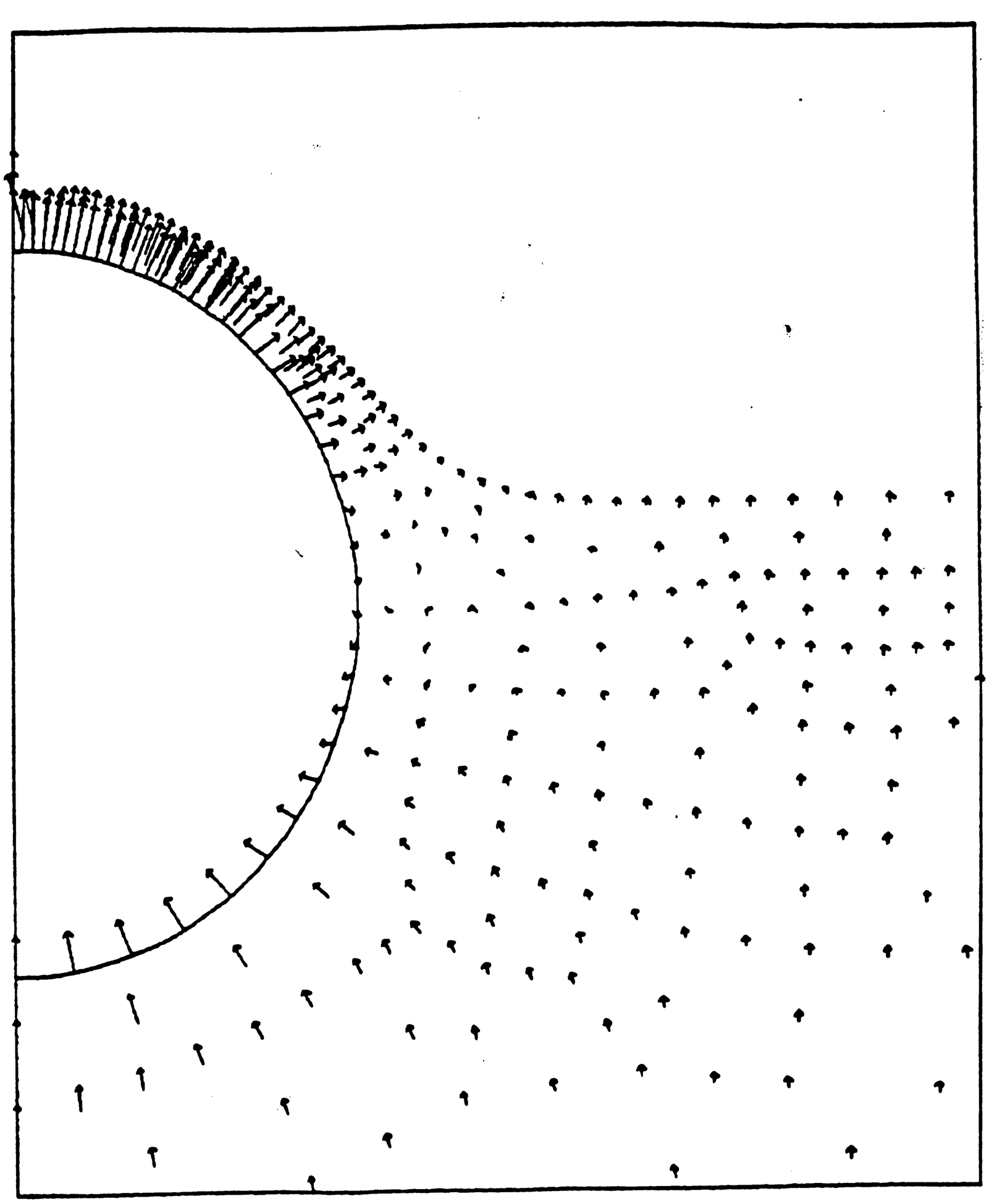

Figure 67. The vector field of absolute gas velocity highlighting the area near to the bubble for bubble center height at 19.85 d_b and K = 1.1

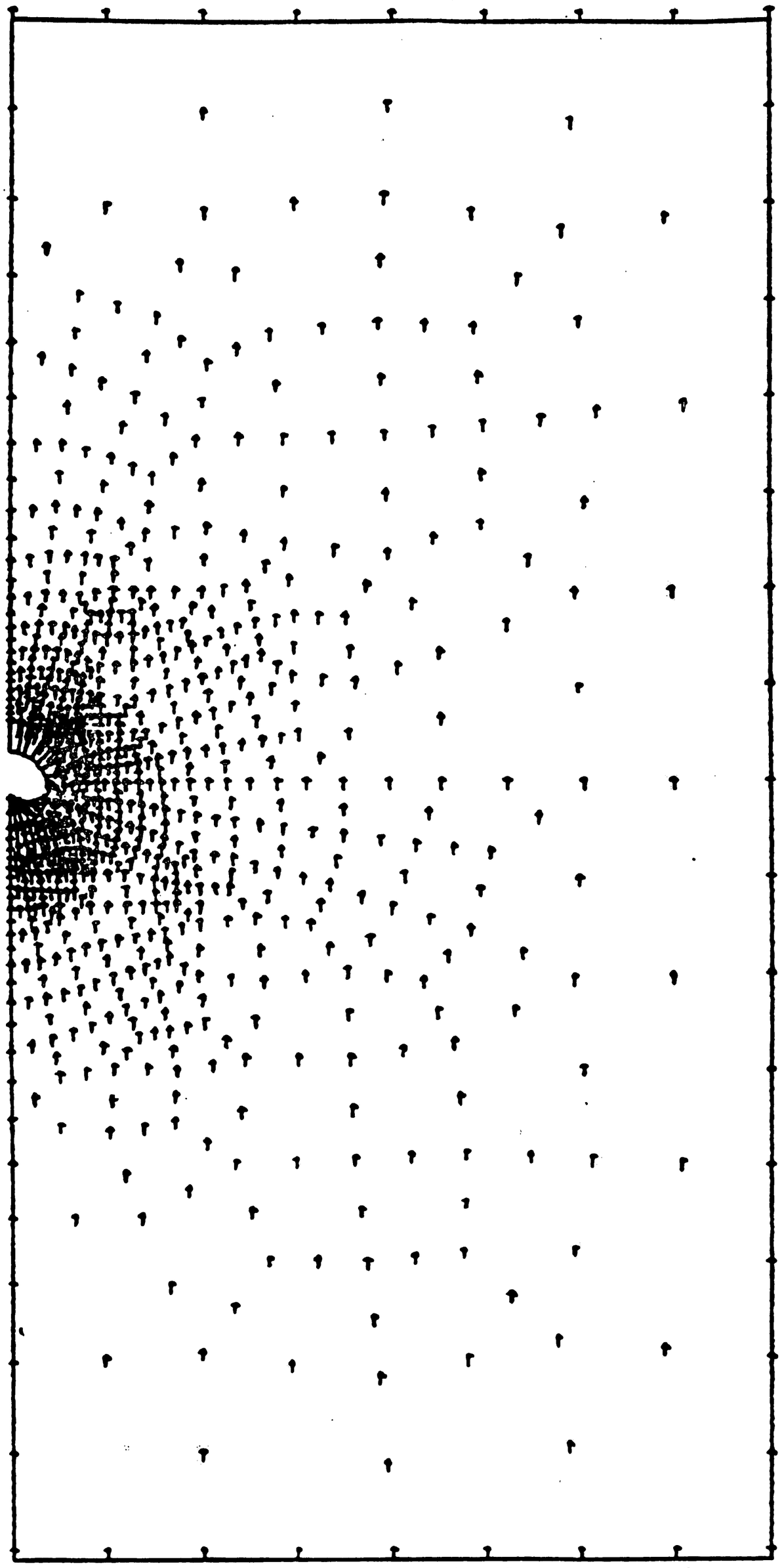

Figure 68. The vector field of absolute gas velocity for bubble center height at 10 d_b and K = 10

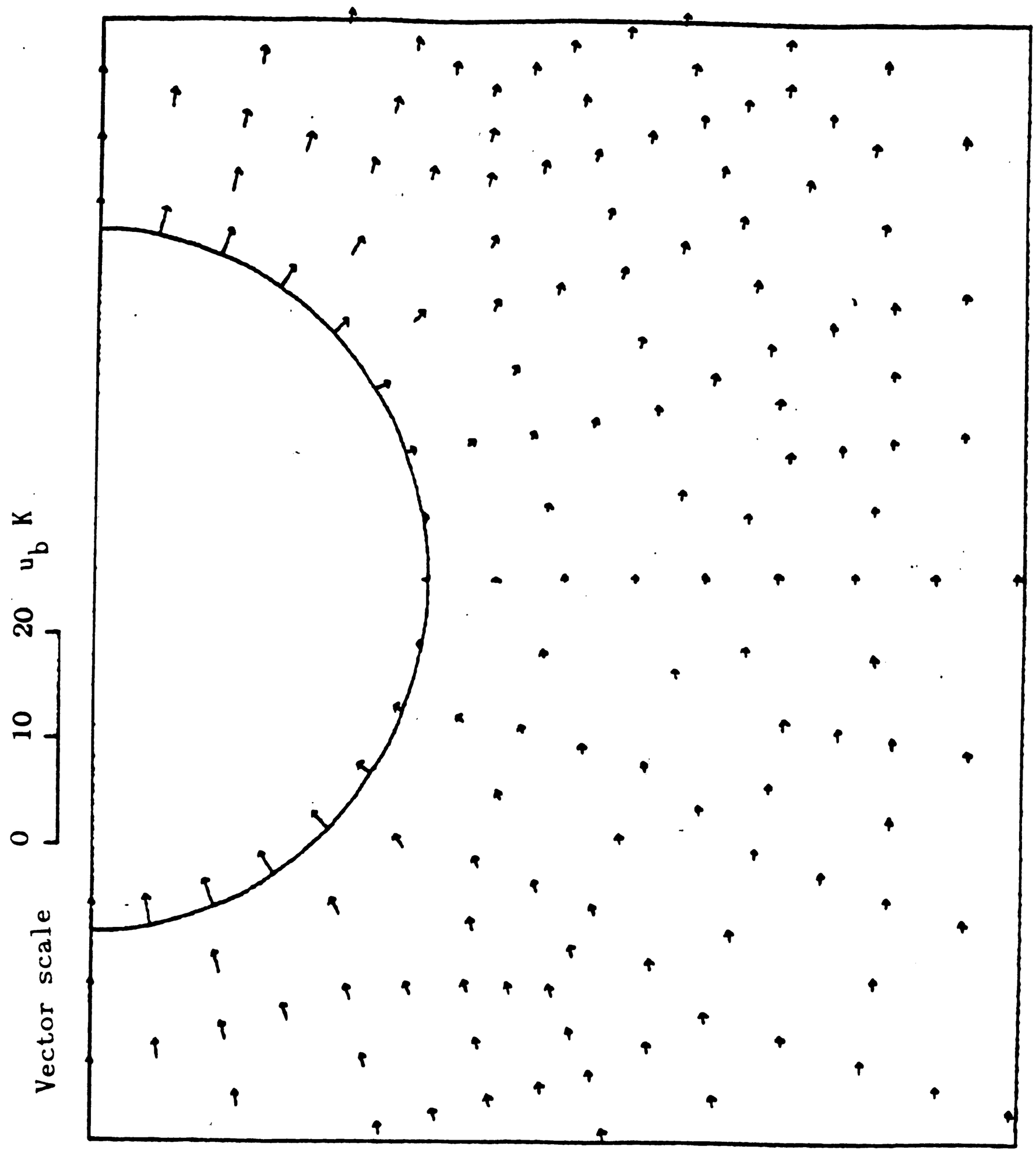

Figure 69. The vector field of absolute gas velocity highlighting the area near to the bubble for bubble center height at 10 d_b and K = 10

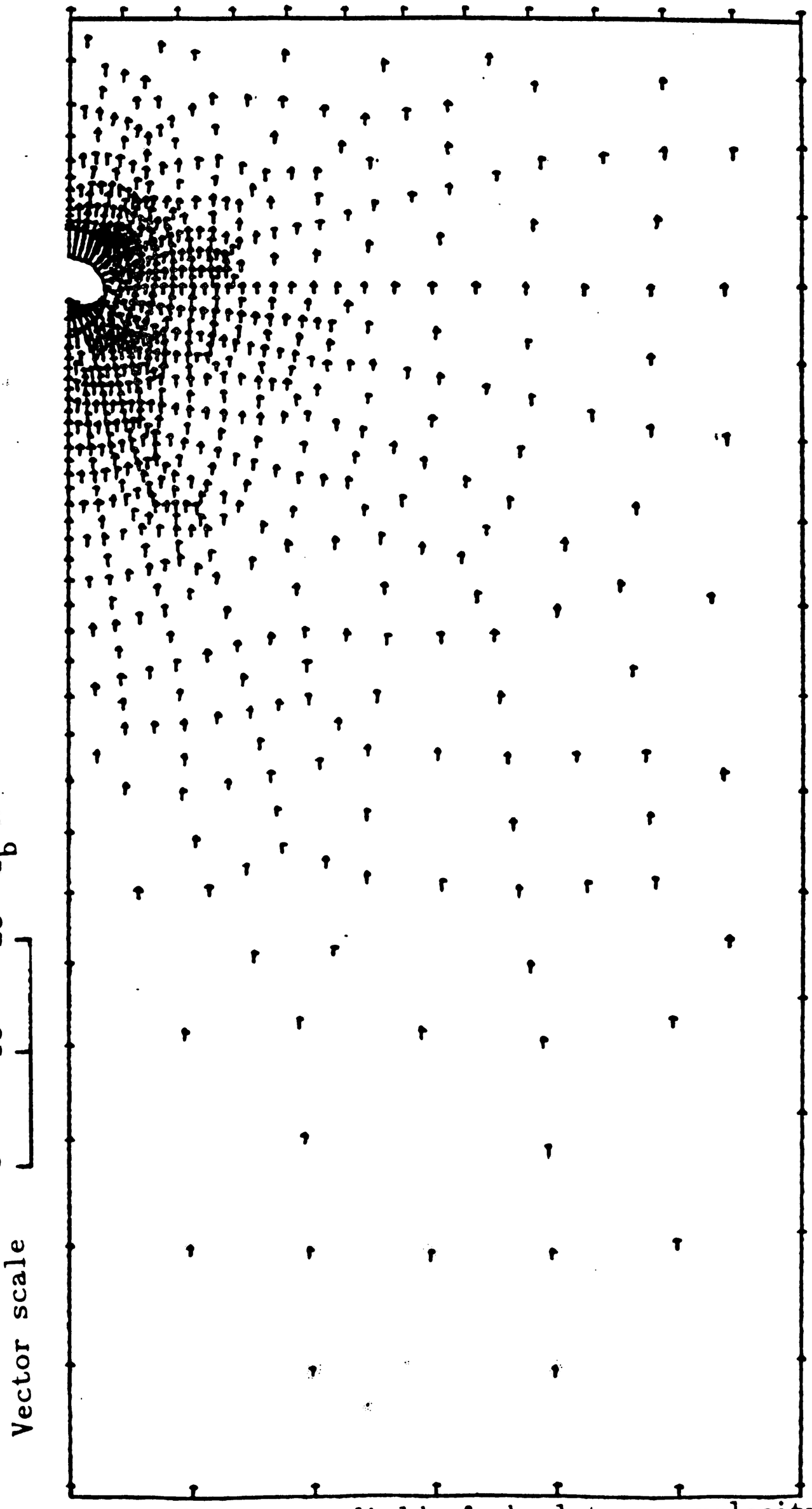

Figure 70. The vector field of absolute gas velocity for bubble center height at 16.25 d_b and K = 10

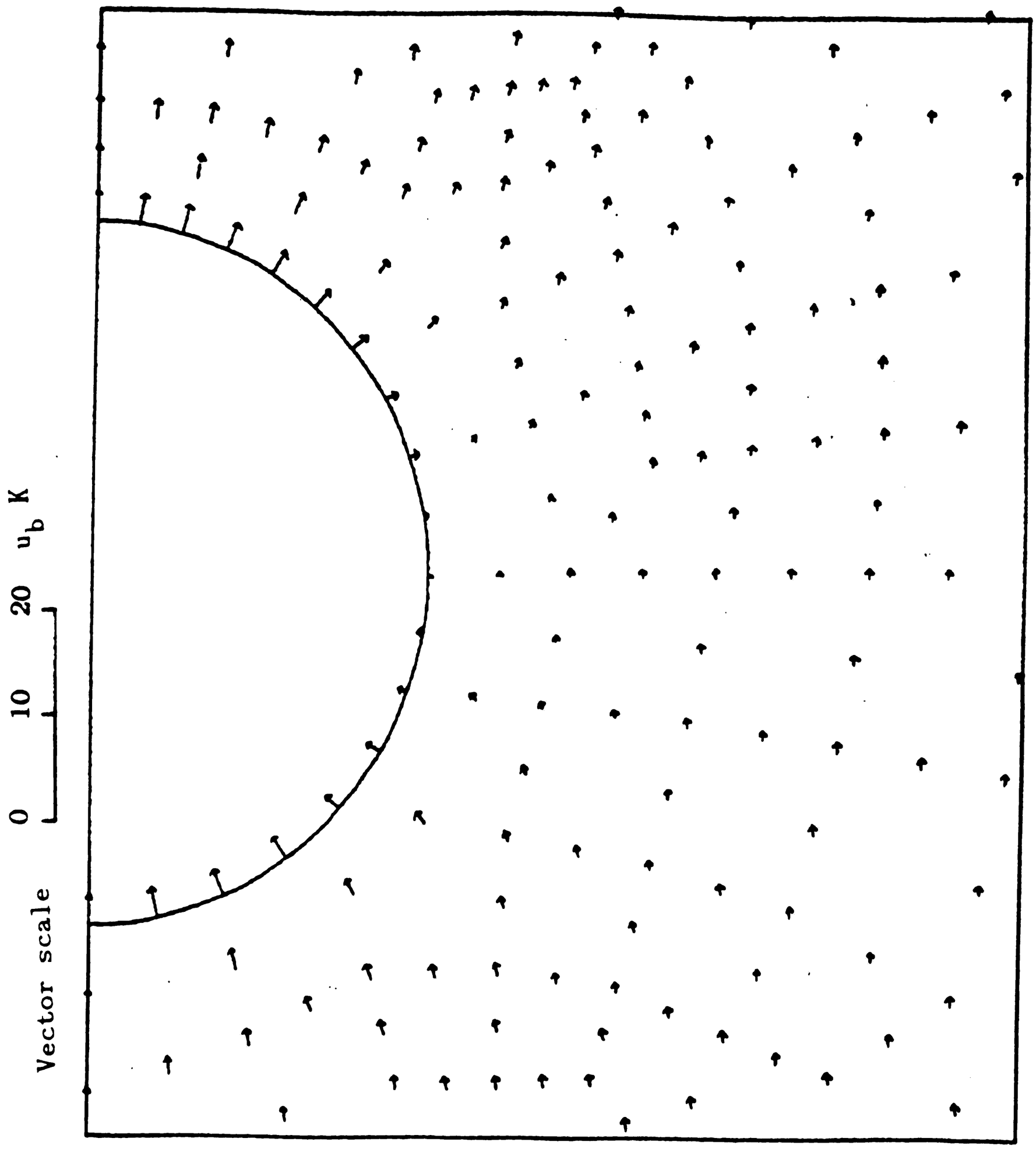

Figure 71. The vector field of absolute gas velocity highlighting the area near to the bubble for bubble center height at 16.25 d_b and K = 10

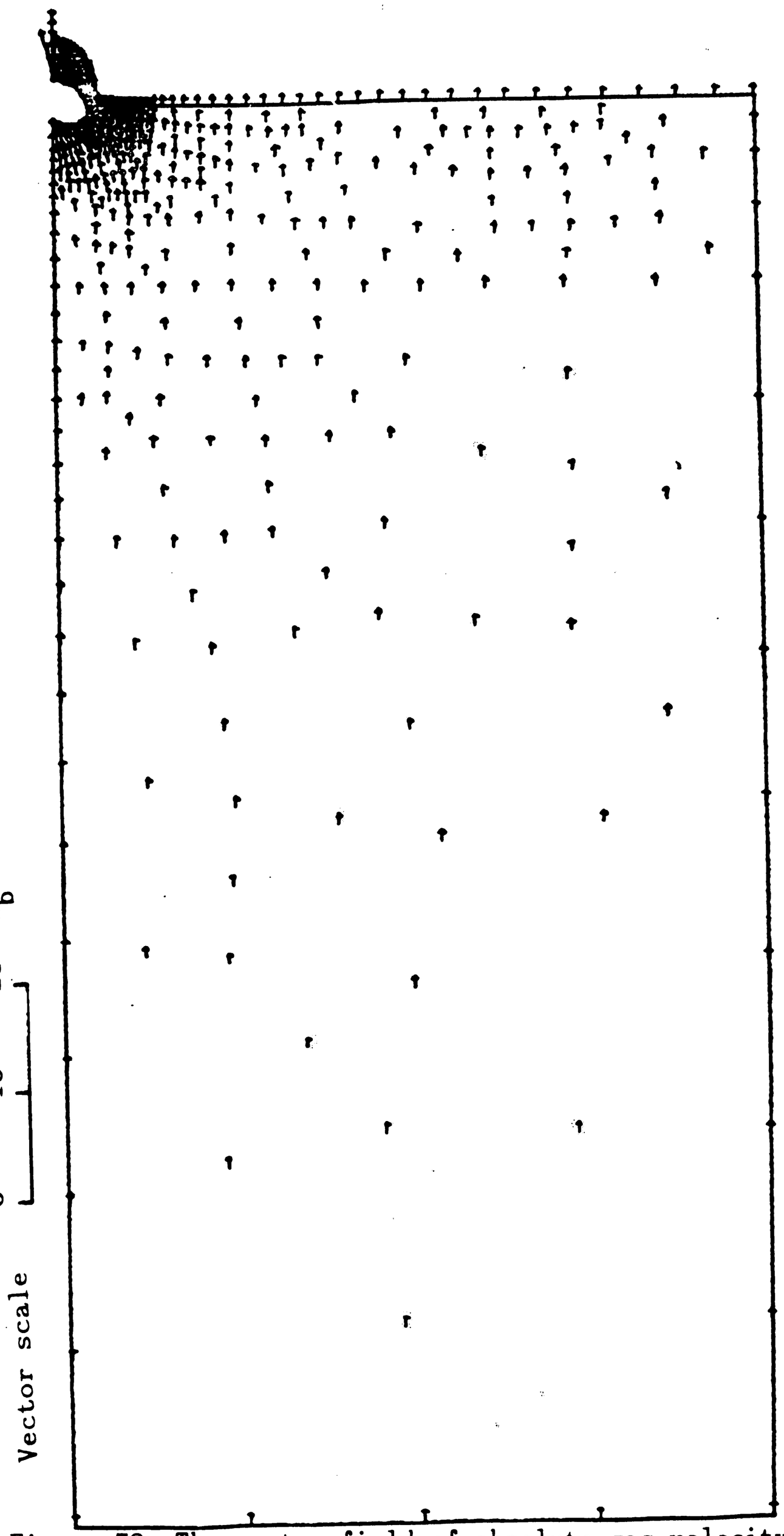

Figure 72. The vector field of absolute gas velocity for bubble center height at 19.85 d_b and K = 10

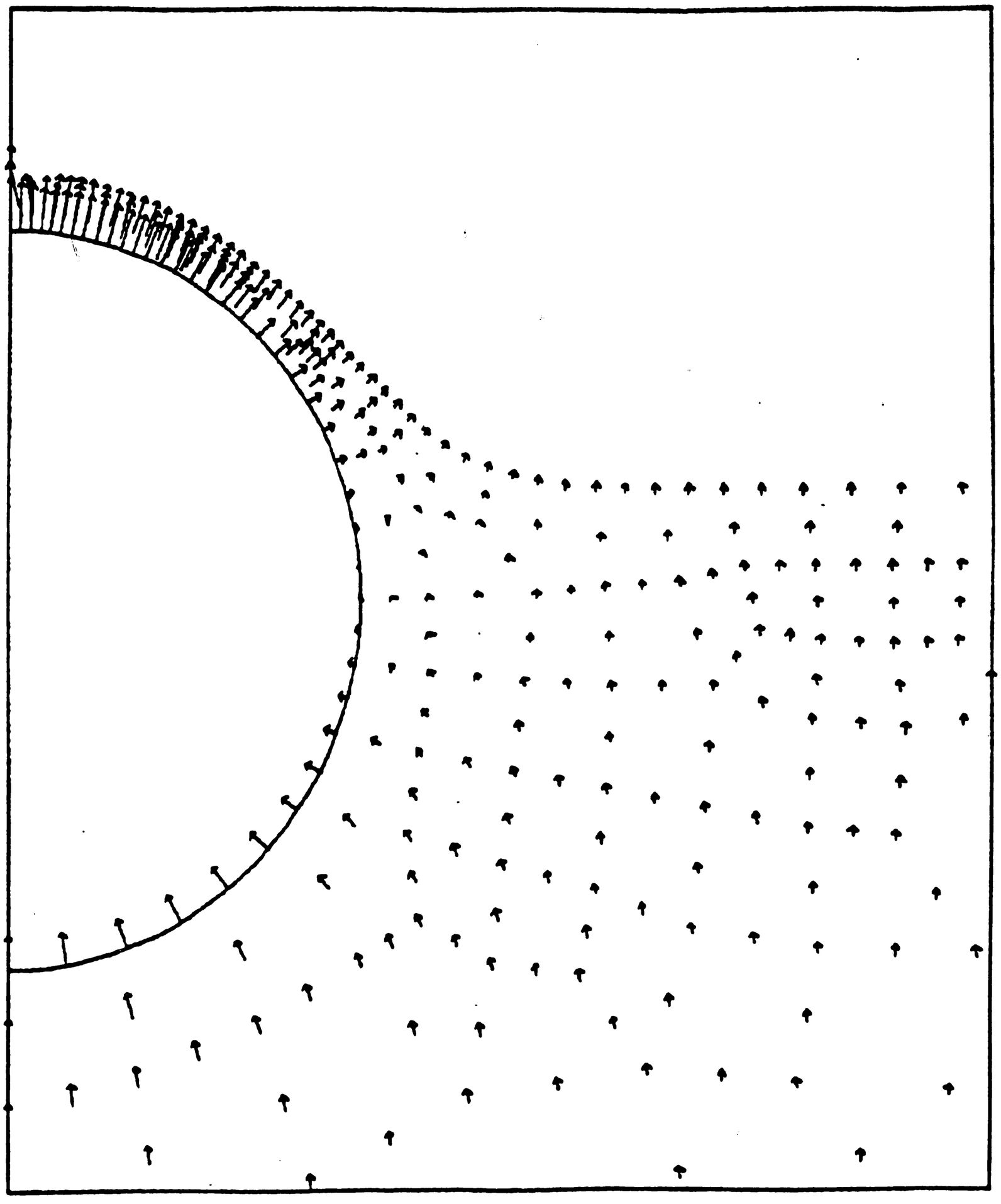

Figure 73. The vector field of absolute gas velocity highlighting the area near to the bubble for bubble center height at 19.85 d_b and K = 10

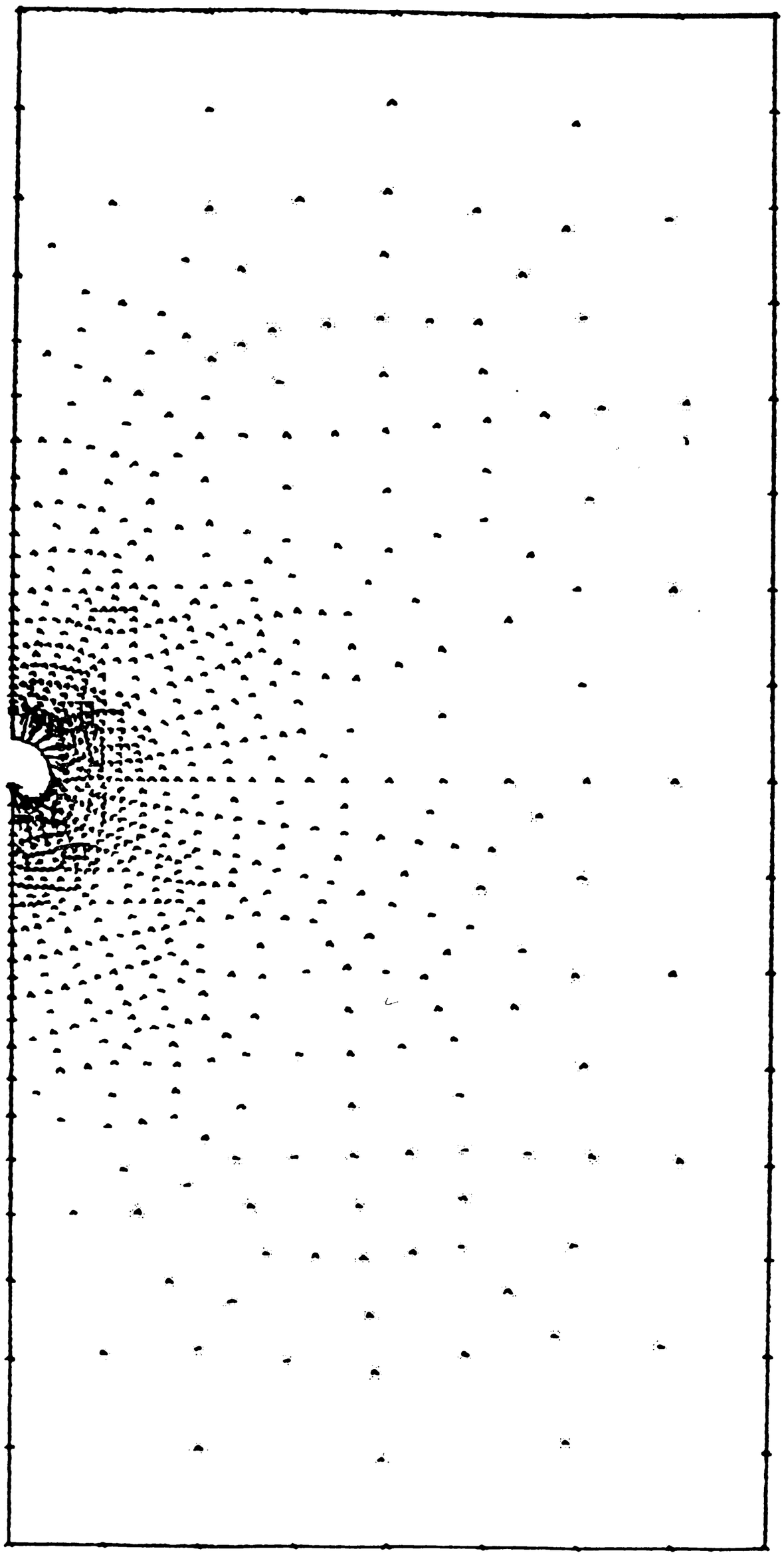

Figure 74. The vector field of gas velocity relative to the bubble for bubble center height at 10 d_b and K = 1.1

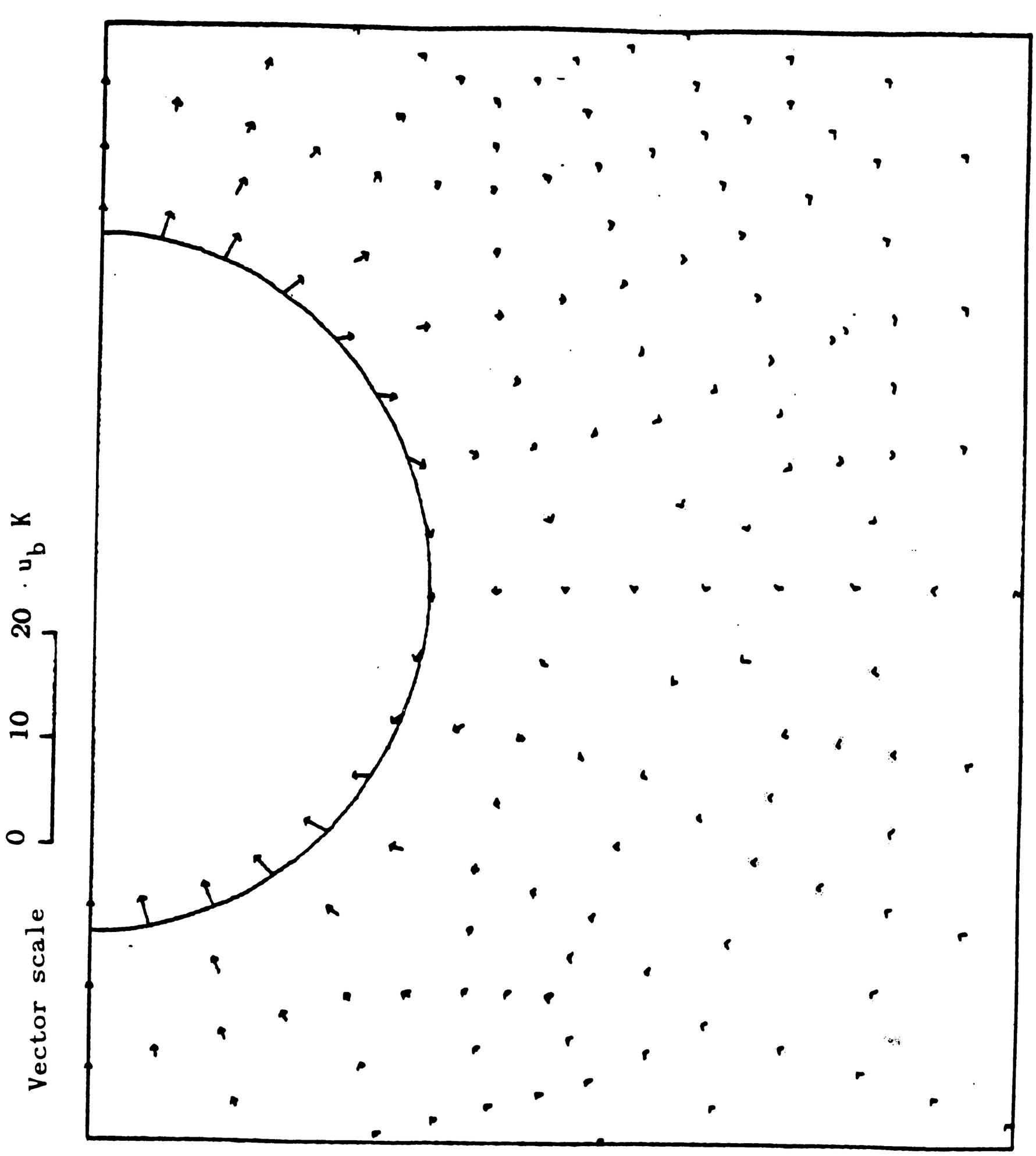

Figure 75. The vector field of gas velocity relative to the bubble highlighting the area near to the bubble for bubble center height at 10 d_b and K = 1.1

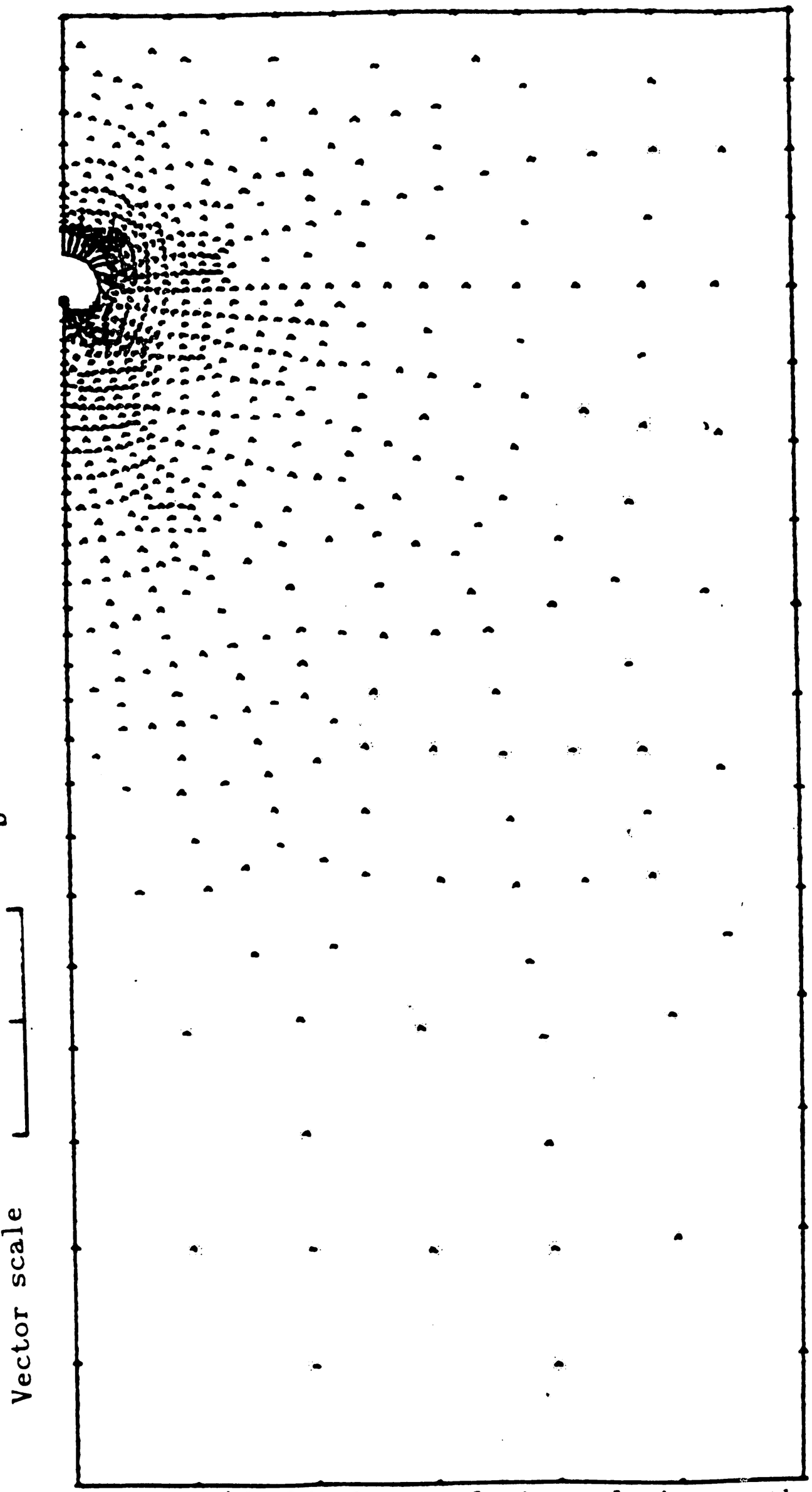

Figure 76. The vector field of gas velocity relative to the bubble for bubble center height at 16.25 d_b and K = 1.1

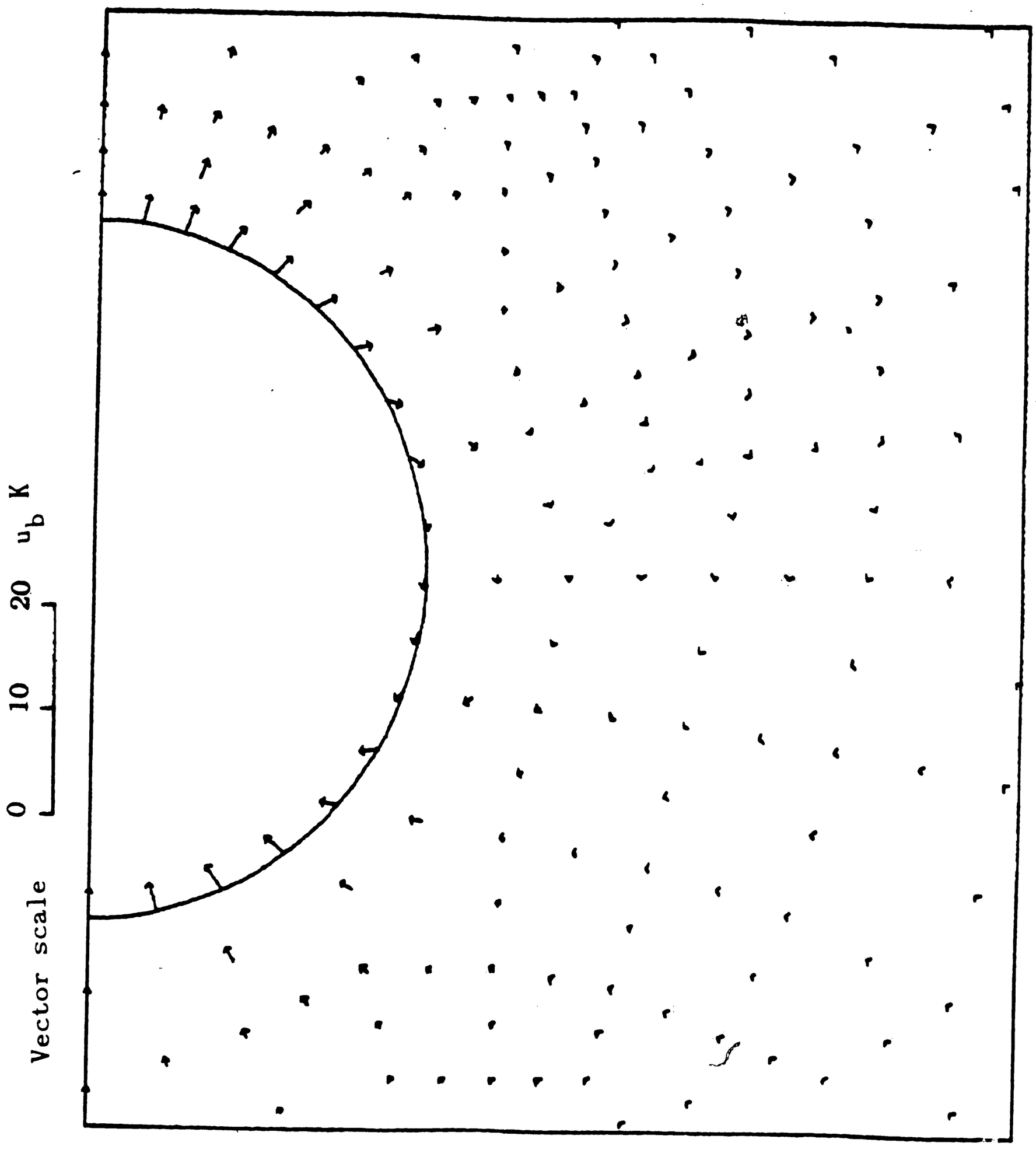

Figure 77. The vector field of gas velocity relative to the bubble highlighting the area near to the bubble for bubble center height at 16.25 d_b and K = 1.1

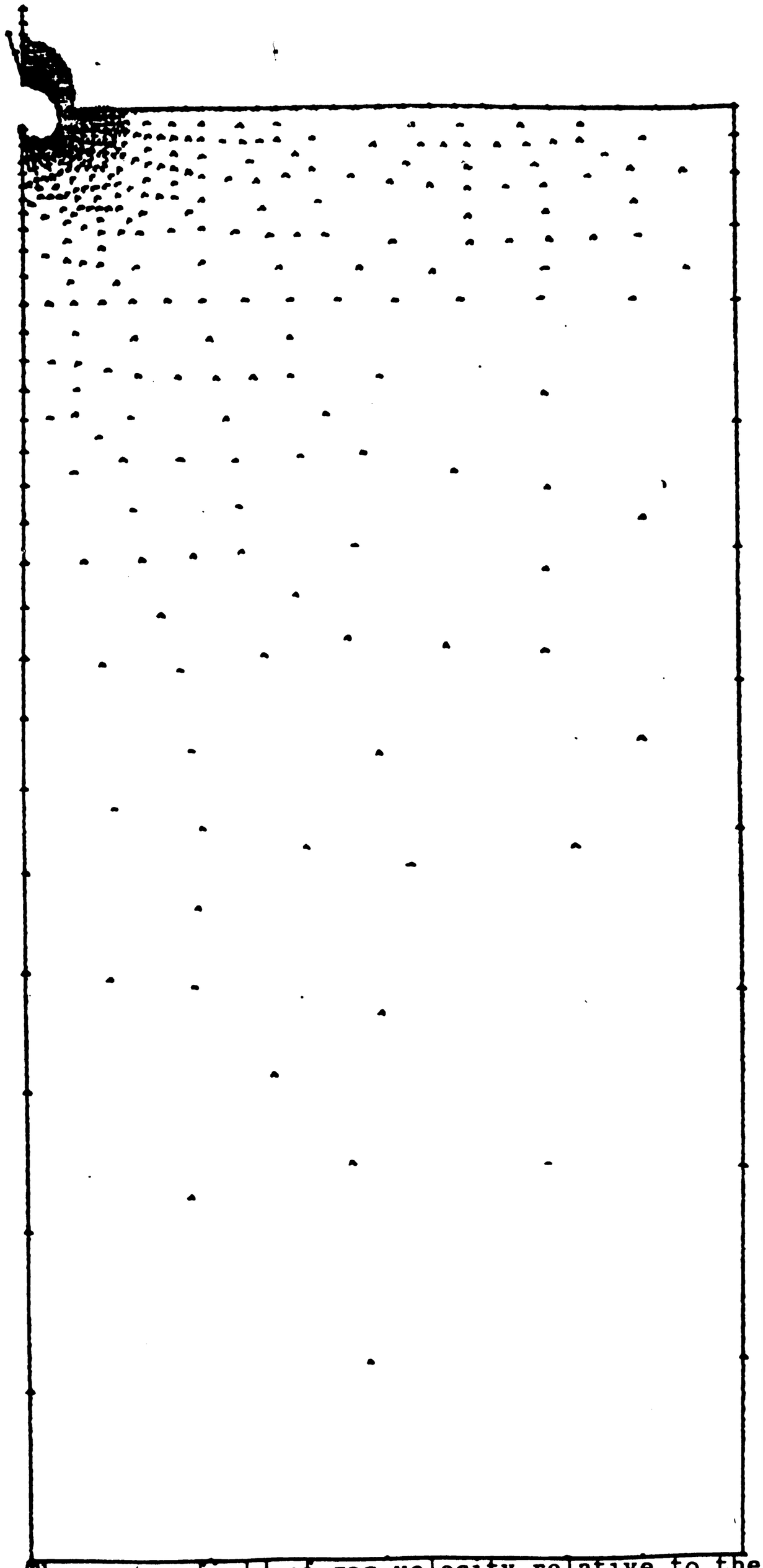

Figure 78. The vector field of gas velocity relative to the bubble for bubble center height at 19.85 d_b and K = 1.1

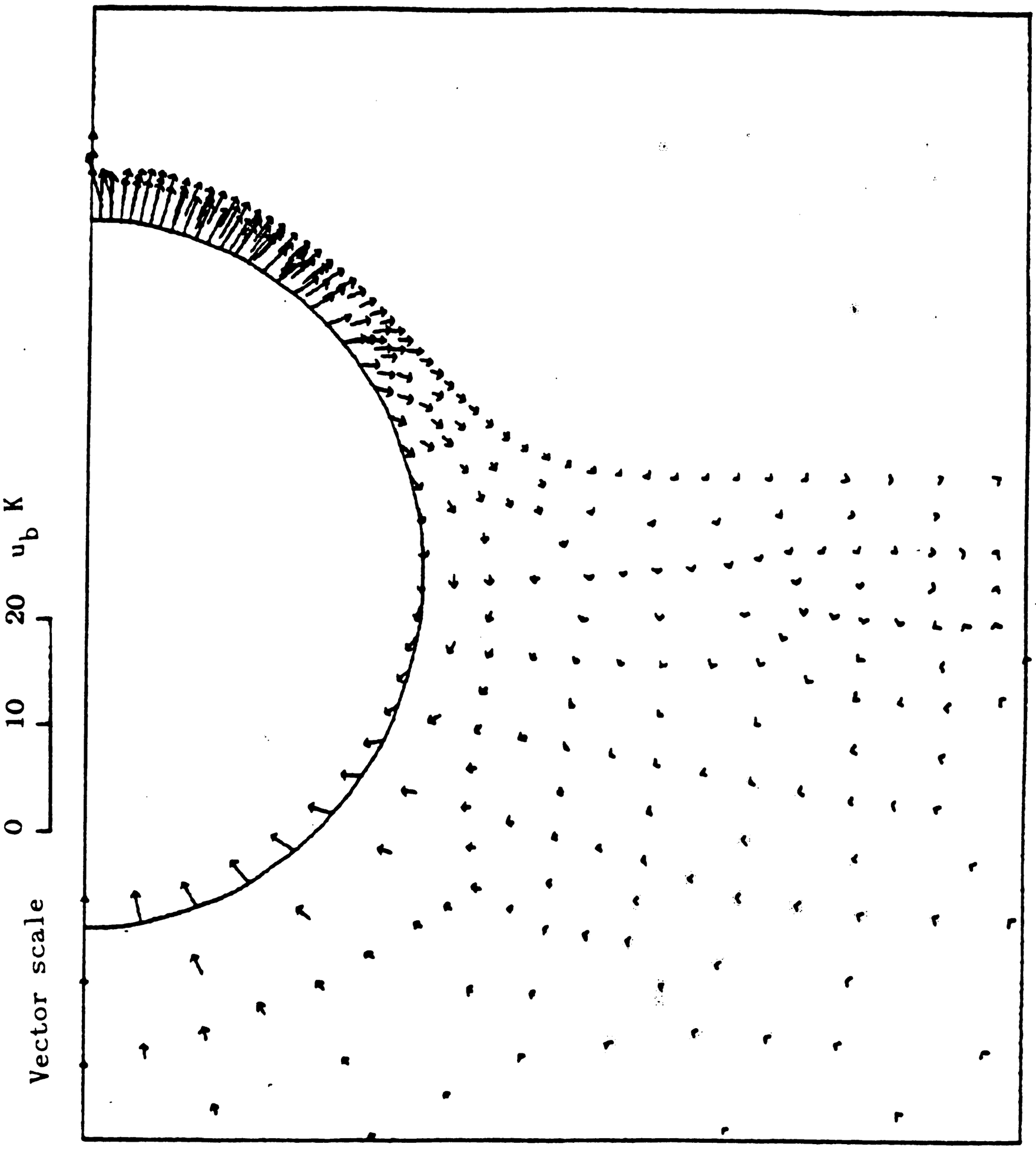

Figure 79. The vector field of gas velocity relative to the bubble highlighting the area near to the bubble for bubble center height at 19.85 d_b and K = 1.1

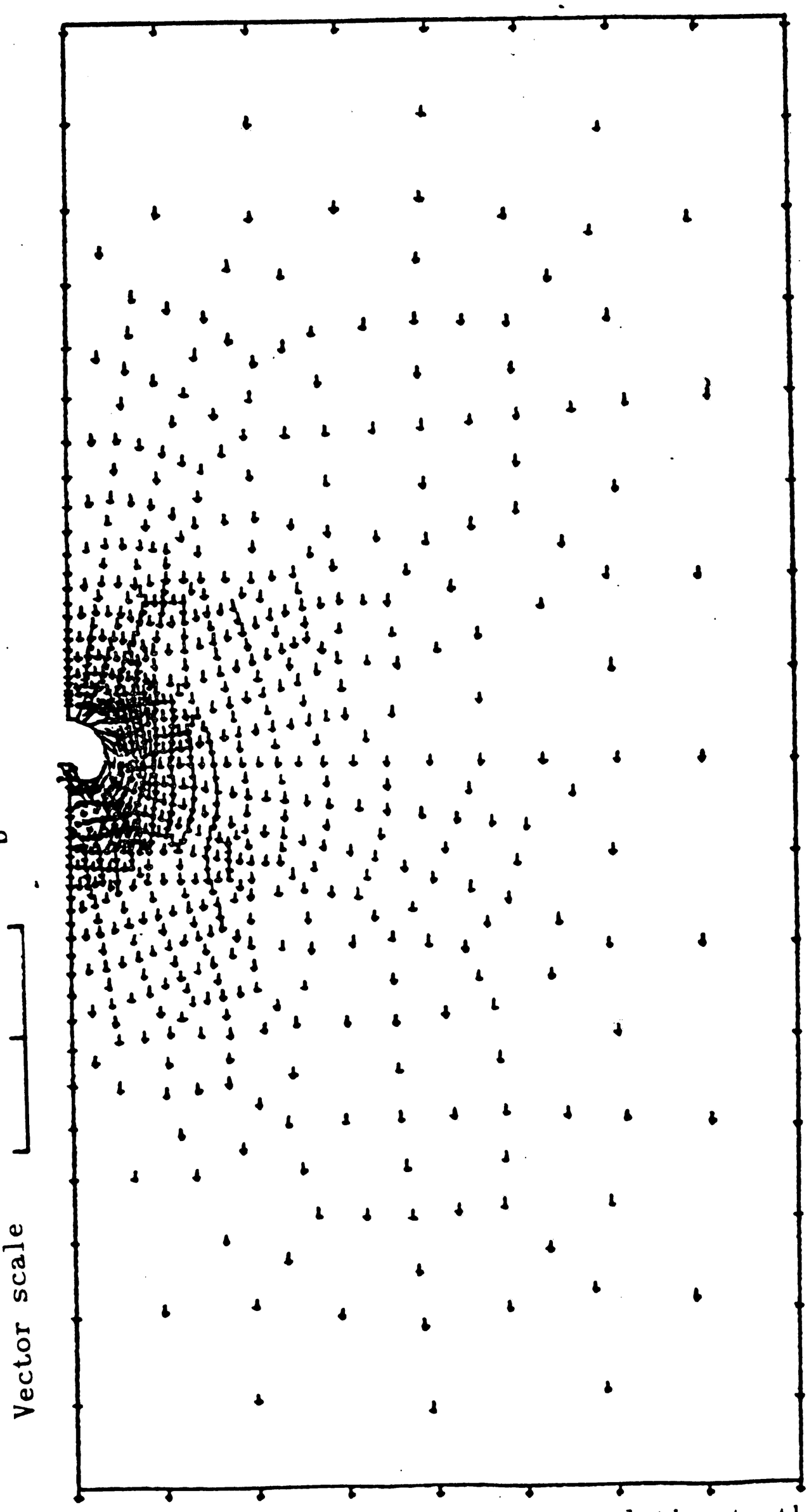

Figure 80. The vector field of gas velocity relative to the bubble for bubble center height at 10 d_b and K = 0.5

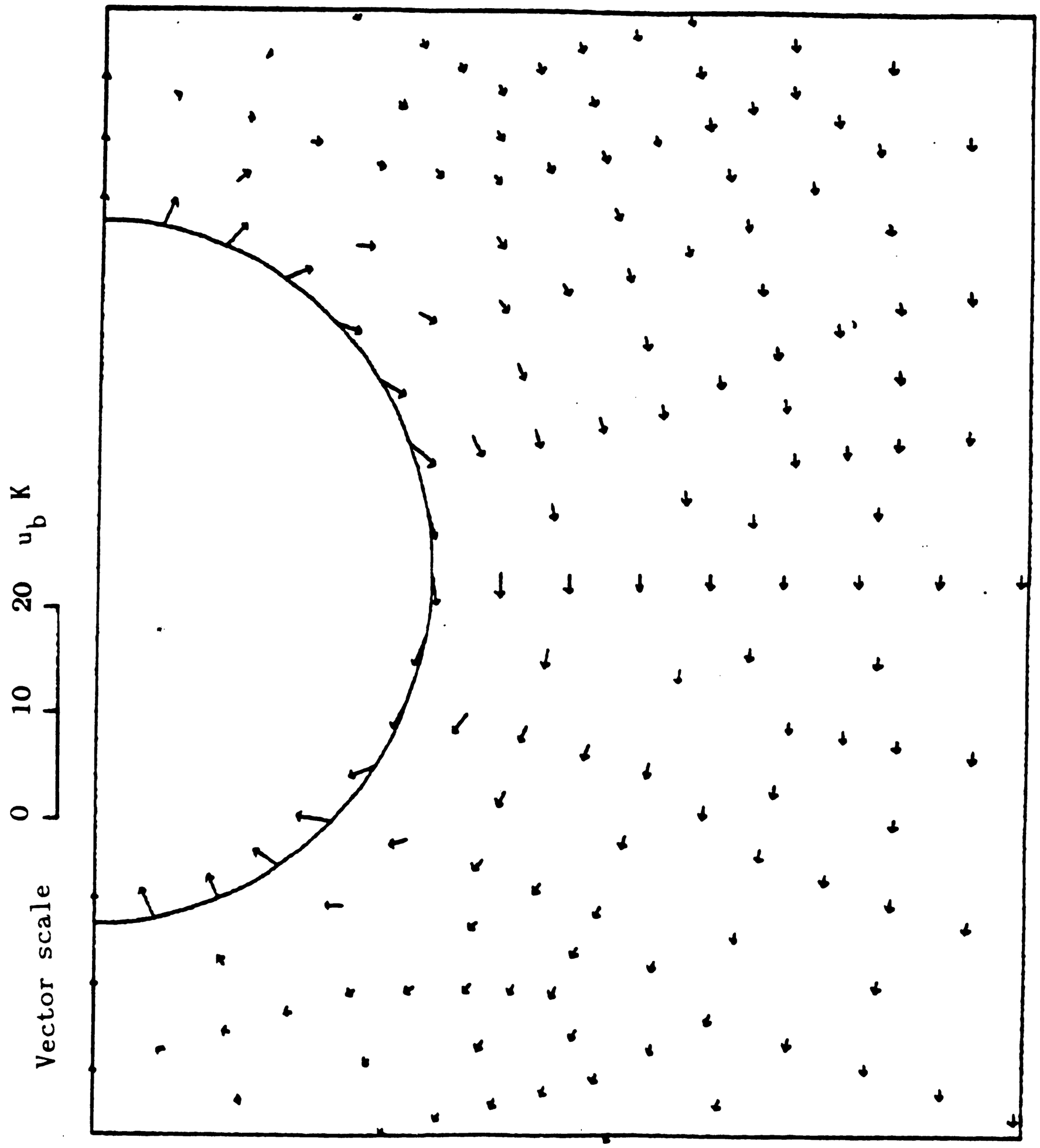

Figure 81. The vector field of gas velocity relative to the bubble highlighting the area near to the bubble for bubble center height at 10 d_b and K = 0.5

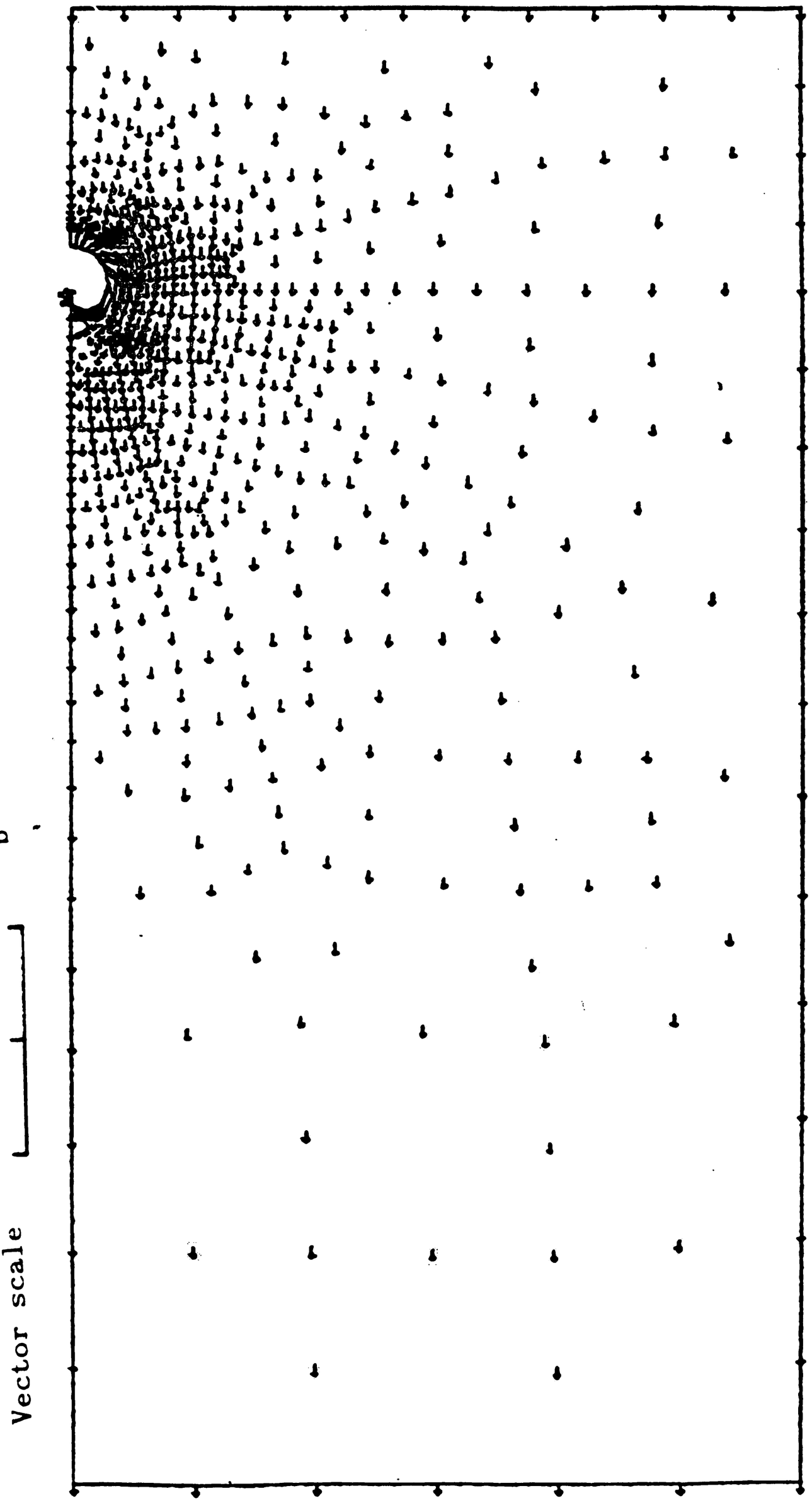

Figure 82. The vector field of gas velocity relative to the bubble for bubble center height at 16.25 d_b and K = 0.5

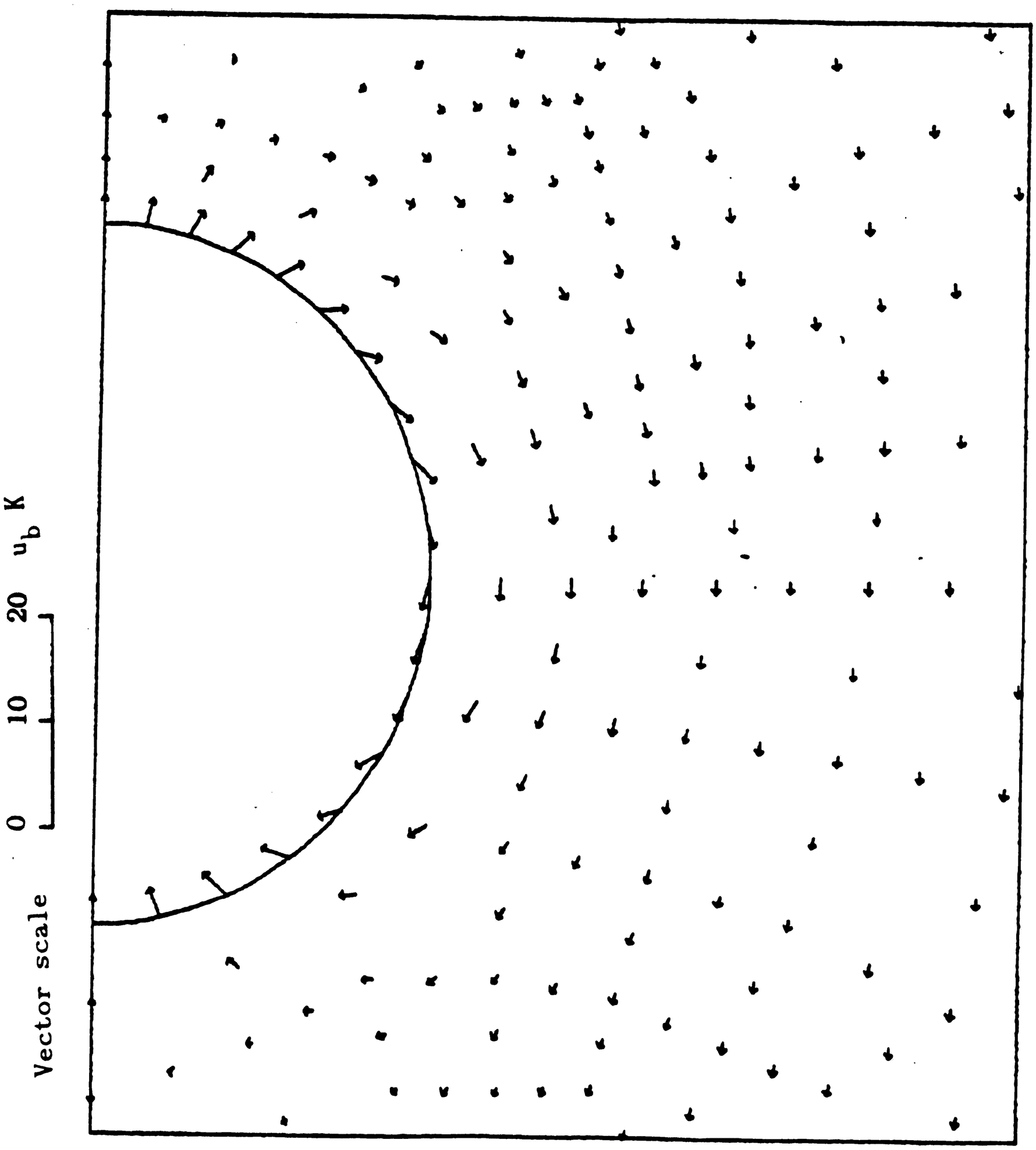

Figure 83. The vector field of gas velocity relative to the bubble highlighting the area near to the bubble for bubble center height at 16.25 d_b and K = 0.5

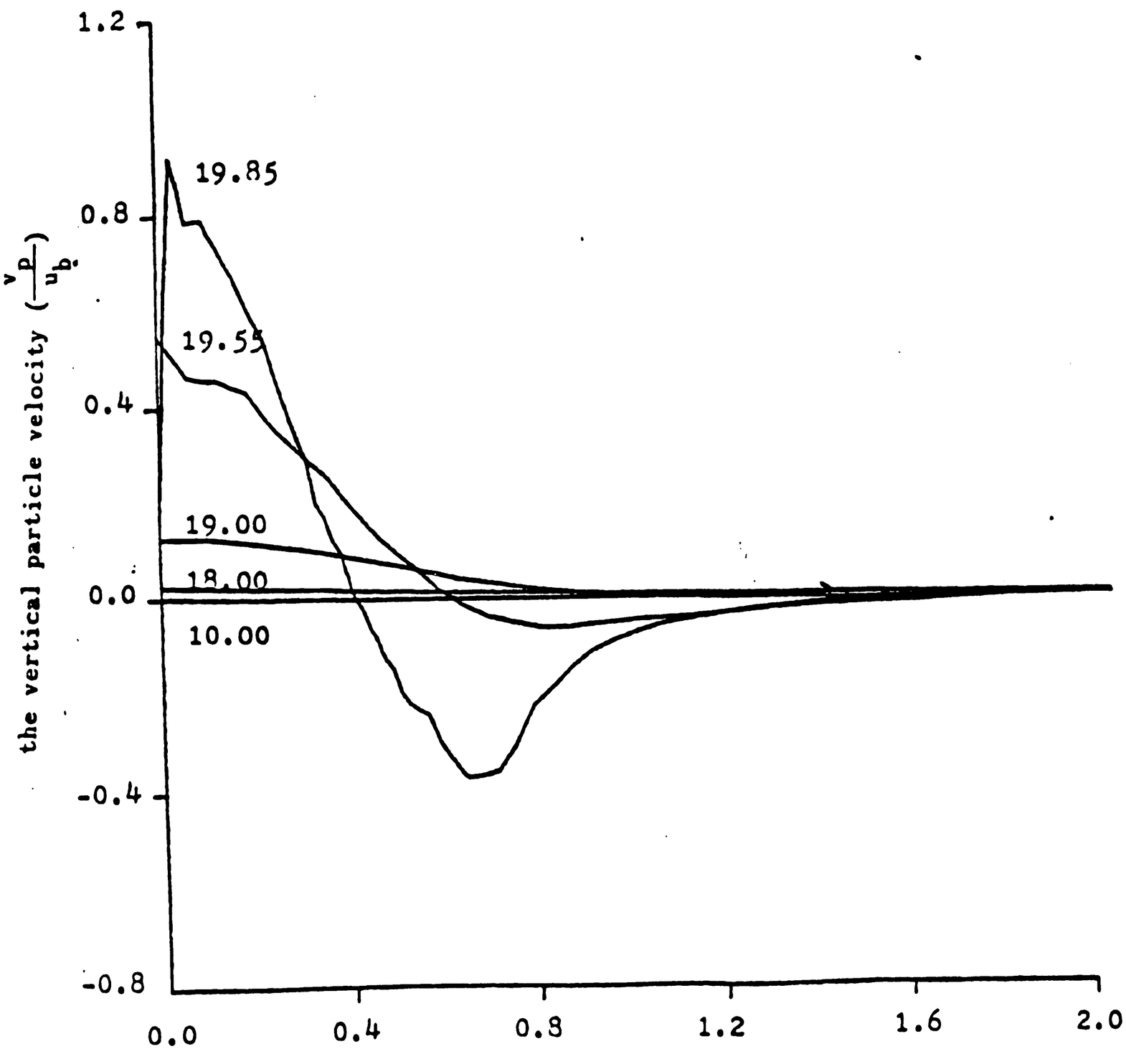

Figure 84. The vertical particle velocity at the free surface

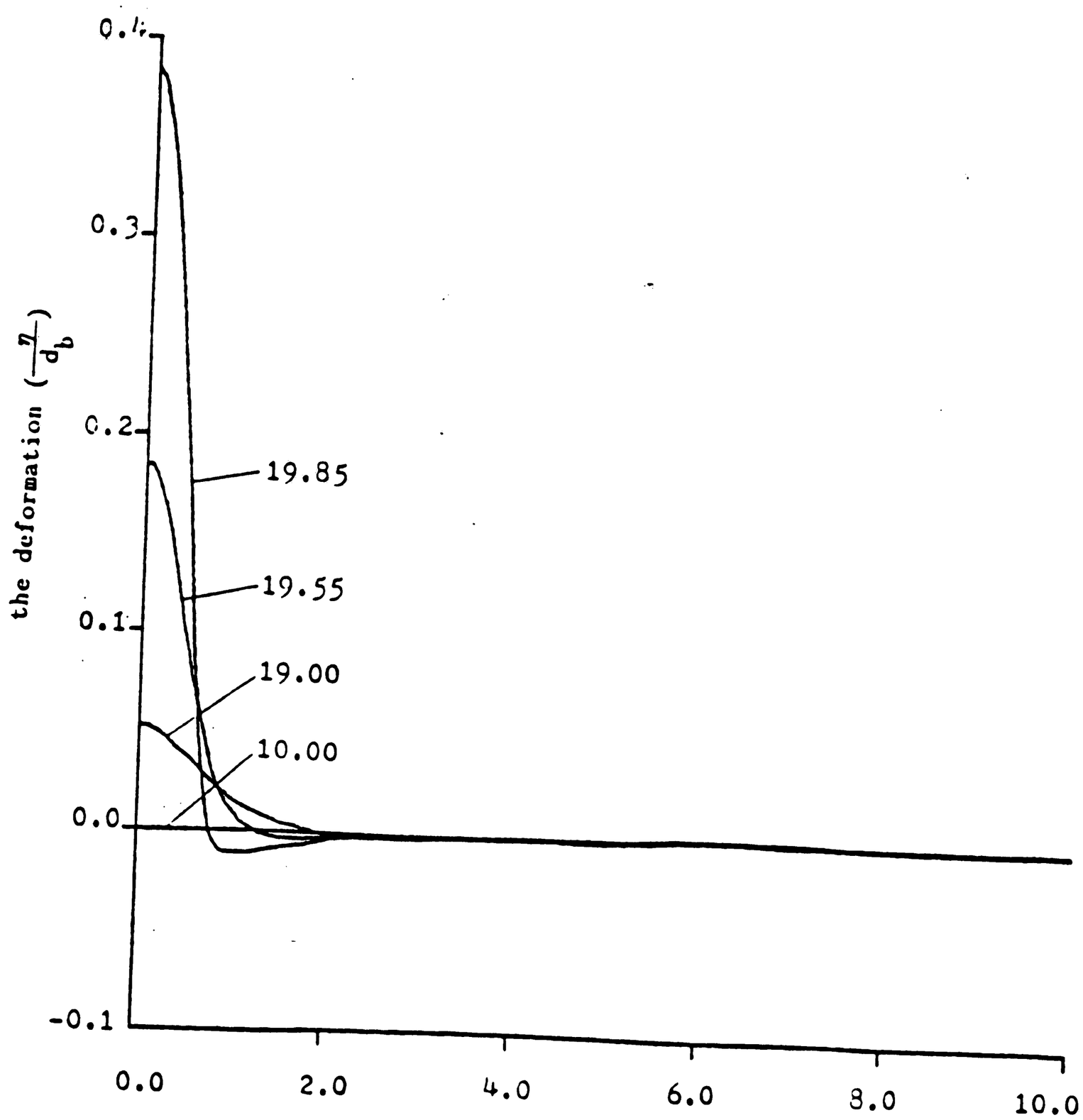

Figure 85. The deformation of the free surface

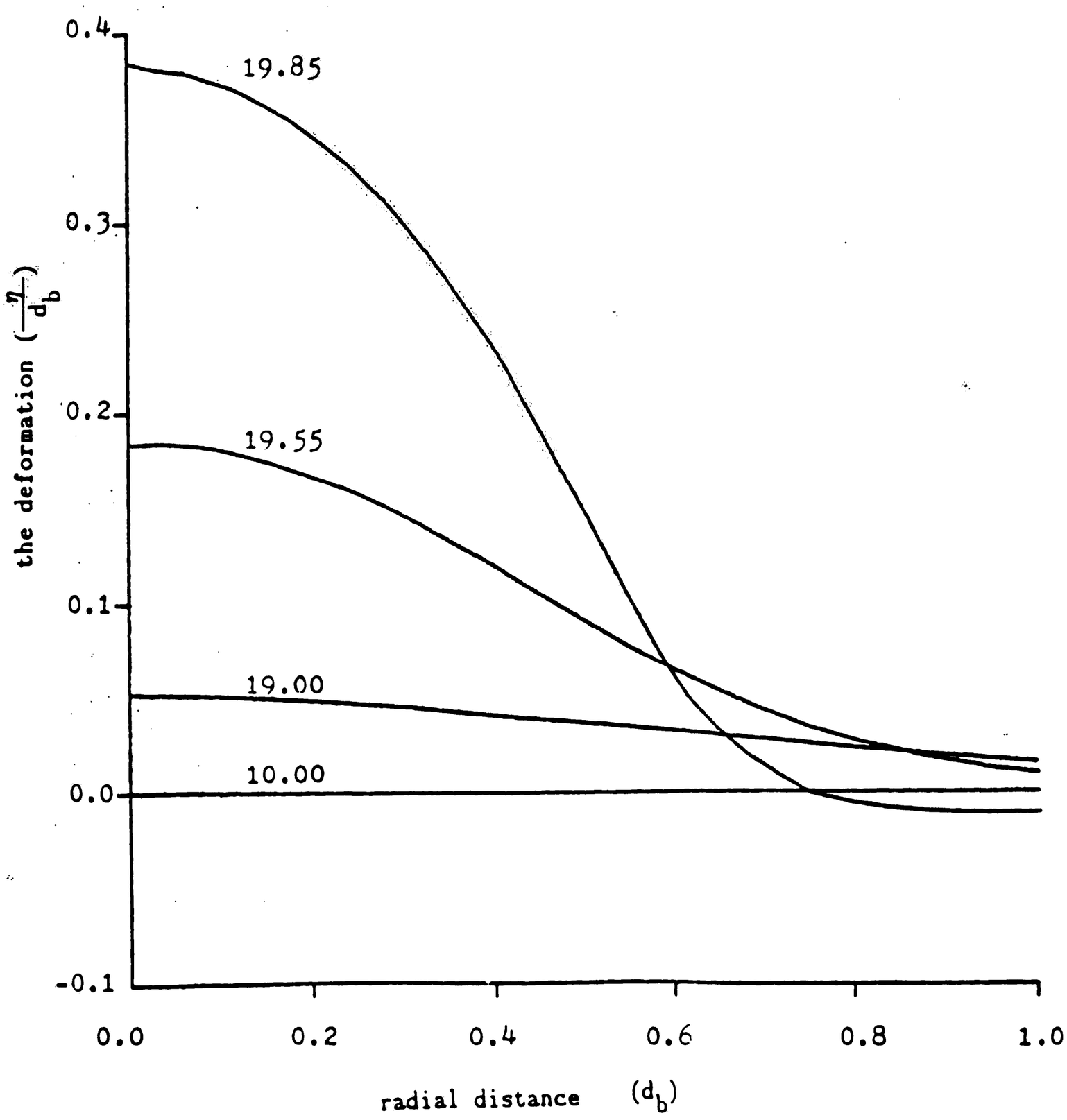

Figure 86. The deformation of the free surface highlighting the area in the vicinity of the bubble centerline

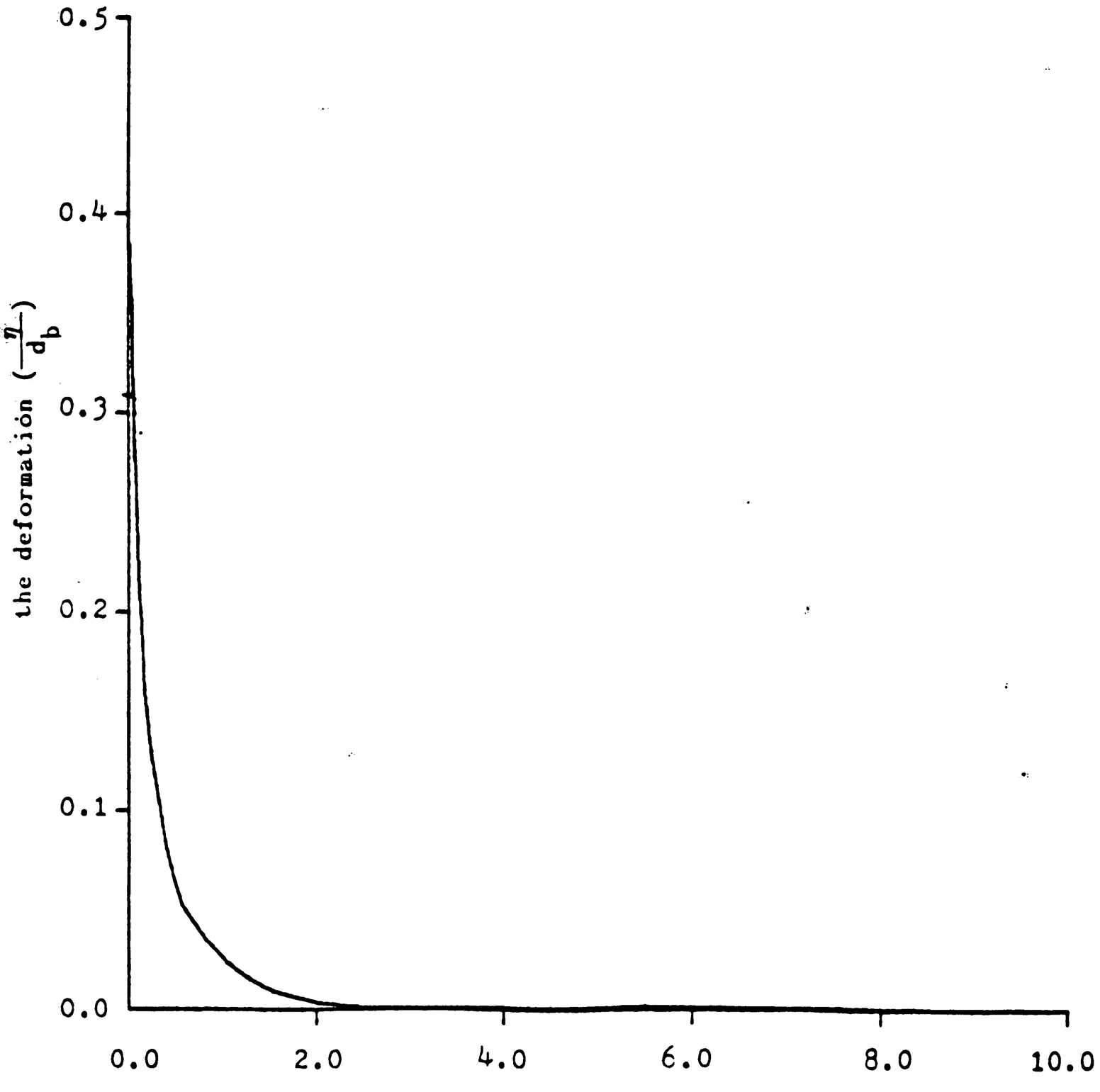

Figure 87. The deformation of the free surface at the bubble centerline related to the bulge thickness at bubble centerline

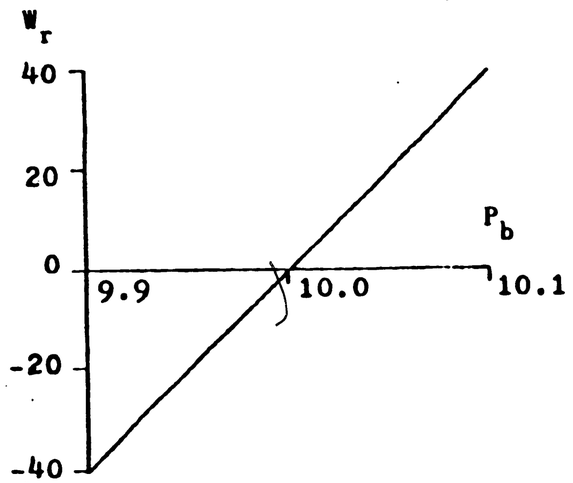

(for $z_c = 10d_b$)

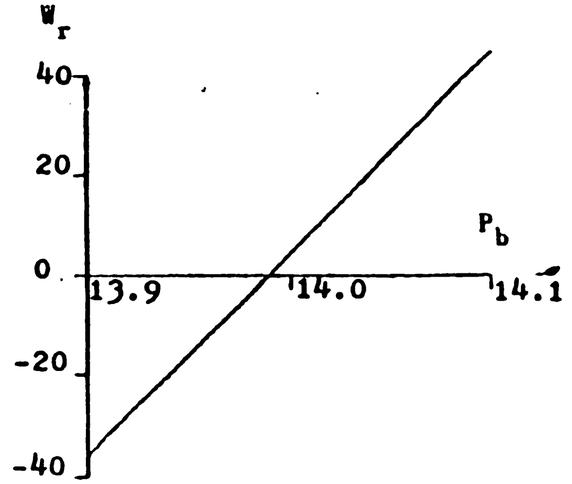

(for $z_c = 14d_b$)

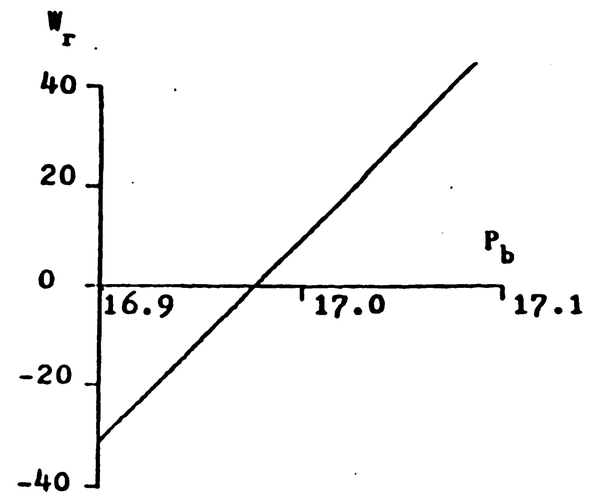

(for $z_c = 17d_b$)

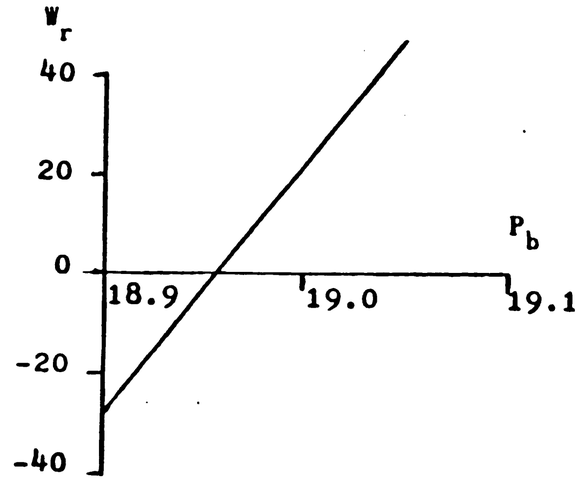

(for $z_c = 19d_b$)

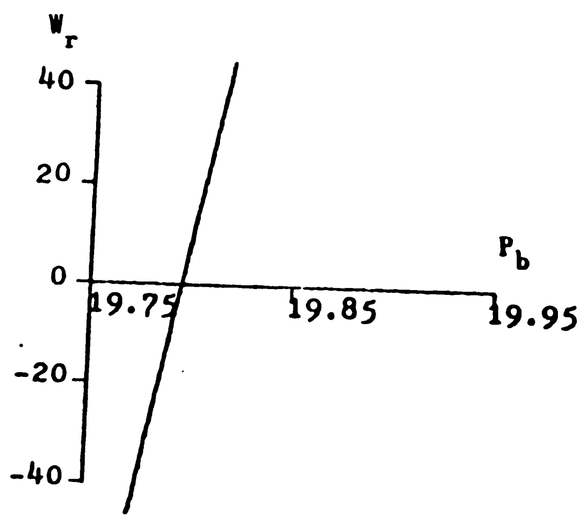

(for $z_c = 19.85d_b$)

Figure 88 . Residual gas flow through the bubble related to the bubble pressure (for K= 100)

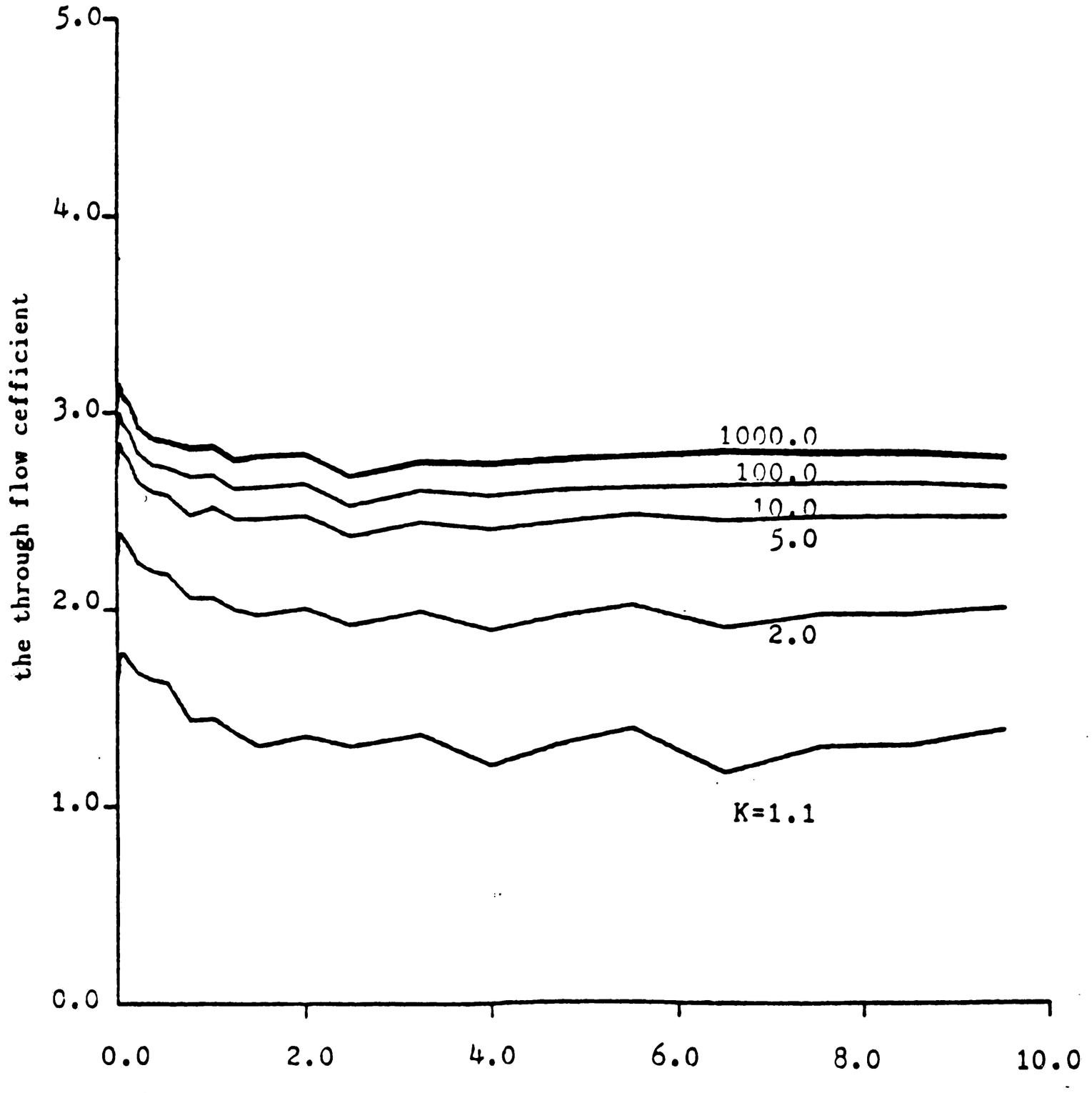

Figure 89. The through flow coefficient of the bubble related to the bulge thickness ($\epsilon_{mf} = 0.4$)

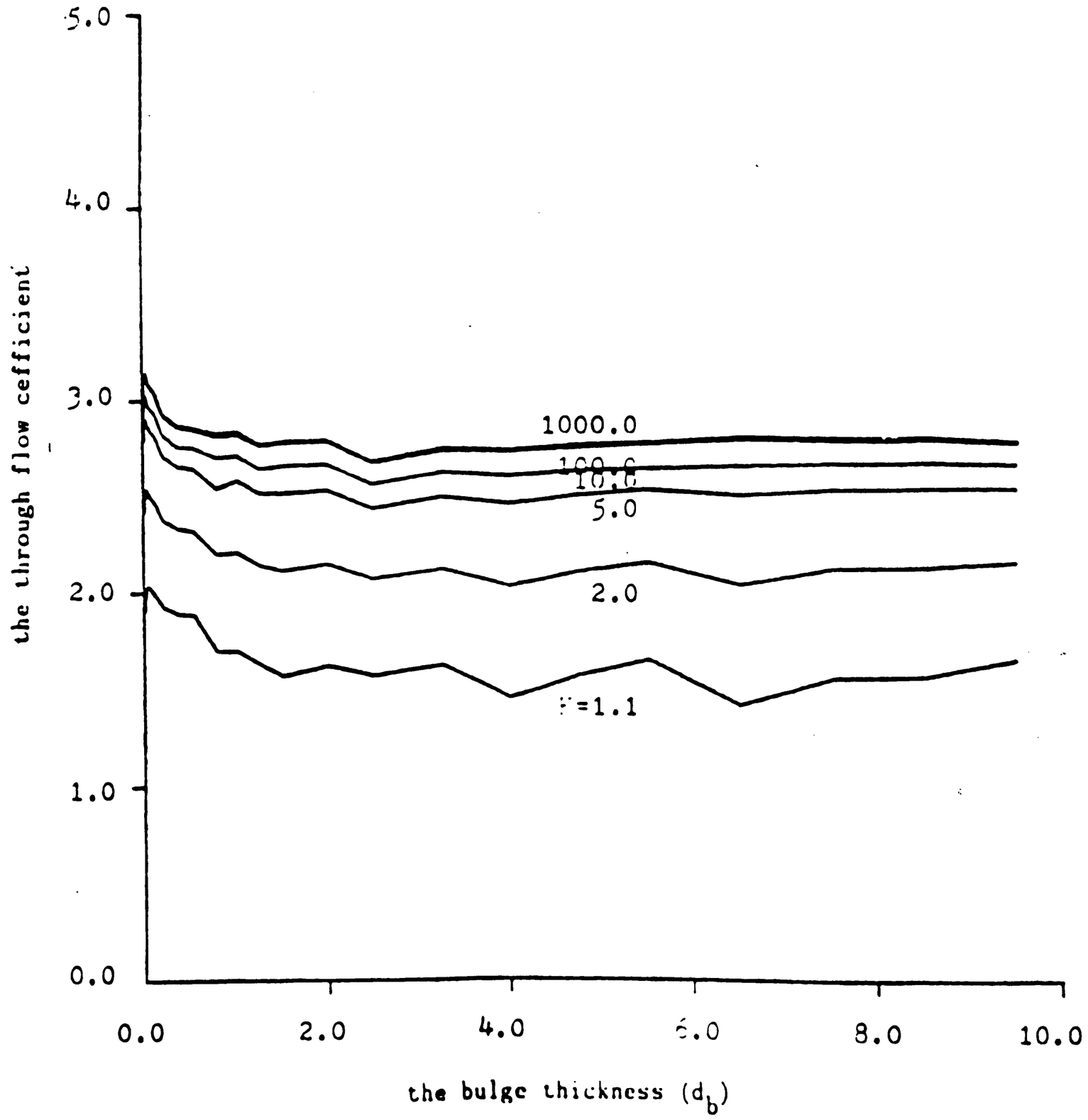

Figure 90. The through flow coefficient of the bubble related to the bulge thickness (ϵ_{mf} = 0.45)

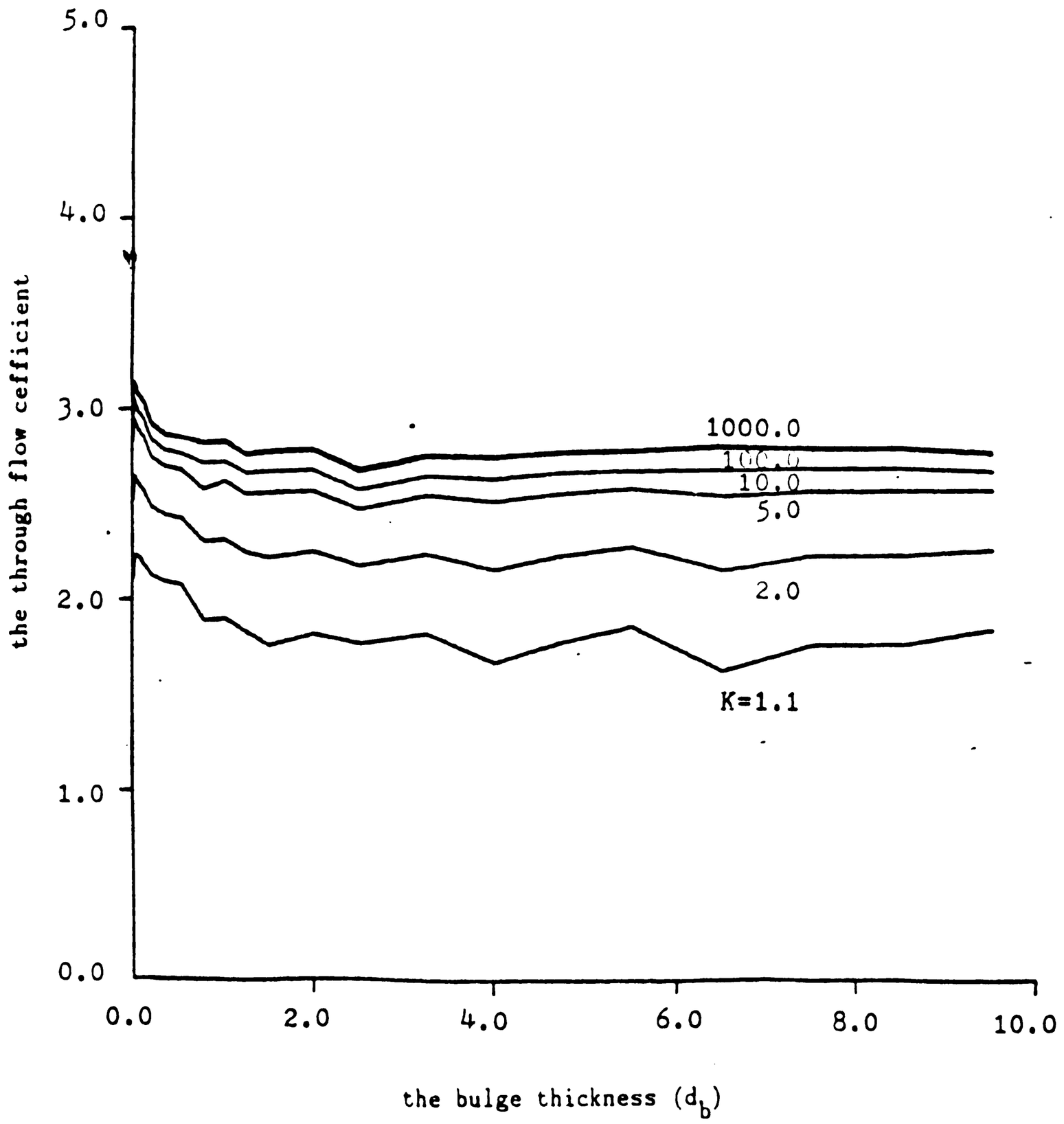

Figure 91. The through flow coefficient of the bubble related to the bulge thickness (ϵ_{mf} = 0.5)

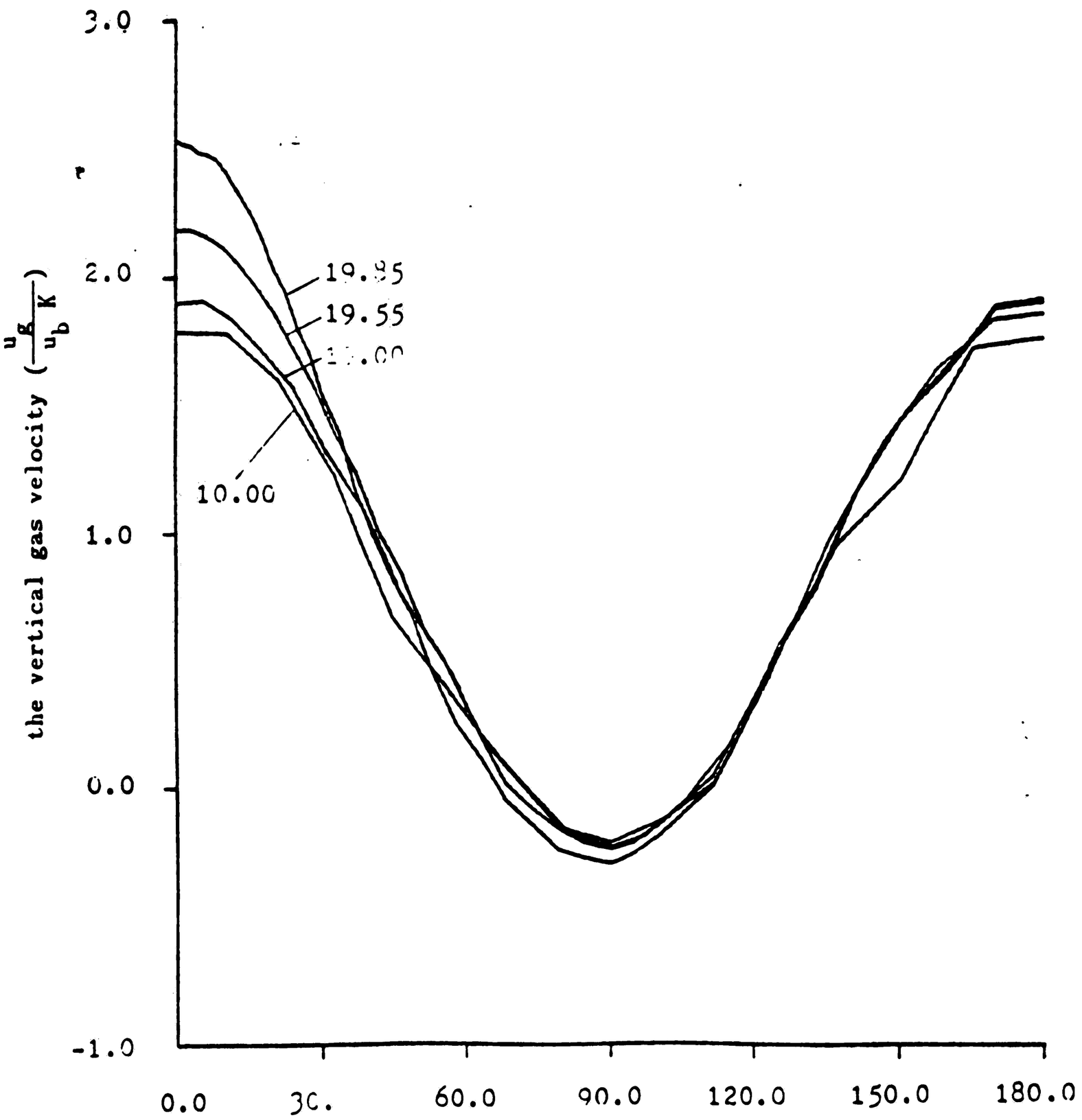

Figure 92. The vertical component of gas velocity around the bubble for K = 1.1

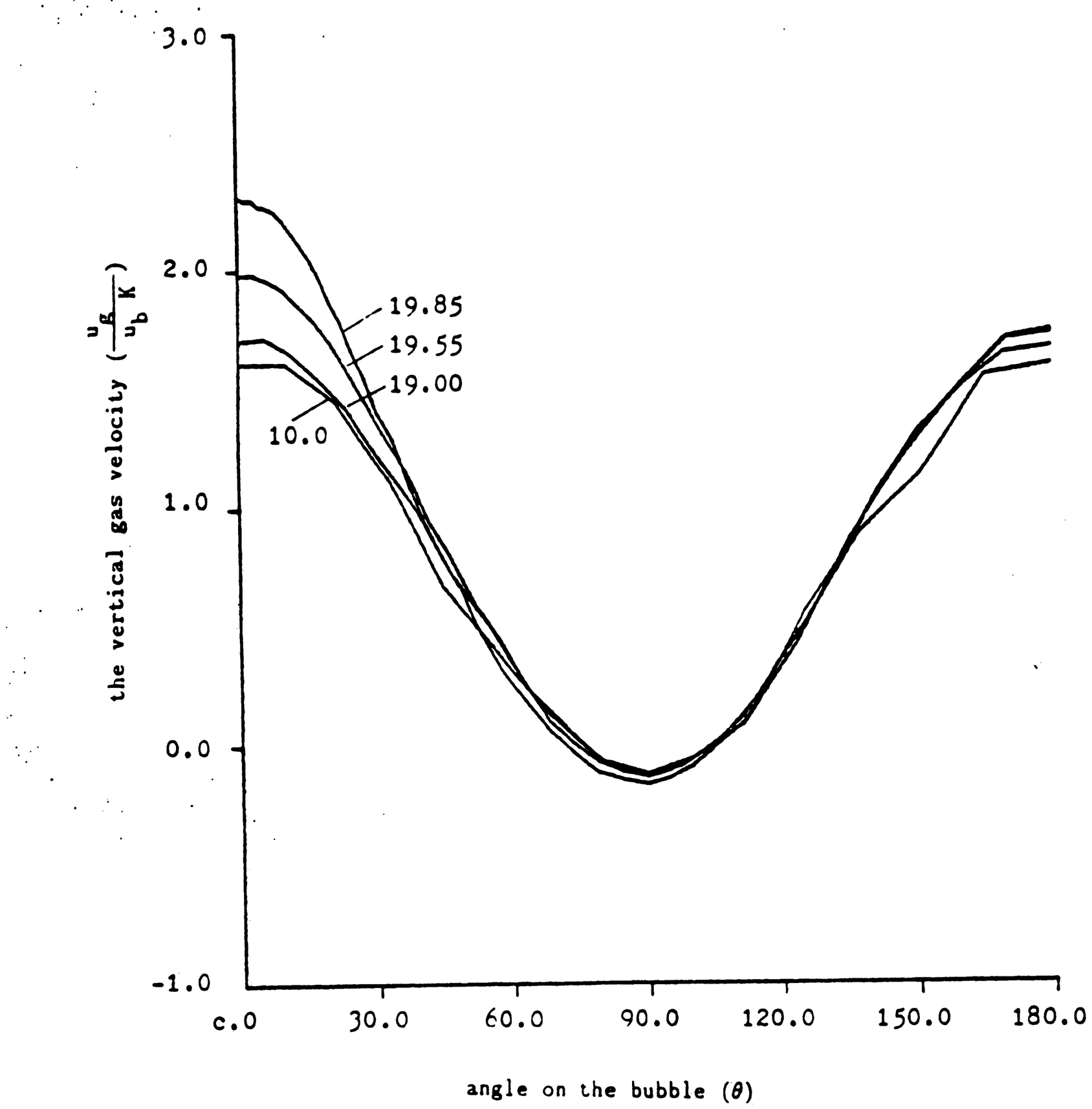

Figure 93. The vertical component of gas velocity around the bubble for K = 2

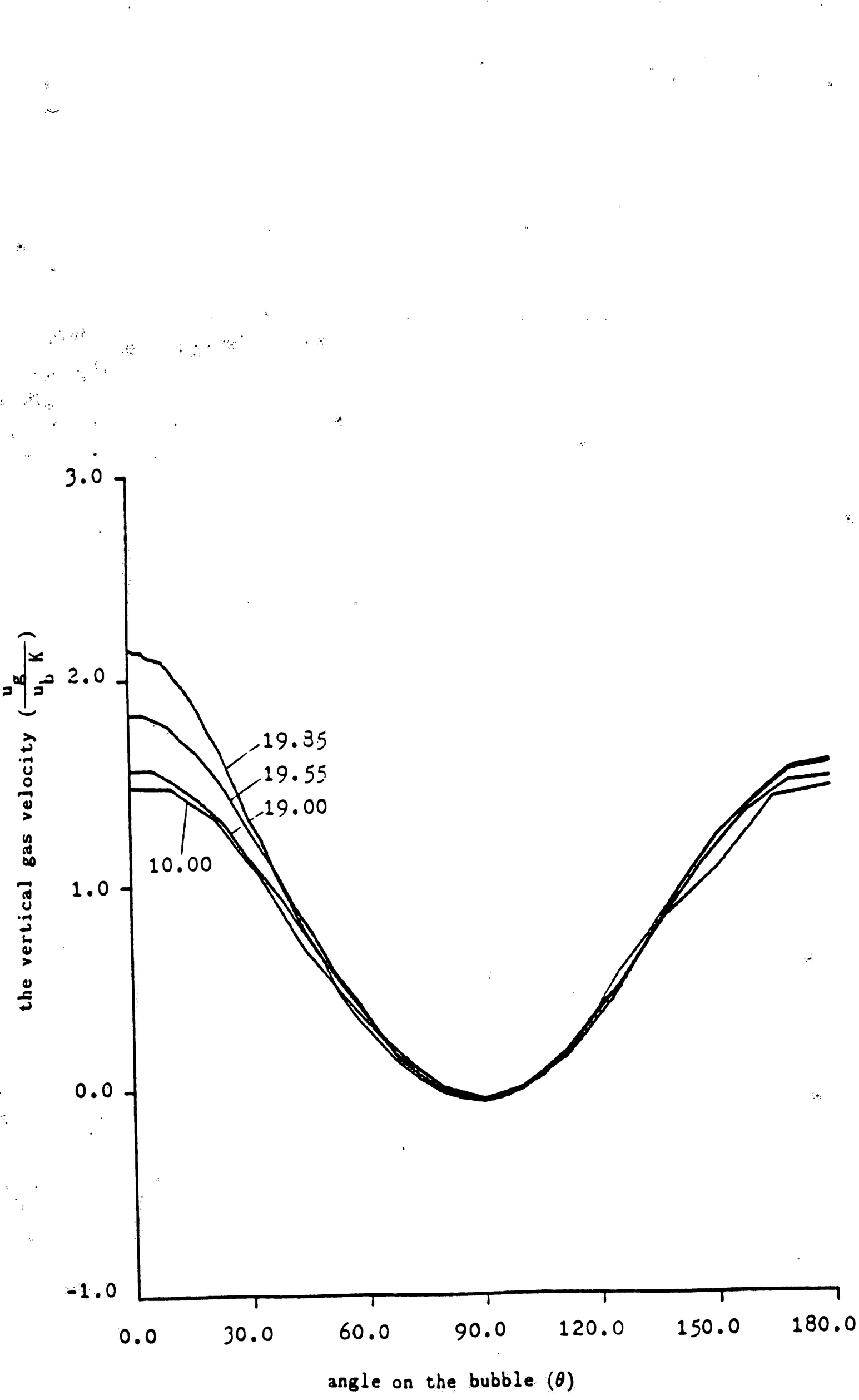

Figure 94. The vertical component of gas velocity around the bubble for K = 5

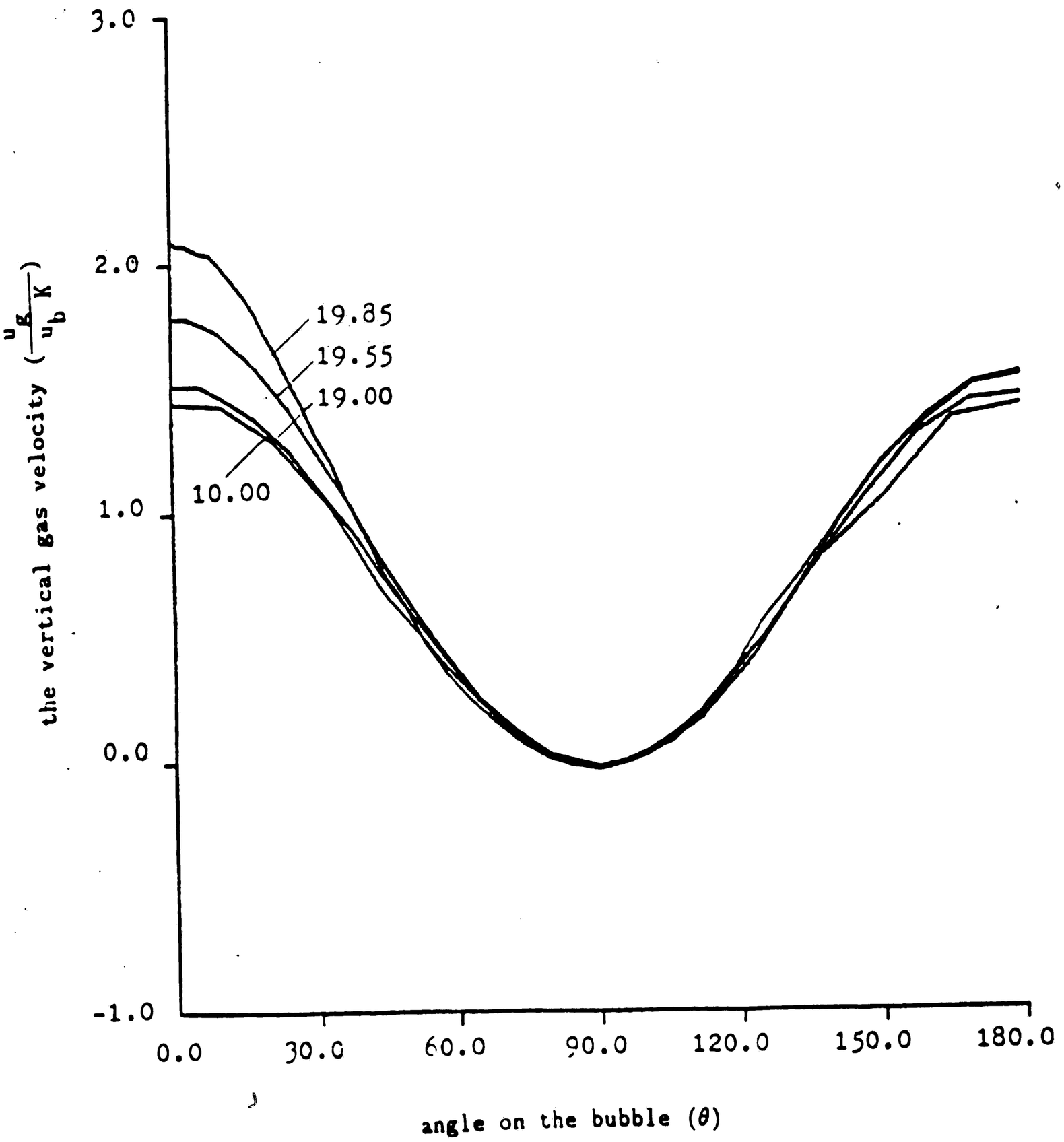

Figure 95. The vertical component of gas velocity around the bubble for K = 10

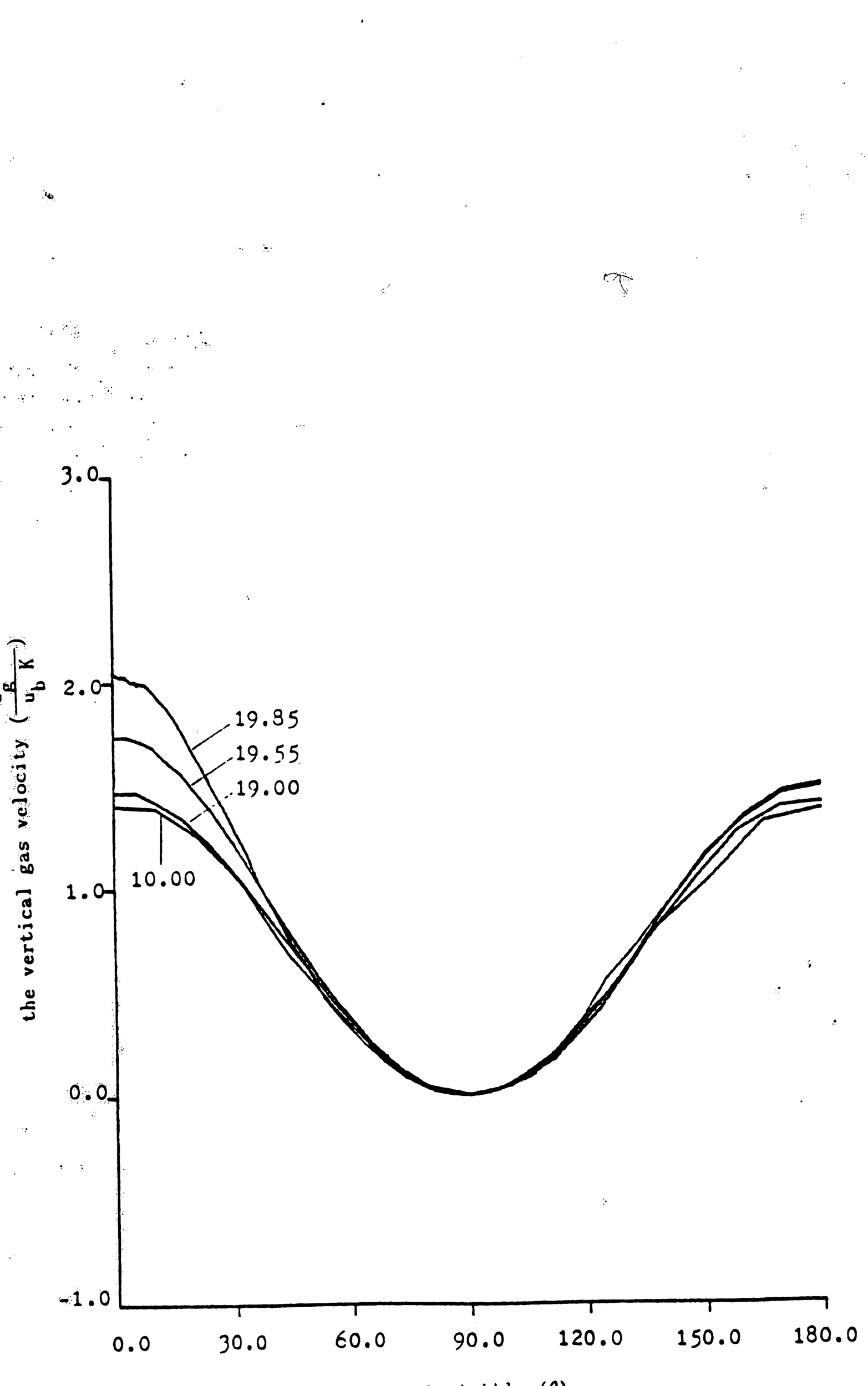

Figure 96. The vertical component of gas velocity around the bubble for K = 100

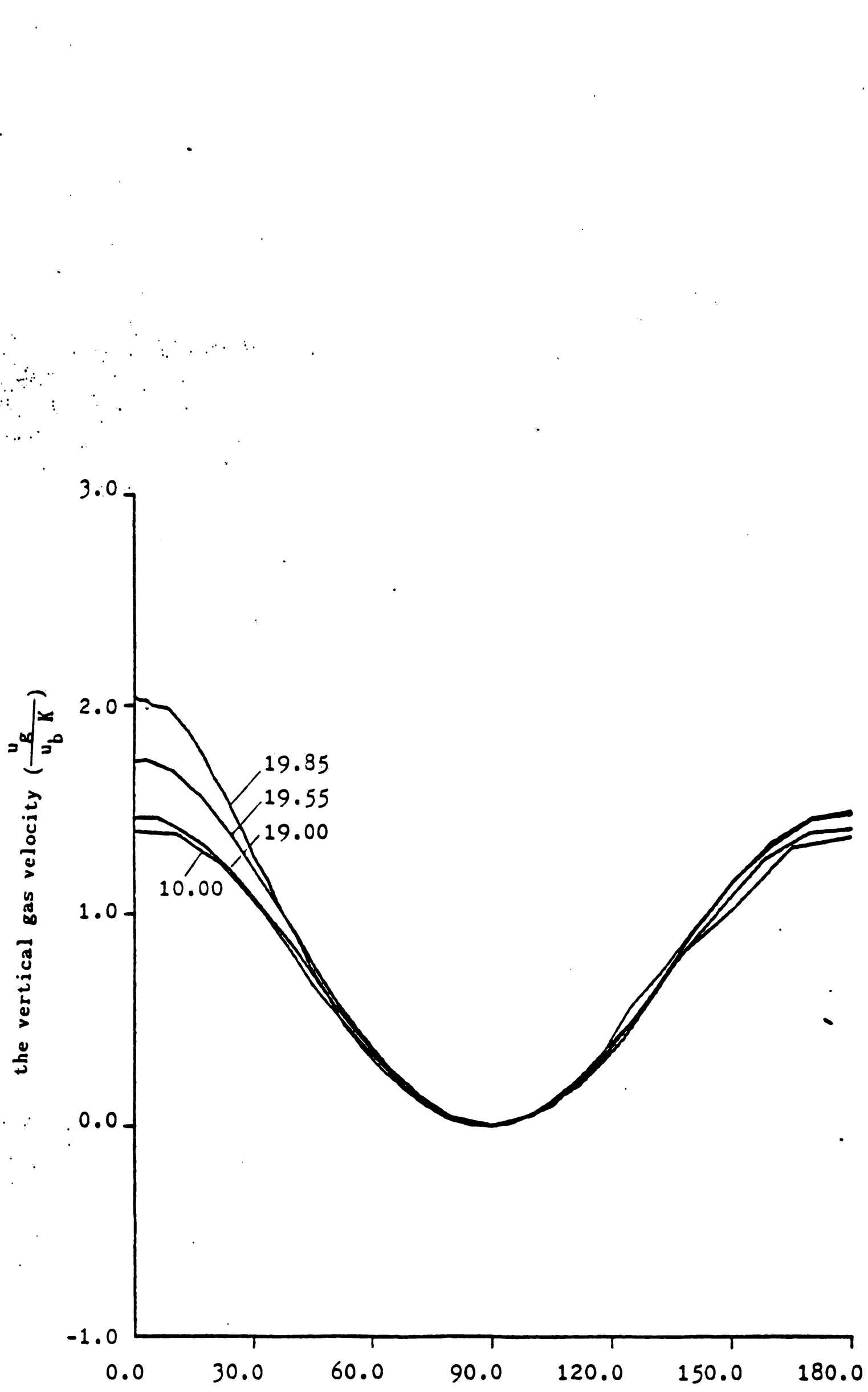

Figure 97. The vertical component of gas velocity around the bubble for K = 1000

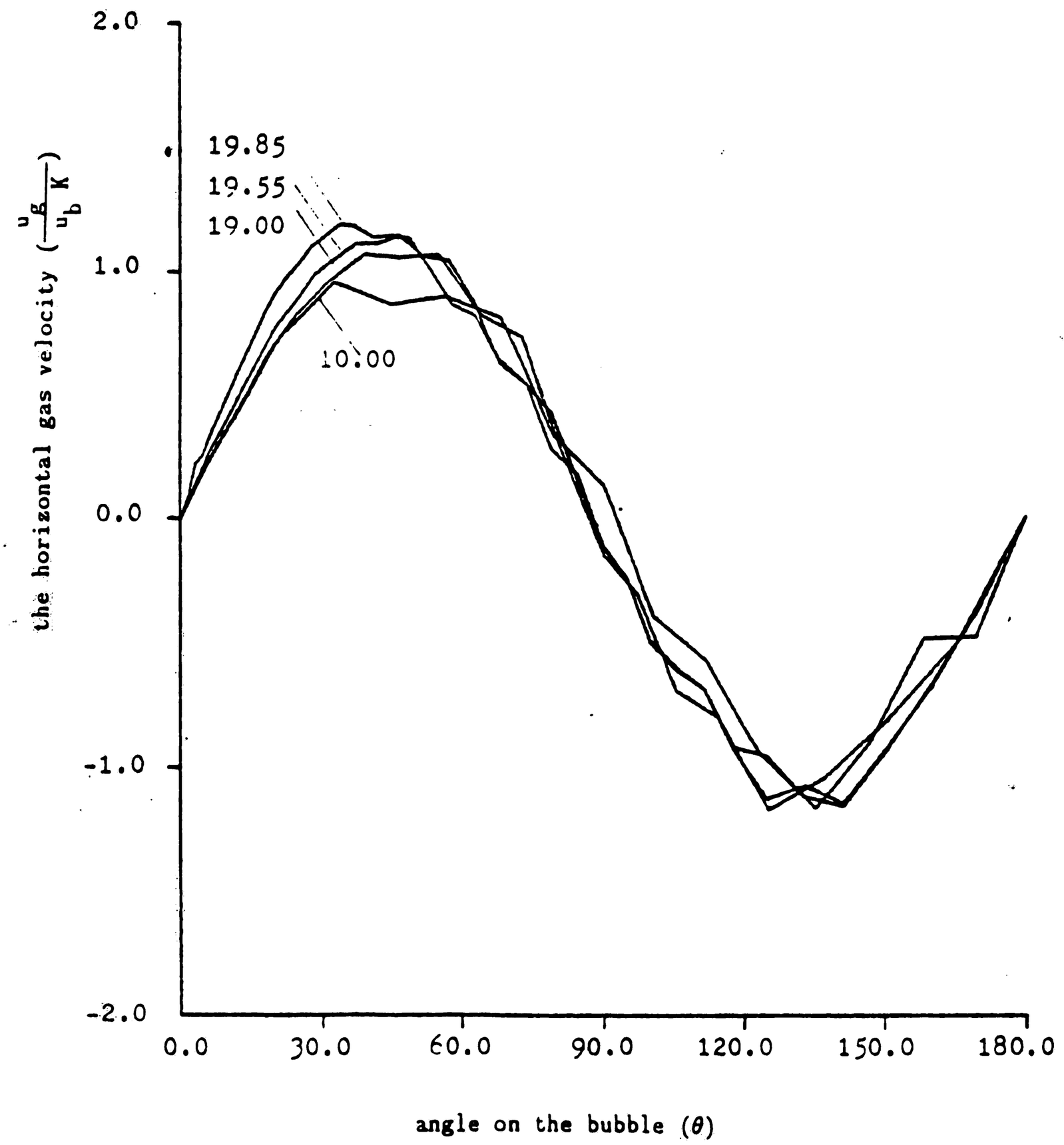

Figure 98. The horizontal component of gas velocity around the bubble for K = 1.1

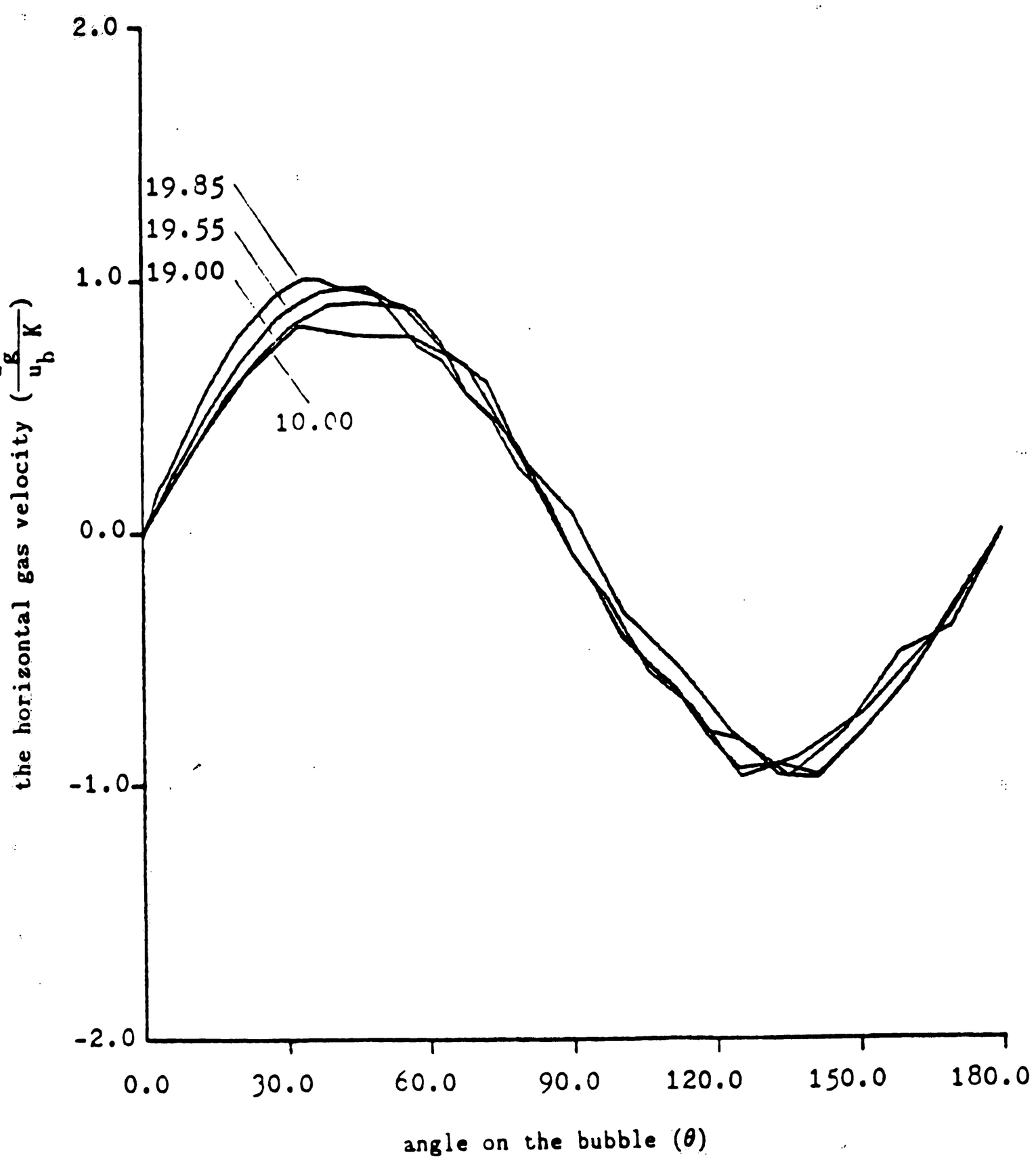

Figure 99. The horizontal component of gas velocity around the bubble for K = 2

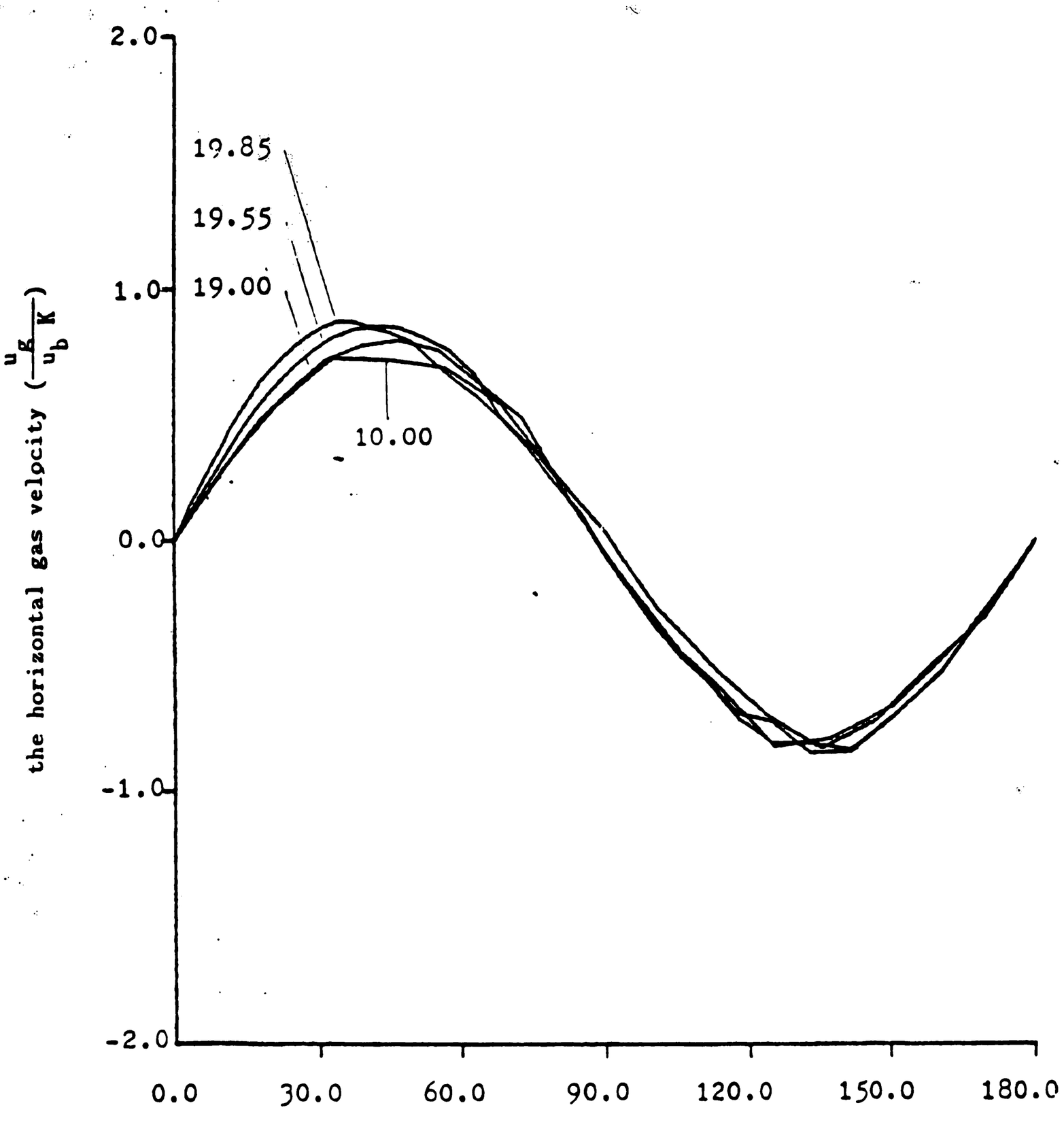

Figure 100. The horizontal component of gas velocity around the bubble for K = 5

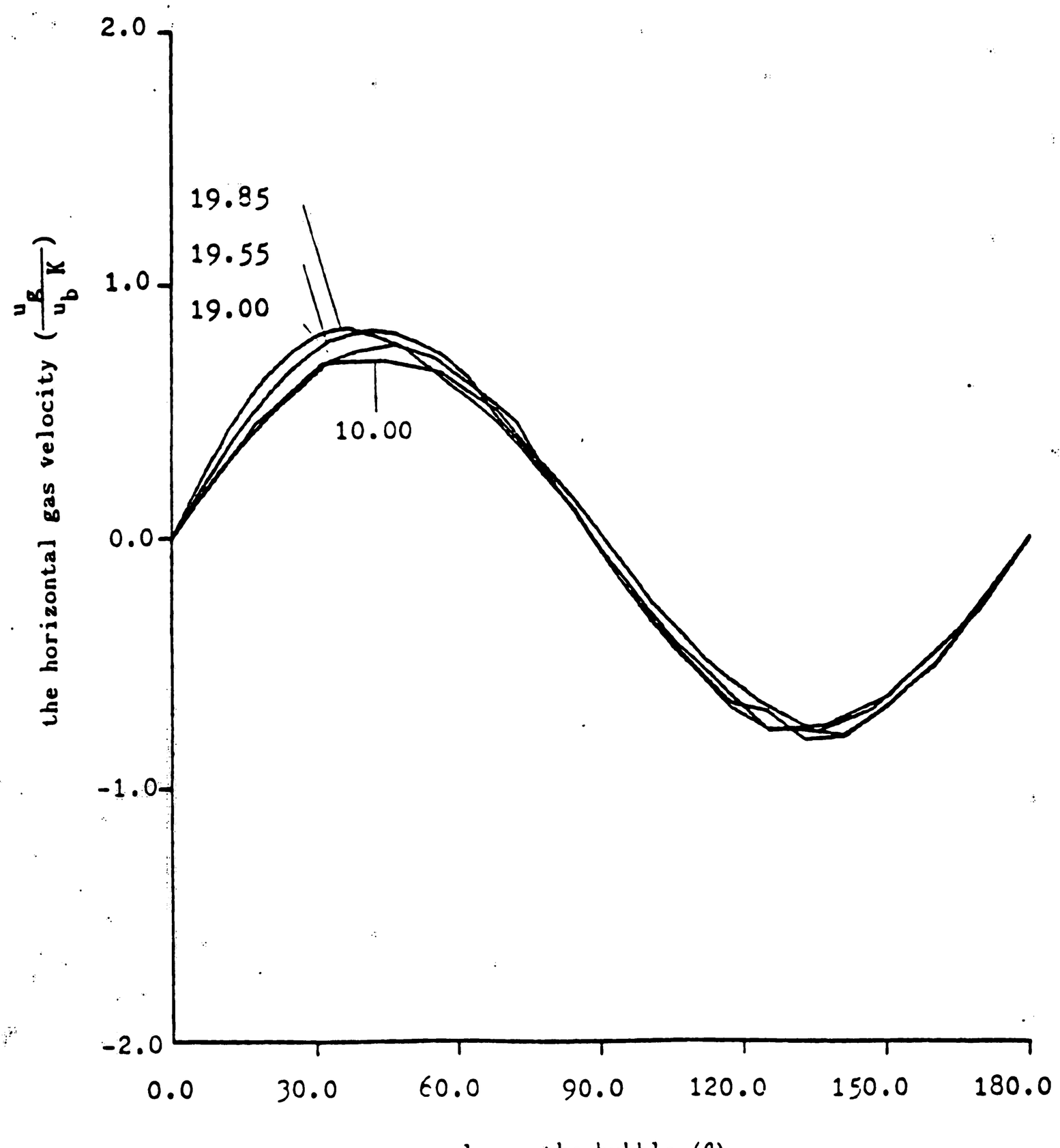

Figure 101. The horizontal component of gas velocity around the bubble for K = 10

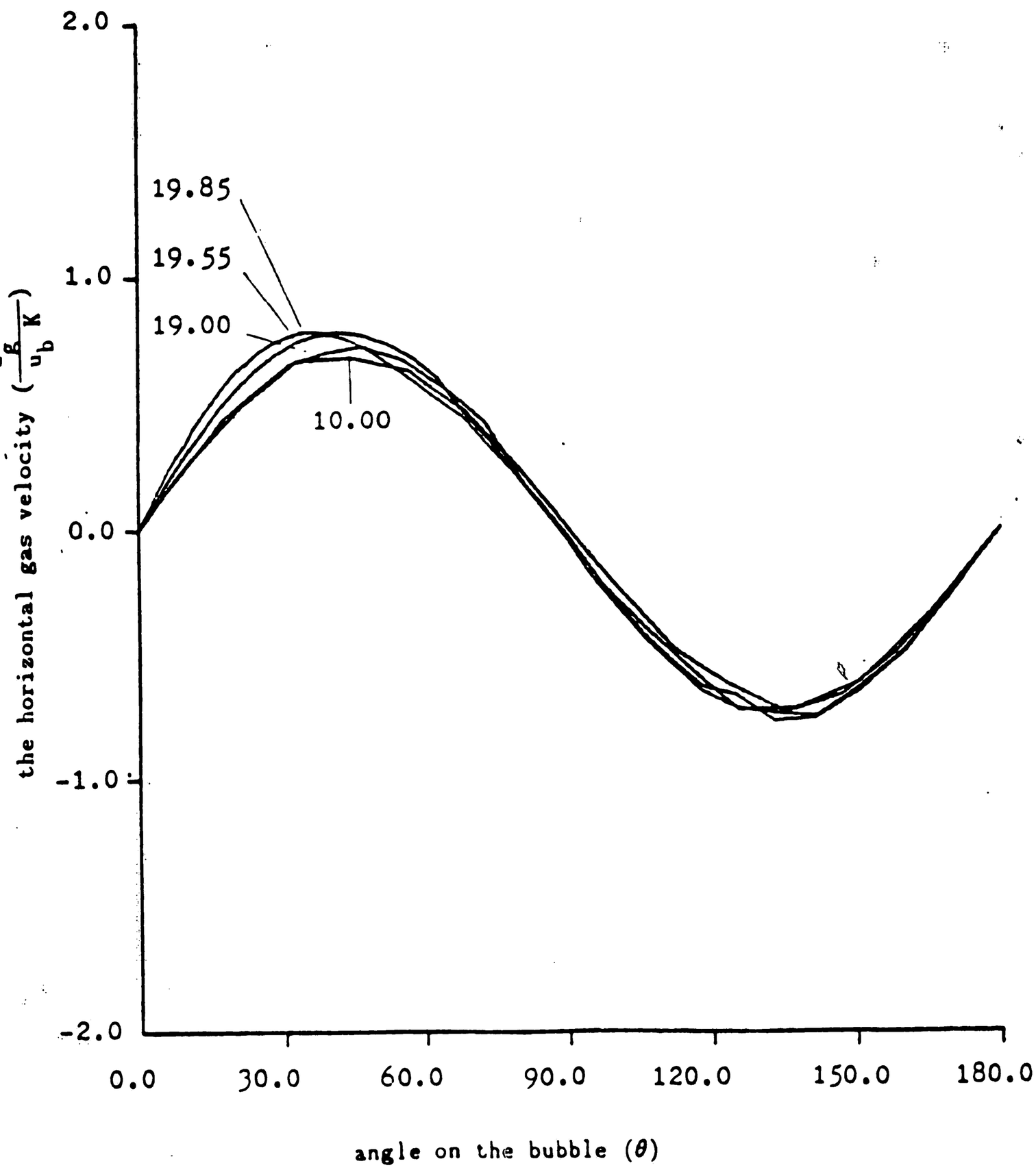

Figure 102. The horizontal component of gas velocity around the bubble for K = 100

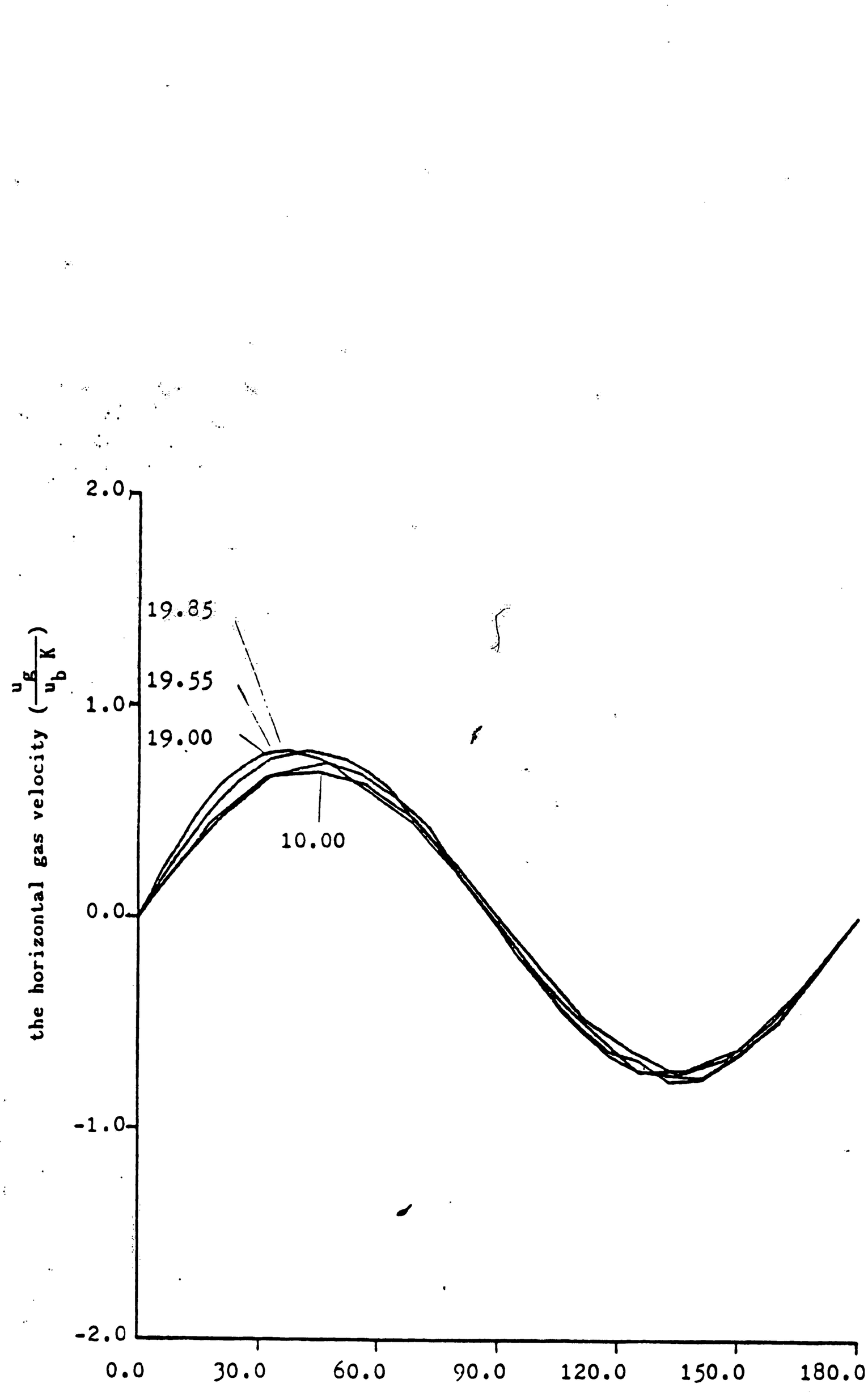

Figure 103. The horizontal component of gas velocity around the bubble for K = 1000

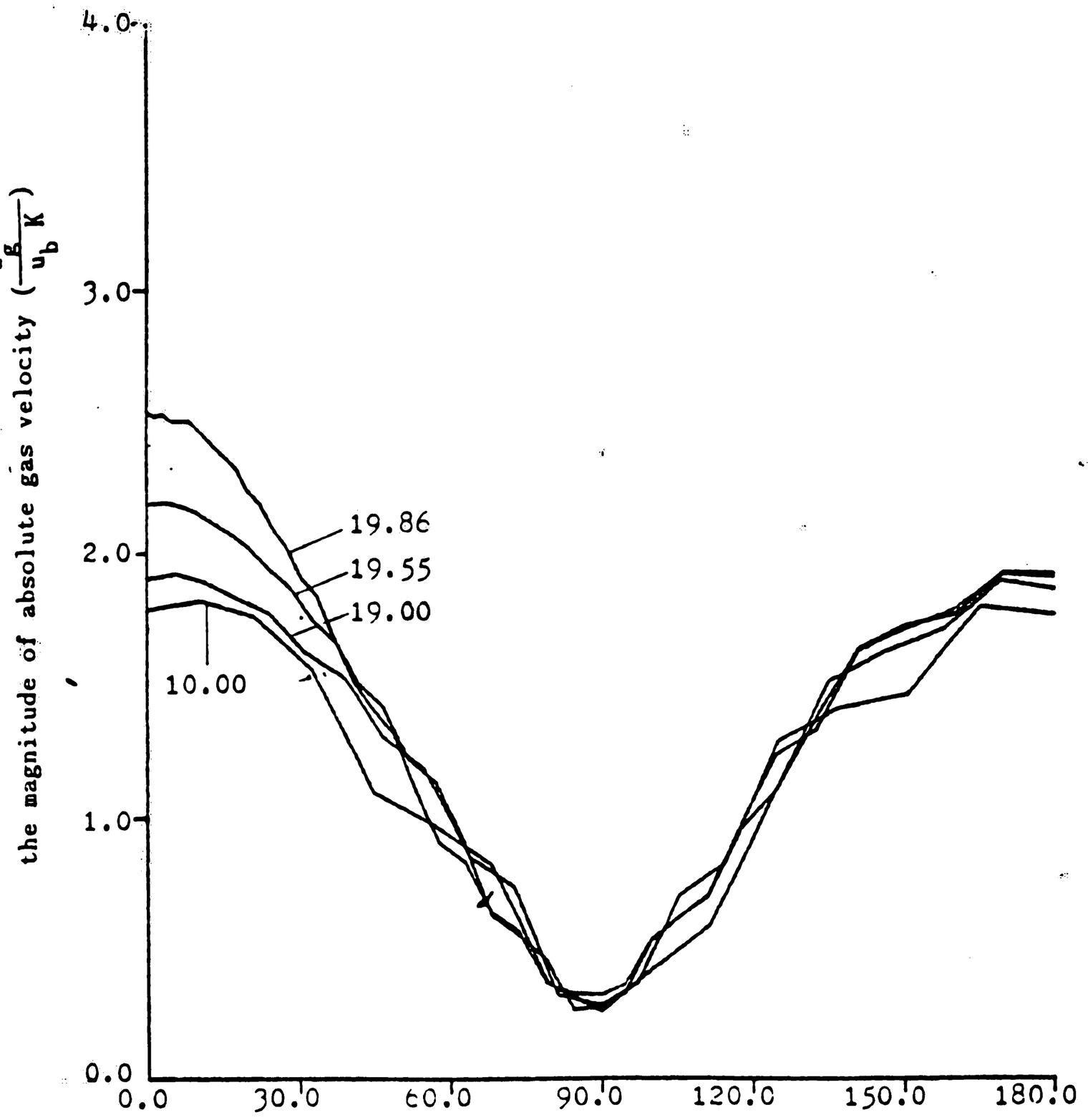

Figure 104. The magnitude of gas velocity around the bubble for K = 1.1

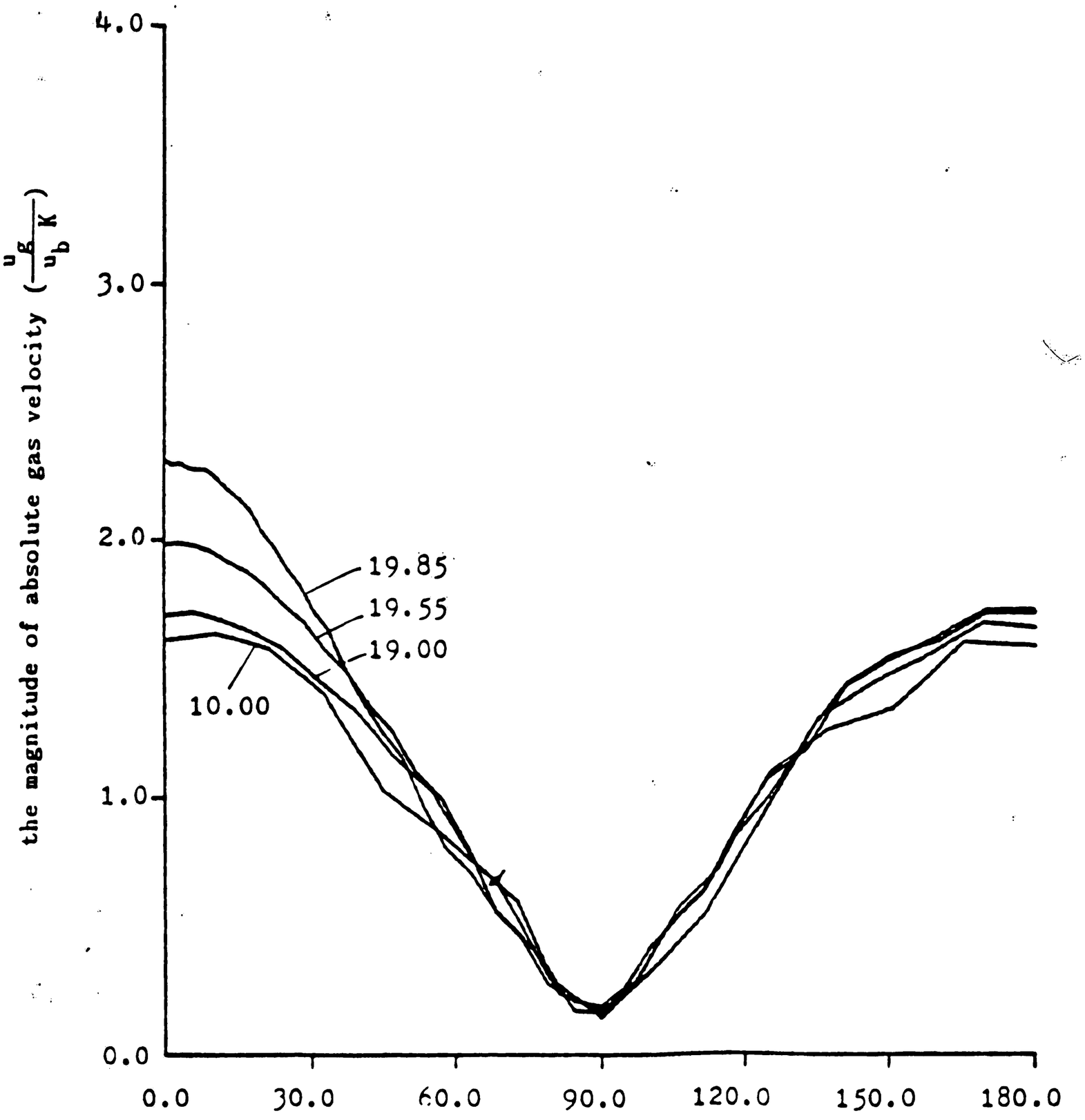

Figure 105. The magnitude of gas velocity around the bubble for K = 2

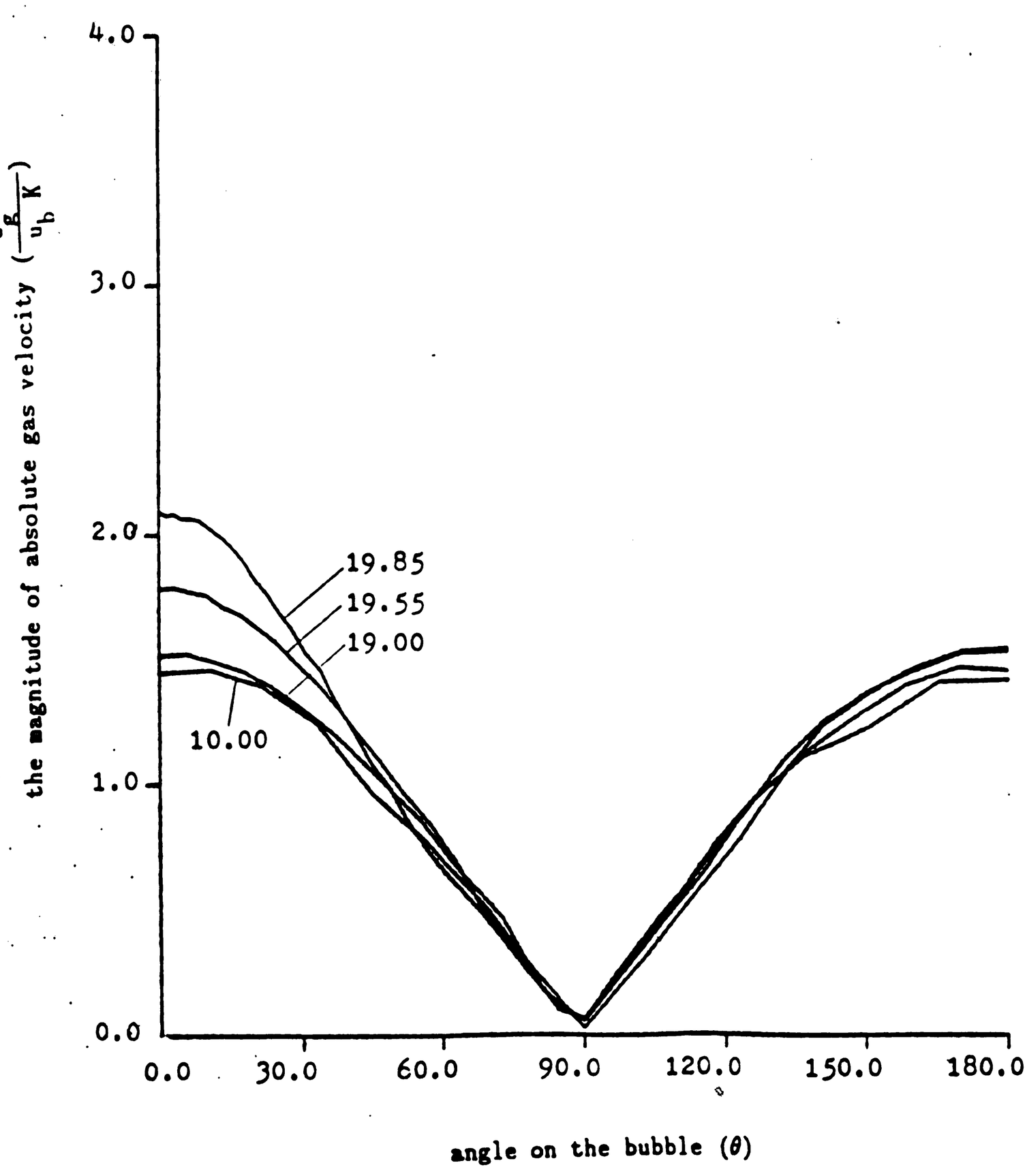

Figure 106. The magnitude of gas velocity around the bubble for K = 5

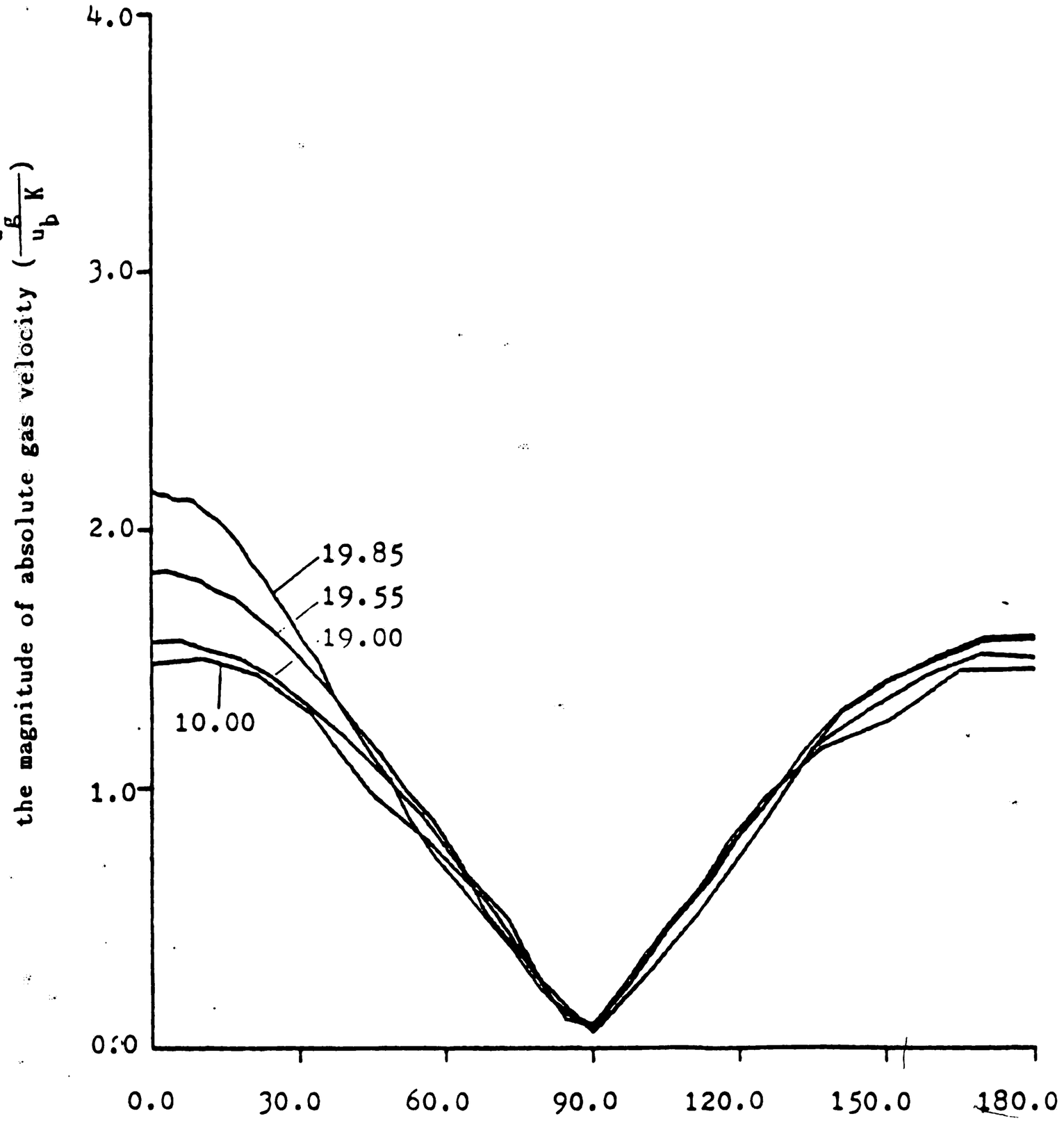

Figure 107. The magnitude of gas velocity around the bubble for K = 10

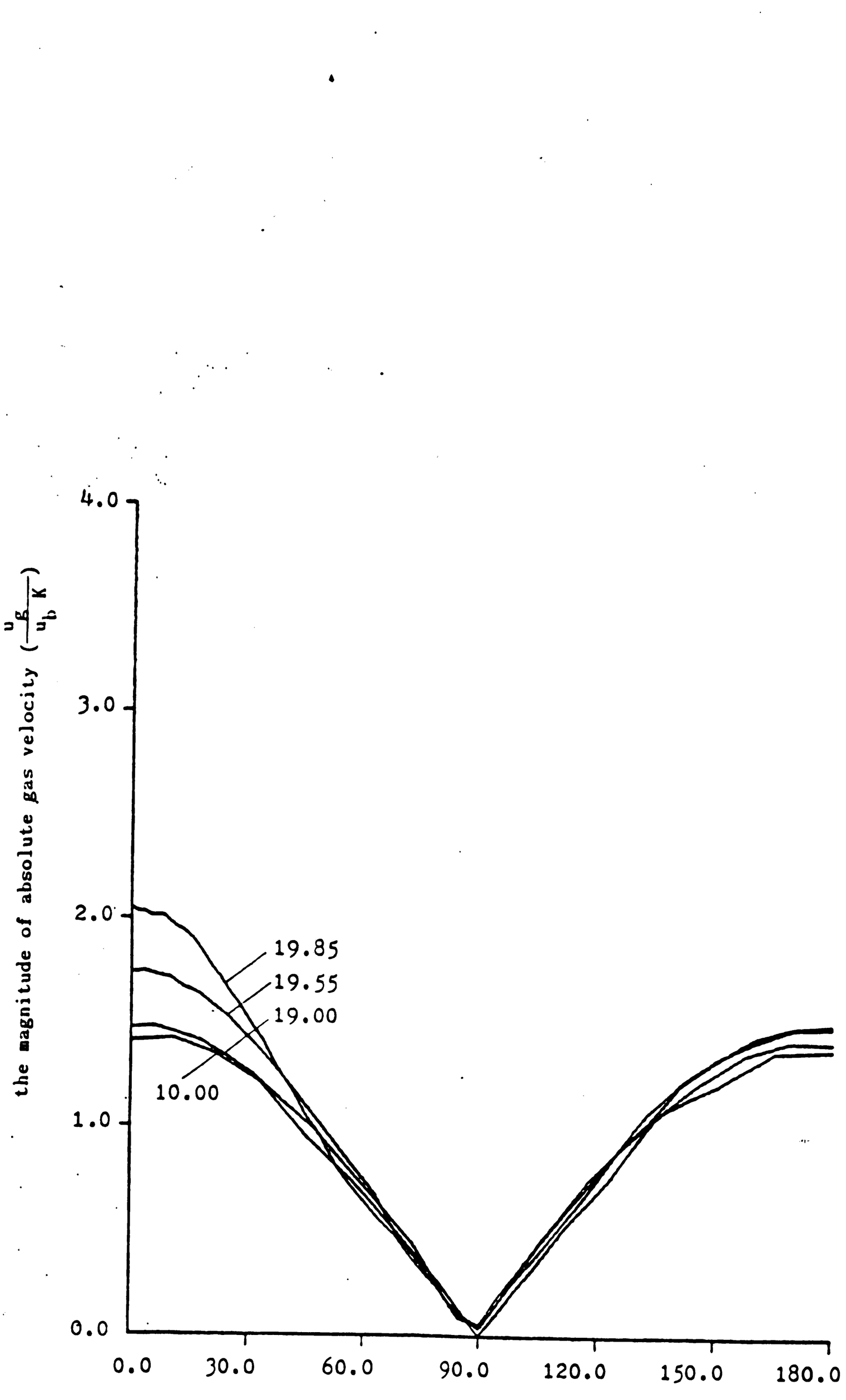

Figure 108. The magnitude of gas velocity around the bubble for K = 100

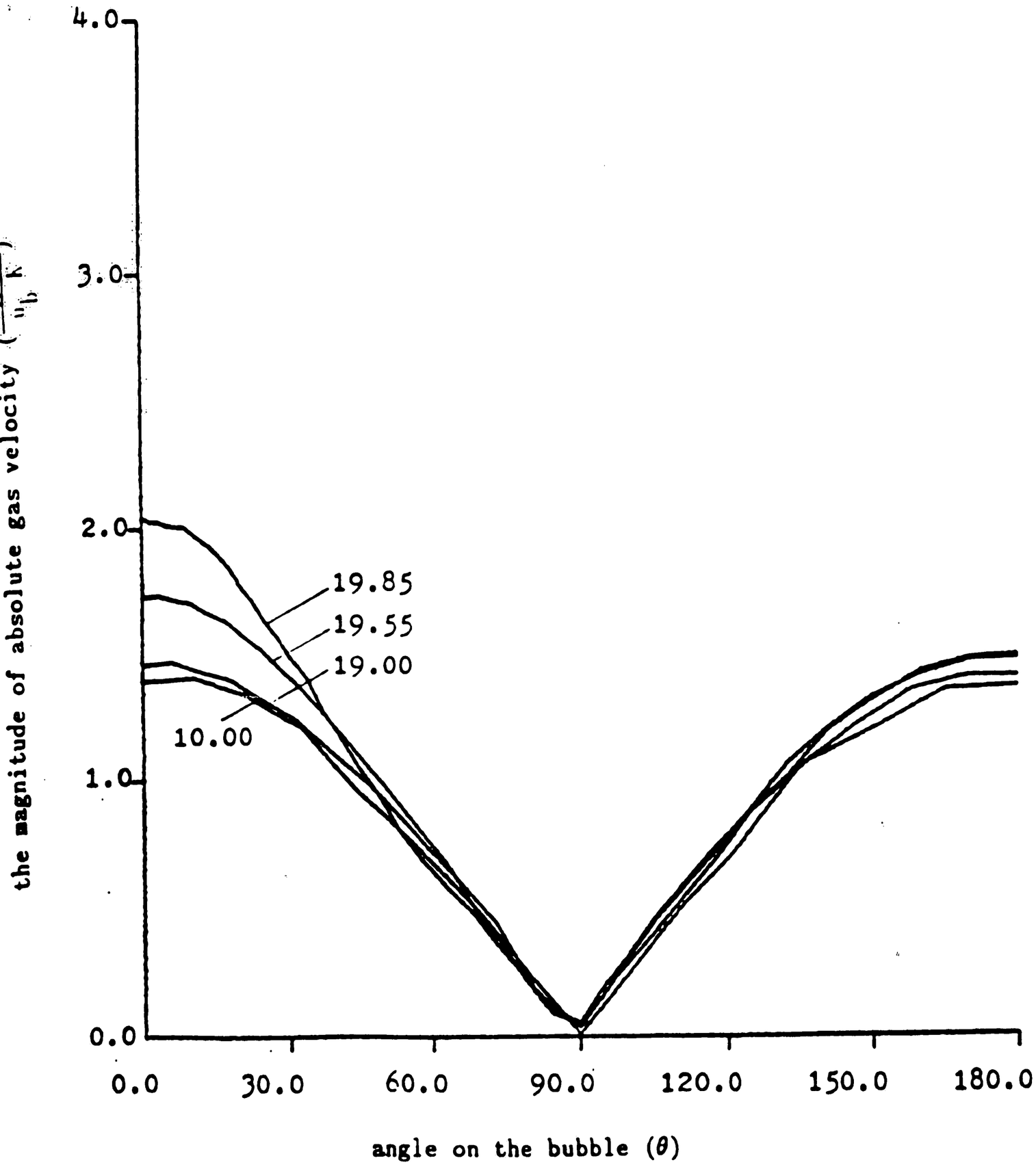

Figure 109. The magnitude of gas velocity around the bubble for K = 1000

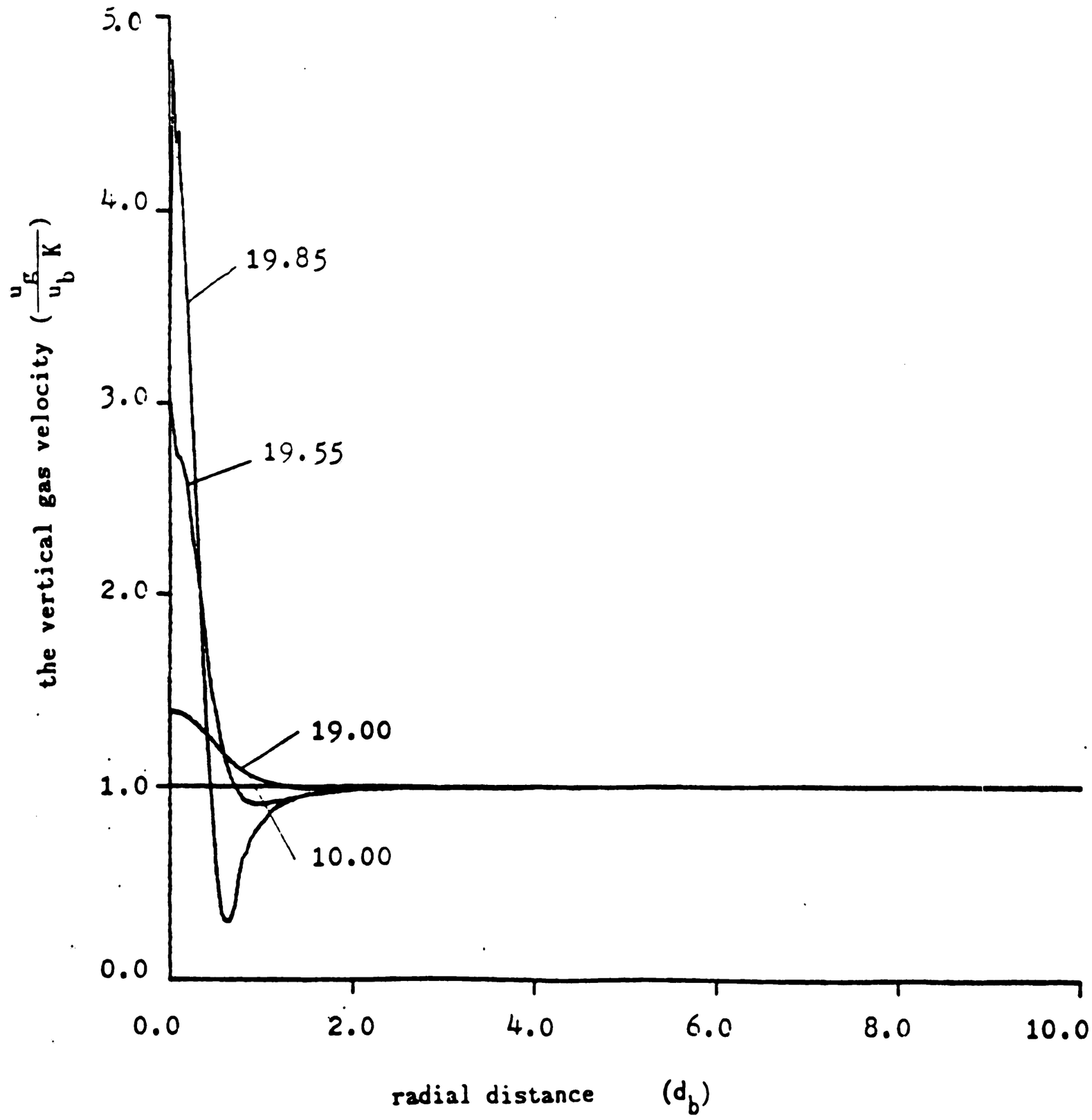

Figure 110. The vertical component of gas velocity at the free surface for K = 1.1

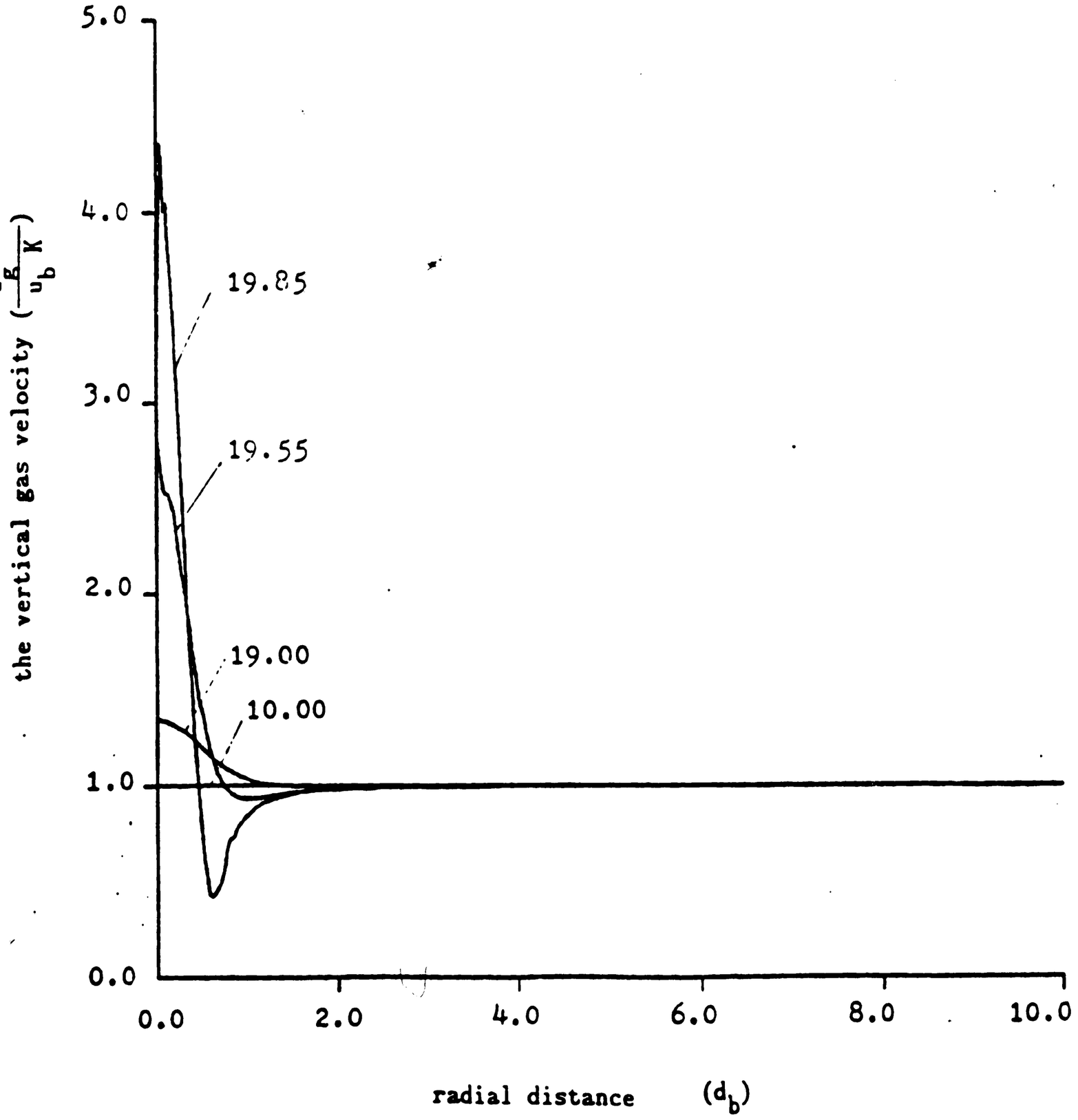

Figure 111. The vertical component of gas velocity at the free surface for K = 2

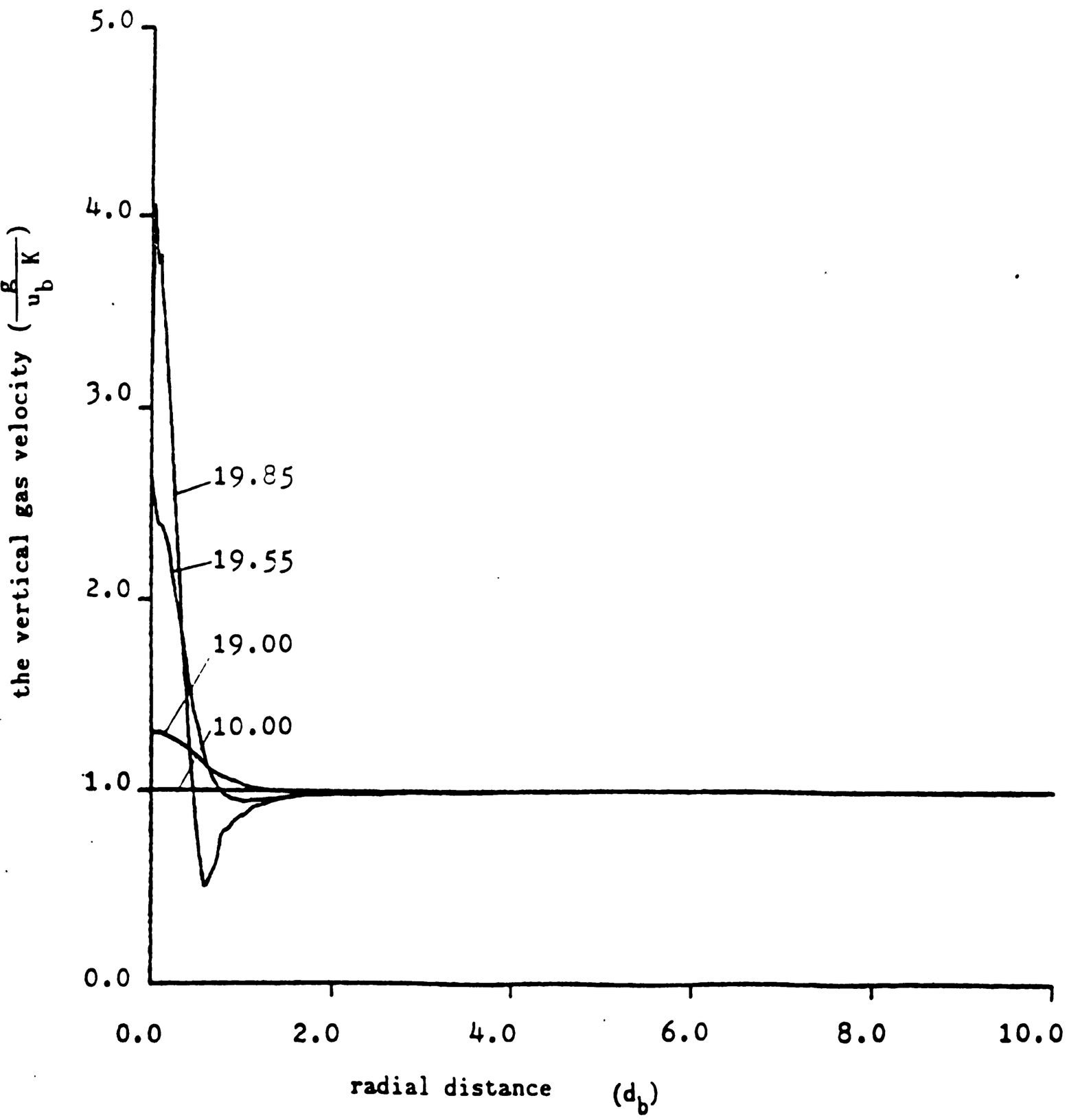

Figure 112. The vertical component of gas velocity at the free surface for K = 5

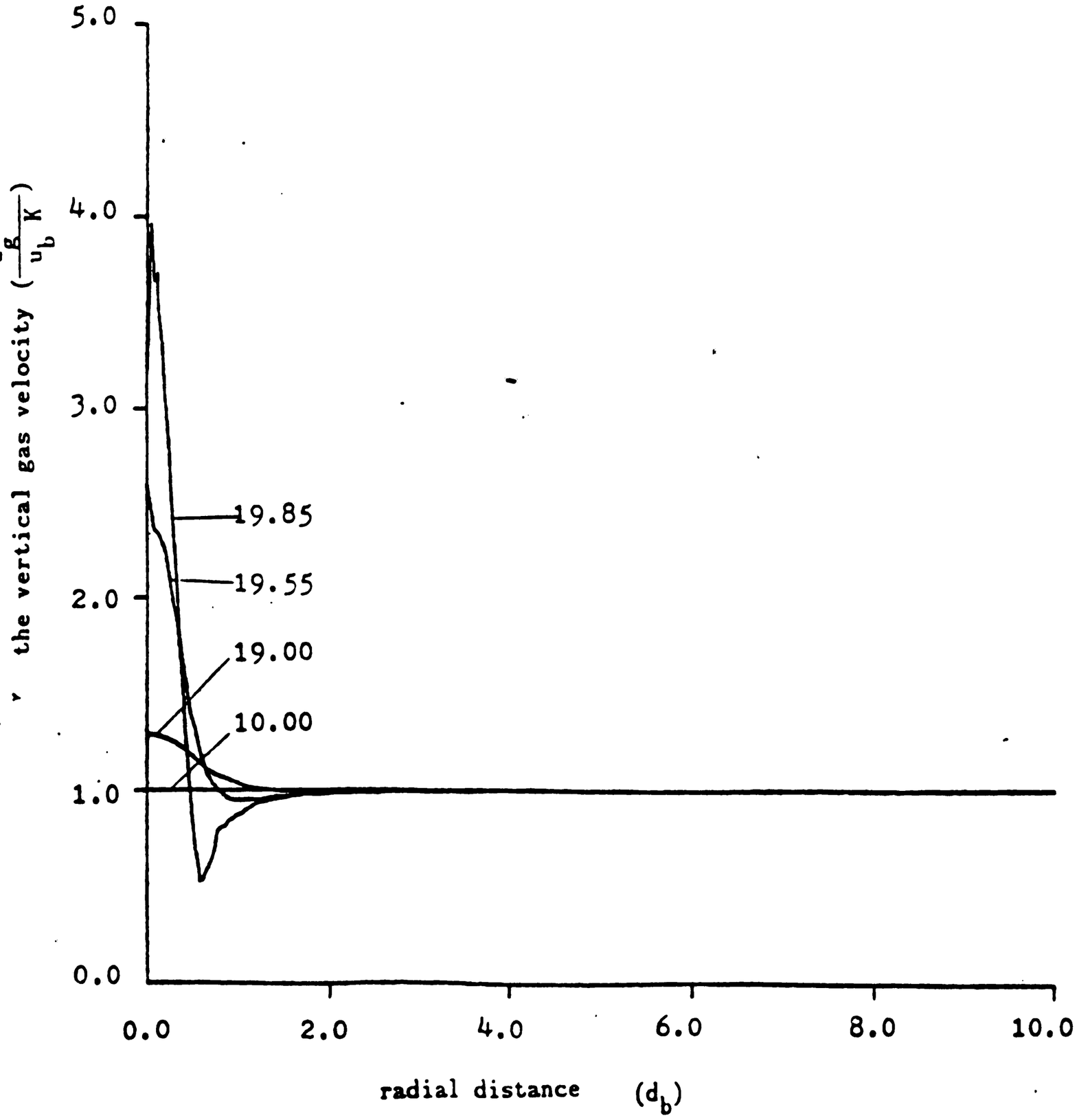

Figure 113. The vertical component of gas velocity at the free surface for K = 10

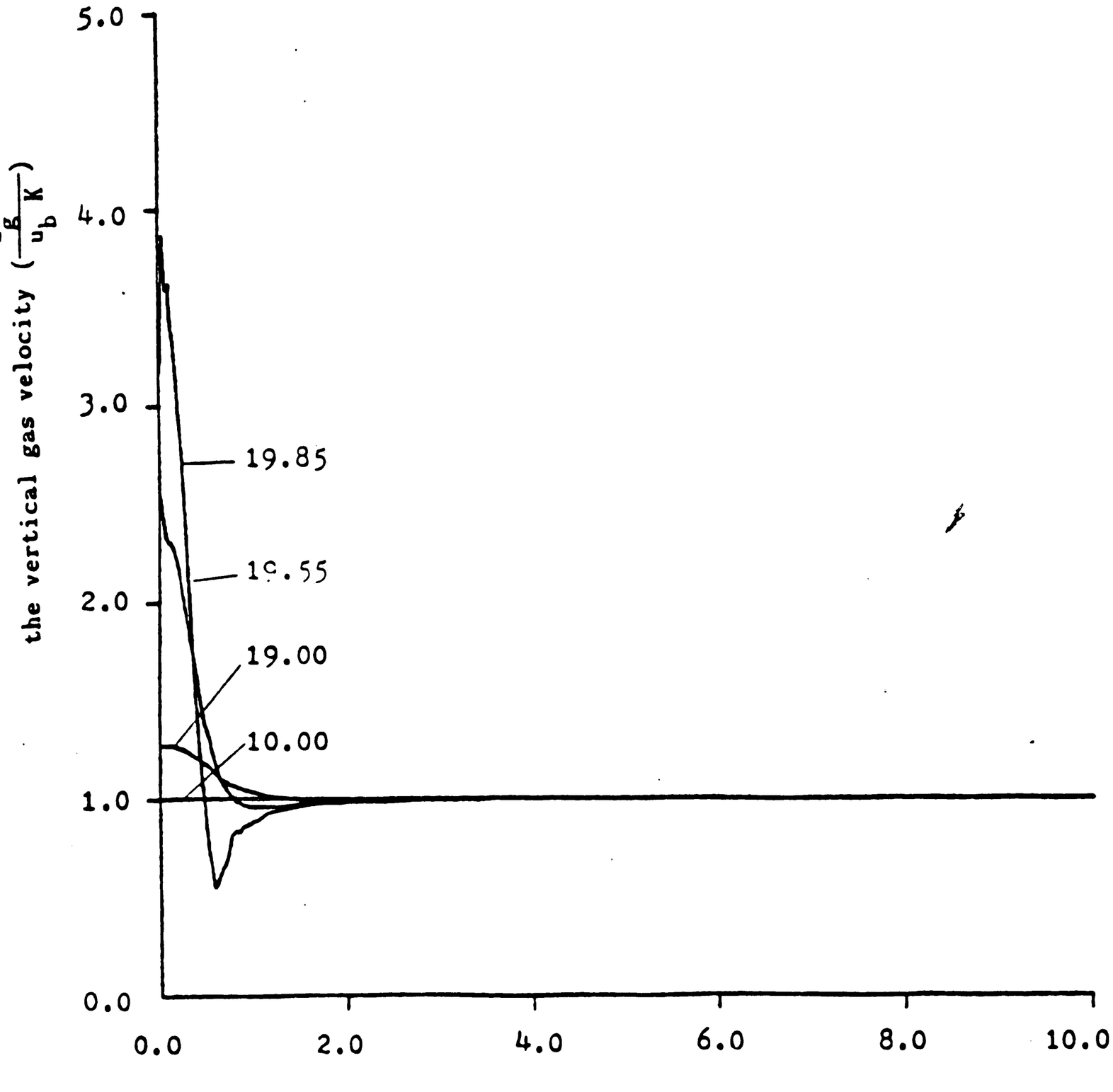

Figure 114. The vertical component of gas velocity at the free surface for K = 100

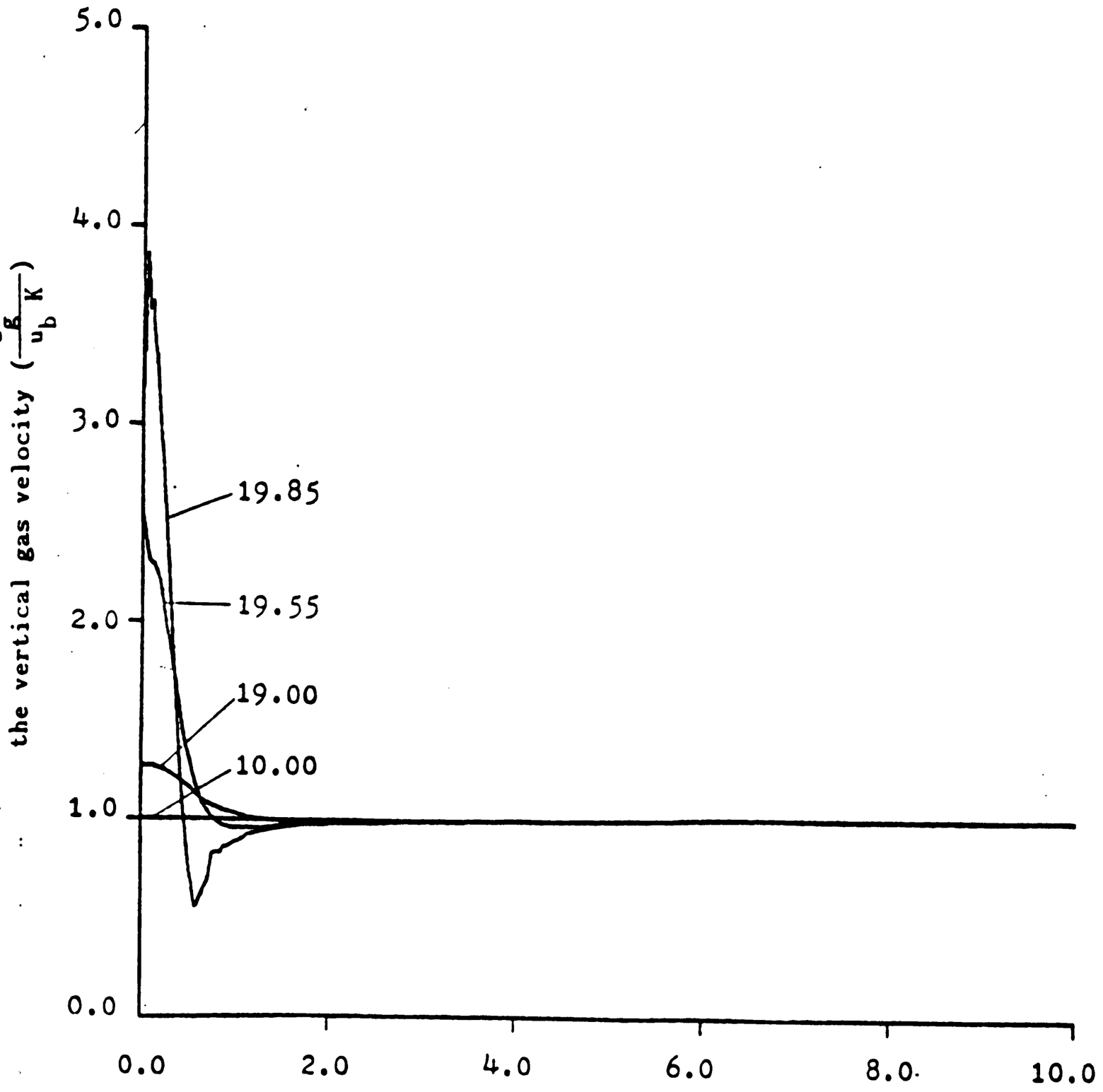

Figure 115. The vertical component of gas velocity at the free surface for K = 1000

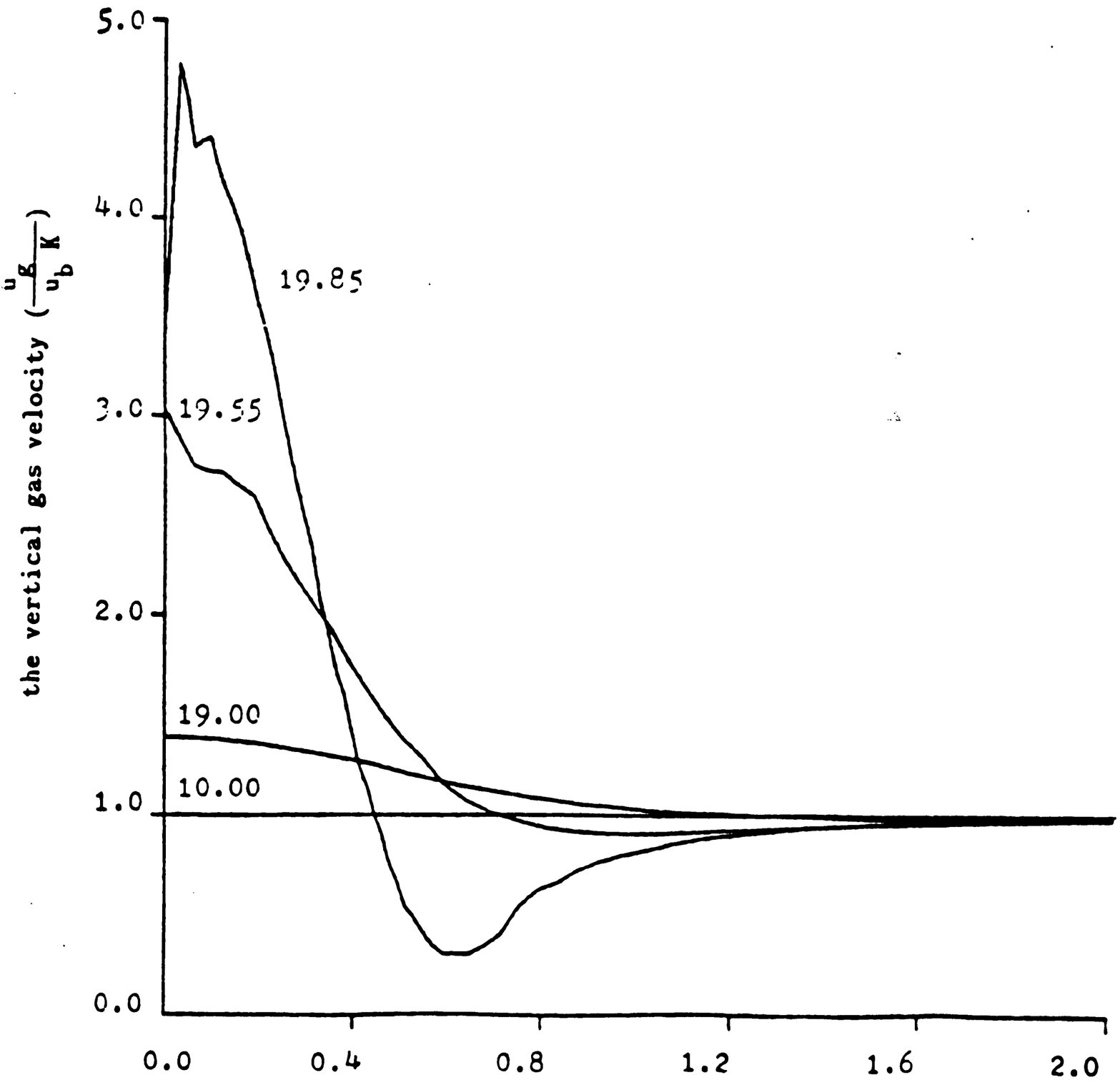

Figure 116. The vertical component of gas velocity
at the free surface
highlighting the area near to the bubble for K = 1.1

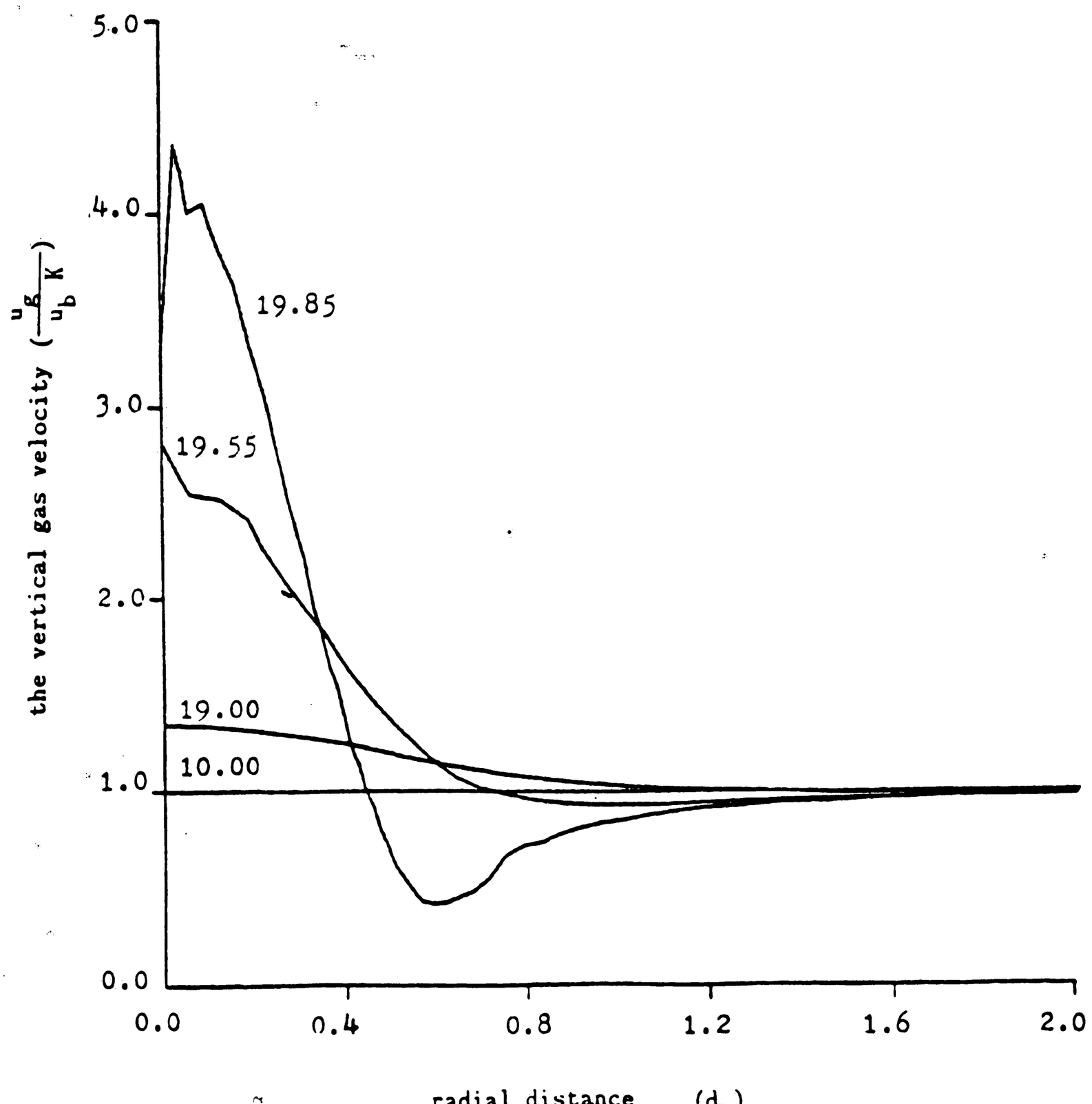

Figure 117. The vertical component of gas velocity at the free surface highlighting the area near to the bubble for K = 2

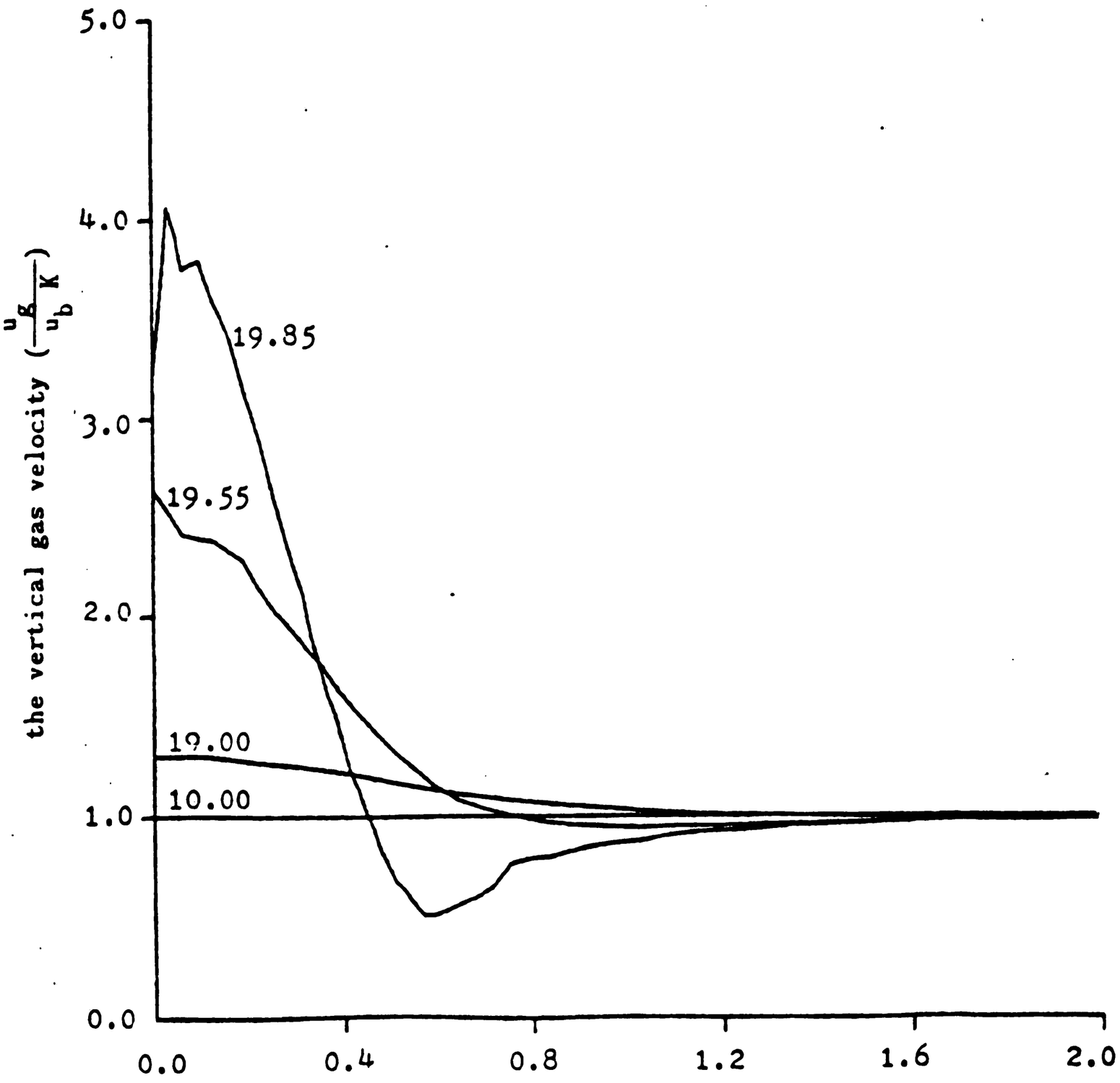

Figure 118. The vertical component of gas velocity at the free surface
highlighting the area near to the bubble for K = 5

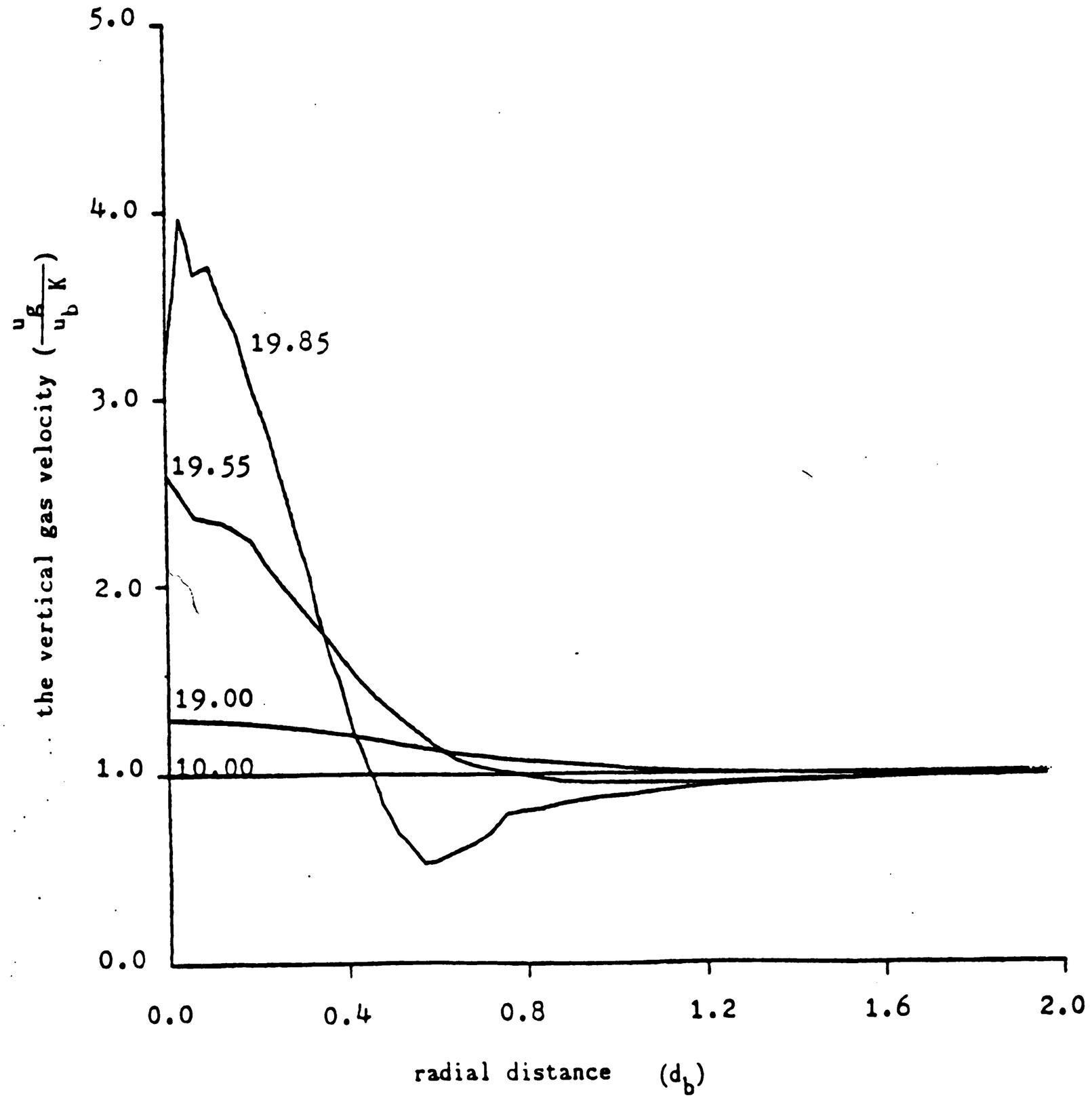

Figure 119. The vertical component of gas velocity
at the free surface
highlighting the area near to the bubble for K = 10

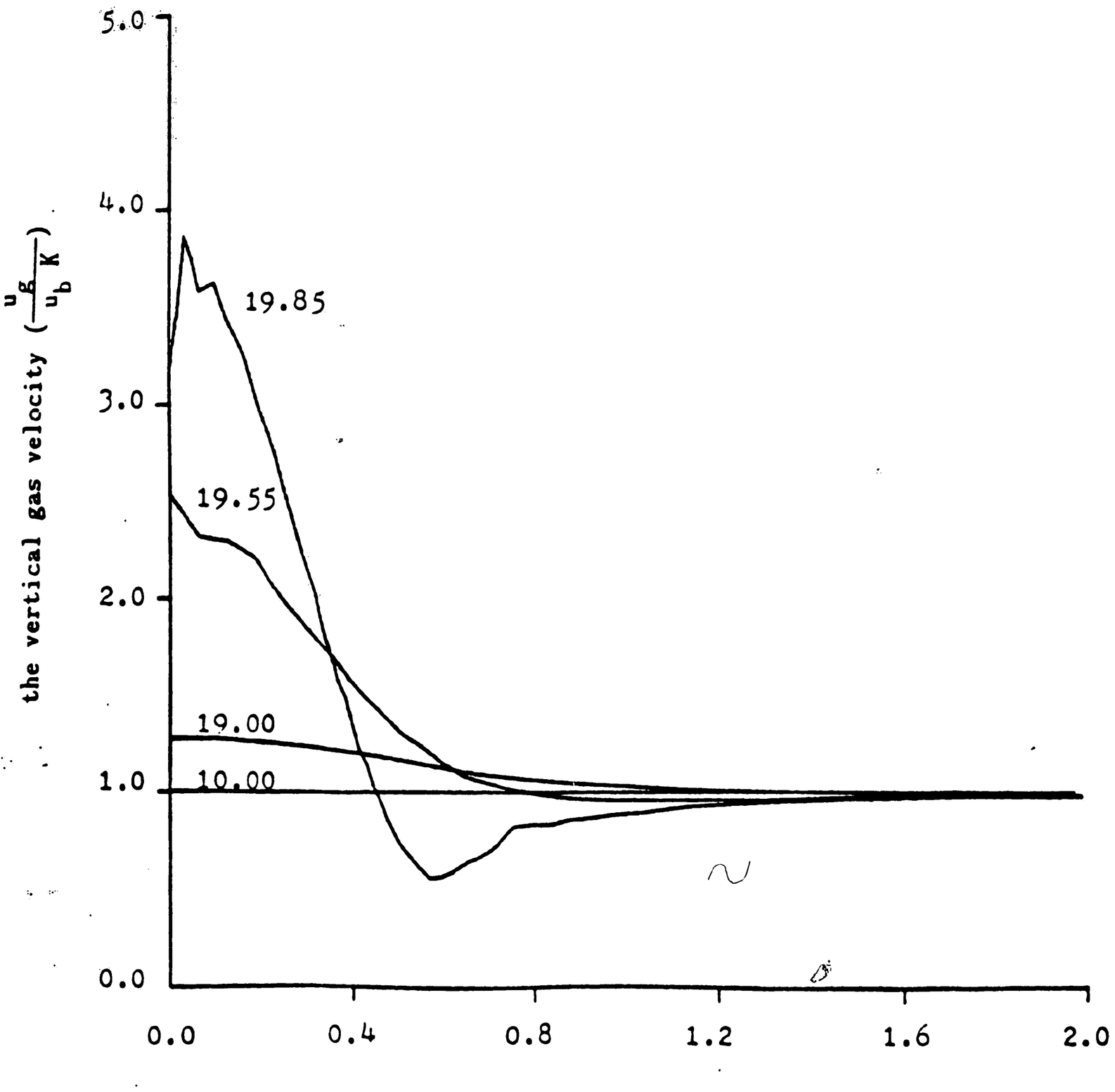

Figure 120. The vertical component of gas velocity
at the free surface
highlighting the area near to the bubble for K = 100

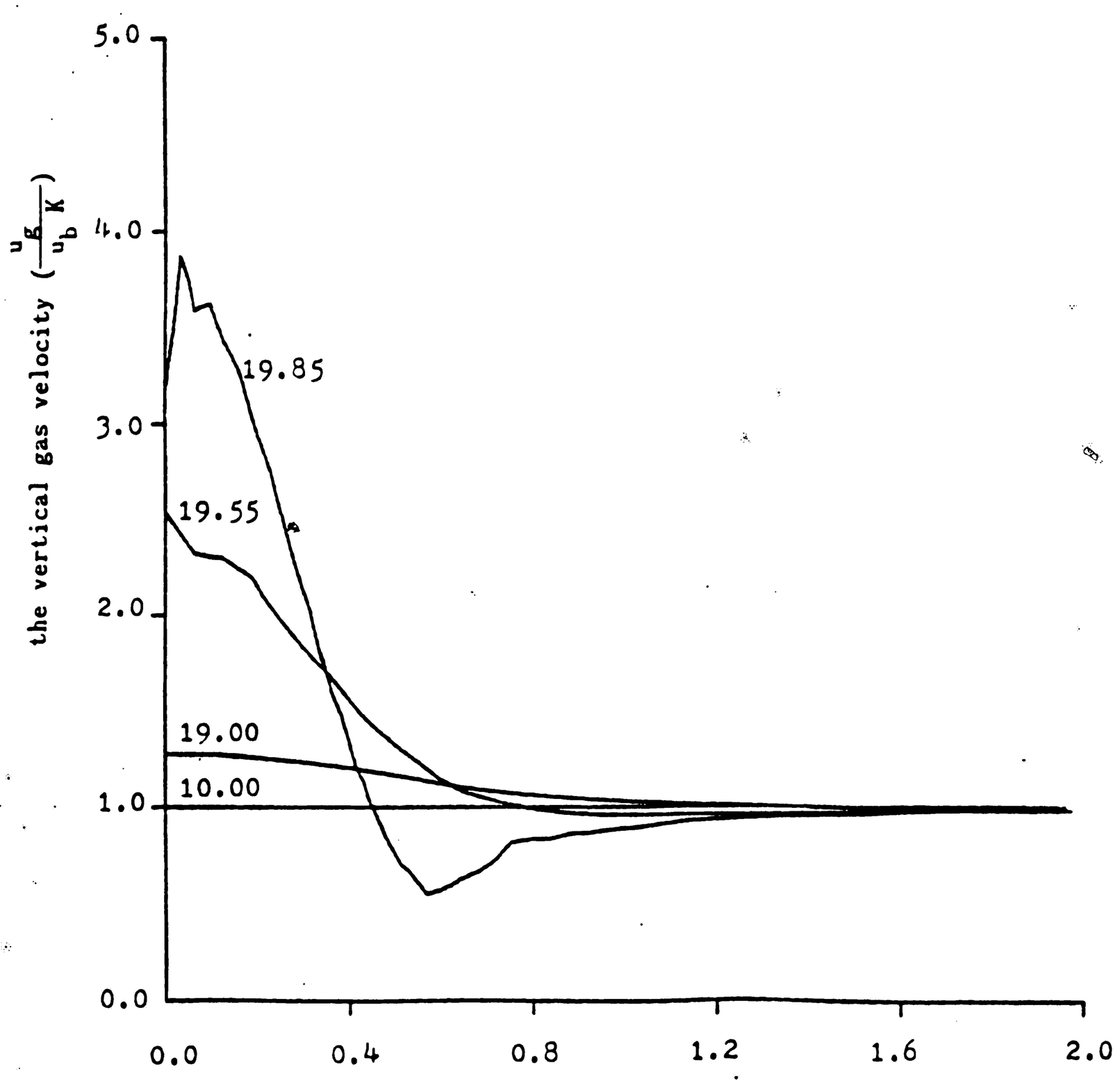

Figure 121. The vertical component of gas velocity
at the free surface
highlighting the area near to the bubble for K = 1000

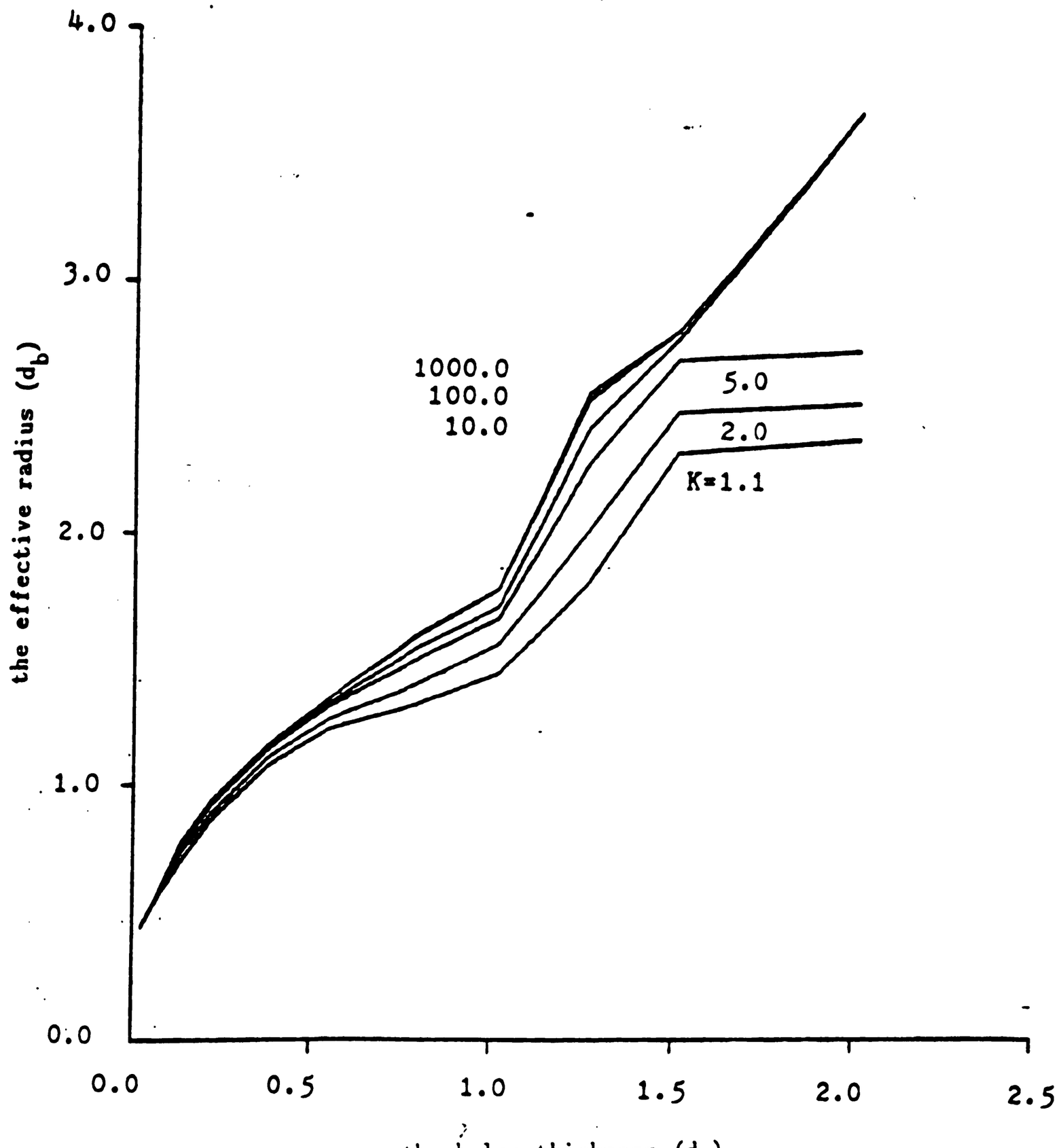

Figure 122. The effective radius related to the bulge thickness at bubble centerline

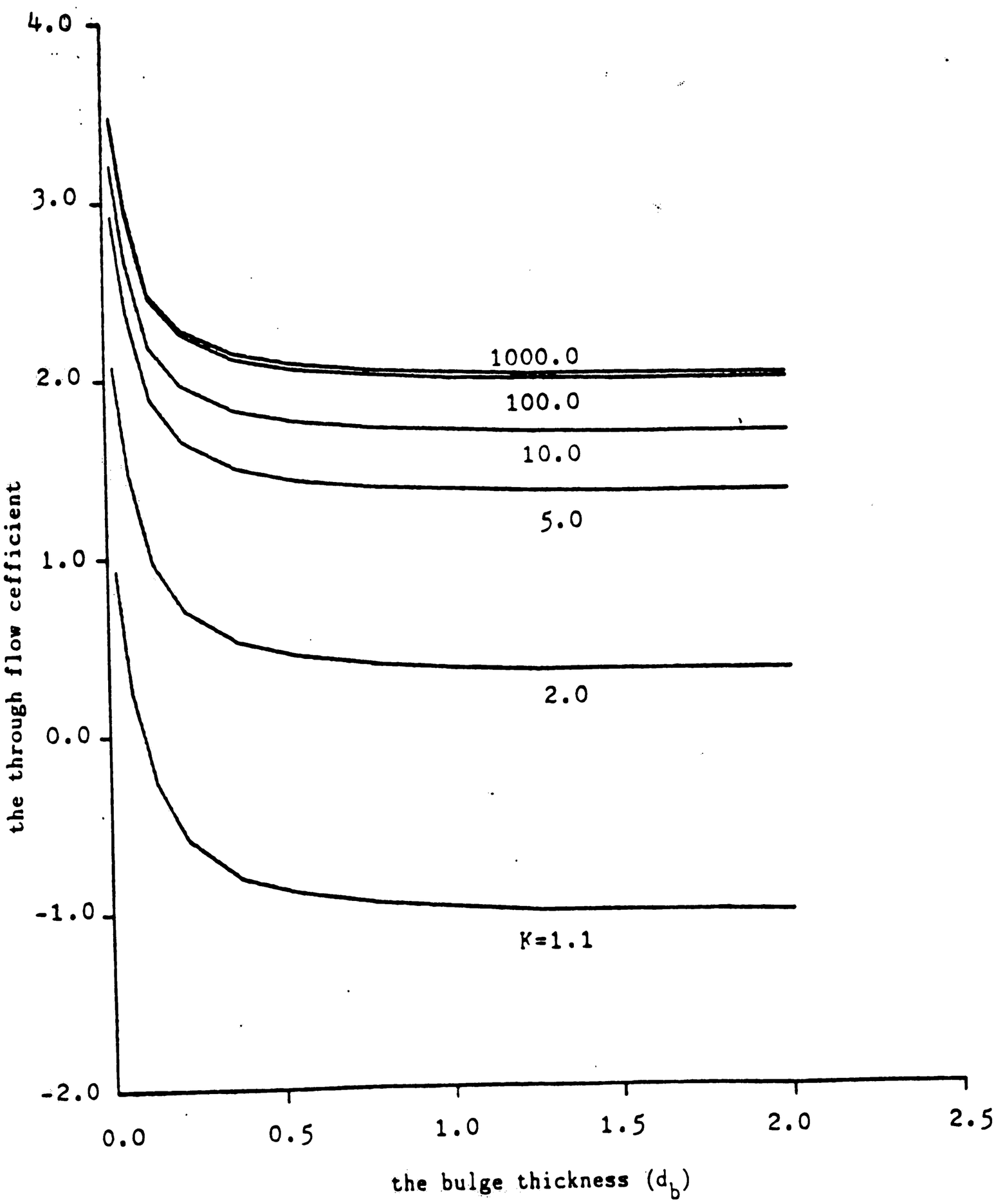

Figure 123. The through flow coefficient at the free surface related to the bulge thickness ($\epsilon_{mf} = 0.4$)

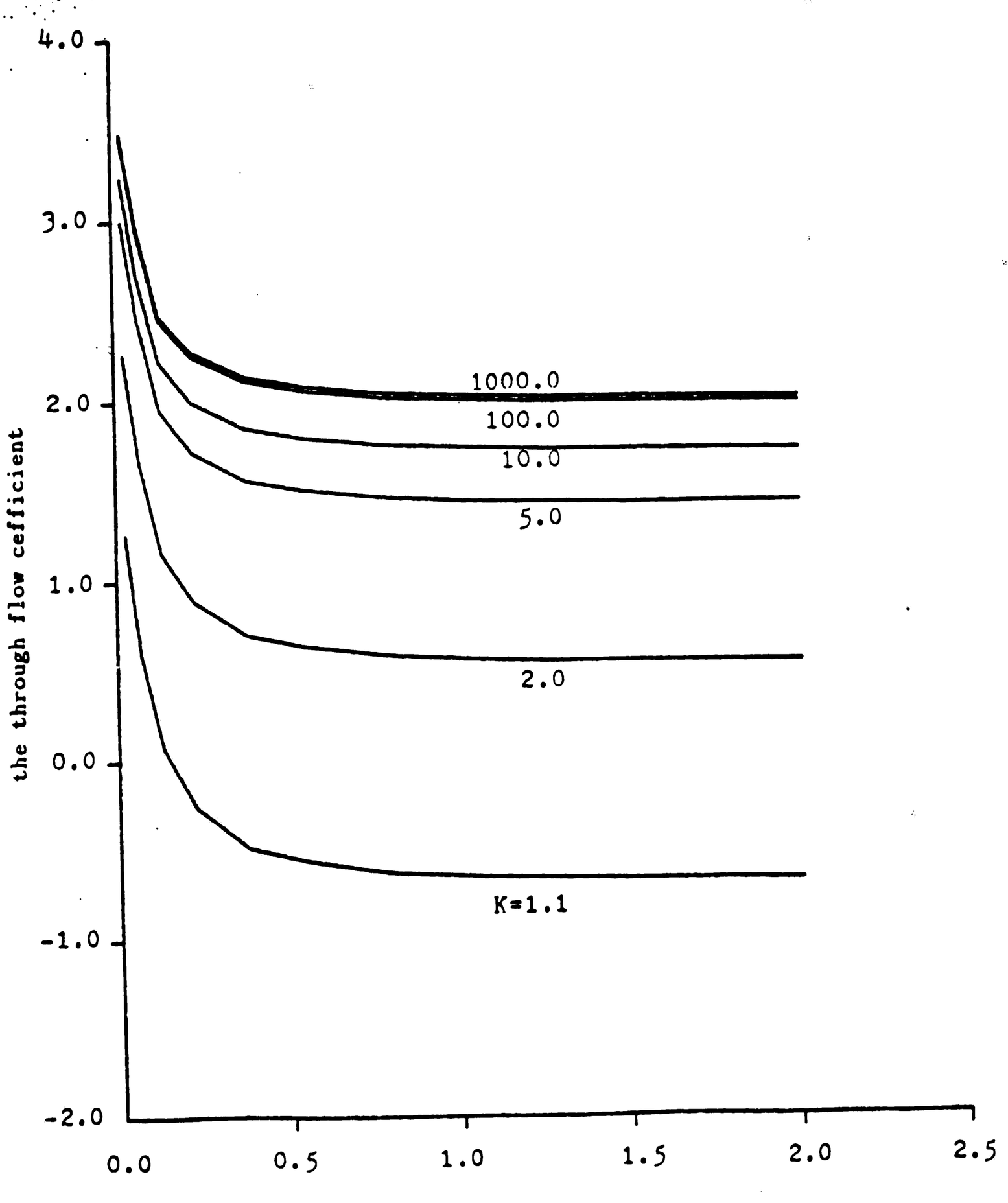

Figure 124. The through flow coefficient at the free surface related to the bulge thickness (ϵ_{mf} = 0.45)

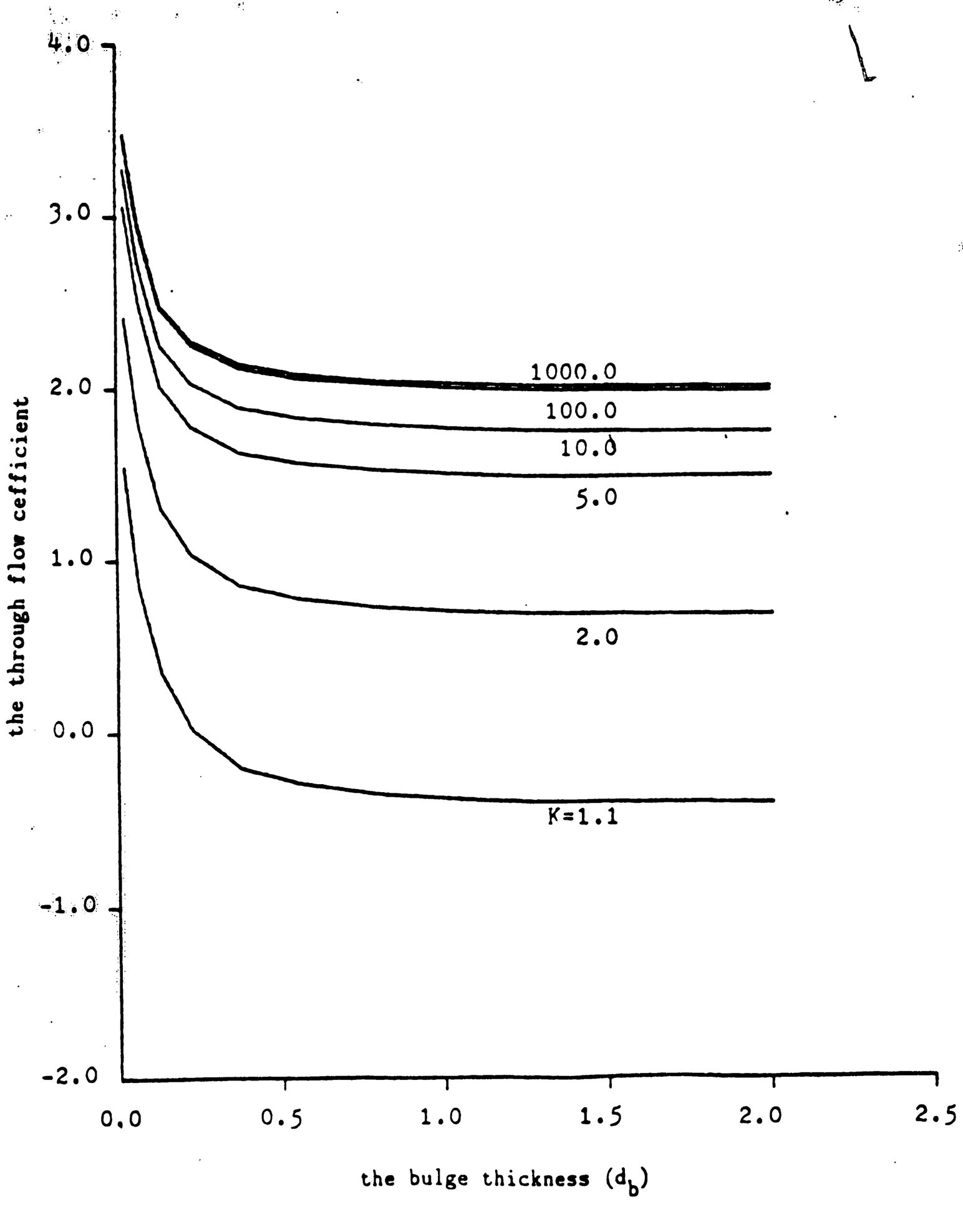

Figure 125.The through flow coefficient at the free surface related to the bulge thickness (ϵ_{mf} = 0.5)

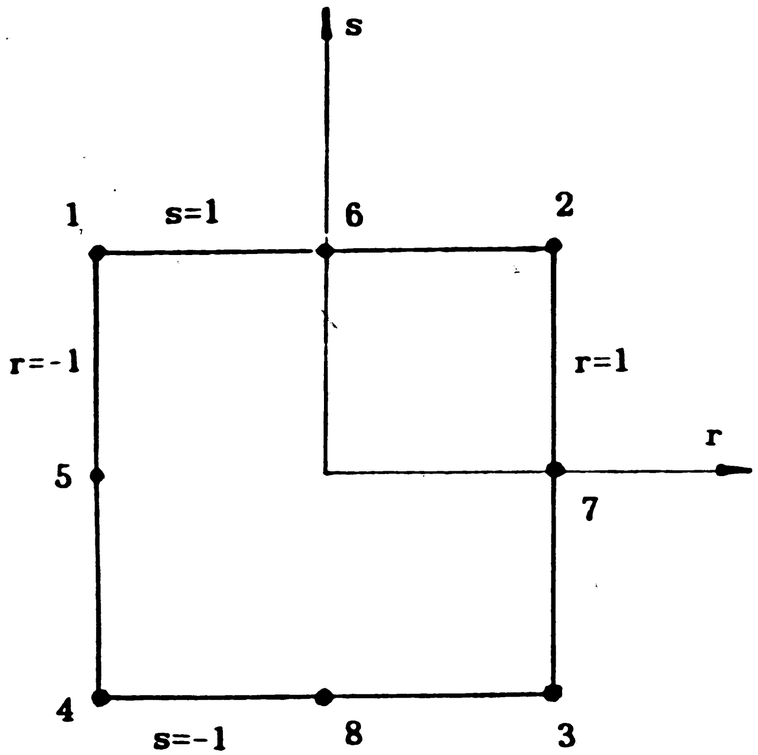

local coordinate

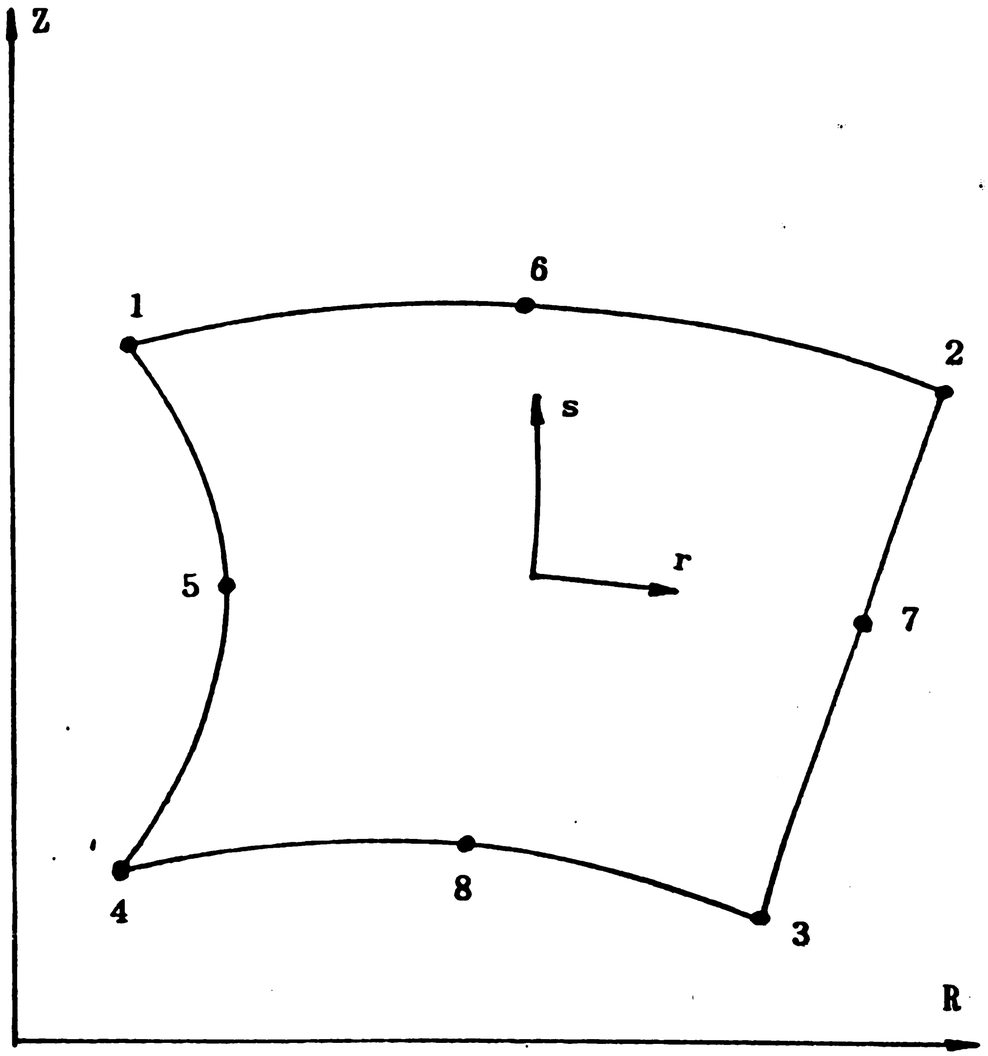

global coordinate

Figure 126 . A curve-sided quadrilateral element resulting from mapping the rectangular parent element.

REFERENCE

1. Zenz, F. A. and Weil, N. A., "A Theoretical-Empirical Approach to the Mechanism of Particle Entrainment from Fluidized Beds", AICHE Journal , 1958.

2. George, S. and Grace, J., "Entrainmaent of Particles from Aggregrative Fluidized Beds", AICHE symp., 176, vol 74.

3. Levy, E. K., Alken, I.and Caram, H., "Characteristics of Erupting Bubbles in a Three Dimensional Fluidized Bed", AICHE symp. 241, vol 80, 1984.

4. Rowe, P. N. and Partridge, B. A.,"The Mechanisms of Solids Mixing in Fluidized Beds", Trans. Instn Chem. Engrs, Vol 43, 1965

5. Do, H. T., Grace, J. R. and Clift, R., "Particle Ejection and Entrainmentd from Fluidized Bed", Power Technology, Vol 6, 1972.

6. Levy, E. K., Caram, H. S., Dille, J. C. and Sergio Edelstein, "Mechanisms for Solids Ejection from Gas-Fluidized Beds" AICHE Journal, 1983.

7. Davidson, J. F., Trans Instn Chem. Engrs, Vol 39, 1961.

8. Jackson, R., Trans Instn Chem. Engrs, Vol 41, 1963.

9. Murray, J. D., "Mathematical Aspects of Bubble Motion in Fluidized Beds", J. Fluid Mechanics, Vol 21 1967.

10. Collins, R., "An Extension of Davidson"s Theory of Bubble in Fluidized Beds"

11. Radcliff, R.A. "Mathematical Model of a Bubble Approaching the Free Surface of a Fluidized Bed" master's thesis, Lehigh University, 1984.

12. Davidson, J.F., and Harrison, D., Fluidized particles, Cambridge University press., 1963.

13. Jackson, R., "Fluid Mechanical Theory" in Fluidization edited by Davidson, J.F., and Harrison, D., Acadmeic press, 1971.

14. Milne, L.M., and Thomson, C.B.E., Theoretical Hydrodynamics. The Macmillan company, New York, 1960.

15. Gill, P.E., and Miller, G.F., "An Algorithm for the Integration of Unequally Spaced Data", Comput. J. 15, 80-83.

16. Zienkiewicz, O.C. The Finite Element Method. 3rd ed. McGraw Hill, New York.

NOMENCLATURE LIST

a	radius of the spherical-cap.
dA	differential area in spherical coordinates.
C	absolute constant.
C(t)	instantaneous constant.
F_i	value of velocity potential or pressure at node i.
$\{\bar{F}\}$	the column matrix of nodal unknown for the assemblage,
Frd	Froude number.
H	dimensionless deformation of the free surface.
I	functional.
J	pressure gradient in the vertical direction far from the bubble which just supports the weight of the particles.
k	constant characteristic of the particles and of the fluidising gas.
K	dimensionless interstitial gas velocity far from the bubble.
M	total number of elements in the assemblage.
m_b	gas through flow coefficient of the bubble.
m_f	gas through flow coefficient at the free surface.
n	the number of nodes assigned to an element.
N,N+1	consecutive levels of time separated by the interval Δt.
N_i	interpolation function.
p	pressure.
P	dimensionless pressure.
p_f	pressure at free surface of bed.
P_s	dimensionless pressure at the bubble surface.

$\dot{q}$ flow rate of gas through a bubble.

$\dot{q}_{FS}$ total gas flow rate across the effective circular eruption area at the free surface of the bed.

$\dot{q}_{net}$ the net volumetric absolute flow rate of gas across the surface of the bubble.

$\dot{q}_{in}$ magnitude of the total absolute flow rate of gas into the bubble.

$\dot{q}_{out}$ magnitude of the total absolute flow rate of gas out of the bubble.

r,s local coordinate system in finite element analysis.

R,Z global coordinate system in finite element analysis.

r_b radius of the bubble.

r_1 effective radius of the circular eruption area through which gas flows vertically across the surface of the bed.

S_1, S_2 boundary surface.

t time.

T dimensionless time.

u_b bubble velocity.

u_g absolute interstitial gas velocity.

U_g dimensionless absolute interstitial gas velocity.

$u_{g\infty}$ absolute interstitial fluid velocity far from the bubble.

u_{GB} average absolute superficial gas velocity flowing through the bubble.

u_{GF} average absolute superficial gas velocity flowing through the area πr_1^2 at the free surface of the bed.

u_{mf} absolute superficial fluid velocity at minimum fluidization.

$u_n(\theta)$ absolute interstitial gas velocity normal to the sphere surface.

$U_n(\theta)$ dimensionless absolute interstitial gas velocity normal to the sphere surface.

u_r, u_θ components of interstitial gas velocity relative to the bubble in three dimensional axi-symmetric coordinate system.

u_z vertical component of absolute interstitial gas velocity.

U_z dimensionless vertical component of absolute interstitial gas velocity.

v_p particle velocity.

V_p dimensionless particle velocity.

v_r, v_z components of particle velocity at the free surface in the r,z directions.

z_c the height of the bubble center

z_f the height of the free surface.

z_o the height of the undisturbed free surface.

Z_o dimensionless height of the undisturbed free surface.

a_f the bubble flow area shape factor.

Δ the bulge thickness.

ϵ_{mf} voidage of the bed at the minimum fluidization velocity.

ϕ particle velocity potential.

Φ dimensionless particle velocity potential.

η the deformation of the free surface.

ρ_s density of the particle phase.

APPENDIX A

1. Derivation of the dimensionless ratio K

From D'Arcy's law, the difference between the interstitial gas and particle velocities is a constant k times the pressure gradient (grad p).

$$u_g = v_p - k\ \nabla p \tag{A1}$$

Using the dimensionless ratios shown in chapter 3, this equation becomes

$$U_g\ u_b = V_p\ u_b - k\ \nabla P\ \frac{\rho_s(\ 1-\epsilon_{mf})\ d_b\ g/g_c}{d_b} \tag{A2}$$

$$U_g = V_p - \frac{k}{u_b}\ \rho_s(\ 1-\epsilon_{mf})\ g/g_c\ \nabla P \tag{A3}$$

Far from the bubble and from the upper and lower surfaces the constant k times $(\frac{\partial p}{\partial z})_\infty$ will equal the interstitial gas velocity $u_{g\infty}$.

Therefore

$$u_{g\infty} = -\ k\ (\ \frac{\partial p}{\partial z})_\infty \tag{A4}$$

If the gas density is assumed to be negligible, the pressure gradient $(\frac{\partial p}{\partial z})_\infty$ equals a constant.

$$-\ (\ \frac{\partial p}{\partial z})_\infty = \rho_s\ (\ 1-\ \epsilon_{mf})\ g/g_c \tag{A5}$$

Then

$$u_{g\infty} = k\ \rho_s\ (\ 1-\ \epsilon_{mf})\ g/gc \tag{A6}$$

Substituting into equation (A3), this becomes

$$U_g = V_p - \frac{u_{g\infty}}{u_b}\ \nabla P \tag{A7}$$

Defining

$$K = \frac{u_{g\infty}}{u_b} \qquad \text{(A8)}$$

we obtain

$$U_g = V_p - K \nabla P \qquad \text{(A9)}$$

and K is the dimensionless ratio for the interstitial gas velocity far from the bubble.

2. Derivation of the pressure boundary conditions on the right and bottom edges

If the gas density is assumed to be negligible, the pressure gradient $(\frac{\partial p}{\partial z})_\infty$ would equal to a constant, $-\rho_s\ (1-\epsilon_{mf})\ g/g_c$, thus

$$\Delta p = -\Delta z\ \rho_s\ (1-\epsilon_{mf})\ g/g_c \qquad \text{(A10)}$$

From the dimensionless ratio

$$p = P\ d_b\ \rho_s\ (1-\epsilon_{mf})\ g/g_c$$

(A10) becomes

$$\Delta P = -\frac{\Delta z}{d_b} = -\Delta Z \qquad \text{(A11)}$$

Referring to the Figure 4., z is the vertical coordinate of the boundary, then

$$\Delta z = z - z_o - \eta \qquad \text{(A12)}$$

Nondimensionlizing the equation (A12) and substituting it into (A11), the boundary conditions of the right and bottom edges could be expressed as

$$\Delta P = -\Delta Z = Z_o + H - Z \qquad \text{(A13)}$$

APPENDIX B

Finite element formulation

The finite element method is used in this investigation for solving the governing equation (Laplace's equation) with boundary conditions.

$$\nabla^2 F = 0. \tag{B1}$$

where F is either velocity potential or pressure function, with two kinds of boundary conditions.

(1) Dirichlet boundary condition:

$$F = \bar{F} \text{ on } S_1. \tag{B2}$$

(2) Neumann boundary condition:

$$\frac{\partial F}{\partial n} = q \text{ on } S_2 \tag{B3}$$

According to the principle of variation of calculus, we specify the problem requiring the stationary of a functional

$$I = \iiint_D [\frac{1}{2} (\frac{\partial F}{\partial R})^2 + \frac{1}{2} (\frac{\partial F}{\partial Z})^2] \, dV - \iint_{S_2} q \, F \, dS \tag{B4}$$

If the distribution of F within each element is assumed to be

$$F^{(e)}(R,Z) = \sum_{i=1}^{n} N_i(R,Z) \, F_i = [N] \, \{F\}^{(e)} \tag{B5}$$

where n is the number of nodes assigned to an element (e)

F_i is the value of velocity potential or pressure at node i

N_i is the interpolation function.

then we substitute this approximation into the functional I and obtain

$$I = \iiint_D \frac{1}{2} (\frac{\partial [N]}{\partial R} \{F\}^{(e)})^2 dV + \iiint_D \frac{1}{2} (\frac{\partial [N]}{\partial Z} \{F\}^{(e)})^2 dV - \iint_{S_2} q \, [N] \, \{F\}^{(e)} \, dS \tag{B6}$$

On diferentiating with respect to a typical F_i and requiring $\frac{\partial I}{\partial F_i} = 0$:

we have the finite element equations:

$$\frac{\partial I}{\partial F_i} = \iiint_D \left[\left(\frac{\partial N_i}{\partial R} \right) \left(\frac{\partial [N]}{\partial R} \right) + \left(\frac{\partial N_i}{\partial Z} \right) \left(\frac{\partial [N]}{\partial Z} \right) \right] \{F\}^{(e)} dV$$

$$- \iint_{S_2} q \, N_i \, dS = 0. \qquad \text{(B7)}$$

$$i = 1, \ldots\ldots, n$$

or in matrix notation

$$[K]^{(e)} \{F\}^{(e)} = \{C\}^{(e)} \qquad \text{(B8)}$$

where

$$K_{ij}^{(e)} = \iiint_D \left[\left(\frac{\partial N_i}{\partial R} \right) \left(\frac{\partial N_j}{\partial R} \right) + \left(\frac{\partial N_i}{\partial Z} \right) \left(\frac{\partial N_j}{\partial Z} \right) \right] dV$$

$$C_i = \iint_{S_2} q \, N_i \, dS$$

The above matrix equations express the properties of individual elements. To find the properties of the overall model, we must assemble all the element properties. Then the complete system of equations is

$$[\bar{K}] \{\bar{F}\} = \{\bar{C}\} \qquad \text{(B9)}$$

where $\{\bar{F}\}$ is the column matrix of nodal unknown for the assemblage,

$$[\bar{K}] = \sum_{e=1}^{M} [K]^{(e)}$$

$$\{\bar{C}\} = \sum_{e=1}^{M} \{C\}^{(e)}$$

and M is the total number of elements in the assemblage.

Solving the system of equations, we can obtain the solution of potential velocity or pressure (F) at all nodes.

In order to improve the accuracy on curved boundaries, axisymmetric parabolic-quadrilateral eight-node isoparametric elements are used in this study. Referring to Zienkiewicz [16], the interpolation function N_i can be defined as

$$N_1 = \frac{1}{4}(1+r)(1+s) - \frac{1}{2}(N_5+N_8) \quad \text{(B10)}$$

$$N_2 = \frac{1}{4}(1-r)(1+s) - \frac{1}{2}(N_5+N_6) \quad \text{(B11)}$$

$$N_3 = \frac{1}{4}(1-r)(1-s) - \frac{1}{2}(N_6+N_7) \quad \text{(B12)}$$

$$N_4 = \frac{1}{4}(1+r)(1-s) - \frac{1}{2}(N_7+N_8) \quad \text{(B13)}$$

$$N_5 = \frac{1}{2}(1-r^2)(1+s) \quad \text{(B14)}$$

$$N_6 = \frac{1}{2}(1-s^2)(1-r) \quad \text{(B15)}$$

$$N_7 = \frac{1}{2}(1-r^2)(1-s) \quad \text{(B16)}$$

$$N_8 = \frac{1}{2}(1-s^2)(1+r) \quad \text{(B17)}$$

where r,s is the local coordinate system.

The nodes in the r-s plane can be mapped into corresponding nodes in the R-S plane by the relations (shown in Figure 126.)

$$R = \sum_{i=1}^{8} N_i(r,s)\, R_i \quad \text{(B18)}$$

$$Z = \sum_{i=1}^{8} N_i(r,s)\, Z_i \quad \text{(B19)}$$

where R, Z is the global coordinate system

VITA

Hai-Kwang Chen, son of Chuan-Lin Chen and Chien-Hu Young, Was born on November 4, 1958 in Taipei, Taiwan, Republic of China. He attended the National Cheng Kung University in Tainan, Taiwan from 1976 and received the Bachelor of Science degree in Mechanical Engineering in June 1980. In December 1983, he was accepted as a graduate student in the Department of Mechanical engineering at Lehigh University.